CHEMICAL SYNTHESIS OF BULKY ISOPRENOID ANALOGUES FOR PROBING PHOSPHOGLYCOSYLTRANSFERASES IN THE BIOSYNTHESIS OF BACTERIAL GLYCANS

by

Dylan C. Morris

A thesis submitted to the faculty of
The University of North Carolina at Charlotte
in partial fulfillment of the requirements
for the degree of Master of Science in
Chemistry

Charlotte

2024

Approved by:

_____
Dr. Jerry Troutman

_____
Dr. Adam Fessler

_____
Dr. Michael Walter

_____
Dr. Kausik Chakrabarti

ABSTRACT

DYLAN MORRIS. Chemical Synthesis of Bulky Isoprenoid Analogues for Probing Phosphoglycosyltransferases in the Biosynthesis of Bacterial Glycans.
(Under the direction of DR. JERRY TROUTMAN)

The bacterial cell wall serves as a protective barrier that encapsulates the cell and features an array of macromolecules, including polysaccharides. These sugar polymers form an extracellular coating that is crucial for bacterial survival and can contribute to infections in host organisms. Bacterial glycans are biosynthesized in a process that is typically initiated by an important class of enzymes called phosphoglycosyltransferases (PGTs). PGTs are integral membrane proteins that are responsible for the first committed step in bacterial glycan biosynthesis, which involves catalyzing the transfer of a phosphosugar moiety to a membrane-embedded polyprenyl phosphate substrate. Despite playing an important role in this process, a lack of information remains regarding PGT function and the reactions they catalyze. One approach to studying the function of enzymes involves probing their substrate specificities using small molecules with varying chemical functionalities. Herein, a small library of short-chain isoprenoid analogues with bulky aromatic groups was developed to probe the effects of substrate size on PGT function. Seven neryl phosphate analogues with naphthylamine, aminobiphenyl, and benzylaniline incorporated were utilized in chemoenzymatic reactions to study the monotopic PGTs, PglC (*Campylobacter jejuni*) and WcfS (*Bacteroides fragilis*). It was found that all seven synthetic probes were accepted by PglC, while only two were accepted by WcfS. This was an important development as short-chain analogues previously tested against WcfS were ineffective suggesting that small structural changes in the substrate could impact activity.

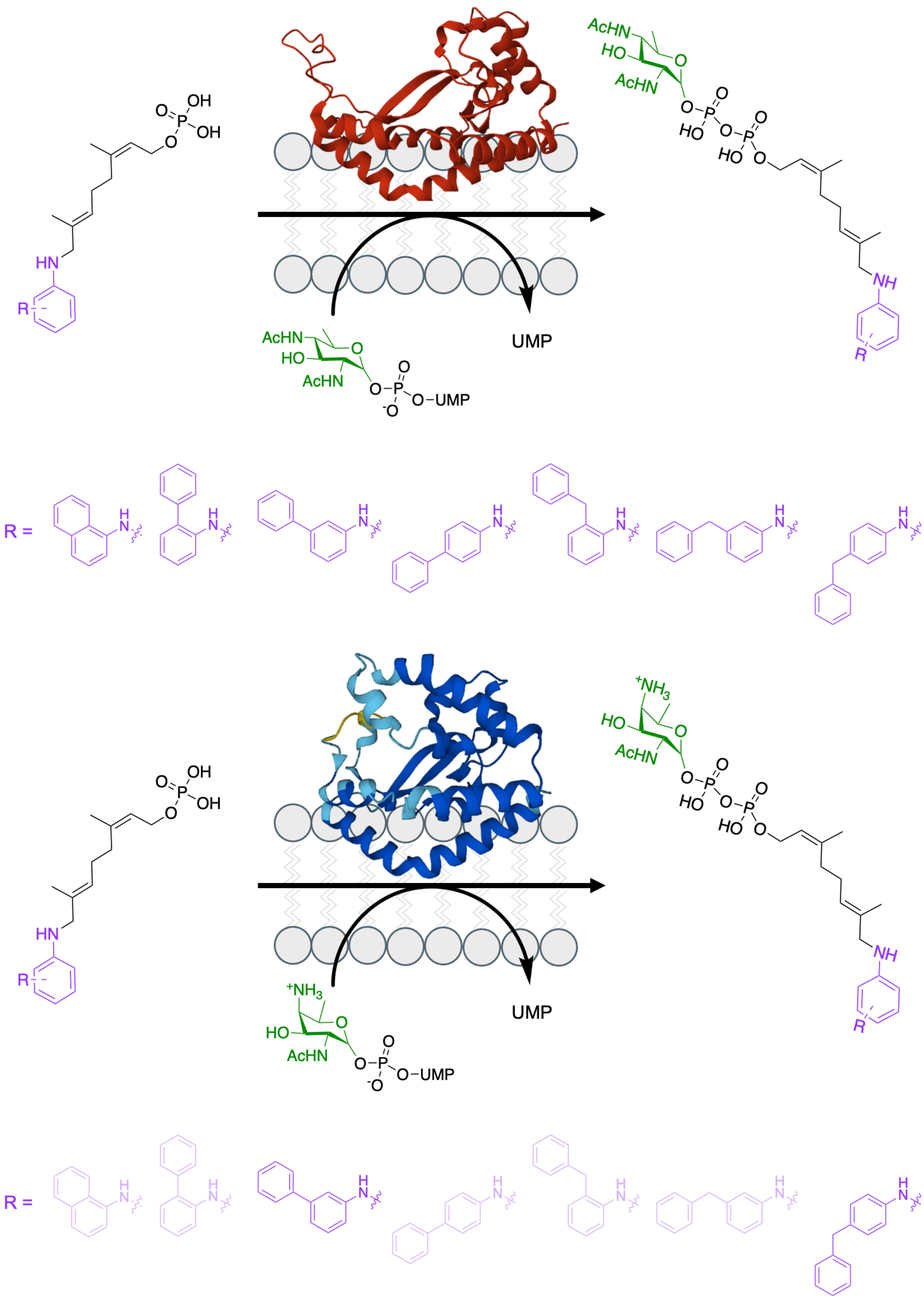
UMP
O-P-O-UMP
R =
UMP
O-P-O-UMP
R =

ACKNOWLEDGMENTS

I would first like to acknowledge Dr. Troutman for introducing me to the master's program at UNC Charlotte and for allowing me to take part in his lab's research. Before coming to Charlotte, I was grappling with imposter syndrome, as I felt I lacked the necessary research experience to become the chemist I had always hoped to be. This was due in part to the COVID-19 pandemic, which greatly limited the academic research opportunities available for me as an undergraduate student. After communicating with Dr. Troutman about the research available at Charlotte, I eventually decided to resign from my job and enroll in the master's program. I want to thank Dr. Troutman for helping me realize my capabilities as a researcher and for allowing me to gain the research experience that I so desperately wanted.

I would also like to acknowledge the other members of the Troutman Lab—including both the former and current students. Starting with the former, I would like to thank Drs. Beth Scarbrough, Amanda Reid, and Katelyn Erickson for their contributions to our lab's research, which helped lay the foundation for my research. Additionally, I want to thank the other members of the lab, who helped me in more direct ways. First, I am immensely grateful to Allena Opoku and Alexis Murray for their friendship and guidance. After moving away from my home in Greensboro, NC, I was alone in a new city without my friends and family nearby. Both Allena and Alexis welcomed me to Charlotte and kindly introduced me to the Troutman Lab. They eventually became two of my closest friends and graciously helped me in numerous ways. Allena was especially helpful with preparing me to teach CHEM 1251L and with providing useful insight for questions regarding analytical chemistry.

After joining the Troutman Lab, I was able to meet some other remarkable people who made a positive impact on my life and academic career. Manoj Dooda was one of the first

graduate students in the Troutman Lab to train me on several useful techniques—namely, culturing bacteria, protein expression, and operating the LC-MS. He kindly shared his knowledge of microbiology and was always willing to help in times of need. I also want to acknowledge Ryan Spillane, who proved to be a great friend in addition to being my chemical synthesis partner. I enjoyed working with Ryan and exchanging ideas about our projects. Thank you to the other members of the lab—Supriya Kurra, Sara Salamat, Alaina Rosen, Jenna Costelloe, and Hope Clements—for making our group feel like a family and for making our work more enjoyable. I especially want to thank Claire Moneghan for offering to host events for the group and for always being friendly, encouraging, helpful, and informative.

Lastly, this thesis and the accompanying research would not exist without the involvement of my thesis committee. Thank you, Drs. Fessler, Walter, and Chakrabarti for agreeing to join my committee and for offering your expertise. I greatly appreciate your interest in my research and your willingness to help me succeed.

DEDICATION

This work is dedicated to every student striving to accomplish their academic goals. Those students who are fully determined and willing to make personal sacrifices, devote long hours, and put in great effort in their studies. Regardless of whether your commitment is recognized by your peers, just know that you are exceptional, capable of greatness, and an important asset. Despite your disabilities, personal struggles, or the numerous adversities you may endure, don’t give up; don’t lose focus; don’t get tripped up by the obstacles along your path to success. Always remember: You can do anything if you set your mind to it and work hard for it. Good luck and enjoy the experience!

TABLE OF CONTENTS

LIST OF TABLES

LIST OF FIGURES

LIST OF ABBREVIATIONS

1-NA	1-naphthylamine
1-NA-NP	1-naphthylamine neryl monophosphate
1-NA-NPP	1-naphthylamine neryl diphosphate
1-NA-NPPP	1-naphthylamine neryl triphosphate
1-NA-OAc	1-naphthylamine neryl acetate
1-NA-OH	1-naphthylamine neryl alcohol
2-ABP	2-aminobiphenyl
2-ABP-NP	2-aminobiphenyl neryl monophosphate
2-ABP-NPP	2-aminobiphenyl neryl diphosphate
2-ABP-NPPP	2-aminobiphenyl neryl triphosphate
2-ABP-OAc	2-aminobiphenyl neryl acetate
2-ABP-OH	2-aminobiphenyl neryl alcohol
2-BA	2-benzylaniline
2-BA-NP	2-benzylaniline neryl monophosphate
2-BA-NPP	2-benzylaniline neryl diphosphate
2-BA-NPPP	2-benzylaniline neryl triphosphate
2-BA-OAc	2-benzylaniline neryl acetate
2-BA-OH	2-benzylaniline neryl alcohol
2AA-GPP	2-amideanilinogeranyl diphosphate
2AB-N-P	2-aminobenzamide neryl phosphate
2CN-NP	2-nitrileanilinoneryl phosphate
2CNA-GPP	2-nitrileanilinogeranyl diphosphate

3-ABP	3-aminobiphenyl
3-ABP-NP	3-aminobiphenyl neryl monophosphate
3-ABP-NPP	3-aminobiphenyl neryl diphosphate
3-ABP-NPPP	3-aminobiphenyl neryl triphosphate
3-ABP-OAc	3-aminobiphenyl neryl acetate
3-ABP-OH	3-aminobiphenyl neryl alcohol
3-BA	3-benzylaniline
3-BA-NP	3-benzylaniline neryl monophosphate
3-BA-NPP	3-benzylaniline neryl diphosphate
3-BA-NPPP	3-benzylaniline neryl triphosphate
3-BA-OAc	3-benzylaniline neryl acetate
3-BA-OH	3-benzylaniline neryl alcohol
4-ABP	4-aminobiphenyl
4-ABP-NP	4-aminobiphenyl neryl monophosphate
4-ABP-NPP	4-aminobiphenyl neryl diphosphate
4-ABP-NPPP	4-aminobiphenyl neryl triphosphate
4-ABP-OAc	4-aminobiphenyl neryl acetate
4-ABP-OH	4-aminobiphenyl neryl alcohol
4-BA	4-benzylaniline
4-BA-NP	4-benzylaniline neryl monophosphate
4-BA-NPP	4-benzylaniline neryl diphosphate
4-BA-NPPP	4-benzylaniline neryl triphosphate
4-BA-OAc	4-benzylaniline neryl acetate

4-BA-OH	4-benzylaniline neryl alcohol
AADGal	acetamido-4-amino-6-deoxygalactopyranose
Acetyl-CoA	acetyl coenzyme A
AGPP	8-anilinogeranyl diphosphate
A. hydrophila	*Aeromonas hydrophila*
aq	aqueous
Asp	aspartic acid
Az-NP	azide neryl phosphate
Bac	2,4-diacetamido-2,4,6-trideoxyglucose
B. fragilis	*Bacteroides fragilis*
BP	bactoprenyl phosphate
BPP	bactoprenyl diphosphate
$CDCl_3$	deuterated chloroform
C. jejuni	*Campylobacter jejuni*
CPS	capsular polysaccharide
Cps2E	a phosphoglycosyltransferase
diNAcBac	2,4-diacetamido-2,4,6-trideoxyglucose
DMAPP	dimethylallyl diphosphate
D_2O	deuterium oxide
ECA	enterobacterial common antigen
E. coli	*Escherichia coli*
EHEC	enterohemorrhagic *Escherichia coli*
EPS	exopolysaccharide

Et_3N	triethylamine
EtOAc	ethyl acetate
FPP	farnesyl diphosphate
FTase	farnesyltransferase
GalNAc	*N*-acetylgalactosamine
GGPP	geranylgeranyl diphosphate
GGPPS	geranylgeranyl diphosphate synthase
GGTase-I	geranylgeranyltransferase type I
GlcNAc	*N*-acetylglucosamine
Glu	glutamic acid
GPP	geranyl diphosphate
GPPS	geranyl diphosphate synthase
GST	glutathione S-transferase
GT	glycosyltransferase
HGP	Human Genome Project
His	histidine
HOAc	acetic acid
HPLC	high performance liquid chromatography
IMAC	immobilized metal affinity chromatography
IPP	isopentenyl diphosphate
IPPS	isopentenyl diphosphate synthase
*i*PrOH	isopropanol
IPTG	isopropyl-β-D-1-thiogalactopyranoside

LB	Luria-Bertani
LC-MS	liquid chromatography-mass spectrometry
LPS	lipopolysaccharide
MeOH	methanol
monoPGT	monotopic phosphoglycosyltransferase
MWCO	molecular weight cut-off
m/z	mass-to-charge ratio
$NaBH(OAc)_3$	sodium triacetoxyborohydride
NAD^+	nicotinamide adenine dinucleotide
NDP-sugar	nucleoside diphosphate-linked sugar glycoside
Ni-NTA	nickel-nitrilotriacetic acid
NMP-sugar	nucleoside monophosphate-linked sugar glycoside
NMR	nuclear Magnetic Resonance
NPP	neryl diphosphate
OD_{600}	optical density at 600 nm
PBS	phosphate-buffered saline
Pgl	protein glycosylation
PglB	an oligosaccharyl transferase
PglC	a phosphoglycosyltransferase
PglJ	a glycosyltransferase
PGT	phosphoglycosyltransferase
PHPT	polyisoprenol-phosphate hexose-1-phosphate transferase
PLP	pyridoxal 5’-phosphate

PNPT	polyisoprenol-phosphate N-acetylaminosugar-1-phosphate transferase
polyPGT	polytopic phosphoglycosyltransferase
Pren-P	prenyl-phosphate
R-NOAc	an aniline (R)-incorporated neryl acetate analogue
R-NOH	an aniline (R)-incorporated neryl alcohol analogue
R-NP	an aniline (R)-incorporated neryl monophosphate analogue
Ras	a G protein
R_f	retention factor
RT	room temperature
RXN	reaction
SDS-PAGE	sodium dodecyl sulfate-polyacrylamide gel electrophoresis
S. enterica	*Salmonella enterica*
SIM	selected ion monitoring
S. pneumoniae	*Streptococcus pneumoniae*
TEAP	bis-triethylammonium phosphate
TNBAP	tetra-*n*-butylammonium dihydrogen phosphate
Tris	tris(hydroxymethyl)aminomethane
Tris-Acetate	tris(hydroxymethyl)aminomethane (pH adjusted with acetic acid)
Tris-HCl	tris(hydroxymethyl)aminomethane (pH adjusted with hydrochloric acid)
TLC	thin-layer chromatography
UDP	uridine 5’-diphosphate
Und-P	undecaprenyl phosphate
Und-PP	undecaprenyl pyrophosphate

UPEC	uropathogenic *Escherichia coli*
UppS	undecaprenyl pyrophosphate synthase
UV	ultraviolet
WbaP	a phosphoglycosyltransferase
WcfS	a phosphoglycosyltransferase
WecA	a phosphoglycosyltransferase
WecG	a glycosyltransferase
WecF	a glycosyltransferase
WecP	a phosphoglycosyltransferase

CHAPTER 1: INTRODUCTION

1.1: Bacterial Cell Wall

Bacterial cells are completely encapsulated by a cell wall that acts as a physical barrier and functions simultaneously to contain internal cellular components and protect the cell externally from the environment. The cell wall itself is composed of multiple layers with an array of complex macromolecules, including lipids, proteins, and carbohydrates (**Figure 1**). Lipids exist primarily as fatty acid hydrocarbons, forming the hydrophobic layer of the phospholipid membrane. Proteins are embedded within and along the surface of the membrane and fulfill various functions as enzymes, receptors, transporters, and structural anchors. Carbohydrates are present as long polysaccharide chains that extend out of the membrane and into the extracellular space and play a crucial role in bacterial survival.

The bacterial glycocalyx is an extracellular sugar coating that surrounds the outer surface of bacterial cells.[13] It is within this coating that the various bacterial surface polysaccharides—also known as bacterial glycans—can be found. Bacterial glycans are responsible for maintaining cellular structure and physiology: They can protect the cell from osmotic stress, changes in temperature or pH, and desiccation.[5, 14] These sugars are also necessary for cellular adhesion and biofilm formation, which immobilizes bacteria onto surfaces to facilitate growth and host colonization.[5] Additionally, bacterial glycans can either be immunogenic and trigger an immune response in host organisms, or they can assist a bacterium in evading a provocation with the immune system.[5, 15]

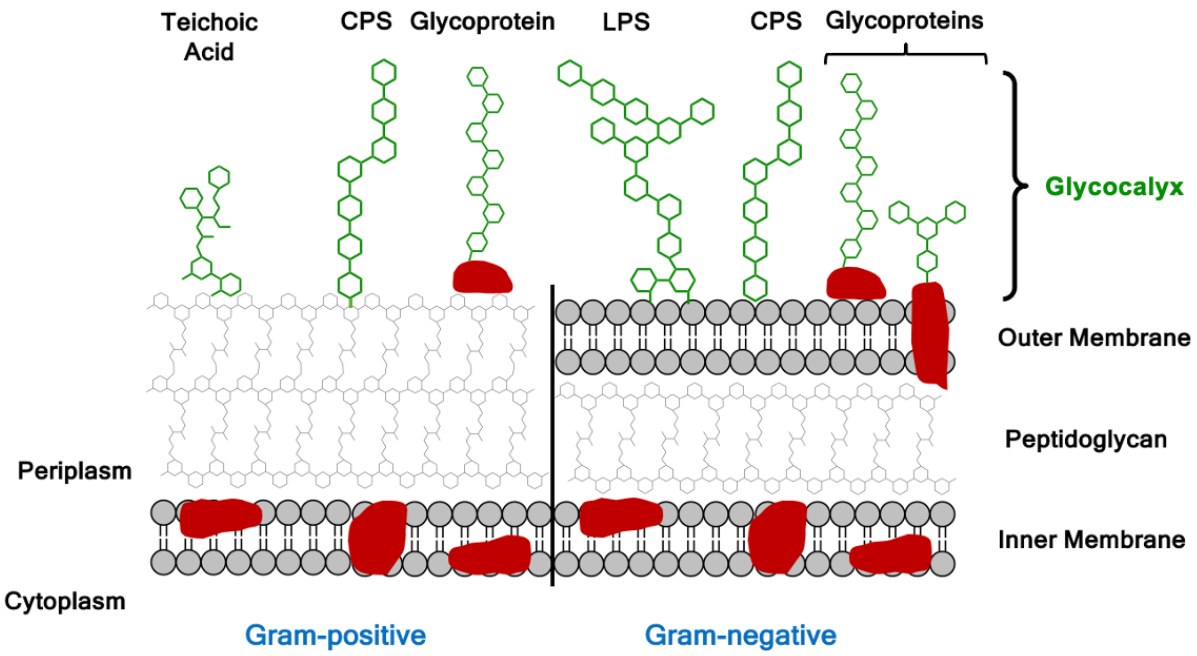

Figure 1: Bacterial cell wall. A representation of macromolecules in the cell wall, including proteins (red amorphous shapes), lipids (dark gray phospholipid membrane), and carbohydrates (green chains and light gray peptidoglycan). The glycans in the glycocalyx and the composition of the membrane structure are unique features for each Gram classification.

Most bacteria are either Gram-positive or Gram-negative, which distinguishes the type of cell wall and the accompanying bacterial glycans associated with it (**Figure 1**). Gram-positive bacteria have characteristically thick layers of peptidoglycan and a single phospholipid inner membrane.[16] The glycans produced by these species include capsular polysaccharide (CPS) and polyol phosphate polymers made of teichoic acids.[17, 18] Gram-negative bacteria have a cell wall containing a phospholipid inner and outer membrane that are separated by a thin layer of peptidoglycan in the periplasmic space. These bacteria usually produce lipopolysaccharide (LPS) in addition to capsular polysaccharide in the outer membrane.[18]

There are essentially two main classifications of surface polysaccharides: exopolysaccharides (EPSs) and capsular polysaccharides (CPSs). These terms are used to describe whether the polysaccharide is loosely attached—EPS—or firmly attached—CPS—to

the cell surface. However, they are often used interchangeably due to the difficulty of discerning how each type of glycan is attached.[19, 20] Bacteria often use EPSs to interact with the environment, adhere to surfaces, respond to environmental stress, and maintain homeostasis.[5, 21] Colanic acid (**Figure 2A**), for example, is an EPS produced by *Enterobacteriaceae*, which is a family of Gram-negative bacteria including *Escherichia coli*. *E. coli* has been found to secrete colonic acid when exposed to harshly acidic environments.[22] CPSs and lipopolysaccharides (LPSs) are virulence factors that contribute to pathogenicity and can elicit or evade an immune response in host organisms.[5, 21] For example, lipid A—also known as endotoxin—(**Figure 2B**) is the hydrophobic lipid domain of LPS. This glycan is found in the outer membrane of most Gram-negative bacteria, covering approximately 40% of the surface, and triggers an innate immune response.[23, 24]

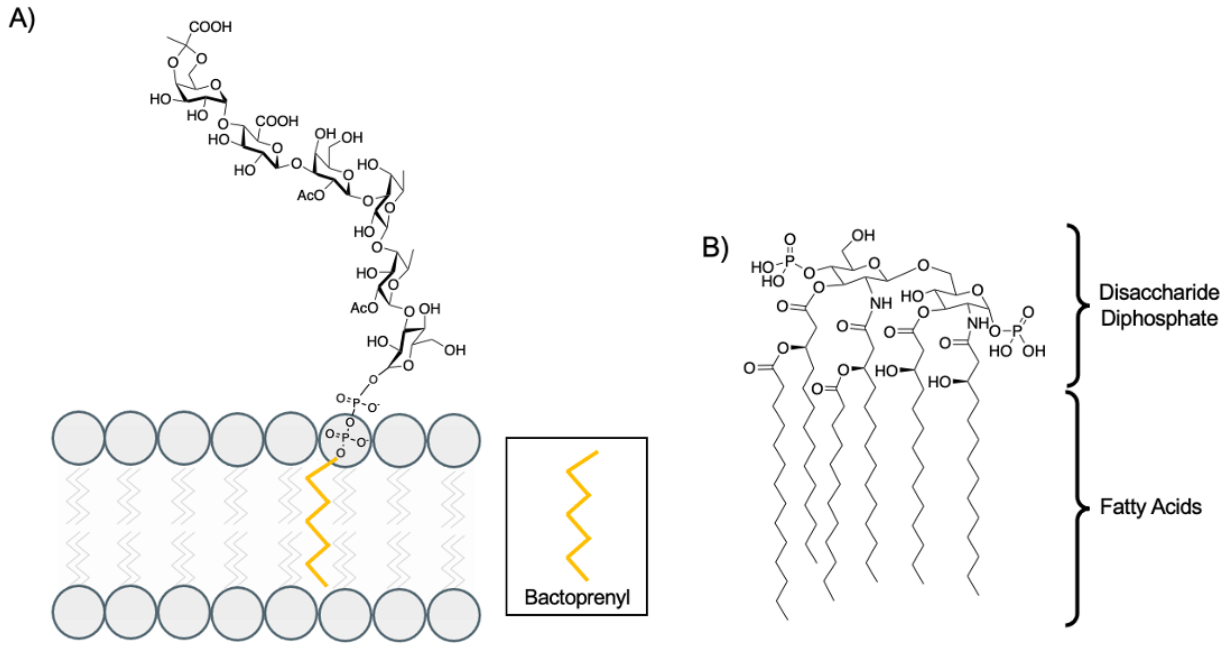

Figure 2: Chemical structures of Colanic acid (**A**) and lipid A (**B**).[1, 2]

1.2: Bacterial Infections and Treatment Options

1.2.1: Bacterial Pathogenicity

Certain strains of bacteria are classified as pathogenic, and therefore capable of causing disease in the infected host. For example, *Campylobacter jejuni* is a Gram-negative species of pathogenic bacteria that infects an estimated 1.5 million people each year in the United States, according to the Center for Disease Control and Prevention.[25, 26] *C. jejuni* causes gastroenteritis and can lead to more severe illnesses such as Guillain-Barré syndrome.[27, 28] Conversely, *Bacteroides fragilis* is also a Gram-negative bacterium, but it is typically nonpathogenic and commensal inside the human colon. *B. fragilis* is a prominent constituent of the human microbiota that supports digestion and can benefit the immune system.[29]

It is a common misconception that all bacteria are harmful, disease-causing germs. As the scientific community learns more about the vast number of bacterial species and how they interact with their environments, more information is illuminating the immense diversity of bacterial species and the uniqueness of various bacterial strains. One of the best examples demonstrating this observation is with *E. coli*, a species so common and versatile that it is frequently used in numerous areas of scientific research.[30, 31] Since the first time the organism was described in 1885, several different strains have been identified.[30] *E. coli* is one of the first bacterial species to inhabit infant colons and usually remains a commensal and nonpathogenic member of the human gut microbiome. Only certain strains of the species are harmful, such as enterohemorrhagic *E. coli* (EHEC), which causes mild to severe diarrhea, and uropathogenic *E. coli* (UPEC), which causes urinary tract infections.[31, 32]

1.2.2: Antibiotic Resistance

Despite the fact that bacteria constitute approximately 90% of the cells in the human body and carry out essential bodily functions, including assisting with digestion, aiding metabolism, and boosting the immune system, they are still often regarded as harmful invaders.[29, 32] Modern medicine is currently struggling with the drastic and concerning rise of antibiotic resistance due to the overuse and misuse of antibiotics. Since 1928, when Sir Alexander Fleming discovered penicillin, people have greatly benefitted from the life-saving aid of antibiotics. However, as with every other organism in nature, natural selection determines which species are better suited for survival. The few strains of bacteria resistant to antibiotics remain unaffected, thrive, and eventually propagate their advantageous genes for resistance (**Figure 3**).[33] As a repercussion of this phenomenon, certain antibiotics are no longer effective against various strains of bacteria.[18]

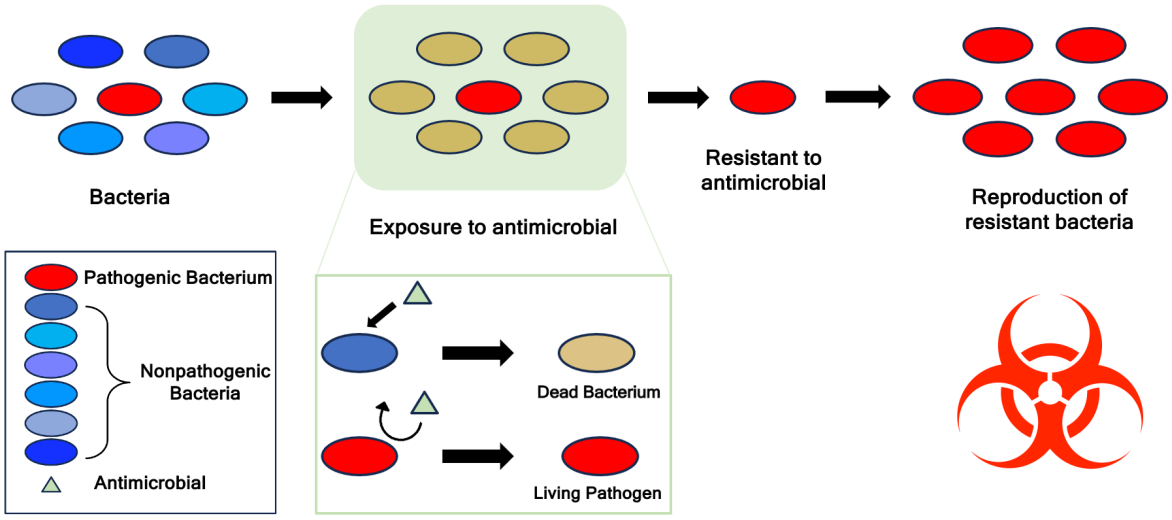

Figure 3: The progression of antibiotic resistance. When bacteria are exposed to an antimicrobial substance, some bacteria remain unaffected and continue living. As resistant pathogens (shown as red ovals) propagate, antimicrobial drugs become less effective over time and the threat of antibiotic resistance increases.

For years, the healthcare industry has misdiagnosed patients and prescribed them with a suite of antibiotics, that may or may not be appropriate for treating the patient's ailment. In fact, studies have shown that the incorrect treatment was given in 30% to 50% of cases.[33] One of the biggest contributing factors to the antibiotic resistance crisis is the use of broad-spectrum antibiotics. Rather than identifying the specific pathogen causing the patient's disease, medical providers often resort to the ease of administering a multitude of different antibiotics simultaneously and hope that something works to resolve the issue. As an unintentional result, however, the likelihood of antibiotic resistance increases, and a myriad of nonpathogenic and commensal bacteria are decimated in the process. In doing so, the human gut microbiome can be drastically altered for years, potentially effecting human health in deleterious ways.[18, 34]

The number of available antibiotics that remain effective is consequentially being outpaced by the number of pathogenic bacterial species, which is exacerbating the need for new and better treatments.[18, 35] There are, however, potentially promising antimicrobial alternatives to broad-spectrum antibiotics that could improve the crisis. These alternatives involve treating infections with microorganism-specific medicines, such as narrow-spectrum antibiotics or antivirulence drugs. Both options treat an infection by selectively targeting the pathogen of interest, as opposed to killing a multitude of different bacteria. Antivirulence drugs work by targeting bacterial virulence factors—products that can either cause harm to the host or evade host immunity. These drugs go after the things that cause disease instead of outright killing the pathogen itself. The major advantage of treating bacterial infections with this approach is that antivirulence drugs do not put as much selective pressure on bacteria for survival and therefore avoid the development of resistance.[35]

The main challenge of using microorganism-specific drugs for treating pathogenic infections is the need for effective diagnostic testing to identify the pathogen.[34] Additionally, specific drugs would need to be developed to selectively target specific bacteria. As one would imagine, this endeavor takes time to research the pathogenicity of each microbe. Furthermore, in order to successfully identify specific pathotypes, there is a significant need for assaying bacterial serotypes, which largely involves studying bacterial glycans. Considering how different strains of bacteria seemingly have unique glycan repertoires, it is paramount that more and better methods are developed to characterize bacterial glycans and fully comprehend the native biosynthesis of these sugar structures.[18, 36]

1.3: Bacterial Glycan Biosynthesis

There is an immense diversity among bacterial species due to the unique composition of sugars that form along the surface of the cell wall.[36, 37] Bacteria are completely covered in polysaccharides that are made up of hundreds to thousands of sugar monomers.[13] Each glycan structure is composed of individual monosaccharide units, that can either be common (e.g., glucose) (**Figure 4A**) or rare sugars (e.g., diNAcBac) (**Figure 4B**), depending on the respective species.[37] And yet, while distinct glycans are produced by various species and strains of bacteria, each glycan shares some commonality. Most bacterial glycans are produced along the surface of the cell, where they elongate sequentially and extend out into the surrounding environment (**Figure 4C**). Additionally, these complex polysaccharide structures are also biosynthesized by similar reactions with similar starting materials or substrates.[5]

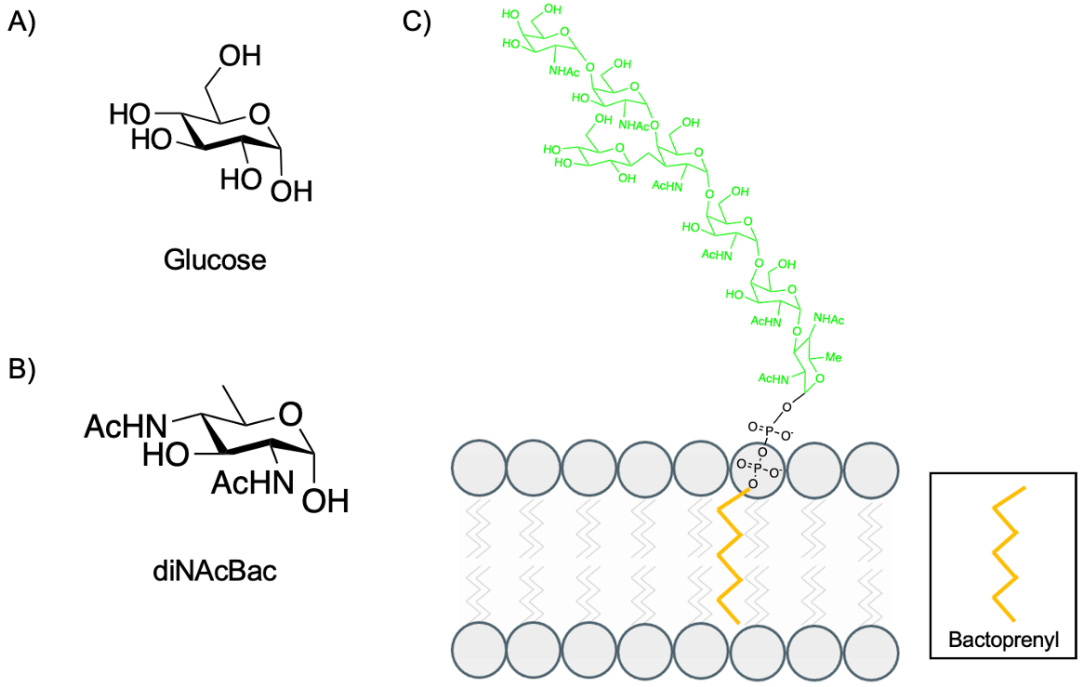

Figure 4: **A**) Glucose is a common sugar, while **B**) diNAcBac is rare. **C**) The chemical structure of a heptasaccharide produced by *C. jejuni*.[3] Bacterial glycans typically consist of an oligosaccharide chain (shown in green) that is attached to the cellular membrane by a lipid anchor (shown in yellow).

Bacterial glycan biosynthesis begins at the inner membrane in Gram-negative bacteria and the cytoplasmic membrane in Gram-positive bacteria (**Figure 5**). There, monosaccharides are sequentially appended to a lipid substrate that anchors the growing glycan structure to the membrane.[22] After the nascent oligosaccharide is fully formed, it is flipped *en bloc* across the membrane to the periplasm. In Gram-positive bacteria, the polysaccharide structure can either extend out of the multiple layers of peptidoglycan and into the extracellular space, or it can be covalently bonded to the surface or become attached to proteins as a glycoconjugate.[18, 38] In Gram-negative bacteria, the glycan is similarly flipped across the inner membrane and translocated to the outer membrane, where it can also become a glycoconjugate and extend outwardly.[38]

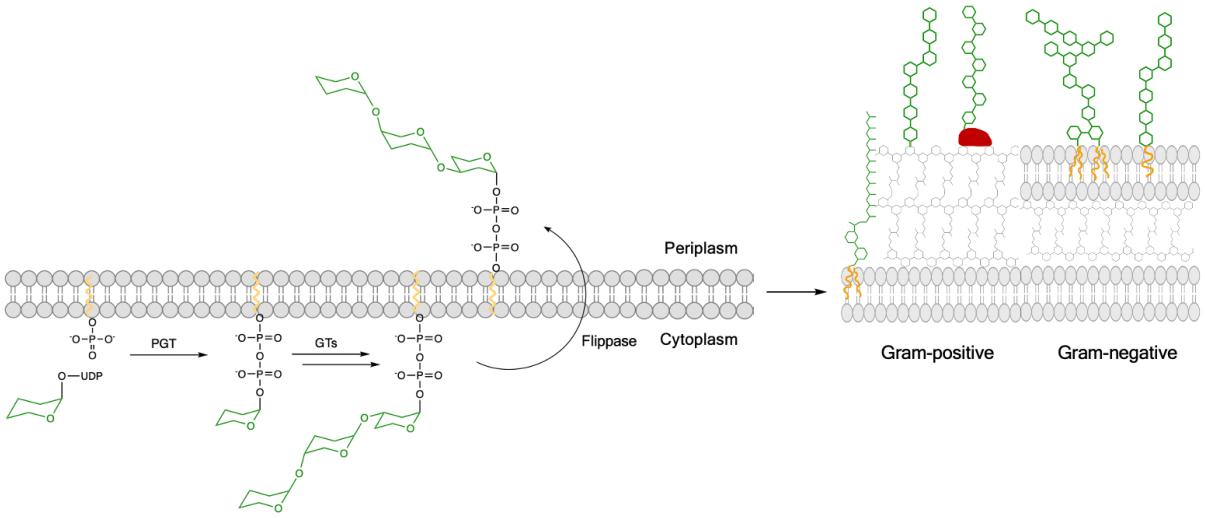

Figure 5: General bacterial glycan biosynthetic pathway. Glycans are assembled in multiple steps by the sequential addition of monosaccharides (shown in green) to a membrane-embedded lipid anchor (shown in yellow). The fully formed oligosaccharides are later flipped from the cytoplasm inside the cell to the periplasm, where the glycans can extend out of the cell.

The lipid substrate generally used by bacteria in glycan biosynthesis is the 55-carbon isoprenoid, bactoprenyl phosphate (BP)—also known as undecaprenyl phosphate (Und-P).[22] BP is a long-chain, linear isoprenoid made up of 11 isoprene units (**Figure 6A**).[11, 39] The biopolymer is composed of 2 isoprene units with the *trans* (E) double-bond configuration and 8 isoprene units with the *cis* (Z) double-bond configuration.[39] BP is synthesized in the cytosol by undecaprenyl pyrophosphate synthase (UppS), which is a soluble prenyltransferase (**Figure 6B**). This type of enzyme is selective for its allylic substrates and only forms products with a specific chain length.[11, 40] UppS polymerizes BP *de novo* by linking 1 molecule of the 15-carbon isoprenoid, farnesyl diphosphate (FPP) to 8 molecules of the 5-carbon isoprenoid, isopentenyl diphosphate (IPP) (**Figure 6B**).[11, 40, 41] Following catalysis with UppS, the resulting precursor, bactoprenyl diphosphate (BPP)—also known as undecaprenyl pyrophosphate (Und-PP)—is dephosphorylated to the monophosphate substrate.[40]

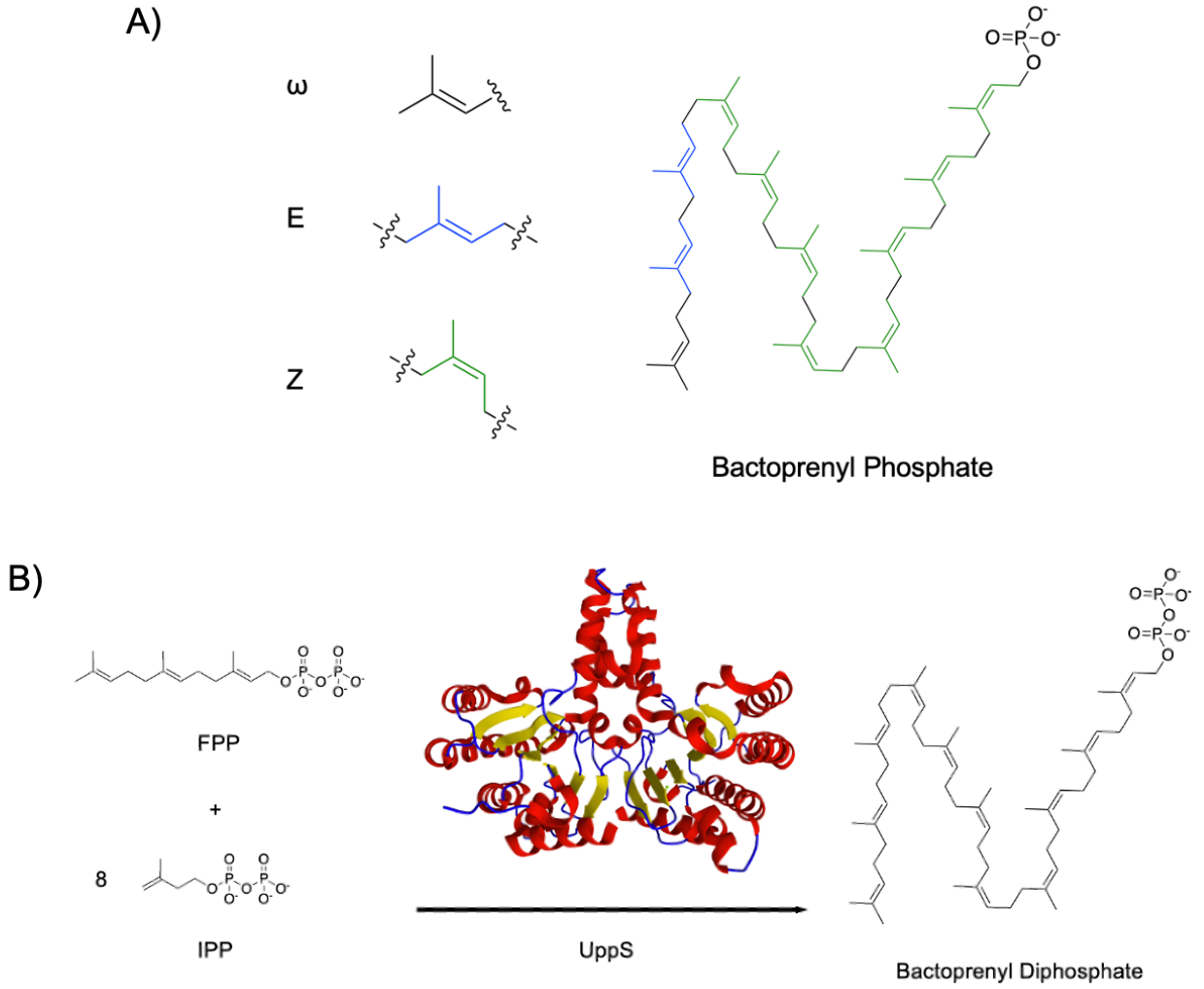

Figure 6: **A**) Bactoprenyl phosphate is composed of 2 isoprene units with *trans* (E) double bonds (shown in blue) and 8 isoprene units with *cis* (Z) double bonds (shown in green). **B**) UppS polymerizes bactoprenyl diphosphate from 1 molecule of farnesyl diphosphate (FPP) and 8 molecules of isoprentenyl diphosphate (IPP).[4] BPP is later converted to the monophosphate in a dephosphorylation reaction not shown.

Once BP is formed, bacterial glycans are biosynthesized through a series of enzymatic reactions with phosphoglycosyltransferases (PGTs), glycosyltransferases (GTs), and additional modifying enzymes (**Figure 5**). The process begins with a PGT appending the first sugar to the membrane-embedded BP substrate. Following this, GT enzymes further elaborate the growing oligosaccharide by sequentially linking additional sugars together. Glycosylation involves GTs

catalyzing the transfer of a monosaccharide from a nucleoside diphosphate-linked sugar glycoside (NDP-sugar) to the oligosaccharide chain.[42] In *E. coli*, for example, the enterobacterial common antigen (ECA) is biosynthesized by the PGT, WecA, and then glycosylated by the GTs, WecG and WecF (**Figure 7**).[5] Lastly, the process ends with the complete polysaccharide being flipped across the membrane to the periplasm by a flippase enzyme.[5, 43] As an essential substrate in the biosynthetic process, BP is recycled and can be reused later for synthesizing additional glycans.[40]

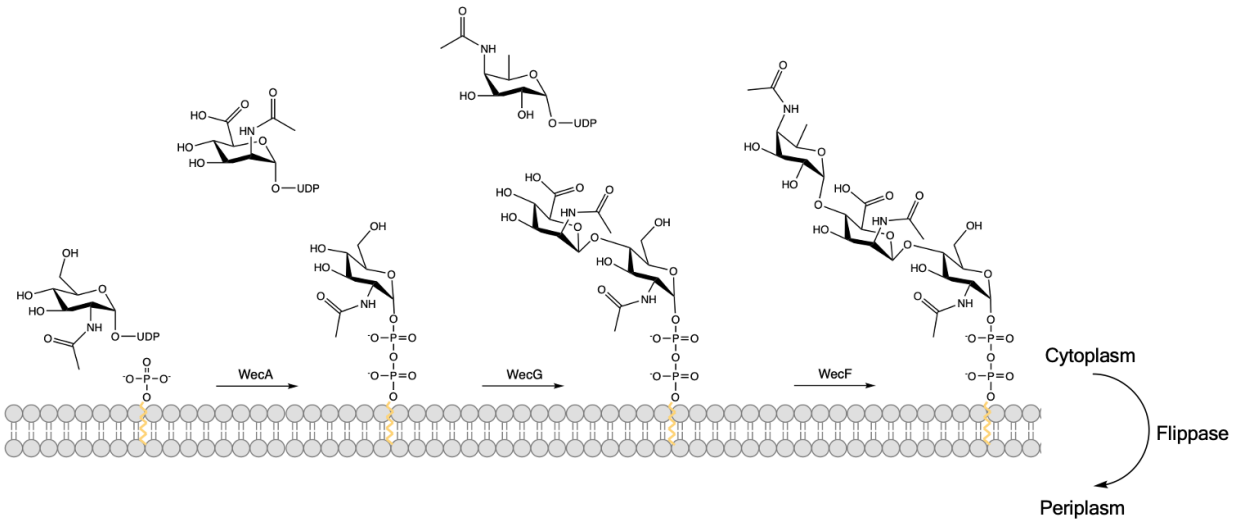

Figure 7: The biosynthesis of the ECA repeat unit in *E. coli*. WecA is a PGT that appends the first sugar to BP (shown in yellow), which is further glycosylated by the GTs, WecG and WecF. Additional enzymes are also involved in making the sugar substrates, but they were omitted for clarity of the overall biosynthetic process.[5]

1.4: Phosphoglycosyltransferases

The first step of bacterial glycan biosynthesis involves a class of enzymes called, phosphoglycosyltransferases (PGTs). These enzymes are often denoted as “initiating” or “priming” GTs, due to their important roles as the first enzymes involved in the multistep biosynthesis of bacterial glycans.[42] In addition to initiating biosynthesis, PGTs also act as the

first committed step in an extensive series of biochemical reactions. Moreover, the identity of the final glycan product is ultimately determined by this first reaction.[36]

As integral membrane proteins, PGTs are embedded in the membrane and are therefore readily accessible to the lipid substrate. In Gram-positive bacteria, PGTs are located along the cytoplasmic face of the membrane.[42] In Gram-negative bacteria, PGTs are similarly located in the inner membrane, and the resulting glycan product is flipped across the membrane to the periplasm.[38, 42] In one classification system, PGTs have been categorized into two distinct superfamilies according to their topology with respect to the membrane—either as monotopic or polytopic. Monotopic PGTs (monoPGTs) are only partially embedded in the membrane: A single part of the protein penetrates through a single leaflet of the phospholipid bilayer (**Figure 8**). PglC and WcfS, for example, are monoPGTs in *C. jejuni* and *B. fragilis*, respectively.[3, 44] Conversely, polytopic PGTs (polyPGTs) cross the entire membrane at multiple points (**Figure 8**).[43] WecA is an example of a polyPGT in *E. coli*.[45]

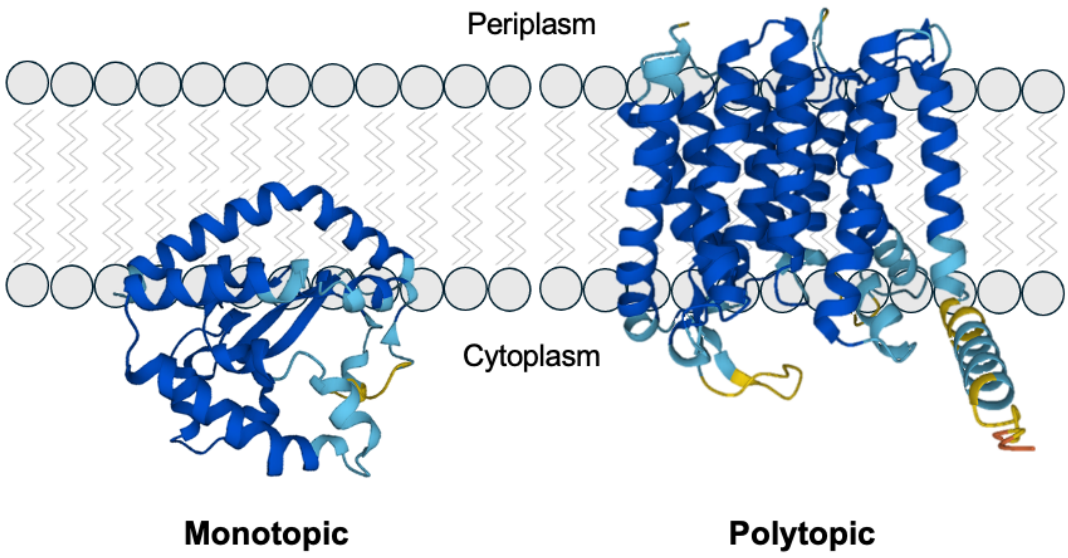

Figure 8: Predicted structures and membrane topologies of the monotopic PGT, WcfS and polytopic PGT, WecA. The protein structures were generated using AlphaFold.[6, 7]

PGTs have also been categorized in an older classification system that groups the different enzymes according to their substrate preferences and the microorganisms that express them. In this system, PGTs are also divided into two broad superfamilies based on sequence homology and function.[42] Polyisoprenol-phosphate hexose-1-phosphate transferases (PHPTs) are PGTs only found in bacteria, whereas polyisoprenol-phosphate N-acetylaminosugar-1-phosphate transferases (PNPTs) occur in prokaryotes and eukaryotes.[42, 46] As the names imply, PHPTs append hexose-1-phosphate sugars (e.g., glucose) to the substrate, while PNPTs append HexNAc phosphosugars (e.g., N-acetylglucosamine). Cps2E in *Streptococcus pneumoniae* is a PHPT that appends glucose (**Figure 9A**), whereas PglC, WcfS, and WecA (**Figure 9B**), are all PNPTs that append diNAcBac (2,4-diacetamido-2,4,6-trideoxyglucose), AADGal (acetamido-4-amino-6-deoxygalactopyranose), and GlcNAc (*N*-acetylglucosamine), respectively.[3, 44, 45, 47]

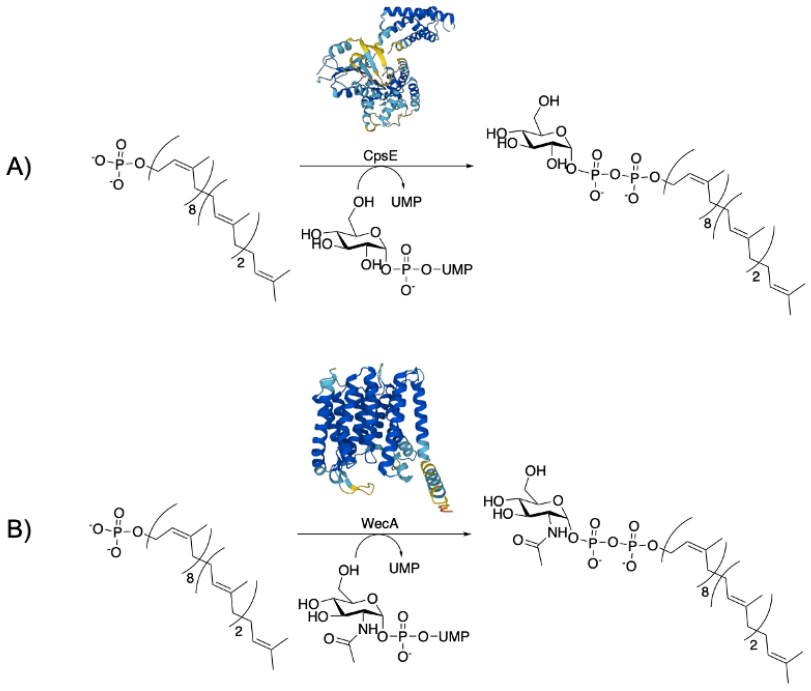

Figure 9: **A**) Cps2E is a PNPT that catalyzes the transfer of glucose to BP. **B**) WecA is a PHPT that appends GlcNAc to BP. The protein structures were generated using AlphaFold.[6, 7]

The catalytic function of polyPGTs in bacteria is best exemplified by WecA, which is involved in the biosynthesis of O-antigen LPS and EPS in multiple enterobacterial species.[45] PolyPGTs are understood to form a ternary complex with a conserved Asp-Asp-Xaa-Xaa-Asp motif.[10] In comparison to polyPGTs, the structure and function of monoPGTs are considerably less understood.[48] However, PglC is often used as a model monoPGT, considering it is the most extensively studied monoPGT, and it is the first and only monoPGT with a high-resolution X-ray crystal structure that was experimentally determined in 2018 (**Figure 10**).[49] The enzyme has a dual domain architecture, comprised of a soluble C-terminal domain and a membrane-embedded N-terminal domain.[48] The former is globular and contains approximately 180 residues, while the latter is a single reentrant membrane helix and contains approximately 20 residues.[48, 50]

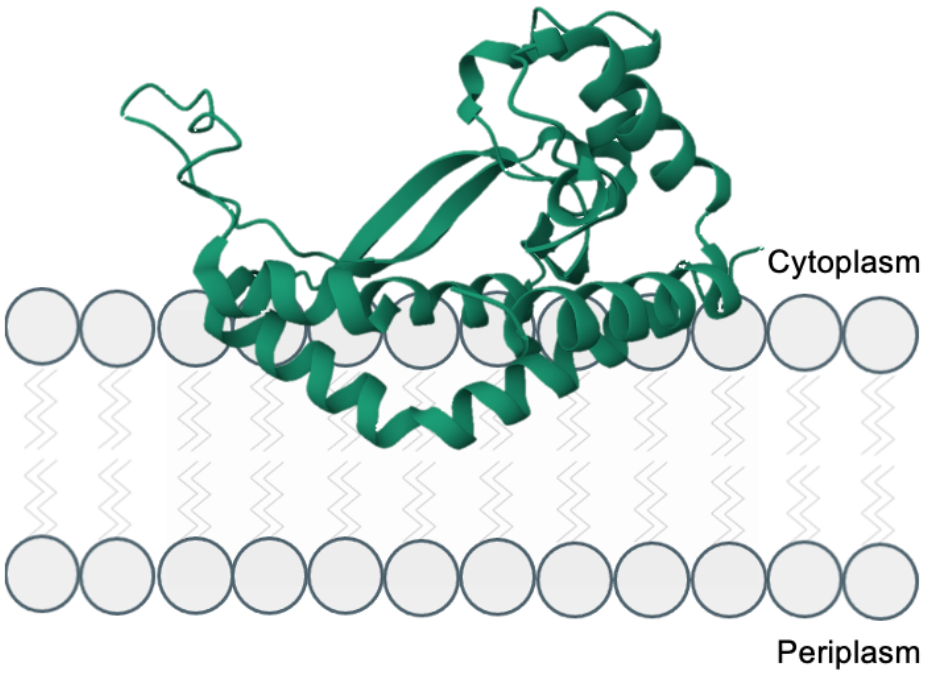

Figure 10: PglC crystal structure.[8] PglC is a monoPGT with a membrane-embedded N-terminal domain and a soluble C-terminal domain that protrudes into the cytoplasm.

PglC is encoded by the *pgl* gene cluster, which was revealed to carry out N-linked glycosylation in the bacterial domain. *C. jejuni* has a general N-linked glycosylation pathway, in which a preassembled heptasaccharide (GalNAc-α1,4-GalNAc-α1,4-(Glcβ1,3)-GalNAc-α1,4-GalNAc-α1,4-GalNAc-α1,3-Bac-α1-PP-Und; where Bac is 2,4-diacetamido-2,4,6-trideoxyglucose) is transferred *en bloc* from a bactoprenyl pyrophosphate-linked donor to a protein acceptor (**Figure 11**).[3] The highly conserved active site has an Asp-Glu dyad that has been proposed to perform a Bi-Bi ping-pong mechanism.[10, 43] Catalysis by this enzymatic mechanism occurs in two main steps: A phosphosugar-enzyme intermediate is formed, which is subsequently followed by the transfer of the phosphosugar donor to a polyprenyl phosphate acceptor (**Figure 12**).[50]

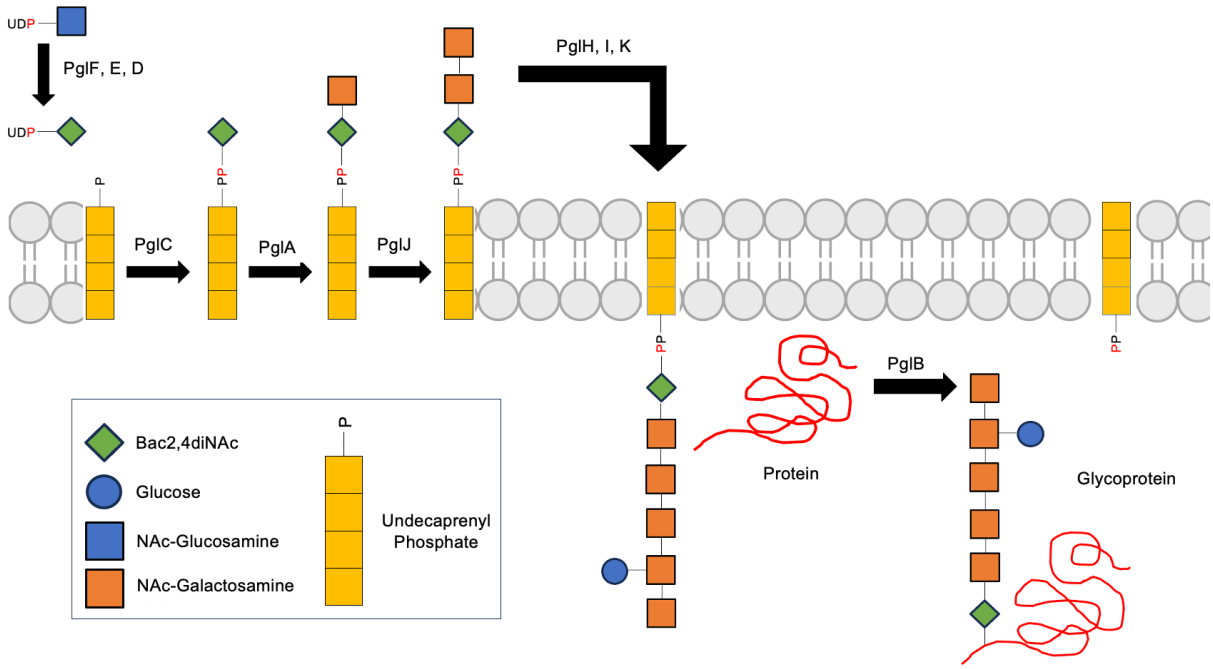

Figure 11: *C. jejuni* N-linked glycosylation pathway (adapted from Chen, M. M., et al.).[9]

In the first reaction, the nucleoside diphosphate-linked sugar glycoside (NDP-sugar) enters the active site and forms a covalent enzyme-substrate intermediate; the nucleophilic aspartic acid (Asp93) attacks the α-phosphate on the NDP-sugar, and the NMP byproduct is released.[10, 42, 48] Second, the covalent adduct undergoes nucleophilic attack by the membrane-embedded prenyl-phosphate substrate (Pren-P/Und-P), which results in the phosphosugar moiety being transferred to the Pren-P substrate.[43, 48] Within the active site, a resident Mg^{2+} cofactor is believed to coordinate with the diphosphate group, orient the substrate for catalysis, neutralize electrostatic repulsion between the phosphate and acidic residues, and activate the NDP-sugar by increasing the nucleophilicity of the α-phosphate.[48]

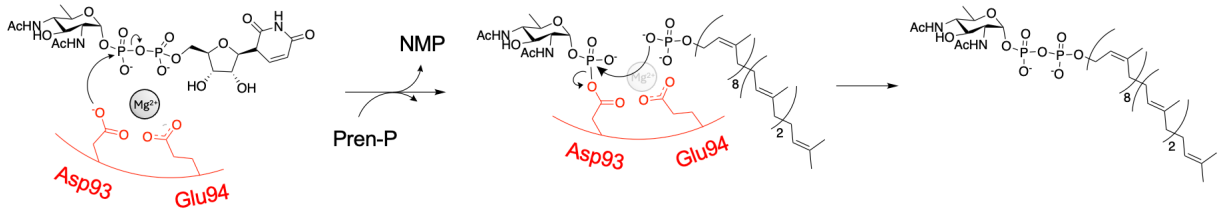

Figure 12: Proposed catalytic mechanism of PglC with an Asp-Glu dyad forming the active site shown in red (adapted from Anderson, A. J., et al.).[10]

While the protein structure and catalytic function of PglC is gradually becoming elucidated, there is still a significant lack of information regarding the other monoPGTs. Unfortunately, monoPGTs are challenging to study due to their being membrane proteins. Despite representing between 20-30% of the proteome in most organisms, membrane proteins have gained notoriety for being extremely difficult to study. These proteins are hydrophobic and are often unstable and flexible, which leads to numerous experimental challenges.[51] Since membrane proteins are embedded in the cellular membrane, the hydrophobic interactions with the lipid bilayer have to be disrupted using amphipathic detergents. However, treatment with

detergent may cause the proteins to aggregate and precipitate out of solution, and they could potentially distort the protein structure and function.[10] Additional challenges include low expression levels and issues with purification and crystallization.[10, 51]

There continues to be a severe lack of information regarding the structure and function of PGTs and their biosynthetic roles in bacterial glycan bioassembly.[10] Relying solely or predominantly on protein sequence and homology between similar species greatly limits our understanding of these important enzymes.[22] In order to overcome this gap in knowledge, more and better analytical methods are needed. One alternative technique that could potentially resolve these concerns involves probing the catalytic activity of PGTs without fully characterizing the protein structure beforehand. This approach would circumvent the painstaking challenges of characterization methods reliant on X-ray crystallography, while also gleaning necessary information about the biosynthetic function of these important enzymes.

1.5: Enzyme Probes

1.5.1: Enzyme Probe Development

Following the successful completion of the Human Genome Project (HGP) in April 2003, subsequent questions and research ventures arose, in an attempt to contextualize the new information and expand upon it.[52] With the central dogma of molecular biology in mind, the HGP sparked a curiosity in understanding the expansive correlations between genomics and proteomics. Over time, it became evident that proteins play a crucial role in biological systems, and those roles can have a significant impact on human health. This point is possibly best exemplified by the discovery that genetic mutations and the post-translational modification of certain proteins have been linked to various diseases, including cancer.[53, 54] For this reason, there

has been a considerable level of interest in studying proteins—especially for drug discovery and development—and uncovering the relationship between protein structures and their coinciding functions.[55, 56]

Over the past couple of decades, the scientific research community has become more concerned with identifying proteins and discovering ways to characterize them using novel techniques and tools. Most of these techniques involve probing proteins of interest with purposely designed synthetic chemicals to evaluate the reactivity of proteins with specific substrates. Chemical probes are usually designed as small-molecule reagents that react with a protein and modulate its function in a particular way. By design, the chemical reactivity of the probe is already known, so characterizing the product of the reaction can then be used to determine the phenotypic structure and mechanistic function of the protein.[56]

Different probes have been developed for different applications, and the construction of each is largely dependent on the intended purpose. Some prevalent examples include activity-, affinity-, and substrate-based probes.[57, 58] Activity-based probes, for example, share a similar design that is comprised of three main components: a recognition group, a linker chain, and a reporter tag (**Figure 13**).[55, 58] The recognition group is responsible for binding the probe to the enzyme and consists of a functional group that reacts with the enzyme's active site residue(s). Connected to the recognition group is the linker, which is often a mimetic substrate (e.g., an alkyl chain or peptide sequence) that functions simultaneously to connect and separate the reactive recognition group and the reporter tag.[58-60] Upon binding to the enzyme, the enzyme-probe complex can be detected and purified with the incorporation of a reporter molecule, such as a fluorophore, radioisotope label, antibody, or an additional biomolecule (e.g., biotin).[58, 61]

Enzyme probes have proven to be instrumental in garnering crucial information regarding proteins of interest, and depending on their design, they can be tuned for diverse applications.

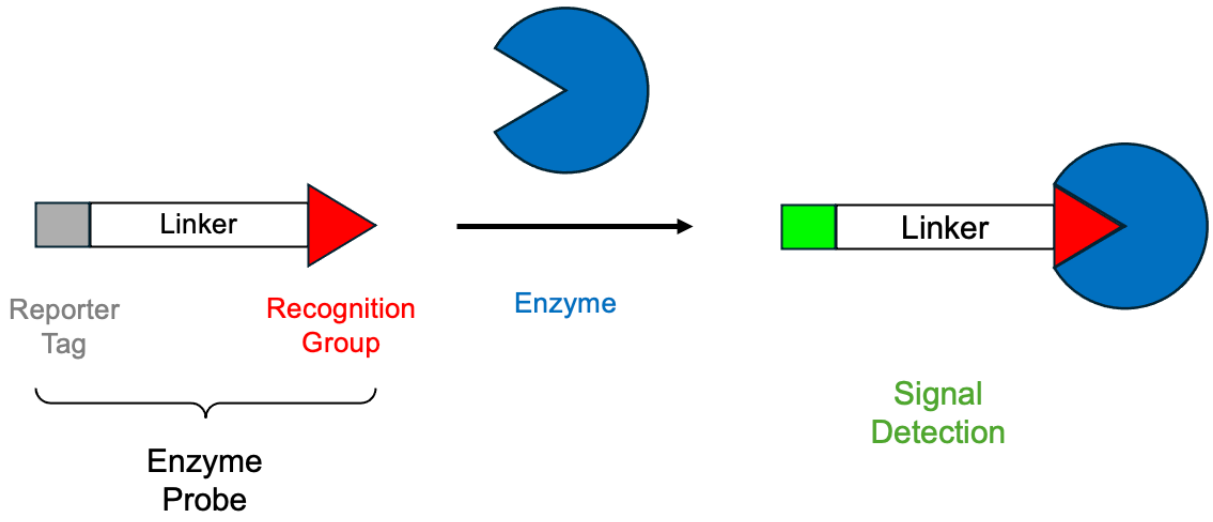

Figure 13: The general schematic of an activity-based enzyme probe. After the probe binds to the enzyme (shown in blue), a signal can be detected from the reporter tag (shown in green).

1.5.2: Isoprenoid Analogues and Prenyltransferases

Isoprenoids are suitable scaffolds for building enzyme probes, considering they are the most abundant and structurally diverse natural products found in all domains of life.[62] These hydrocarbon analogues are composed of a 5-carbon building block called an isoprene unit, which defines the overall chemical structure (**Figure 14A**).[63] Isoprenoids are part of a broad class of compounds that are universally derived from the precursors, isopentenyl diphosphate (IPP) and its isomer, dimethylallyl diphosphate (DMAPP).[63, 64] Prior to 1993, the mevalonate pathway was the only know source of isoprenoids in eukaryotes and some Gram-positive prokaryotes, and it remains the most studied IPP biosynthetic pathway. Through the mevalonate pathway, IPP is

biosynthesized in multiple steps by converting acetyl-CoA to mevalonate, which undergoes additional steps to form IPP.[64]

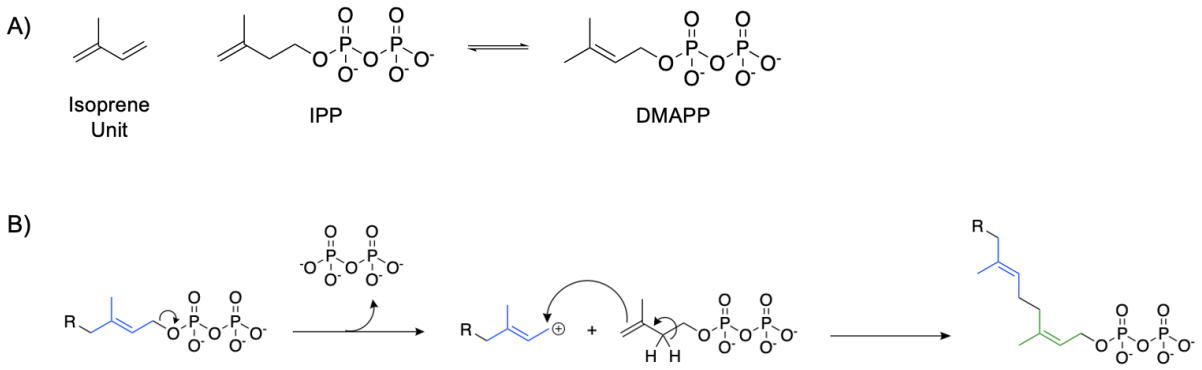

Figure 14: **A**) An isoprene unit for comparison to the isoprenoid precursors, isopentenyl diphosphate (IPP) and dimethylallyl diphosphate (DMAPP). **B**) A proposed head-to-tail elongation mechanism catalyzed by prenyltransferases in the synthesis of isoprenoids.[11]

Following the synthesis of IPP and DMAPP, isoprenoids are elongated by enzymes called, isoprenyl diphosphate synthases (IPPS)—also commonly referred to as prenyltransferases. These enzymes catalyze the sequential 1'-4, head-to-tail condensations of IPP with an allylic diphosphate, and they are classified according to their product's chain length and double bond stereochemistry (**Figure 14B**).[62, 64, 65] The known *cis*-prenyltransferases mostly synthesize products with longer chains that have *cis* (Z) double bonds, while *trans*-prenyltransferases generally form products with up to 50 carbons that have *trans* (E) double bonds.[62] The latter group is further classified according to the chain length of the final products: short- (C_{10}-C_{25}), medium- (C_{30}-C_{35}), and long-chain (C_{40}-C_{50}).[62, 65] Three of the most prevalent short-chain isoprenoids and their respective prenyltransferases are the 10-carbon geranyl diphosphate (GPP), the 15-carbon farnesyl diphosphate (FPP), and the 20-carbon geranylgeranyl

diphosphate (GGPP), which are synthesized by GPP synthase (GPPS), FPP synthase (FPPS), and GGPP synthase (GGPPS) respectively (**Figure 15**).[62, 64]

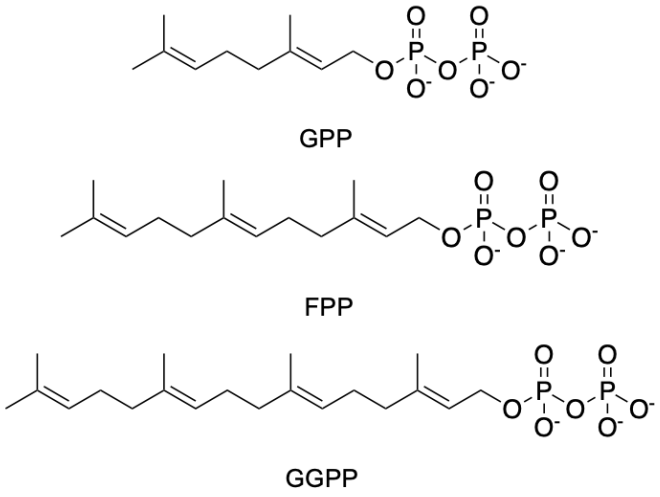

Figure 15: The short-chain isoprenoids, geranyl diphosphate (GPP), farnesyl diphosphate (FPP), and geranylgeranyl diphosphate (GGPP).

Isoprenoids became a major focus in biochemical research during the late 1970s and early 1980s, when it was discovered that these lipids can modify polypeptides through a process called protein prenylation.[63, 66] After polypeptides are synthesized, they can undergo post-translational modifications, which involves covalently attaching modifying groups, such as phosphoryl, glycosyl, and prenyl groups to polypeptides.[67, 68] Protein prenylation occurs when a farnesyl group from FPP or a geranylgeranyl group from GGPP are linked to a cysteine residue on a protein substrate by a thioester linkage.[69] These findings were especially important because modified proteins are structurally different than their unmodified counterparts and therefore serve different biochemical and cellular functions.

Prenylated proteins are ubiquitous in eukaryotic cells and are important for maintaining proper cellular activity.[66] For example, Ras is a G protein that participates in signal transduction

pathways that control cell growth and differentiation; the prenylation of Ras is necessary for membrane localization and cellular transformation.[63, 70] Protein prenylation gained a significant level of interest when it was discovered that mutated forms of Ras are oncogenic and were detected in 30% of all human cancers.[69] Addition interest went into studying the prenyltransferases, farnesyltransferase (FTase) and geranylgeranyltransferase type I (GGTase-I), since they were found to be responsible for the first, obligatory step in protein prenylation.[70] In learning this, various chemicals were synthesized to probe prenyltransferases with the intention of inhibiting them. The purpose of doing so was to develop chemicals that could prevent the post-translational modification of Ras and therefore act as potential cancer chemotherapies.[69, 70]

1.5.3: Probing Bacterial Glycan Biosynthesis

In bacteria, glycans are vital cellular structures that are conjugated to the 55-carbon lipid anchor, BP.[22] This long-chain isoprenoid is biosynthesized by the *cis*-prenyltransferase, UppS, through the consecutive condensation of FPP with 8 IPP precursor molecules. Considering the important roles that BP and UppS play in bacterial glycan biosynthesis, both biomolecules are attractive targets for the rational design of antibacterial drugs.[71] Similarly to the relationship between the aforementioned Ras protein and FTase, various chemicals have been developed to probe the production of BP by UppS with the intention of inhibiting bacterial glycan biosynthesis.

One of the biggest challenges with studying bacterial polysaccharides is the lack of established chemical tools for studying the complex process. This predicament is largely due to the lack of chemical handles or chromophores in either the oligosaccharides or the bactoprenyl substrate.[72] Additionally, the native bactoprenol—with 2 *trans* (E) and 8 *cis* (Z) geometry—is

relatively difficult to procure (**Figure 16**).[2, 39, 72] And while undecaprenol is commercially available, the non-native compound is isolated from a plant source (i.e., *Magnolia kobus*), and the stereochemistry is different: 3 *trans* (E), 7 *cis* (Z) (**Figure 16**).[72-74] Multiple methods have been proposed to mitigate these challenges, including one in which the oligosaccharide is hydrolyzed from its isoprenoid substrate, and the free sugar structure is labeled with a fluorescent moiety.[75, 76] However, an alternative method by the Troutman Group has shown to be effective at probing UppS and tracking glycan biosynthesis without disrupting the natural bioassembly process.[75]

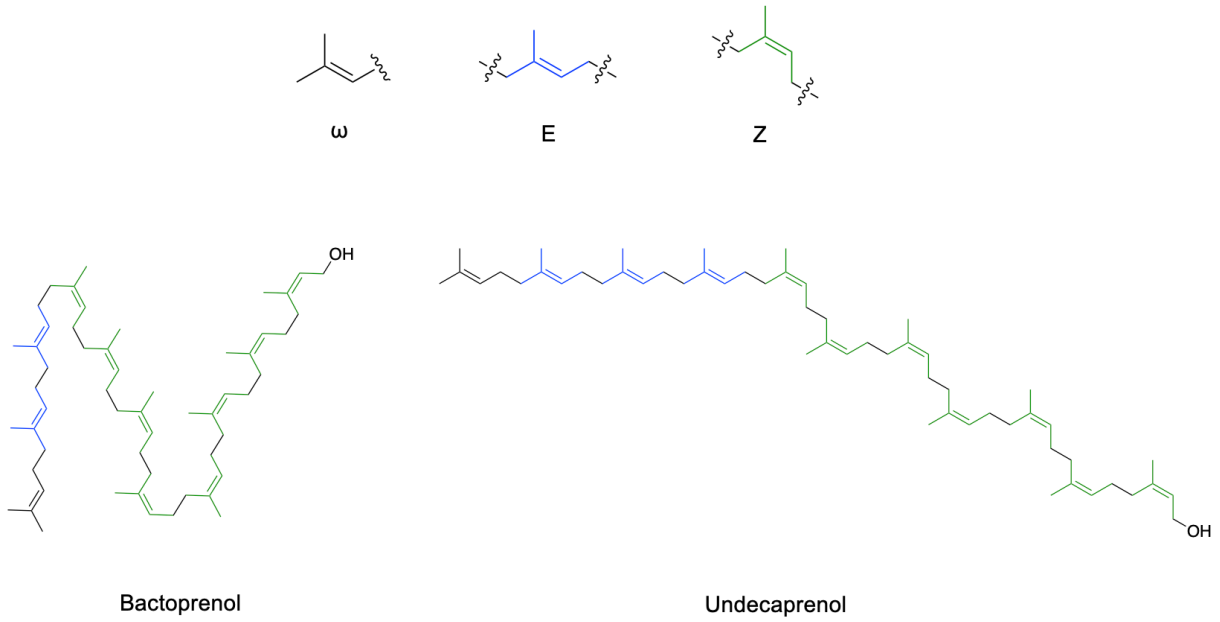

Figure 16: Structural comparison of bactoprenol and undecaprenol. Individual isoprene units are color coded according to their double bond geometry: *trans* (E) double bonds are shown in blue and *cis* (Z) double bonds are shown in green.

The Troutman Group developed a set of fluorescently labeled FPP analogues that can react with UppS to incorporate a fluorescent tag directly into the bactoprenyl substrate.[75] Two examples of these fluorescent probes include 2-amideanilinogeranyl diphosphate (2AA-GPP)

and 2-nitrileanilinogeranyl diphosphate (2CNA-GPP), which respectively have an anthranilamide and nitrile at the terminal end of the farnesyl analogue (**Figure 17**).[41] The diphosphate head of the FPP analogue is coordinated to polar residues in the binding site of UppS, where IPP is in close proximity. As UppS elongates the isoprenoid chain, the farnesyl end gradually travels through what is believed to be a hydrophobic tunnel in each monomer of the homodimer.[41, 75] The final product is eventually released from the prenyltransferase once the growing chain reaches a length-determining helical floor.[75]

A major advantage of tagging the isoprenoid substrate in these enzyme probes is the ability to assay their optical activity throughout the chemoenzymatic reactions and determine whether they are accepted by UppS.[77] It was found that 2CNA-GPP displayed an increase in fluorescent upon elongation with UppS from three different species (i.e., *Bacteroides fragilis*, *Vibrio vulnificus*, and *Escherichia coli*), while 2AA-GPP only worked with $UppS_{Bf}$. These results were rather surprising, since all three UppS enzymes fulfil the same biological function, but only one species accepted 2AA-GPP as an alternative substrate.[41] Based on the results of this study, it is reasonable to conclude that regardless of structural homology, certain enzymes from different species might have unique substrate specificities.

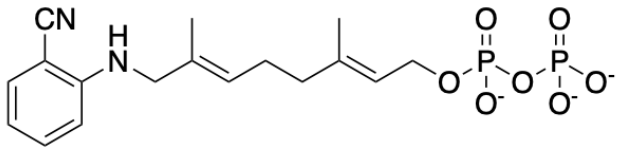

2CNA-GPP

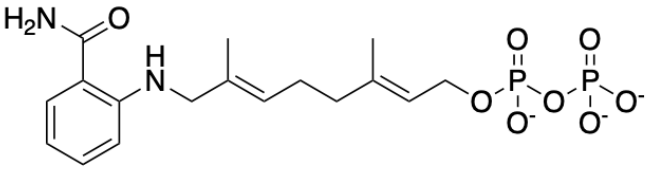

2AA-GPP

Figure 17: UppS probes developed by the Troutman Group. These farnesyl analogues contain an anthranilamide (in 2CNA-GPP) and nitrile (in 2AA-GPP) at the terminal end of the molecule—on the opposite side of the diphosphate.

1.5.4: PGT Probes

PGTs are an important class of integral membrane proteins that function by initiating the multistep bioassembly of bacterial glycans and serve as the first committed step in the overall biosynthetic process.[42] Despite the crucial roles these enzymes play, there is still a significant lack of information regarding their unique structures and functions in different species of bacteria. Currently, monoPGTs are often characterized based on their sequence similarities and structural homologies to the prototypic model PGT, PglC, from the Gram-negative enteropathogen, *C. jejuni*.[49] It is imperative that more tools are developed to study the different PGT variants and elucidate any mechanistic differences among various species of bacteria.

In order to garner more information about an enzyme's catalytic activity, it is necessary to identify what the enzyme can and cannot accept as substrates.[72, 75] An effective strategy for rapidly acquiring this kind of information is by building directed libraries of substrate analogues.[78] This strategy involves synthesizing a series of molecules with closely related

structures that feature slightly different functionalities. The purpose of the library is to explore the reactivity of multiple compounds with an enzyme target and explore the subtle effects of their focused chemical diversity.[41, 78] Previous work with prenyltransferases—including FTase and UppS—utilized directed libraries of FPP analogues to determine which alternative substrates could be acceptable for their respective enzyme targets.[75, 79] The same logic can be applied to PGTs as a method for studying their substrate specificities and catalytic activity in the biosynthesis of bacterial glycans.

While BP is the native substrate generally used by bacteria for biosynthesizing glycans, the long-chain isoprenoid would not act as an ideal scaffold for developing PGT probes. The 55-carbon chain is difficult to work with experimentally because it is very hydrophobic and readily adsorbs to glassware. Conversely, short-chain prenyl phosphates are amphiphilic and mitigate these experimental challenges by being water soluble.[42] Short-chain prenyl phosphates, such as farnesyl phosphate, geranyl phosphate, and neryl phosphate have been utilized previously in the development of other enzyme probes (**Figure 18**). These compounds are also attractive reagents because they can be purchased or synthesized from commercially available starting materials that are generally affordable.

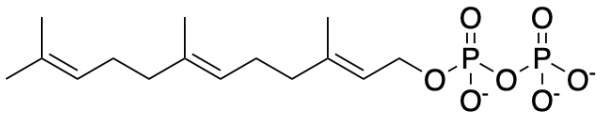

FPP

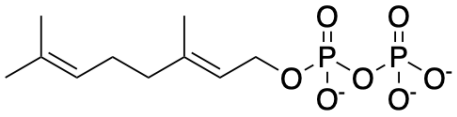

GPP

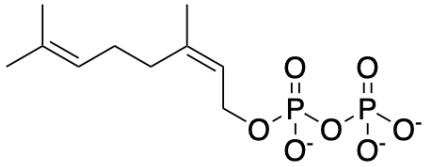

NPP

Figure 18: The short-chain prenyl phosphates, farnesyl diphosphate (FPP), geranyl diphosphate (GPP), and neryl diphosphate (NPP).

Previous studies have been published using short-chain isoprenoid analogues, but their efficacy as scaffolds for PGT probes remains inconclusive. For example, the Troutman Group reported that a 2-aminobenzamide probe using geranyl phosphate and neryl phosphate (i.e., 2AB-G-P and 2AB-N-P) did not work as substrates for WcfS and suggested that longer chain isoprenoids were necessary.[75] However, the Imperiali Group performed multiple kinetic analyses using a panel of isoprenoid substrates that varied in length, saturation, and double bond geometry with multiple enzymes, including PglC, and found that the length of the isoprenoid chain had seemingly little effect on catalytic turnover.[9] It is reasonable to conclude from both studies that various enzymes demonstrate differences in substrate specificities and additional tests with alternative PGT substrates would be greatly informative.

1.5.5: PGT Probe Design

When designing an enzyme probe, it is imperative to consider the effect of substrate complementarity: An enzyme is more likely to accept alternative substrates that closely resemble its native substrate.[66] The Imperiali analyses demonstrated that polyisoprenyl phosphates serve more important roles in bacterial glycan biosynthesis beyond simply acting as physical membrane anchors. They found that the isoprenoid saturation and double bond geometry were significant features that affected the catalytic turnover of three Pgl enzymes: PglC, PglJ, and PglB. These three enzymes exhibited a preference for isoprenoid substrates with *cis* (Z) double bond geometry and α-unsaturatation.[9]

Linear poylprenols are conventionally named using Greek letters to designate the location of specific isoprene units spanning a polyisoprenyl chain. In a polyprenyl phosphate, for example, the isoprene adjacent to the phosphate is designated α, while the terminal isoprene on the opposite side of the chain is ω (**Figure 19**).[70, 74] The native BP contains only unsaturated double bonds, and the α-isoprene is in the *cis* (Z) configuration.[39, 74] Of the short-chain prenyl phosphates previously described for the development of PGT probes, allylic neryl phosphate displays the most comparable double bond geometry as BP. The small molecule is composed of two isoprene units: one terminal ω-isoprene linked to a second *cis* (Z) α-isoprene (**Figure 20**). Due to its similar α-isoprene configuration as BP, neryl phosphate could act as a mimetic short-chain scaffold for building PGT probes.[80]

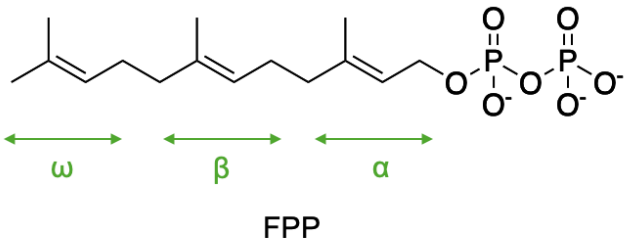

Figure 19: Farnesyl diphosphate (FPP) with its individual isoprene units labeled according to the linear polyprenol Greek nomenclature.

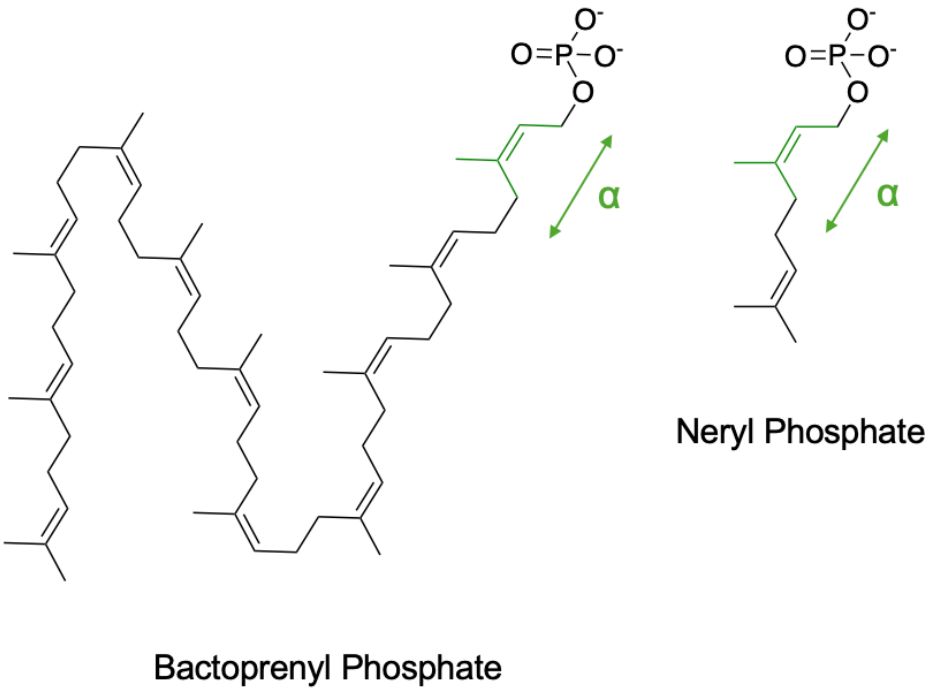

Figure 20: A structural comparison of the α-isoprene (shown in green) in native bactoprenyl phosphate and neryl phosphate. Both molecules have an α-isoprene in the *cis* (Z) configuration.

A considerable amount of information can be gleaned from the decades' worth of research published on the topic of prenyltransferases—namely FTase—and the sizable library of FPP analogues that were chemically synthesized for probing these enzymes. Multiple studies were conducted to systematically determine how subtle changes in the isoprenoid structures of FPP analogues might influence their reactivity and competitiveness with FTase. Some

noteworthy characteristics focused on in these studies were the effects of isoprenoid length, as well as the size and shape of the ω-terminus.[70] This work led to a particularly insightful discovery that the terminal isoprene is isosteric with aryl substituents and ultimately resulted in the synthesis of an array of FPP analogues with aromatic moieties.[79, 81]

A prime example of an ω-arylated FPP analogue is 8-anilinogeranyl diphosphate (AGPP) (**Figure 21**). This compound consists of a 10-carbon GPP chain with an aniline group replacing the ω-isoprene moiety; the two components combine to form an isoprenoid approximately the same size as the 15-carbon FPP.[70, 71] The aniline group in AGPP is a significant isostere because it can serve as a convenient platform for incorporating numerous functional groups into the FPP chain—including fluorophores or additional aromatic groups.[79] However, there are some limitations to this type of modification. It was found that the size of certain substituents and their position on the aniline ring altered the reactivity of FPP analogues.[70] Additionally, although multiple ω-arylated FPP analogues were tested, the extent of isosterism with subsequent arylation was not fully investigated. Moreover, it remains inconclusive whether analogues are functional when additional isoprene units within a polyisoprenyl chain are replaced by consecutive aromatic groups.

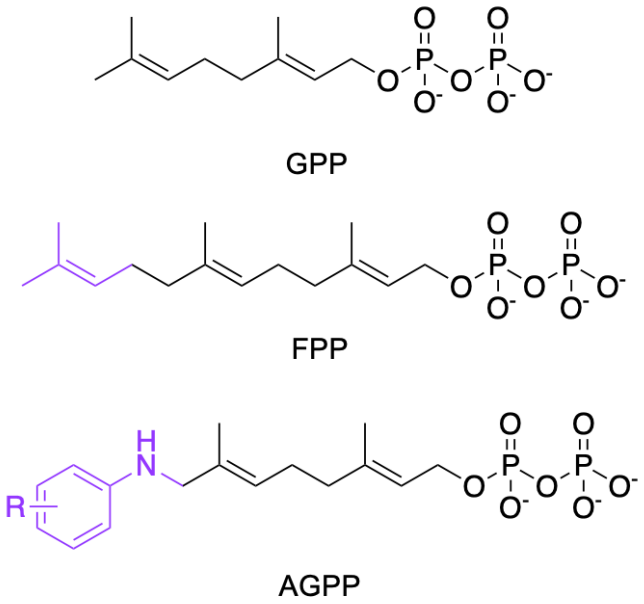

Figure 21: The chemical structure of 8-anilinogeranyl diphosphate (AGPP) compared to Farnesyl diphosphate (FPP) and geranyl diphosphate (GPP). The aniline on AGPP and the terminal isoprene in FPP are shown in purple to demonstrate the isosteric relationship.

In the context of PGTs and bacterial glycan biosynthesis, there is still a considerable gap in knowledge regarding the structural requirements of isoprenoid substrates and how these enzymes select for their substrates. While certain aspects are relatively well known, such as the functionality of the monophosphate with residues in the active site, other structural details concerning the lipid substrate are unknown. To further elucidate the substrate specificities of PGTs, it would be beneficial to design a set of isoprenoid analogues to probe the interactions between alternative lipid substrates with PGTs. One approach to this endeavor would be to utilize the structural characteristics of the isoprenoid analogues described above as references for designing novel PGT enzyme probes.

Considering how PGTs catalyze the transfer of a phosphosugar moiety to a monophosphorylated lipid substrate, synthetic PGT probes would also need to contain a monophosphate at the reactive end of the analogue. Based on the Imperiali analyses, an

unsaturated short-chain prenyl phosphate with a *cis* (Z) α-isoprene—such as neryl monophosphate—could act as a suitable scaffold for the probe. Additionally, the information acquired from FTase concerning the isosteric relationship between aromatic groups and isoprene units may be applicable to PGTs as well. An aryl group—such as the aniline in AGPP—could be included at the ω-terminus to incorporate select functionality into the probe (**Figure 22A**).

Using the AGPP analogues as a reference, the size of bulky aromatic groups and their position on the aniline ring could impact PGT activity, which might be a useful indicator of substrate specificity. To test the effects of substrate size, a set of anilinoneryl monophosphate analogues could be synthesized that feature a selection of aromatic groups with varying levels of bulkiness incorporated at the ω-terminus (**Figure 22B**). The bulky groups include: naphthylamine, an *ortho*-fused ring system; aminobiphenyl, two rings connected by a single bond; and benzylaniline, two rings separated by a methylene. In addition to size, the stereochemical arrangement of these groups may impact reactivity as well. Therefore, alternating the position of the second ring at the *ortho*-, *meta*-, and *para*- positions on the aniline could be useful to analyze the potential impact of steric hinderance between the analogue and the PGT.

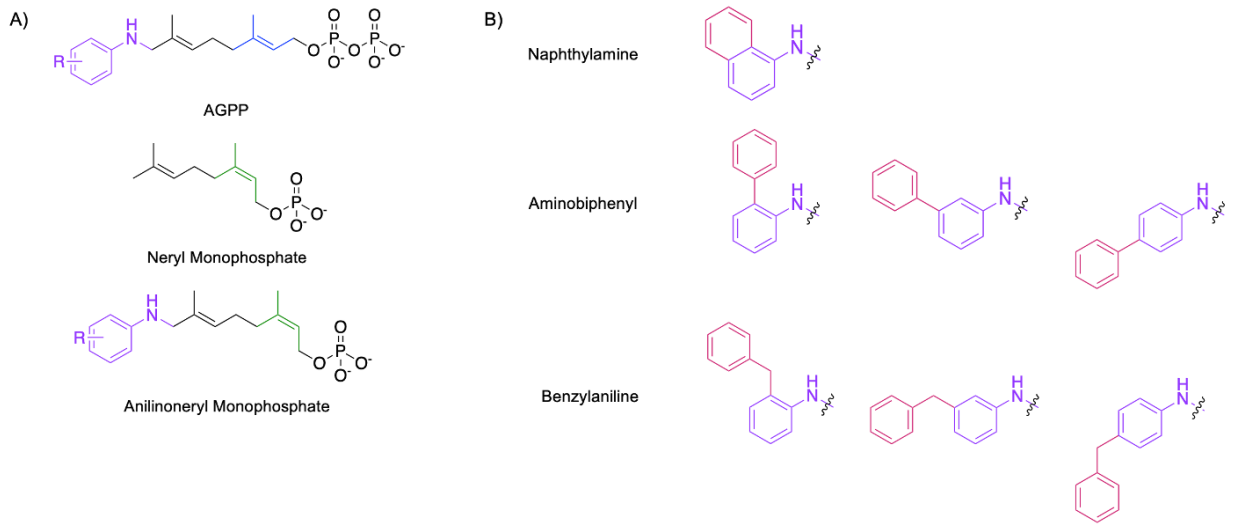

Figure 22: PGT probe design. **A**) Anilinoneryl monophosphate is constructed by incorporating the aniline from AGPP (shown in purple) with the short-chain neryl monophosphate. The α-isoprene geometry in AGPP and neryl monophosphate are color coded for comparison: blue for *trans* (E) double bonds and green for *cis* (Z) double bonds. **B**) A set of bulky groups (shown in burgundy) to test the effects of substrate size on PGT specificity.

Building a library of small-molecule isoprenoid analogues may prove to be an effective strategy for developing PGT enzyme probes. These tools could be instrumental to learning more about the structure and function of PGTs and further characterize these important enzymes. The enzymes utilized for this objective include the model monoPGT, PglC (**Figure 23A**), from pathogenic *C. jejuni*, as well as WcfS (**Figure 23B**) from the commensal, nonpathogenic *B. fragilis*. In addition to these PGTs, a selection of other well-studied PGTs that are prevalent in bacterial glycan research could also prove insightful: WecA from *E. coli*, Cps2E from *S. pneumoniae*, WecP from *Aeromonas hydrophila,* and WbaP from *Salmonella enterica* (**Figure 23C**). By observing the unique interactions between various PGTs and a series of purposely designed synthetic compounds, it may be possible to detect the substrate specificities of each enzyme and coincidingly deduce what each protein accepts as alternative substrates.

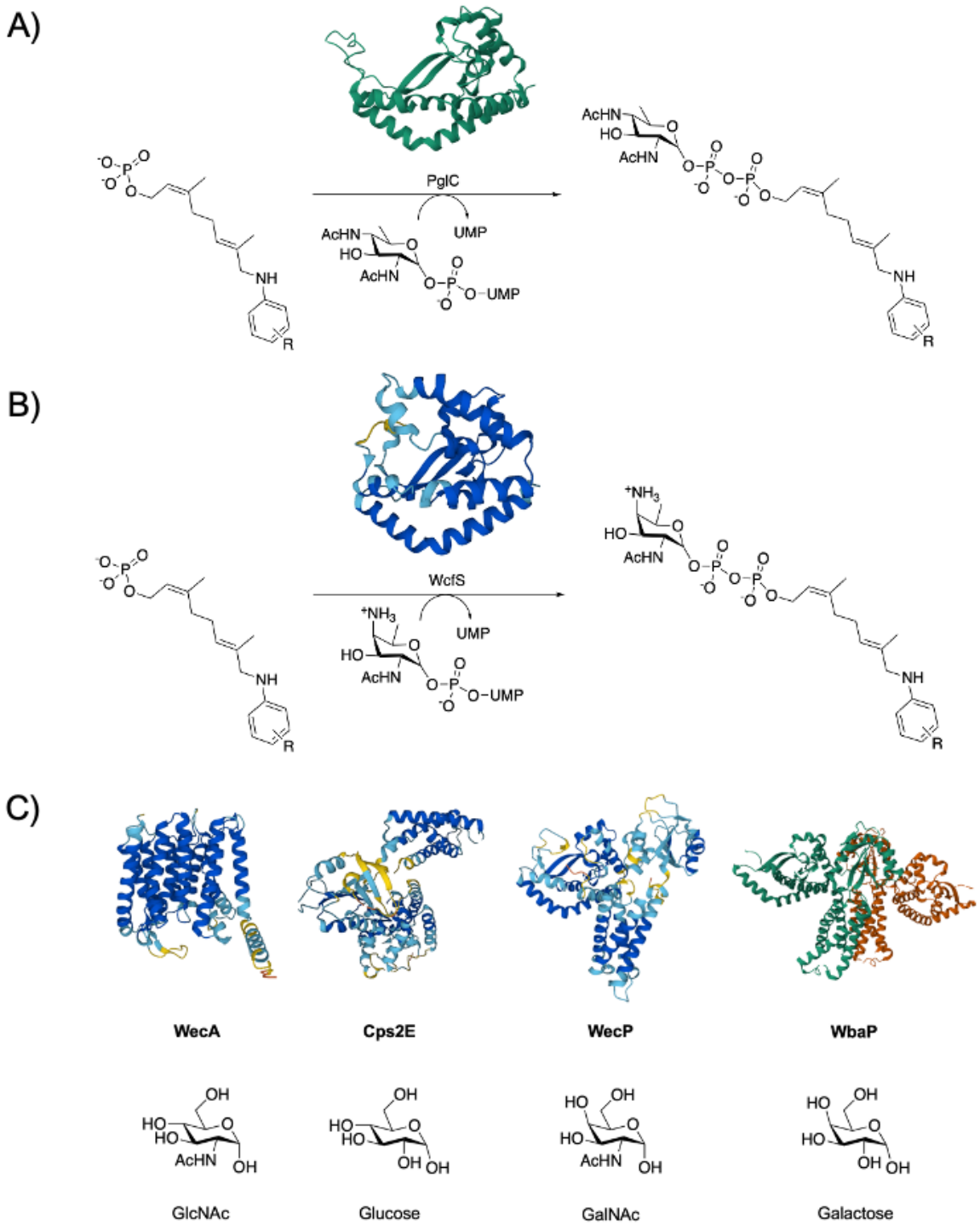

Figure 23: A chemoenzymatic reaction with the anilinoneryl monophosphate analogues and the PGTs, PglC (**A**) and WcfS (**B**). **C**) Additional PGTs and the sugars they typically append to the lipid substrate. The protein structures for PglC and WbaP were sourced from the RCBS Protein Data Bank.[8, 12] The protein structures for WcfS, WecA, Cps2E, and WecP were generated using AlphaFold.[6, 7]

The chemoenzymatic reactions described in this work could provide some critical information that may be useful for multiple reasons. First, employing a series of PGT probes may help with understanding the role of an important class of enzymes involved in the biosynthesis of cellular structures that are associated with countless bacterial infections. Second, these results could potentially influence a plethora of future applications. Some of which include building bacterial glycan libraries, establishing detection methods to differentiate and target bacterial species (e.g., pathogenic vs. non-pathogenic), finding new ways to combat antibiotic resistance, discovering PGT inhibitors to prevent the initiation of bacterial glycan biosynthesis, and developing antivirulence drugs for treating bacterial infections.

CHAPTER 2: METHODS

2.1: Chemical Synthesis of Isoprenoid Analogues

2.1.1: General Procedures

Neryl Aldehyde Synthesis

Neryl acetate was oxidized according to a previously described method with some modifications.[79, 82] In a clean and dry 500 mL round-bottom flask, SeO_2 (0.1 mol equiv.) and salicylic acid (0.1 mol equiv.) were added and suspended in 75 mL CH_2Cl_2. The flask was cooled to 0 °C in an ice bath. While stirring, 70% *tert*-butyl hydroperoxide (5.3 mol equiv.) was added to the suspension and stirred until homogenous. After approximately 10 min, neryl acetate (1.0 mol equiv.) was slowly poured into the flask. The mixture was stirred on ice for 5 h. Afterword, the flask was removed from the ice bath and left to stir at RT for 18-24 h. Thin layer chromatography (TLC) was used to monitor the reaction progress (30% EtOAc/hexanes).

The solvent was removed by rotary evaporation until a viscous, oily residue remained. The residue was dissolved in 100 mL ether and poured into a 1000 mL separatory funnel. An additional 100 mL ether was used to wash down the sides of the flask. The mixture was extracted with 50 mL 5% $NaHCO_3$ to remove H_2SeO_3, and the aqueous layer was discarded. Additionally, 50 mL of the following were added individually: 5 M brine, saturated aq NaS_2O_3 (2x), $CuSO_4$ (2x), and 5 M brine—discarding the aqueous layers between each extraction. The organic layer was dried with $MgSO_4$ and filtered under vacuum. Then the solvent was removed by rotary evaporation to afford a pale-yellow crude oil. The oxidation reaction produces a mixture of alcohol, aldehyde, and carboxylic acid; the aldehyde was purified by flash chromatography on silica gel with 5% EtOAc/hexanes. TLC was used to determine the column conditions.

Reductive Amination

Neryl aldehyde underwent reductive amination according to a previously reported method with some modifications and adaptations.[79, 83] A clean 250 mL round-bottom flask was flame-dried under flowing argon gas to remove any moisture. 30 mL $C_2H_4Cl_2$ was added to the flask, along with neryl aldehyde (1.0 mol equiv.), the aniline (1.4 mol equiv.) dissolved in 2 mL $C_2H_4Cl_2$, and glacial acetic acid (12 mol equiv.). The solution was stirred at RT for 0.5 min before adding $NaBH(OAc)_3$ (3.0 mol equiv.). The solution was stirred under argon at RT for 5 h, after which TLC (30% EtOAc/hexanes) was performed to ensure the reaction had gone to completion. After 5 h, the reaction mixture was quenched with 200 mL 5% $NaHCO_3$ in a 1000 mL separatory funnel and extracted with 300 mL ether. The organic layer was dried with $MgSO_4$ and filtered by vacuum before the solvent was removed by rotary evaporation. The residue was then dissolved in 5% EtOAc/hexanes and purified by flash chromatography (5% EtOAc/hexanes).

Saponification

The neryl acetate analogues were deacetylated according to the following modified saponification reaction.[81] In a 250 mL round-bottom flask, the acetate (1.0 mol equiv.) was dissolved in 50 mL methanol. To this mixture, a solution of potassium carbonate (4.5 mol equiv.) dissolved in 12 mL water was added and stirred at RT for 5 h or overnight. After this time, 20 mL water was added. The reaction mixture was then extracted with 200 mL CH_2Cl_2 (two 100 mL rinses) in a 1000 mL separatory funnel and washed with 100 mL 5 M brine. After the aqueous layer was discarded, the organic layer was dried with $MgSO_4$, filtered under vacuum, and concentrated by rotary evaporation. The concentrated oil was purified by flash chromatography

(10-20% EtOAc/hexanes). TLC (30% EtOAc/hexanes) was used to monitor the conversion of the starting acetate to the alcohol product.

Phosphorylation

Neryl Alcohol analogues were phosphorylated according to the following modified method for monophosphorylation.[84, 85] First, three solutions (solutions A-C) were prepared before starting the reaction. A solution of bis-triethylammonium phosphate (TEAP) was prepared by slowly combining solution A (25 mL phosphoric acid and 94 mL acetonitrile) and solution B (110 mL triethylamine and 100 mL acetonitrile) [38% solution A and 62% solution B]. Then, a mobile phase (solution C) was prepared with *i*PrOH/conc. NH_4OH/H_2O (6:2.5:0.5).

In a 15 mL Falcon tube, trichloroacetonitrile (49 mol equiv.) was added along with the neryl alcohol analogue (1.0 mol equiv.). To this mixture, 1 mL TEAP was added and heated in a water bath at 40 °C for 5 min. After this time, another 1 mL TEAP was added and heated for an additional 5 min. This process of TEAP addition and heating was repeated 3 times in total, before transferring the mixture to a 50 mL Falcon tube and diluting the reaction mixture fivefold in mobile phase (solution C) [5.5 mL reaction mixture in 27.5 mL solution C]. The mixture was then centrifuged for 15 min at 2500 RCF to remove the resulting precipitate. After which, the supernatant was filtered using a 0.20 μm CHROMAFIL PET-20/15 MS syringe filter to remove any remaining precipitate.

Isolation and Purification of Monophosphates

The phosphorylation reaction produces a mixture of mono-, di-, and triphosphates in addition to some unreacted alcohol. TLC was done using solution C as a mobile phase to monitor

the formation of the monophosphate. The monophosphate was isolated and purified by reverse-phase HPLC using an Agilent Eclipse XDB-C18, 5 μm, 9.4 x 250 mm column on an Agilent 1100 HPLC system. Isolations were performed at 3 mL/min in a 20:80 mixture of acetonitrile and 25 mM ammonium bicarbonate, increasing acetonitrile from 20 to 100% over 20 min. The compounds were detected with an excitation wavelength respective to each alcohol. Fractions containing the isolated monophosphate were frozen overnight at -80 °C and lyophilized until a white powder remained.

Bis-triethylammonium phosphate is used in the phosphorylation reaction to solubilize the phosphate in organic solvents. Following phosphorylation, the triethylammonium ion remains loosely associated with the phosphorylated product. Ion exchange was performed in an attempt to exchange the bulky triethylammonium ion with a smaller ammonium cation. The dried powder was dissolved in approximately 10 mL 25 mM ammonium bicarbonate and passed through an ion exchange column packed with Dowex 50WX8, 100-200 mesh resin in the ammonium form with approximately 250 mL 25 mM ammonium bicarbonate. 10 mL fractions were collected, and the fluorescent compounds were assayed under a 254 nm UV lamp (**Figure A1**). Fluorescent fractions were pooled, frozen overnight at -80 °C, and lyophilized. Non-fluorescent compounds were collected without UV analysis in the combined 250 mL flow-through and similarly lyophilized.

To ensure the ion exchange method was successful, the samples were characterized by ^{1}H and ^{31}P NMR. The dried powder was dissolved in 1 mL D_2O, forming a turbid solution, which was centrifuged at 14.1 RCF for 15 min in a microcentrifuge tube. An insoluble white solid was pelleted, and the supernatant was collected for ^{1}H and ^{31}P NMR analysis using a Bruker Ascend 500 MHz NMR. Following NMR, the monophosphorylated compounds were subsequently

characterized via LC-MS in SIM mode (negative ion mode) using an XBridge Peptide BEH C18, 3.5 μm, 4.6 x 50 mm column on an Agilent 1260 Infinity II system. Analyses were performed at 1 mL/min with a gradient of 0.1% ammonium hydroxide and *n*-propanol, increasing *n*-propanol from 5 to 90% over 15 min. The samples were stored in microcentrifuge tubes at -80 °C.

2.1.2: Specific Procedures

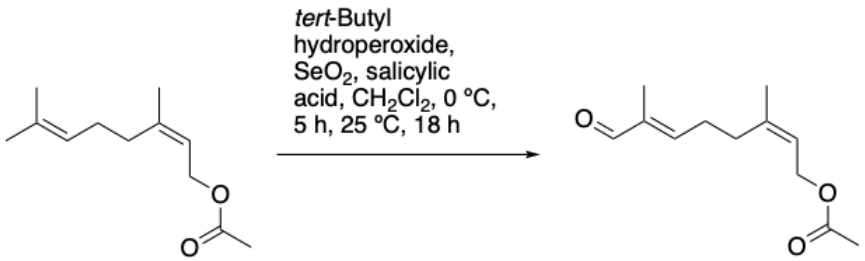

1

Neryl Aldehyde (**1**). 1.1806 g (0.010639 mol) SeO_2 and 1.4304 g (0.010356 mol) salicylic acid were suspended in 75.0 mL CH_2Cl_2 and cooled to 0 °C. While stirring, 51.0 mL (0.53 mol) 70% *tert*-butyl hydroperoxide was added until homogenous. 21.5 mL (0.100 mol) chilled neryl acetate was slowly poured into the flask and stirred on ice for 5 h and then at RT for an additional 18 h. The solvent was removed by rotary evaporation and extracted in 200 mL ether with 50 mL 5% $NaHCO_3$, 5 M brine, saturated aq NaS_2O_3 (2x), $CuSO_4$ (2x), and 5 M brine. The organic layer was dried with $MgSO_4$, concentrated, and purified by flash chromatography on silica gel (5% EtOAc/hexanes), yielding 5.1533 g of **1** (24.4%); R_f: 0.41 (30% EtOAc/hexanes); ^{1}H NMR (500 MHz, $CDCl_3$): δ 9.42 (s, 1H); 6.49 (t, J = 7.3 Hz, 1H); 5.47 (t, J = 7.3 Hz, 1H); 4.60 (d, J = 7.4 Hz, 2H); 2.52 (q, J = 7.0 Hz, 2H); 2.35 (t, J = 7.5 Hz, 2H); 2.06 (s, 3H); 1.82 (s, 3H); 1.78 (s, 3H).

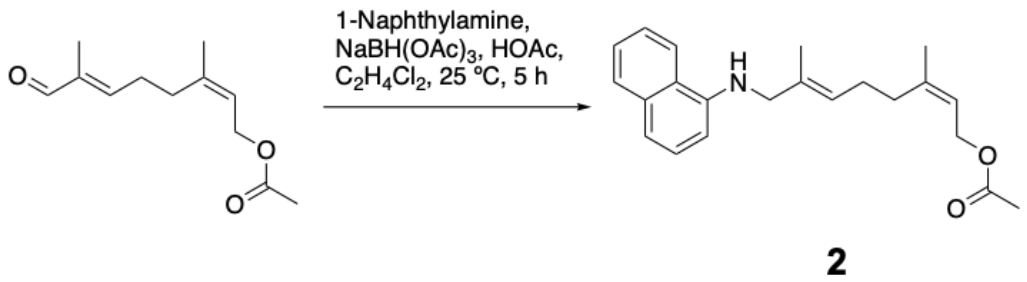

2

1-Naphthylamine neryl acetate (**2**). A solution of 30.0 mL $C_2H_4Cl_2$, 1.0469 g (4.9788 mmol) neryl aldehyde (**1**), 0.9656 g (6.744 mmol) 1-naphthylamine dissolved in 2.0 mL $C_2H_4Cl_2$, and 3.0 mL glacial acetic acid was added to a flame-dried 250 mL round-bottom flask under flowing argon gas. After 0.5 min, 3.0355 g (14.390 mmol) $NaBH(OAc)_3$ was added to the solution and stirred under argon at RT for 5 h. The solution was quenched with 200 mL 5% $NaHCO_3$ and extracted with 300 mL ether. The organic layer was dried with $MgSO_4$, concentrated, and purified by flash chromatography (5% EtOAc/hexanes), yielding 1.2597 g of **2** (74.978%); R_f: 0.57 (30% EtOAc/hexanes); ^{1}H NMR (500 MHz, $CDCl_3$): δ 7.87 (m, 1H); 7.82 (m, 1H); 7.47 (m, 2H); 7.36 (t, J = 8.1 Hz, 1H); 7.25 (d, J = 8.1 Hz, 1H); 6.61 (d, J = 7.6 Hz, 1H); 5.53 (t, J = 7.0 Hz, 1H); 5.41 (t, J = 7.2 Hz, 1H); 4.59 (d, J = 6.3 Hz, 2H); 3.85 (s, 2H); 3.85 (s, 2H); 2.21 (m, 4H); 2.05 (s, 3H); 1.79 (d, J = 4.3 Hz, 6H).

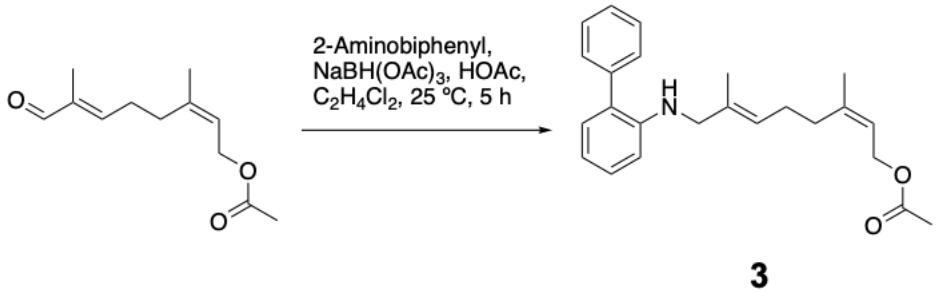

3

2-Aminobiphenyl neryl acetate (**3**). A solution of 30.0 mL $C_2H_4Cl_2$, 1.0781 g (5.1271 mmol) neryl aldehyde (**1**), 0.9707 g (5.736 mmol) 2-aminobiphenyl dissolved in 2.0 mL

$C_2H_4Cl_2$, and 3.0 mL glacial acetic acid was added to a flame-dried 250 mL round-bottom flask under flowing argon gas. After 0.5 min, 3.0926 g (14.592 mmol) $NaBH(OAc)_3$ was added to the solution and stirred under argon at RT for 5 h. The solution was quenched with 200 mL 5% $NaHCO_3$ and extracted with 300 mL ether. The organic layer was dried with $MgSO_4$, concentrated, and purified by flash chromatography (10% EtOAc/hexanes), yielding 1.3792 g of **3** (74.003%); R_f: 0.62 (30% EtOAc/hexanes); ^{1}H NMR (500 MHz, $CDCl_3$): δ 7.47 (m, 3H); 7.38 (td, J = 3.4 Hz, 1H); 7.24 (td, J = 6.8 Hz, 1H); 7.11 (dd, J = 7.5 Hz, 1H); 6.79 (t, J = 7.5 Hz, 1H); 6.69 (d, J = 8.2 Hz, 1H); 5.37 (t, J = 8.7 Hz, 2H); 4.55 (d, J = 7.2 Hz, 2H); 3.64 (s, 2H); 2.14 (s, 4H); 2.04 (s, 3H); 1.76 (s, 3H); 1.64 (s, 3H).

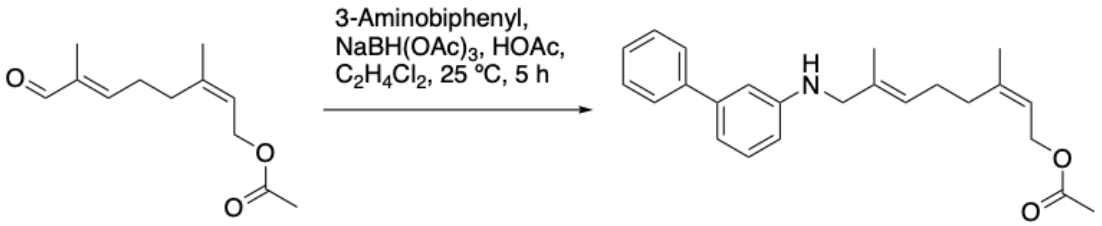

4

3-Aminobiphenyl neryl acetate (**4**). A solution of 30.0 mL $C_2H_4Cl_2$, 1.0913 g (5.190 mmol) neryl aldehyde (**1**), 0.9607 g (5.677 mmol) 3-aminobiphenyl dissolved in 2.0 mL $C_2H_4Cl_2$, and 3.0 mL glacial acetic acid was added to a flame-dried 250 mL round-bottom flask under flowing argon gas. After 0.5 min, 3.0499 g (14.390 mmol) $NaBH(OAc)_3$ was added to the solution and stirred under argon at RT for 5 h. The solution was quenched with 200 mL 5% $NaHCO_3$ and extracted with 300 mL ether. The organic layer was dried with $MgSO_4$, concentrated, and purified by flash chromatography (5% EtOAc/hexanes), yielding 1.0250 g of **4** (54.333%); R_f: 0.58 (30% EtOAc/hexanes); ^{1}H NMR (500 MHz, $CDCl_3$): δ 7.60 (dd, J = 8.6 Hz,

2H); 7.44 (t, *J* = 7.3 Hz, 2H); 7.35 (t, *J* = 8.7 Hz, 1H); 7.26 (t, *J* = 7.8 Hz, 1H); 6.95 (d, *J* = 7.7 Hz, 1H); 6.85 (s, 1H); 6.63 (dd, *J* = 8.1 Hz, 1H); 5.49 (t, *J* = 5.5 Hz, 1H); 5.39 (t, *J* = 7.2 Hz, 1H); 4.59 (d, *J* = 6.1 Hz, 2H); 3.73 (s, 2H); 2.19 (s, 4H); 2.05 (s, 3H); 1.78 (s, 3H); 1.74 (s, 3H).

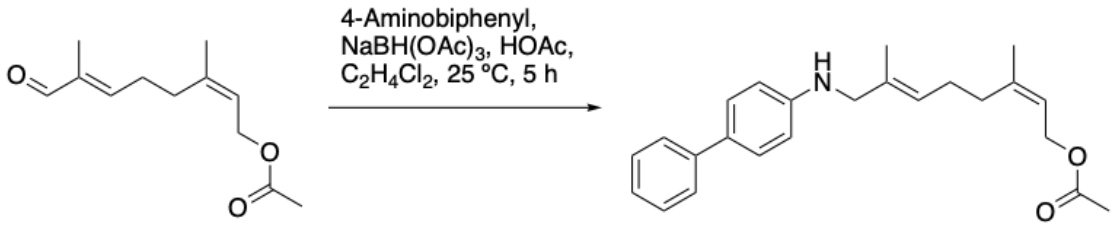

5

4-Aminobiphenyl neryl acetate (**5**). A solution of 30.0 mL $C_2H_4Cl_2$, 1.0913 g (5.190 mmol) neryl aldehyde (**1**), 0.9617 g (5.683 mmol) 4-aminobiphenyl dissolved in 2.0 mL $C_2H_4Cl_2$, and 3.0 mL glacial acetic acid was added to a flame-dried 250 mL round-bottom flask under flowing argon gas. After 0.5 min, 3.0517 g (14.399 mmol) $NaBH(OAc)_3$ was added to the solution and stirred under argon at RT for 5 h. The solution was quenched with 200 mL 5% $NaHCO_3$ and extracted with 300 mL ether. The organic layer was dried with $MgSO_4$, concentrated, and purified by flash chromatography (10% EtOAc/hexanes), yielding 1.7705 g of **5** (93.851%); R_f: 0.57 (30% EtOAc/hexanes); ^{1}H NMR (500 MHz, $CDCl_3$): δ 7.56 (dd, *J* = 8.4 Hz, 2H); 7.45 (d, *J* = 8.7 Hz, 2H); 7.41 (t, *J* = 7.5 Hz, 2H); 7.27 (t, *J* = 7.3 Hz, 3H); 6.70 (d, *J* = 8.7 Hz, 2H); 5.47 (t, *J* = 6.9 Hz, 1H); 5.40 (t, *J* = 5.6 Hz, 1H); 4.59 (d, *J* = 7.2 Hz, 2H); 3.72 (s, 2H); 2.19 (s, 4H); 2.05 (s, 3H); 1.79 (s, 3H); 1.73 (s, 3H).

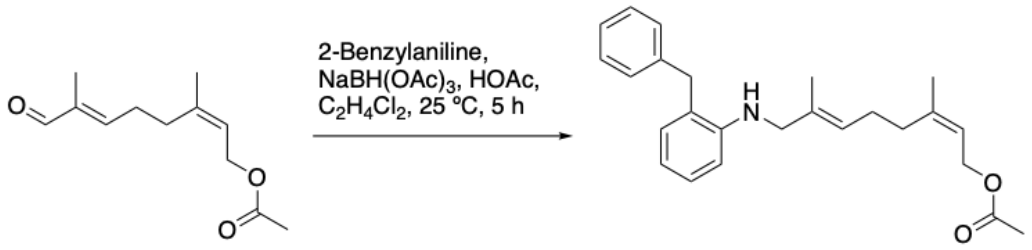

6

2-Benzylaniline neryl acetate (**6**). A solution of 30.0 mL $C_2H_4Cl_2$, 1.0493 g (4.9902 mmol) neryl aldehyde (**1**), 0.9636 g (5.258 mmol) 2-benzylaniline dissolved in 2.0 mL $C_2H_4Cl_2$, and 3.0 mL glacial acetic acid was added to a flame-dried 250 mL round-bottom flask under flowing argon gas. After 0.5 min, 3.0532 g (14.474 mmol) $NaBH(OAc)_3$ was added to the solution and stirred under argon at RT for 5 h. The solution was quenched with 200 mL 5% $NaHCO_3$ and extracted with 300 mL ether. The organic layer was dried with $MgSO_4$, concentrated, and purified by flash chromatography (5% EtOAc/hexanes), yielding 0.9898 g of **6** (52.54%); R_f: 0.61 (30% EtOAc/hexanes); ^{1}H NMR (500 MHz, $CDCl_3$): δ 7.32 (t, J = 7.0 Hz, 3H); 7.24 (t, J = 9.4 Hz, 3H); 7.19 (td, J = 5.6 Hz, 1H); 7.09 (d, J = 7.4 Hz, 1H); 6.74 (td, J = 6.1 Hz, 1H); 6.62 (d, J = 8.1 Hz, 1H); 5.38 (t, J = 7.3 Hz, 1H); 5.23 (t, J = 6.9 Hz, 1H); 4.55 (d, J = 7.4 Hz, 2H); 3.92 (s, 2H); 3.59 (s, 2H); 2.10 (d, 4H); 2.06 (s, 3H); 1.76 (s, 3H); 1.50 (s, 3H).

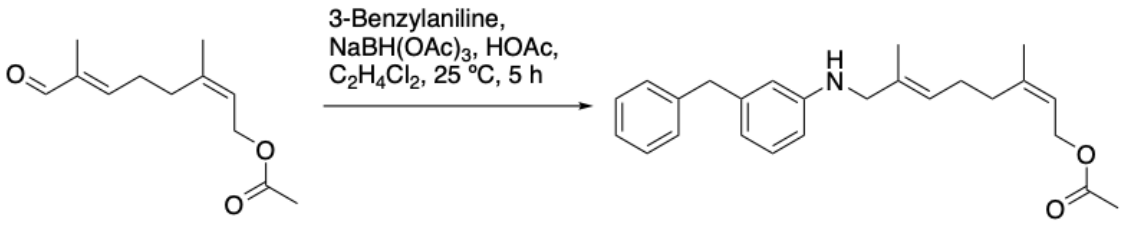

7

3-Benzylaniline neryl acetate (**7**). A solution of 30.0 mL $C_2H_4Cl_2$, 1.0394 g (4.9431 mmol) neryl aldehyde (**1**), 0.9657 g (5.270 mmol) 3-benzylaniline dissolved in 2.0 mL $C_2H_4Cl_2$,

and 3.0 mL glacial acetic acid was added to a flame-dried 250 mL round-bottom flask under flowing argon gas. After 0.5 min, 3.0542 g (14.479 mmol) $NaBH(OAc)_3$ was added to the solution and stirred under argon at RT for 5 h. The solution was quenched with 200 mL 5% $NaHCO_3$ and extracted with 300 mL ether. The organic layer was dried with $MgSO_4$, concentrated, and purified by flash chromatography (5% EtOAc/hexanes), yielding 1.1135 g of **7** (59.667%); R_f: 0.58 (30% EtOAc/hexanes); ^{1}H NMR (500 MHz, $CDCl_3$): δ 7.31 (t, *J* = 7.6 Hz, 3H); 7.23 (m, 3H); 7.11 (t, *J* = 7.8 Hz, 1H); 6.56 (d, *J* = 7.7 Hz, 1H); 6.48 (td, *J* = 4.6 Hz, 2H); 5.40 (m, *J* = 7.0 Hz, 2H); 4.58 (d, *J* = 7.3 Hz, 2H); 3.92 (s, 2H); 3.62 (s, 2H); 2.15 (s, 4H); 2.05 (s, 3H); 1.78 (s, 3H); 1.68 (s, 3H).

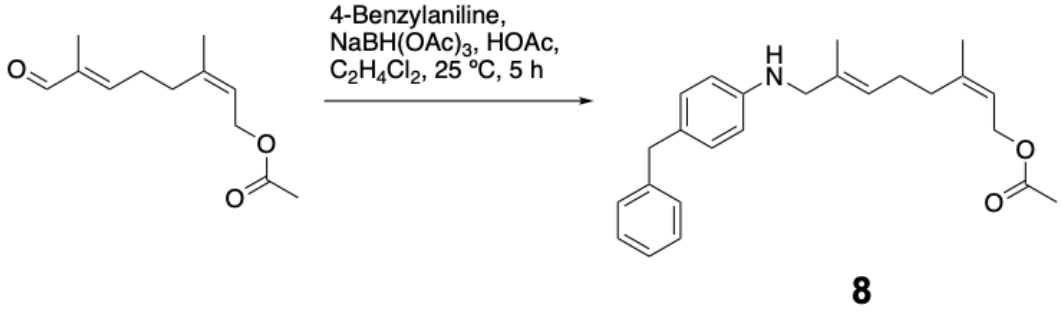

8

4-Benzylaniline neryl acetate (**8**). A solution of 30.0 mL $C_2H_4Cl_2$, 1.0352 g (4.9231 mmol) neryl aldehyde (**1**), 0.9632 g (5.256 mmol) 4-benzylaniline dissolved in 2.0 mL $C_2H_4Cl_2$, and 3.0 mL glacial acetic acid was added to a flame-dried 250 mL round-bottom flask under flowing argon gas. After 0.5 min, 3.0517 g (14.467 mmol) $NaBH(OAc)_3$ was added to the solution and stirred under argon at RT for 5 h. The solution was quenched with 200 mL 5% $NaHCO_3$ and extracted with 300 mL ether. The organic layer was dried with $MgSO_4$, concentrated, and purified by flash chromatography (5% EtOAc/hexanes), yielding 1.1101 g of **8** (59.728%); R_f: 0.53 (30% EtOAc/hexanes); ^{1}H NMR (500 MHz, $CDCl_3$): δ 7.30 (t, *J* = 7.4 Hz,

3H); 7.21 (d, *J* = 7.6 Hz, 3H); 7.01 (d, *J* = 8.6 Hz, 2H); 6.57 (d, *J* = 8.9 Hz, 2H); 5.43 (t, *J* = 2.8 Hz, 1H); 5.39 (t, *J* = 7.2 Hz, 1H); 4.58 (d, *J* = 7.4 Hz, 2H); 3.89 (s, 2H); 3.64 (s, 2H); 2.16 (s, 4H); 2.06 (s, 3H); 1.78 (s, 3H); 1.70 (s, 3H).

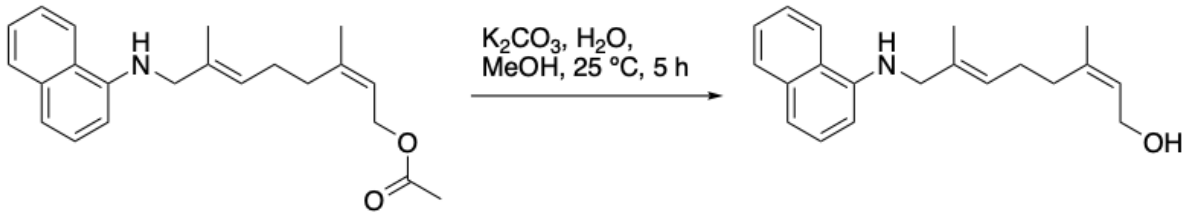

9

1-Naphthylamine neryl alcohol (**9**). In a 250 mL round-bottom flask, 1.2597 g (3.7329 mmol) acetate (**2**) was dissolved in 50.0 mL methanol. A solution of 2.3327 g (16.879 mmol) potassium carbonate dissolved in 12.0 mL water was added and stirred at RT for 5 h. The solution was quenched with 20.0 mL water, extracted with CH_2Cl_2 (2 x 100 mL), and washed with 100 mL 5 M brine. The organic layer was dried with $MgSO_4$, concentrated, and purified by flash chromatography (20% EtOAc/hexanes), yielding 1.0535 g of **9** (95.530%); R_f: 0.28 (30% EtOAc/hexanes); ^{1}H NMR (500 MHz, $CDCl_3$): δ 7.86 (m, 1H); 7.82 (m, 1H); 7.47 (m, 2H); 7.36 (t, *J* = 8.1 Hz, 1H); 7.26 (d, *J* = 8.3 Hz, 1H); 6.62 (d, *J* = 7.6 Hz, 1H); 5.53 (t, *J* = 5.7 Hz, 1H); 5.47 (t, *J* = 7.0 Hz, 1H); 4.11 (d, *J* = 7.0 Hz, 2H); 3.86 (s, 2H); 2.23 (m, 4H); 1.79 (d, *J* = 5.6 Hz, 6H); extinction coefficient ε = 6,559 $M^{-1}cm^{-1}$ at 340 nm.

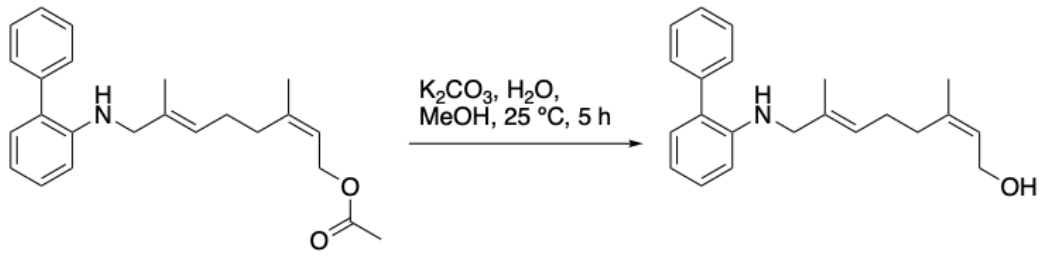

10

2-Aminobiphenyl neryl alcohol (**10**). In a 250 mL round-bottom flask, 0.9708 g (2.671 mmol) acetate (**3**) was dissolved in 50.0 mL methanol. A solution of 2.3406 g (16.936 mmol) potassium carbonate dissolved in 12.0 mL water was added and stirred at RT for 5 h. The solution was quenched with 20.0 mL water, extracted with CH_2Cl_2 (2 x 100 mL), and washed with 100 mL 5 M brine. The organic layer was dried with $MgSO_4$, concentrated, and purified by flash chromatography (20% EtOAc/hexanes), yielding 0.4715 g of **10** (54.91%); R_f: 0.37 (30% EtOAc/hexanes); ^{1}H NMR (500 MHz, $CDCl_3$): δ 7.48 (m, 4H); 7.39 (m, 1H); 7.24 (td, J = 5.7 Hz, 1H); 7.12 (dd, J = 7.5 Hz, 1H); 6.79 (t, J = 7.6 Hz, 1H); 6.67 (d, J = 8.3 Hz, 1H); 5.42 (t, J = 7.2 Hz, 1H); 5.36 (t, J = 5.8 Hz, 1H); 4.04 (d, J = 6.3 Hz, 2H); 3.63 (s, 2H); 2.15 (q, J = 9.9 Hz, 4H); 1.74 (s, 3H); 1.63 (s, 3H); 1.57 (s, 3H); extinction coefficient ε = 3,475 $M^{-1}cm^{-1}$ at 310 nm.

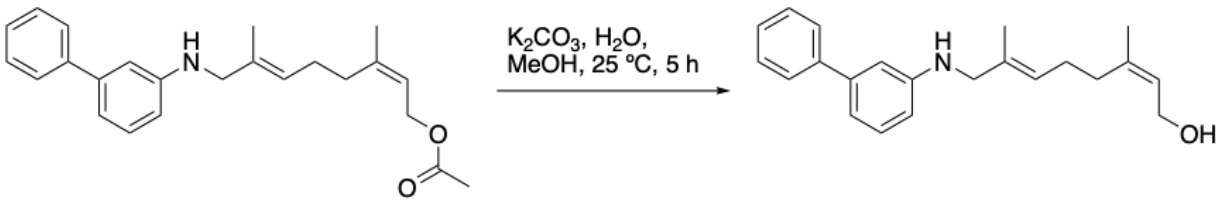

11

3-Aminobiphenyl neryl alcohol (**11**). In a 250 mL round-bottom flask, 1.0250 g (2.8198 mmol) acetate (**4**) was dissolved in 50.0 mL methanol. A solution of 2.3227 g (16.806 mmol) potassium carbonate dissolved in 12.0 mL water was added and stirred at RT for 5 h. The

solution was quenched with 20.0 mL water, extracted with CH_2Cl_2 (2 x 100 mL), and washed with 100 mL 5 M brine. The organic layer was dried with $MgSO_4$, concentrated, and purified by flash chromatography (20% EtOAc/hexanes), yielding 0.9599 g of **11** (105.9%); R_f: 0.29 (30% EtOAc/hexanes); ^{1}H NMR (500 MHz, $CDCl_3$): δ 7.60 (dd, *J* = 8.6 Hz, 2H); 7.45 (t, *J* = 7.4 Hz, 2H); 7.36 (t, *J* = 7.4 Hz, 1H); 7.27 (t, *J* = 7.8 Hz, 1H); 6.95 (d, *J* = 7.6 Hz, 1H); 6.83 (m, 1H); 6.63 (dd, *J* = 8.3 Hz, 1H); 5.47 (m, 2H); 4.09 (d, *J* = 7.0 Hz, 2H); 3.72 (s, 2H); 2.19 (q, *J* = 6.4 Hz, 4H); 1.76 (s, 3H); 1.72 (s, 3H); extinction coefficient ε = 2,220 $M^{-1}cm^{-1}$ at 320 nm.

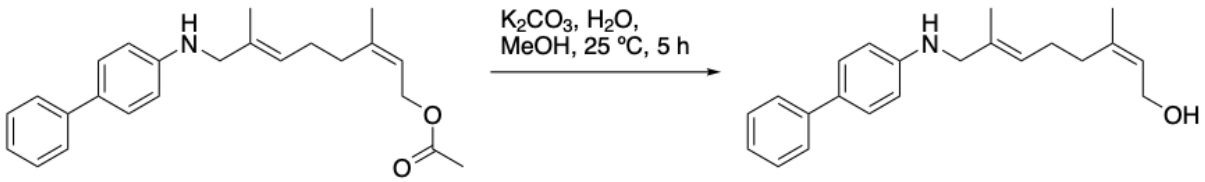

12

4-Aminobiphenyl neryl alcohol (**12**). In a 250 mL round-bottom flask, 1.7705 g (4.8707 mmol) acetate (**5**) was dissolved in 50.0 mL methanol. A solution of 2.3273 g (16.839 mmol) potassium carbonate dissolved in 12.0 mL water was added and stirred at RT for 5 h. The solution was quenched with 20.0 mL water, extracted with CH_2Cl_2 (2 x 100 mL), and washed with 100 mL 5 M brine. The organic layer was dried with $MgSO_4$, concentrated, and purified by flash chromatography (20% EtOAc/hexanes), yielding 1.4170 g of **12** (90.497%); R_f: 0.26 (30% EtOAc/hexanes); ^{1}H NMR (500 MHz, $CDCl_3$): δ 7.57 (dd, *J* = 8.4 Hz, 2H); 7.46 (d, *J* = 10.1 Hz, 2H); 7.42 (t, *J* = 7.5 Hz, 2H); 7.29 (t, *J* = 7.4 Hz, 3H); 6.70 (d, *J* = 8.7 Hz, 2H); 5.47 (m, 2H); 4.11 (d, *J* = 7.2 Hz, 2H); 3.70 (s, 2H); 2.20 (q, *J* = 5.6 Hz, 4H); 1.77 (s, 3H); 1.72 (s, 3H); extinction coefficient ε = 41,787 $M^{-1}cm^{-1}$ at 305 nm.

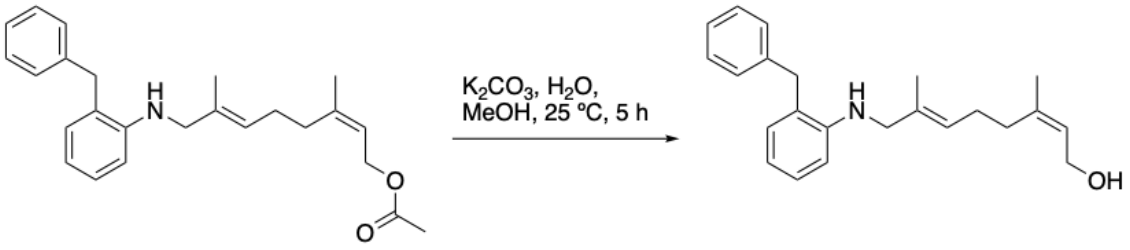

13

2-Benzylaniline neryl alcohol (**13**). In a 250 mL round-bottom flask, 0.9898 g (2.622 mmol) acetate (**6**) was dissolved in 50.0 mL methanol. A solution of 2.3248 g (16.821 mmol) potassium carbonate dissolved in 12.0 mL water was added and stirred at RT for 5 h. The solution was quenched with 20.0 mL water, extracted with CH_2Cl_2 (2 x 100 mL), and washed with 100 mL 5 M brine. The organic layer was dried with $MgSO_4$, concentrated, and purified by flash chromatography (20% EtOAc/hexanes), yielding 0.8615 g of **13** (97.94%); R_f: 0.29 (30% EtOAc/hexanes); ^{1}H NMR (500 MHz, $CDCl_3$): δ 7.32 (t, *J* = 7.0 Hz, 3H); 7.25 (m, 3H); 7.20 (td, *J* = 5.8 Hz, 1H); 7.10 (dd, *J* = 7.3 Hz, 1H); 6.75 (td, *J* = 6.3 Hz, 1H); 6.61 (dd, *J* = 8.1 Hz, 1H); 5.44 (t, *J* = 7.2 Hz, 1H); 5.21 (t, *J* = 5.8 Hz, 1H); 4.05 (d, *J* = 7.2 Hz, 2H); 3.93 (s, 2H); 3.58 (s, 2H); 2.10 (q, *J* = 4.8 Hz, 4H); 1.74 (s, 3H); 1.58 (s, 3H); extinction coefficient ε = 3,498 $M^{-1}cm^{-1}$ at 300 nm.

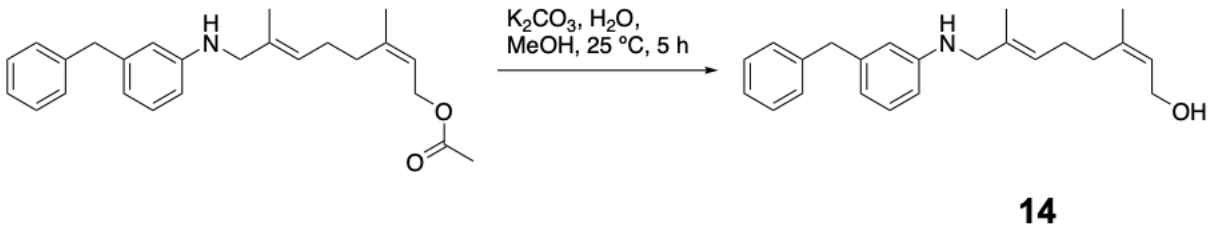

14

3-Benzylaniline neryl alcohol (**14**). In a 250 mL round-bottom flask, 1.1135 g (2.9495 mmol) acetate (**7**) was dissolved in 50.0 mL methanol. A solution of 2.3345 g (16.892 mmol) potassium carbonate dissolved in 12.0 mL water was added and stirred at RT for 5 h. The

solution was quenched with 20.0 mL water, extracted with CH_2Cl_2 (2 x 100 mL), and washed with 100 mL 5 M brine. The organic layer was dried with $MgSO_4$, concentrated, and purified by flash chromatography (20% EtOAc/hexanes), yielding 0.9157 g of **14** (92.54%); R_f: 0.26 (30% EtOAc/hexanes); ^{1}H NMR (500 MHz, $CDCl_3$): δ 7.31 (t, *J* = 8.0 Hz, 3H); 7.23 (d, *J* = 7.5 Hz, 3H); 7.12 (t, *J* = 7.6 Hz, 1H); 6.57 (d, *J* = 7.7 Hz, 1H); 6.48 (td, *J* = 6.4 Hz, 2H); 5.46 (t, *J* = 7.2 Hz, 1H); 5.40 (t, *J* = 5.8 Hz, 1H); 4.09 (d, *J* = 7.0 Hz, 2H); 3.91 (s, 2H); 3.62 (s, 2H); 2.16 (q, *J* = 5.5 Hz, 4H); 1.76 (s, 3H); 1.68 (s, 3H); extinction coefficient ε = 2,845 $M^{-1}cm^{-1}$ at 305 nm.

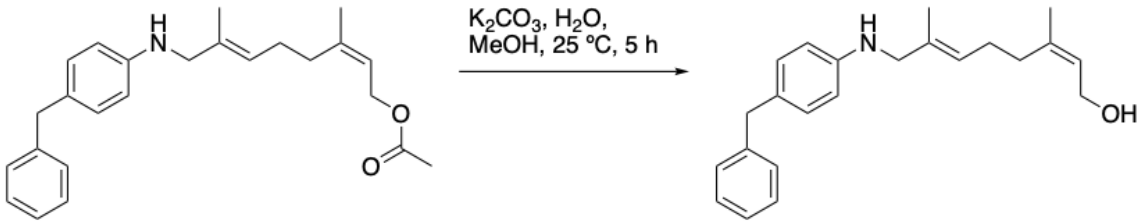

15

4-Benzylaniline neryl alcohol (**15**). In a 250 mL round-bottom flask, 1.1101 g (2.9404 mmol) acetate (**8**) was dissolved in 50.0 mL methanol. A solution of 2.3308 g (16.865 mmol) potassium carbonate dissolved in 12.0 mL water was added and stirred at RT for 5 h. The solution was quenched with 20.0 mL water, extracted with CH_2Cl_2 (2 x 100 mL), and washed with 100 mL 5 M brine. The organic layer was dried with $MgSO_4$, concentrated, and purified by flash chromatography (20% EtOAc/hexanes), yielding 0.9257 g of **15** (93.84%); R_f: 0.24 (30% EtOAc/hexanes); ^{1}H NMR (500 MHz, $CDCl_3$): δ 7.30 (t, *J* = 7.6 Hz, 3H); 7.21 (d, *J* = 6.6 Hz, 3H); 7.01 (d, *J* = 8.6 Hz, 2H); 6.57 (d, *J* = 8.6 Hz, 2H); 5.45 (m, 2H); 4.09 (d, *J* = 8.3 Hz, 2H); 3.89 (s, 2H); 3.63 (s, 2H); 2.18 (q, *J* = 6.6 Hz, 4H); 1.76 (s, 3H); 1.69 (s, 3H); extinction coefficient ε = 2,376 $M^{-1}cm^{-1}$ at 305 nm.

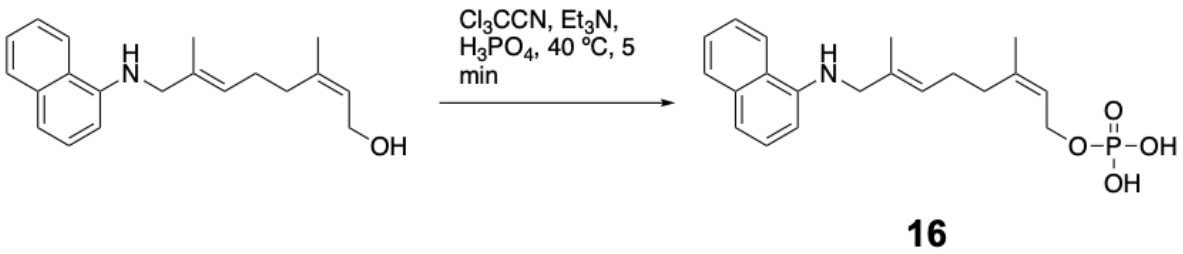

16

1-Naphthylamine neryl monophosphate (**16**). A solution of bis-triethylammonium phosphate (TEAP) was prepared by combining 25.0 mL phosphoric acid and 94.0 mL acetonitrile with 110.0 mL triethylamine and 100.0 mL acetonitrile (38:62 v/v). In a 15 mL Falcon tube, 1 mL (10 mmol) trichloroacetonitrile was added along with 0.0604 g (0.204 mmol) alcohol (**9**). 1 mL TEAP was added and heated at 40 °C for 5 min and then repeated 2 additional times. The mixture was transferred to a 50 mL Falcon tube, diluted fivefold with 27.5 mL mobile phase [*i*PrOH/conc. NH_4OH/H_2O (6:2.5:0.5)], centrifuged for 15 min at 2500 RCF, and the supernatant was filtered. The monophosphate was isolated by RP-HPLC, lyophilized, and passed through an ion exchange column in the ammonium form with 250 mL 25 mM ammonium bicarbonate. Fluorescent fractions were pooled, lyophilized, dissolved in 1 mL D_2O, centrifuged at 14.1 RCF for 15 min, and the supernatant was collected, yielding 11.92 mg of **16** (15.5%); R_f: 0.40 [*i*PrOH/conc. NH_4OH/H_2O (6:2.5:0.5)]; ^{1}H NMR (500 MHz, D_2O): δ 7.97 (m, 1H); 7.82 (m, 1H); 7.49 (m, 2H); 7.35 (t, J = 8.1 Hz, 1H); 7.29 (d, J = 8.1 Hz, 1H); 7.11 (d, J = 7.6 Hz, 1H); 6.75 (m, 2H); 5.38 (m, 2H); 4.20 (m, 2H); 3.81 (s, 2H); 2.07 (m, 4H); 1.60 (m, 6H); ^{31}P NMR (202 MHz, D_2O): δ 3.75; expected *m/z* 374.15, obtained 374.2 *m/z*.

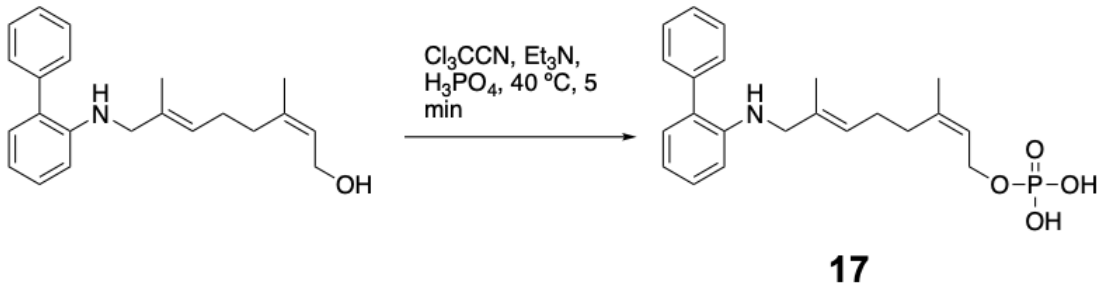

17

2-Aminobiphenyl neryl monophosphate (**17**). A solution of bis-triethylammonium phosphate (TEAP) was prepared by combining 25.0 mL phosphoric acid and 94.0 mL acetonitrile with 110.0 mL triethylamine and 100.0 mL acetonitrile (38:62 v/v). In a 15 mL Falcon tube, 1 mL (10 mmol) trichloroacetonitrile was added along with 0.0607 g (0.189 mmol) alcohol (**10**). 1 mL TEAP was added and heated at 40 °C for 5 min and then repeated 2 additional times. The mixture was transferred to a 50 mL Falcon tube, diluted fivefold with 27.5 mL mobile phase [*i*PrOH/conc. NH_4OH/H_2O (6:2.5:0.5)], centrifuged for 15 min at 2500 RCF, and the supernatant was filtered. The monophosphate was isolated by RP-HPLC, lyophilized, and passed through an ion exchange column in the ammonium form with 250 mL 25 mM ammonium bicarbonate. Fluorescent fractions were pooled, lyophilized, dissolved in 1 mL D_2O, centrifuged at 14.1 RCF for 15 min, and the supernatant was collected, yielding 9.570 mg of **17** (12.6%); R_f: 0.41 [*i*PrOH/conc. NH_4OH/H_2O (6:2.5:0.5)]; ^{1}H NMR (500 MHz, D_2O): δ 7.49 (m, 2H); 7.40 (m, 1H); 7.34 (m, 2H); 7.24 (m, 1H); 6.83 (m, 2H); 5.31 (m, 2H); 4.19 (t, J = 6.1 Hz, 2H); 3.57 (s, 2H); 2.03 (m, 4H); 1.59 (s, 3H); 1.42 (s, 3H); ^{31}P NMR (202 MHz, D_2O): δ 3.04; 2.03; expected *m/z* 400.17, obtained 400.2 *m/z*.

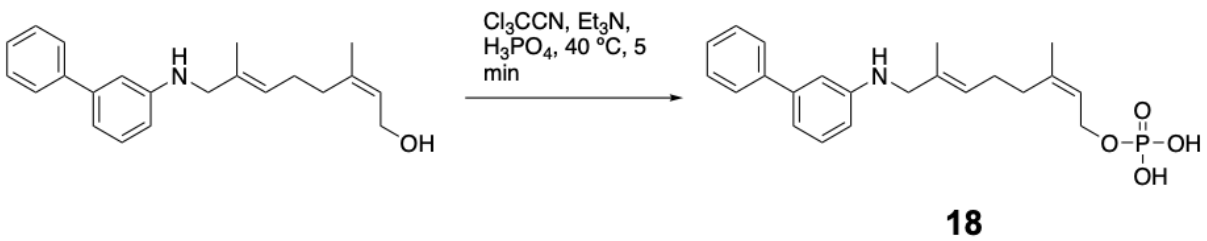

18

3-Aminobiphenyl neryl monophosphate (**18**). A solution of bis-triethylammonium phosphate (TEAP) was prepared by combining 25.0 mL phosphoric acid and 94.0 mL acetonitrile with 110.0 mL triethylamine and 100.0 mL acetonitrile (38:62 v/v). In a 15 mL Falcon tube, 1 mL (10 mmol) trichloroacetonitrile was added along with 0.0604 g (0.188 mmol) alcohol (**11**). 1 mL TEAP was added and heated at 40 °C for 5 min and then repeated 2 additional times. The mixture was transferred to a 50 mL Falcon tube, diluted fivefold with 27.5 mL mobile phase [*i*PrOH/conc. NH_4OH/H_2O (6:2.5:0.5)], centrifuged for 15 min at 2500 RCF, and the supernatant was filtered. The monophosphate was isolated by RP-HPLC, lyophilized, and passed through an ion exchange column in the ammonium form with 250 mL 25 mM ammonium bicarbonate. Fluorescent fractions were pooled, lyophilized, dissolved in 1 mL D_2O, centrifuged at 14.1 RCF for 15 min, and the supernatant was collected, yielding 9.667 mg of **18** (12.8%); R_f: 0.46 [*i*PrOH/conc. NH_4OH/H_2O (6:2.5:0.5)]; ^{1}H NMR (500 MHz, D_2O): δ 7.60 (m, 2H); 7.46 (t, J = 7.2 Hz, 2H); 7.37 (m, 1H); 7.27 (m, 1H); 7.02 (m, 2H); 6.77 (d, J = 6.9 Hz, 1H); 5.39 (m, 2H); 4.19 (m, 2H); 3.67 (s, 2H); 2.07 (m, 4H); 1.58 (m, 6H); ^{31}P NMR (202 MHz, D_2O): δ 3.81; expected *m/z* 400.17, obtained 400.2 *m/z*.

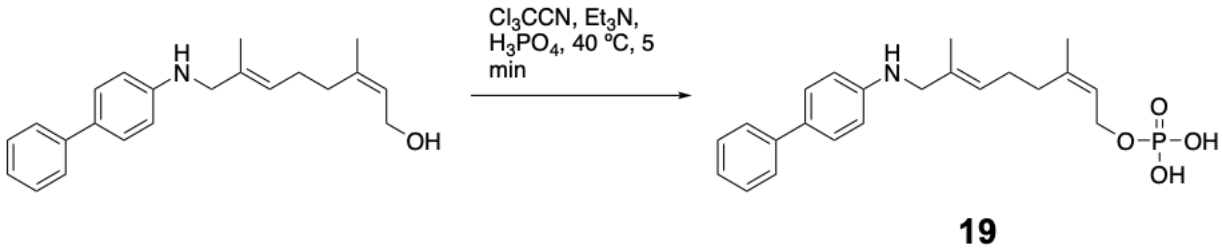

19

4-Aminobiphenyl neryl monophosphate (**19**). A solution of bis-triethylammonium phosphate (TEAP) was prepared by combining 25 mL phosphoric acid and 94 mL acetonitrile with 110 mL triethylamine and 100 mL acetonitrile (38:62 v/v). In a 15 mL Falcon tube, 1 mL (10 mmol) trichloroacetonitrile was added along with 0.0615 g (0.191 mmol) alcohol (**12**). 1 mL TEAP was added and heated at 40 °C for 5 min and then repeated 2 additional times. The mixture was transferred to a 50 mL Falcon tube, diluted fivefold with 27.5 mL mobile phase [*i*PrOH/conc. NH_4OH/H_2O (6:2.5:0.5)], centrifuged for 15 min at 2500 RCF, and the supernatant was filtered. The monophosphate was isolated by RP-HPLC, lyophilized, and passed through an ion exchange column in the ammonium form with 250 mL 25 mM ammonium bicarbonate. Fluorescent fractions were pooled, lyophilized, dissolved in 1 mL D_2O, centrifuged at 14.1 RCF for 15 min, and the supernatant was collected, yielding 0.6046 mg of **19** (0.787%); R_f: 0.45 [*i*PrOH/conc. NH_4OH/H_2O (6:2.5:0.5)]; ^{1}H NMR (500 MHz, D_2O): δ 7.49 (m, 2H); 7.38 (m, 4H); 7.21 (m, 2H); 5.41 (m, 2H); 4.37 (m, 2H); 3.55 (s, 2H); 2.07 (m, 4H); 1.66 (m, 6H); ^{31}P NMR (202 MHz, D_2O): δ 2.38; expected *m/z* 400.17, obtained 400.2 *m/z*.

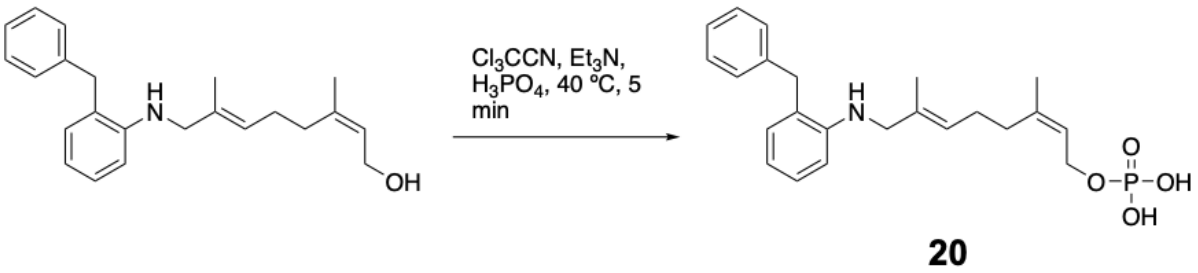

20

2-Benzylaniline neryl monophosphate (**20**). A solution of bis-triethylammonium phosphate (TEAP) was prepared by combining 25.0 mL phosphoric acid and 94.0 mL acetonitrile with 110.0 mL triethylamine and 100.0 mL acetonitrile (38:62 v/v). In a 15 mL Falcon tube, 1 mL (10 mmol) trichloroacetonitrile was added along with 0.0601 g (0.179 mmol) alcohol (**13**). 1 mL TEAP was added and heated at 40 °C for 5 min and then repeated 2 additional times. The mixture was transferred to a 50 mL Falcon tube, diluted fivefold with 27.5 mL mobile phase [*i*PrOH/conc. NH_4OH/H_2O (6:2.5:0.5)], centrifuged for 15 min at 2500 RCF, and the supernatant was filtered. The monophosphate was isolated by RP-HPLC, lyophilized, and passed through an ion exchange column in the ammonium form with 250 mL 25 mM ammonium bicarbonate. The combined flow-through was collected, lyophilized, dissolved in 1 mL D_2O, centrifuged at 14.1 RCF for 15 min, and the supernatant was collected, yielding 1.895 mg of **20** (2.55%); R_f: 0.43 [*i*PrOH/conc. NH_4OH/H_2O (6:2.5:0.5)]; ^{1}H NMR (500 MHz, D_2O): δ 7.10 (m, 7H); 6.58 (m, 2H); 3.99 (m, 2H); 3.69 (s, 2H); 3.34 (s, 2H); 1.78 (m, 4H); 1.41 (s, 3H); 1.12 (s, 3H); ^{31}P NMR (202 MHz, D_2O): δ 3.63; expected *m/z* 414.18, obtained 414.2 *m/z*.

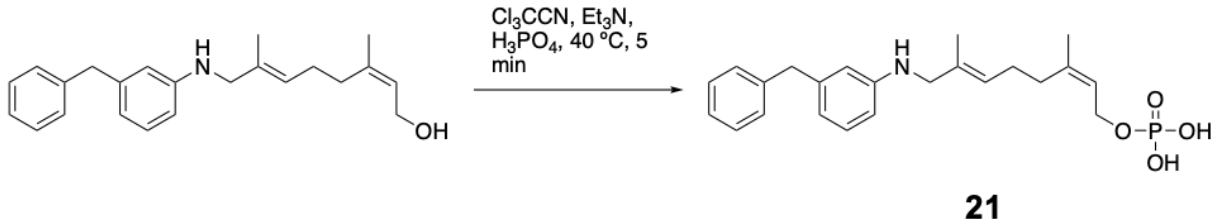

21

3-Benzylaniline neryl monophosphate (**21**). A solution of bis-triethylammonium phosphate (TEAP) was prepared by combining 25.0 mL phosphoric acid and 94.0 mL acetonitrile with 110.0 mL triethylamine and 100.0 mL acetonitrile (38:62 v/v). In a 15 mL Falcon tube, 1 mL (10 mmol) trichloroacetonitrile was added along with 0.0602 g (0.179 mmol) alcohol (**14**). 1 mL TEAP was added and heated at 40 °C for 5 min and then repeated 2 additional times. The mixture was transferred to a 50 mL Falcon tube, diluted fivefold with 27.5 mL mobile phase [*i*PrOH/conc. NH_4OH/H_2O (6:2.5:0.5)], centrifuged for 15 min at 2500 RCF, and the supernatant was filtered. The monophosphate was isolated by RP-HPLC, lyophilized, and passed through an ion exchange column in the ammonium form with 250 mL 25 mM ammonium bicarbonate. The combined flow-through was collected, lyophilized, dissolved in 1 mL D_2O, centrifuged at 14.1 RCF for 15 min, and the supernatant was collected, yielding 2.824 mg of **21** (3.79%); R_f: 0.40 [*i*PrOH/conc. NH_4OH/H_2O (6:2.5:0.5)]; ^{1}H NMR (500 MHz, D_2O): δ 7.17 (m, 7H); 6.52 (m, 2H); 4.06 (m, 2H); 3.70 (s, 2H); 3.42 (s, 2H); 1.88 (m, 4H); 1.48 (s, 3H); 1.36 (s, 3H); ^{31}P NMR (202 MHz, D_2O): δ 3.66; expected *m/z* 414.18, obtained 414.2 *m/z*.

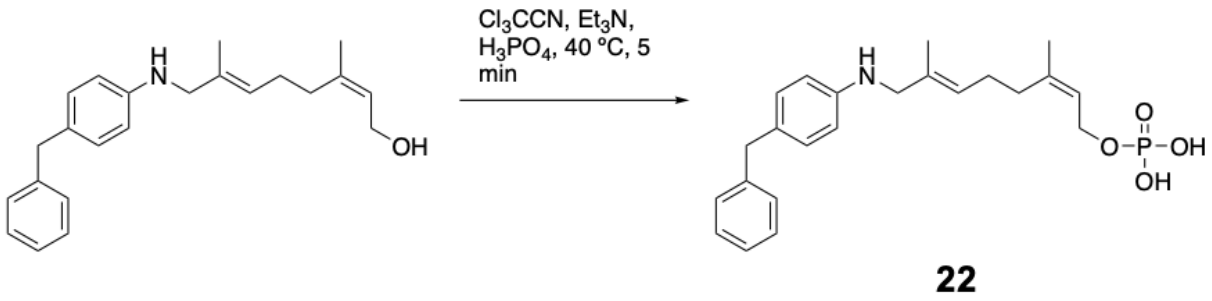

22

4-Benzylaniline neryl monophosphate (**22**). A solution of bis-triethylammonium phosphate (TEAP) was prepared by combining 25.0 mL phosphoric acid and 94.0 mL acetonitrile with 110.0 mL triethylamine and 100.0 mL acetonitrile (38:62 v/v). In a 15 mL Falcon tube, 1 mL (10 mmol) trichloroacetonitrile was added along with 0.0601 g (0.179 mmol) alcohol (**15**). 1 mL TEAP was added and heated at 40 °C for 5 min and then repeated 2 additional times. The mixture was transferred to a 50 mL Falcon tube, diluted fivefold with 27.5 mL mobile phase [*i*PrOH/conc. NH_4OH/H_2O (6:2.5:0.5)], centrifuged for 15 min at 2500 RCF, and the supernatant was filtered. The monophosphate was isolated by RP-HPLC, lyophilized, and passed through an ion exchange column in the ammonium form with 250 mL 25 mM ammonium bicarbonate. The combined flow-through was collected, lyophilized, dissolved in 1 mL D_2O, centrifuged at 14.1 RCF for 15 min, and the supernatant was collected, yielding 26.74 mg of **22** (35.9%); R_f: 0.43 [*i*PrOH/conc. NH_4OH/H_2O (6:2.5:0.5)]; ^{1}H NMR (500 MHz, D_2O): δ 6.79 (m, 7H); 6.26 (m, 2H); 4.15 (m, 2H); 3.39 (s, 2H); 3.24 (s, 2H); 1.87 (m, 4H); 1.45 (s, 3H); 1.31 (s, 3H); ^{31}P NMR (202 MHz, D_2O): δ 3.40; expected *m/z* 414.18, obtained 414.2 *m/z*.

2.2: PGT Protein Expression and Preparation

Protein Expression of PglC and WcfS

A 5 mL liquid starter culture was prepared in a culture tube with Luria-Bertani (LB) broth and 50 μg/mL kanamycin. The culture was inoculated with a transformed strain of *E. coli* containing a pET-24a vector in C41(DE3) expression cells, which were incubated at 37 °C while shaking at 220 rpm overnight. After 12 h, 1 mL of the 5 mL culture was transferred to a 2800 mL Erlenmeyer cell culture flask containing 1 L LB broth and 50 μg/mL kanamycin. The bacteria were further incubated at 37 °C while shaking until an OD_{600} of 0.6-0.8 was reached. At this point, 1 mM isopropyl-β-D-1-thiogalactopyranoside (IPTG) was added to the flask and left at 16 °C while shaking at 220 rpm overnight to induce overexpression of the transformed protein.

Preparation of Membrane Fractions

The next day, 500 mL aliquots of the liquid culture was centrifuged at 5000 RCF for 15 min at 4 °C to pellet the cells and remove the liquid growth media. The LB supernatant was poured off, and the cells were resuspended in 20 mL lysis buffer [50 mM Tris-HCl (pH 8.0), 200 mM NaCl, 20 mM Imidazole]. The cells were lysed via 2 rounds of sonication at an amplitude of 25% for 3 min (1 s on, 1 s off), while keeping the cells on ice. Following sonication, unlysed cells and debris were pelleted and discarded by centrifugation at 2500 RCF for 30 min at 4 °C. Next, the supernatant was transferred to ultracentrifuge vials and spun under vacuum at 150,000 RCF and 4 °C for 60 min to separate membrane fractions into a pellet. The supernatant was discarded, and the pellet was taken up in approximately 2 mL dialysis buffer [500 mM Tris-HCl (pH 8.0), 2 M NaCl]. Expressed proteins were analyzed via SDS-PAGE ran at 180 V for approximately 40-60 min and imaged with Coomassie staining. A Western blot was also

performed using a second gel ran at 380 mA for 60 min, which was later visualized with Ponceau staining and treated with anti-His tag antibodies. Lastly, the proteins were stored in 250 μL aliquots at -80 °C.

2.3: Chemoenzymatic Synthesis of Sugar Substrates

2.3.1: Protein Expression and Purification of PglF, PglE, PglD, and WcfR

Protein Expression

The soluble proteins, PglF, PglE, PglD, and WcfR, were expressed according to the same method described above for the membrane fractions, PglC and WcfS.

Preparation of Soluble Proteins

Following overnight induction with IPTG, 500 mL aliquots of the liquid culture was centrifuged at 5000 RCF for 15 min at 4 °C. The supernatant was poured off, and the cells containing PglE, PglD, and WcfR were resuspended in 20 mL lysis buffer [50 mM Tris-HCl, 200 mM NaCl, 20 mM Imidazole (pH 8.0)], whereas the cells containing PglF were suspended in 20 mL ice-cold PBS buffer [140 mM NaCl, 2.7 mM KCl, 10 mM Na_2HPO_4, and 1.8 mM KH_2PO_4 (pH 7.3) supplemented with 200 μM NAD^+].[86] The cells were lysed via two rounds of sonication at an amplitude of 25% for 3 min (1 s on, 1 s off), while keeping the cells on ice. Following sonication, the lysate was transferred to ultracentrifuge vials and spun under vacuum at 150,000 RCF and 4 °C for 60 min to separate soluble proteins from the pelleted cellular membrane fractions. The supernatant was decanted into a 50 mL Falcon tube and the pellet was discarded.

Purification of His-Tagged PglE, PglD, and WcfR

The plasmids for PglE, PglD, and WcfR were encoded with a terminal polyhistidine tag for purification by immobilized metal affinity chromatography (IMAC). The lysate, containing the His-tagged proteins, was passed through a nickel-nitrilotriacetic acid (Ni-NTA) column packed with 4 mL HisPur Ni-NTA resin; the flow-through was collected and passed through the column a second time. Afterword, 24 mL wash buffer [50 mM Tris-HCl, 50 mM imidazole, 200 mM NaCl (pH 8.0)] was added to the column and collected. Lastly, the adsorbed proteins were eluted from the column and collected in six different microcentrifuge tubes using six additions of 1 mL elution buffer [50 mM Tris-HCl, 500 mM imidazole, 300 mM NaCl (pH 8.0)]. The flow-through, wash, and six elutions were analyzed via SDS-PAGE and Western blotting according to the same method described above for PglC and WcfS. Samples containing the protein of interest were combined and dialyzed overnight at 4 °C in 1 L dialysis buffer [50 mM Tris and 200 mM NaCl (pH 8.0)]. Lastly, the concentration of each protein was determined spectrophotometrically, and the samples were subsequently aliquoted for storage similarly to the membrane fractions.

Purification of GST-Tagged PglF

PglF was encoded with a glutathione S-transferase (GST) tag for purification by affinity chromatography. The lysate was passed through a 1 mL Cytiva GSTrap FF column at a rate of 15 drops/min and collected as a flow-through. Then the column was washed with 5 mL PBS buffer at 30 drops/min. Lastly, the GST-tagged protein was eluted from the column with 5 mL GST elution buffer [50 mM Tris and 10 mM L-glutathione (pH 8.0) supplemented with 200 μM NAD^+] at 30 drops/min and collected sequentially in five 1 mL amounts.[86] The flow-through, wash, and five elutions were analyzed via SDS-PAGE. Samples containing PglF were combined

and dialyzed against PBS three times for approximately 2 h each—the third round went overnight—at 4 °C in 1 L dialysis buffer [50 mM Tris and 200 mM NaCl (pH 8.0), in the presence of 200 μM NAD^+]. The concentration was determined spectrophotometrically and aliquoted for storage according to the same previously described method.

Concentration of PglF, PglE, PglD, and WcfR

Following protein expression and purification, each enzyme was separately concentrated. The dialyzed elutions for each enzyme were combined and spun down in an Amicon Ultra-4 10K MWCO centrifugal filter at 8000 RCF for 20 min at 4 °C. The concentration of the centrifuged proteins was calculated spectrophotometrically at 280 nm using a Thermo Scientific NanoDrop One^C. The proteins were chilled at 4 °C for immediate use in chemoenzymatic reactions and later frozen at -20 °C for long-term storage.

2.3.2: Chemoenzymatic Synthesis and Purification of UDP-diNAcBac

The PglC sugar substrate, UDP-diNAcBac, was chemoenzymatically synthesized according to a previously reported method with some modifications.[86, 87] UDP-diNAcBac was prepared in a total reaction volume of 200 μL with 50 mM Tris-Acetate (pH 7.5), 50 mM NaCl, 5 mM UDP-GlcNAc, 4.0 μM pyridoxal 5'-phosphate (PLP), 15 mM L-glutamate (pH 8.0), and 6 mM acetyl coenzyme A (acetyl-CoA). To this master mixture, 10 μL each of concentrated PglF (2.8 μM) and PglE (4.4 μM) was added and incubated at 37 °C while shaking at 220 rpm for 1 h. Both enzymes were allowed to react in a two-step coupled reaction, to help facilitate the conversion of UDP-4-keto-sugar from UDP-GlcNAc by PglF to UDP-4-amino-sugar by PglE. After 1 h, 10 μL (0.25 mM) PglD was added, and the mixture was incubated while shaking for

an additional hour. A 10 μL aliquot of the reaction mixture was taken after each step and analyzed by reverse-phase HPLC using an Agilent Zorbax NH_2, 5 μm, 4.6 x 150 mm column on an Agilent 1100 HPLC system. Analyses were monitored at 260 nm and performed with an isocratic method at 1 mL/min using a 97% (v/v) mixture of 100 mM ammonium acetate (pH 4.5) and acetonitrile for 15 min. The reaction mixture was later purified using an Amicon Ultra-4 10K MWCO centrifugal filter at 8000 RCF for 20 min at 4 °C.

2.3.3: Chemoenzymatic Synthesis and Purification of UDP-AADGal

The WcfS sugar substrate, UDP-AADGal, was chemoenzymatically synthesized according to a previously reported method with some modifications.[44, 86] UDP-AADGal was prepared in a total reaction volume of 200 μL with 15 mM L-glutamate (pH 8.0), 100 μM pyridoxal 5'-phosphate (PLP), 50 mM Tris-Acetate (pH 8.0), 50 mM NaCl, 1 mM UDP-GlcNAc, and 25 μM NAD^+. To this master mixture, 10 μL each of concentrated PglF (2.8 μM) and WcfR (26 mM) was added in a two-step coupled reaction and incubated at 28 °C while shaking at 150 rpm for 3 h. A 10 μL aliquot of the reaction mixture was taken and analyzed by the same HPLC method described above for the synthesis of UDP-diNAcBac. The reaction mixture was later purified using an Amicon Ultra-4 10K MWCO centrifugal filter at 8000 RCF for 20 min at 4 °C.

2.4: Chemoenzymatic Reactions with Bulky Isoprenoid Analogues and PGTs

All PGT reactions were performed according to a previously reported method with some modifications.[36] The reactions were carried out in a total reaction volume of 40 μL with 200 mM bicine (pH 8.5), 5 mM $MgCl_2$, 100 mM KCl, and 5% (v/v) *n*-propanol. To this mixture, 100 μM

sugar substrate was added, along with 4 μL enzyme and 10 μM isoprenoid analogue—calculated from the stock concentrations provided in **Table 1**. The reaction mixtures were mixed until homogenous and incubated at 37 °C while shaking at 200 rpm for 2 h. Afterword, a 10 μL aliquot of the reaction mixture was analyzed by LC-MS in SIM mode (negative ion mode) using an XBridge Peptide BEH C18, 3.5 μm, 4.6 x 50 mm column on an Agilent 1260 Infinity II system. Analyses were performed at 1 mL/min with a gradient of 0.1% ammonium hydroxide and *n*-propanol, increasing *n*-propanol from 5 to 90% over 15 min.

Table 1: Concentration of isoprenoid analogues

Isoprenoid Analogue	Analogue Concentration (mM)
1-NA-NP	0.7938
2-ABP-NP	0.5960
3-ABP-NP	0.6020
4-ABP-NP	0.03765
2-BA-NP	0.1141
3-BA-NP	0.1700
4-BA-NP	1.609

CHAPTER 3: RESULTS AND DISCUSSION

3.1: Chemical Synthesis of Bulky Neryl Monophosphate Analogues

3.1.1: Forming the Terminal End

The starting point—and arguably the most critical component—of this research involved the chemical synthesis of isoprenoid analogues. These synthetic compounds would act as the necessary tools for investigating the function of various PGTs to help elucidate the substrate specificities of these important enzymes. The short-chain isoprenoid analogues that were designed for this purpose were chemically synthesized according to the synthesis scheme provided in **Figure 24**, adapted from Chehade et al.[79, 81]

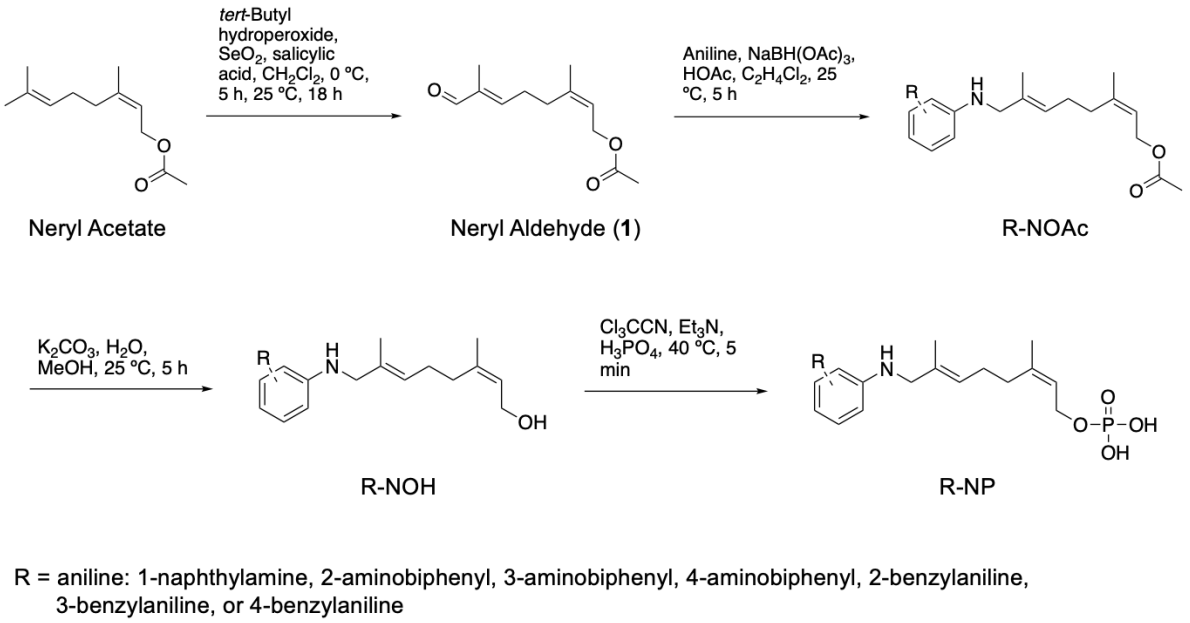

Figure 24: Bulky neryl monophosphate analogue chemical synthesis scheme

The first step of this process utilized neryl acetate, which is commercially available and reasonably affordable. Neryl acetate served as the main scaffold, or linker, of the enzyme probes, on which additional functionality was subsequently incorporated. Neryl acetate has a *cis* (Z) α-

isoprene and was used in place of the isomer, geranyl acetate, in consideration of the reported stereochemical requirements for PGT catalysis.[9] In order to incorporate the chosen anilines, the first step of this synthetic process involved oxidizing the terminal isoprene to an aldehyde using *tert*-butyl hydroperoxide and selenium dioxide. The reaction produces a mixture of neryl alcohol and carboxylic acid in addition to the target aldehyde (**1**) (24% yield), which was purified by flash chromatography on silica gel with a mobile phase of ethyl acetate and hexanes.

The next step of this process involved incorporating a set of chosen anilines with select functionality into the short-chain neryl analogues. Previous work with a different set of probes found that aryl groups are isosteric with isoprene units, so the objective of this research was to determine the extent of isosterism with PGTs by increasing the size of the isoprenoid substrate.[79] Additionally, it was hypothesized that PGTs would be more likely to accept synthetically tractable isoprenoid analogues with aromatic groups that mimicked the native BP substrate (**Figure 25**). To test this hypothesis and study the substrate specificity of multiple PGTs, a set of probes was designed with aromatic groups that varied in size and stereochemical arrangement. Seven different anilines were chosen for this endeavor, including 1-naphthylamine (1-NA), 2-aminobiphenyl (2-ABP), 3-aminobiphenyl (3-ABP), 4-aminobiphenyl (4-ABP), 2-benzylaniline (2-BA), 3-benzylaniline (3-BA), and 4-benzylaniline (4-BA) (**Figure 25**).

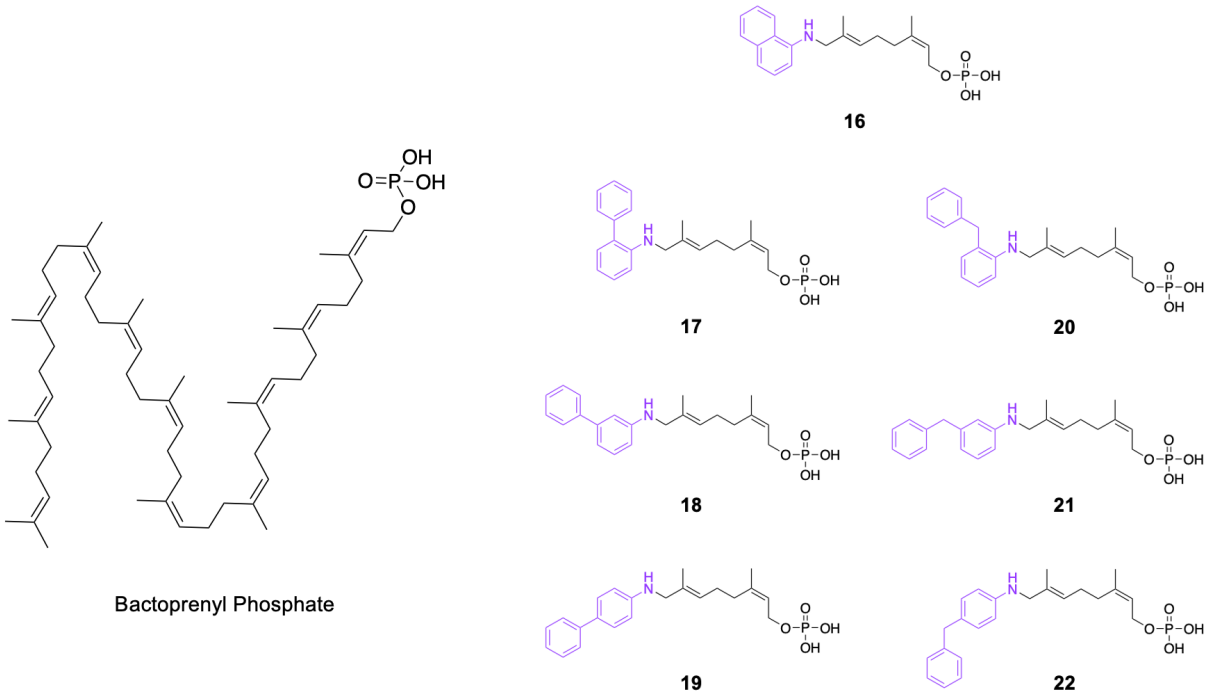

Figure 25: Structural comparison of bactoprenyl phosphate (BP) and the seven bulky isoprenoid analogues (**16-22**), with the anilines (**R-**) shown in purple

Following oxidation, neryl aldehyde (**1**) underwent reductive amination with the respective anilines in separate reactions using sodium triacetoxyborohydride ($NaBH(OAc)_3$) and acetic acid (HOAc) to produce aniline-incorporated neryl acetate (**R-NOAc**). Initial attempts with these reactions included titanium tetrachloride ($TiCl_4$) and pyridine, but the resulting products were difficult to identify and purify due to the formation of numerous side products. $TiCl_4$ was likely too harsh for these reactions, and the milder $NaBH(OAc)_3$ and HOAc combination worked better (53-94% yield) (**Figure 26**). Formation of the fluorescent or UV-active **R-NOAc** products was monitored by TLC, and the products were similarly purified by flash chromatography on silica gel with ethyl acetate and hexanes.

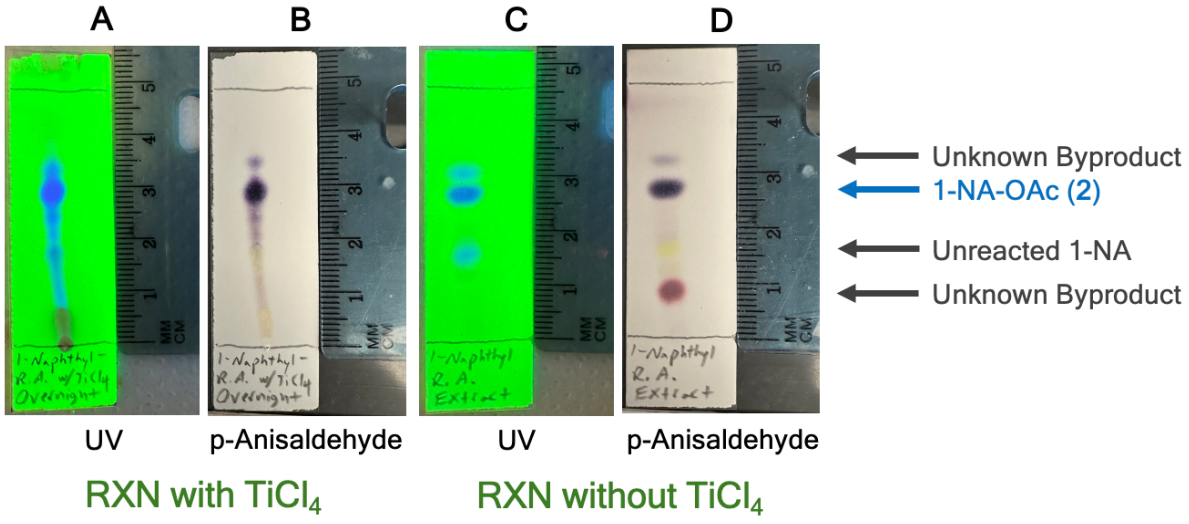

Figure 26: TLCs comparing the 1-naphthylamine reductive amination reaction using titanium tetrachloride (**A** and **B**) versus the reaction without it (**C** and **D**). TLC plates were visualized under 254 nm UV light (**A** and **C**), treated with p-anisaldehyde spray, and heated (**B** and **D**).

3.1.2: Forming the Reactive End

After incorporating the anilines at the terminal end of the molecules, the next part of the synthetic process involved forming the recognition group at the reactive end. For PGTs, the necessary functional group for catalysis is a monophosphate. This process began by deacetylating the **R-NOAc** compounds via a saponification reaction using an alkaline solution of potassium carbonate to cleave the ester into an alcohol (**R-NOH**) (55-100% yield). The resulting alcohols were purified by flash chromatography and analyzed spectrophotometrically (**Table 2**) before proceeding to the phosphorylation reaction. This analysis was performed to determine the maximum absorbance and fluorescence emission values for each compound, which were later used to detect and isolate the final products by HPLC. Additionally, an extinction coefficient was derived from these analyses to quantify the yield of the final phosphorylated product.

Table 2: R-NOH spectrophotometric analysis data

R-NOH Compounds	Maximum Absorbance (nm)	Fluorescence Emission (nm)	Extinction Coefficient ($M^{-1}cm^{-1}$)
1-NA-OH	340	420	6,559
2-ABP-OH	310	420	3,475
3-ABP-OH	320	420	2,220
4-ABP-OH	305	380	41,787
2-BA-OH	300	350*	3,498
3-BA-OH	305	350*	2,845
4-BA-OH	305	360*	2,376

*An unexpected fluorescence emission was detected for the non-fluorescent benzylanilines

The last step of the synthesis pathway to form the monophosphate ultimately proved to be the most challenging. Previous work from the Troutman Group utilized a two-step phosphorylation method that involved brominating the alcohol immediately before phosphorylating with tetra-*n*-butylammonium dihydrogen phosphate (TNBAP).[88] The purpose for using TNBAP was to solubilize an otherwise hydrophilic phosphate in organic solvents to react with the isoprenoid analogues. However, the reaction was notoriously difficult and labor-intensive for multiple reasons. The biggest issue was the need to replace the bulky tetra-*n*-butylammonium ion that associates with the phosphoryl group with a smaller ammonium ion via ion exchange chromatography. This technique required multiple steps to prepare the column before a small volume of sample could be passed through it. After the eluate showed a subtle change in pH, it was collected, and the compound was concentrated by lyophilization. Multiple passes were often required to completely exchange the TNBAP, which consequently led to a significant loss of product.

In an attempt to improve the phosphorylation reaction, an alternative method by Keller et al. was investigated.[84] Rather than brominating the alcohol and phosphorylating with TNBAP, this reaction offered the advantage of directly phosphorylating the alcohol in a single step using

bis-triethylammonium phosphate (TEAP). It was also hypothesized that since TEAP is smaller than TNBAP, the phosphoryl group may be comparatively less hindered when associated with TEAP, or alternatively, the smaller ion could lead to better results with ion exchange chromatography. Conversely, this method had the disadvantage of forming a mixture of mono-, di-, and triphosphates along with some unreacted alcohol, and the monophosphate had to be isolated and purified by HPLC (**Figure 27**).

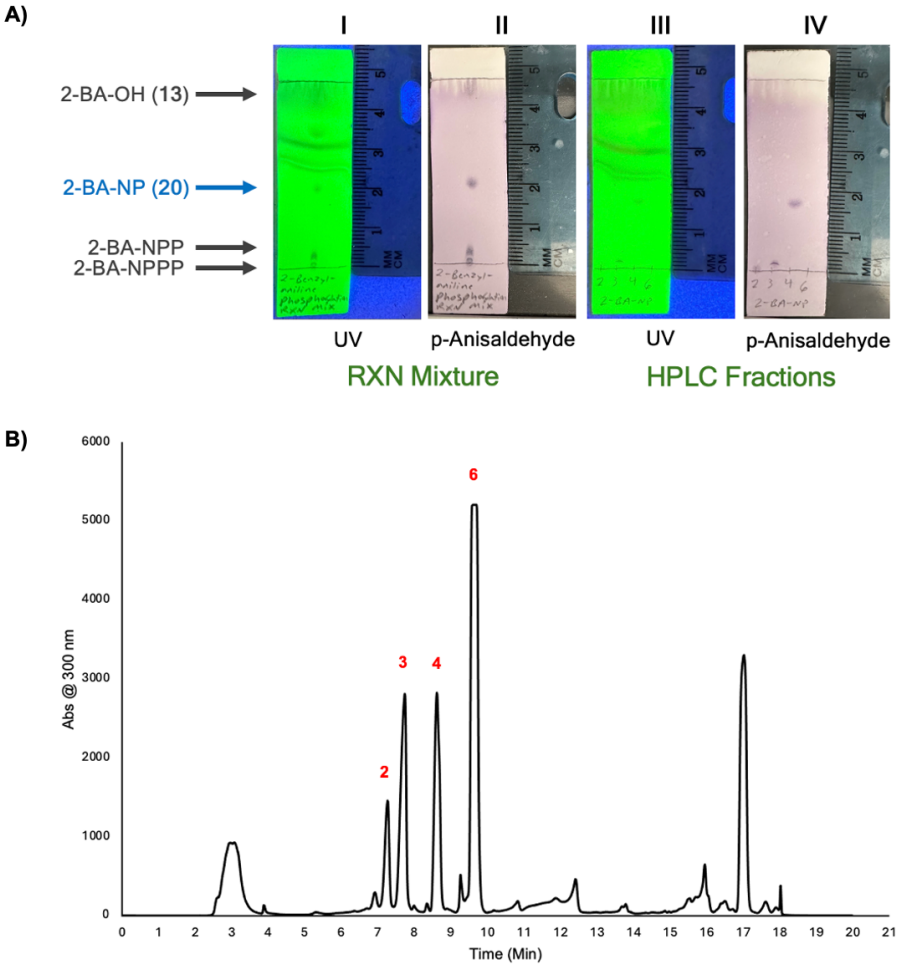

Figure 27: **A**) TLC analysis of the 2-benzylaniline neryl phosphate reaction mixture (**I** and **II**) and fractions 2, 3, 4, and 6, collected by HPLC (**III** and **IV**) [visualized under 254 nm UV light (**I** and **III**), treated with p-anisaldehyde spray, and heated (**II** and **IV**)]. **B**) HPLC chromatogram of the 2-BA-NP (**20**) reaction mixture, with peaks labeled in red corresponding to 2-BA-OH (**13**) (fraction **6**) and the tri- (fraction **2**), di- (fraction **3**), and monophosphate (fraction **4**).

HPLC fractions containing the monophosphate were frozen and lyophilized before undergoing ion exchange with 25 mM ammonium bicarbonate. In an attempt to improve product recovery through the ion exchange process, an alternative collection method was developed by relying on fluorescence instead of pH (**Figure A1**). Considering how most of the analogues were fluorescent (**16-19**), 10 mL aliquots of eluate were separately collected and individually assayed under 254 nm UV light; aliquots that contained the fluorescent product were pooled and concentrated by lyophilization. Lastly, the dried product was dissolved in D_2O and analyzed by ^{1}H and ^{31}P NMR (**Figure 28**). These analyses were mostly qualitative due to the low resolution, which was a consequence of low product concentration (0.8-36% yield). NMR was primarily used to assess the effectiveness of ion exchange and ensure that triethylammonium was no longer present. The samples that appeared to have successfully exchanged triethylammonium were then characterized by LC-MS in SIM mode (**Figure 29**).

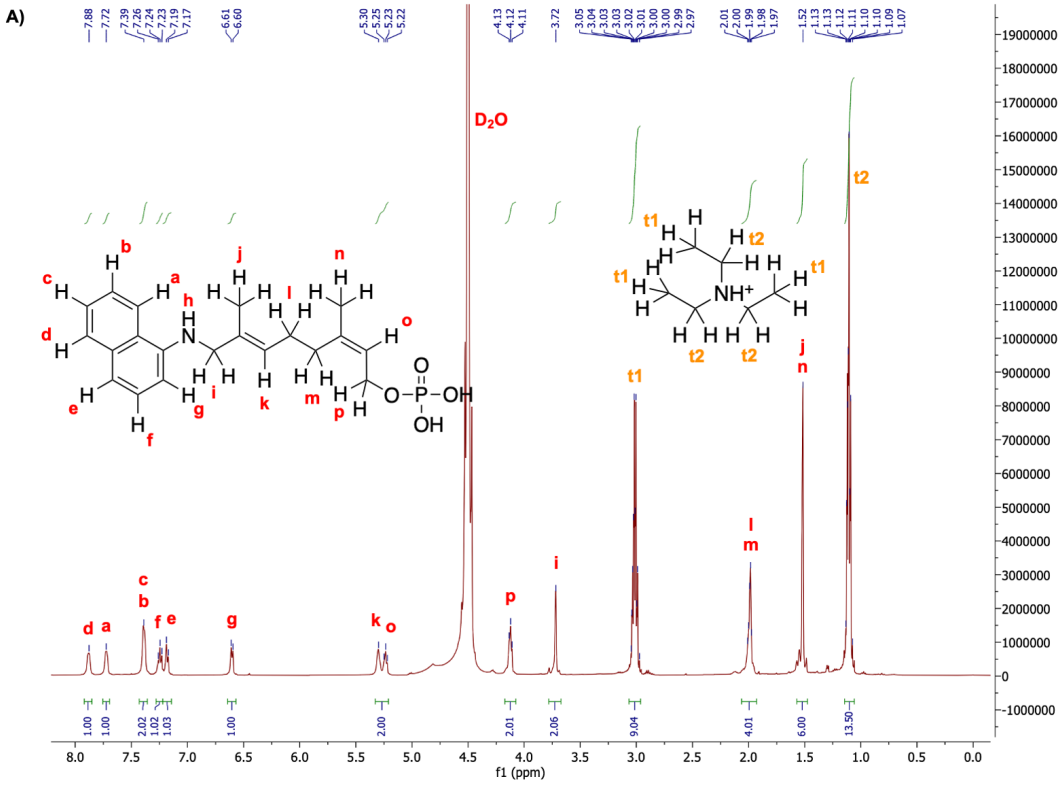

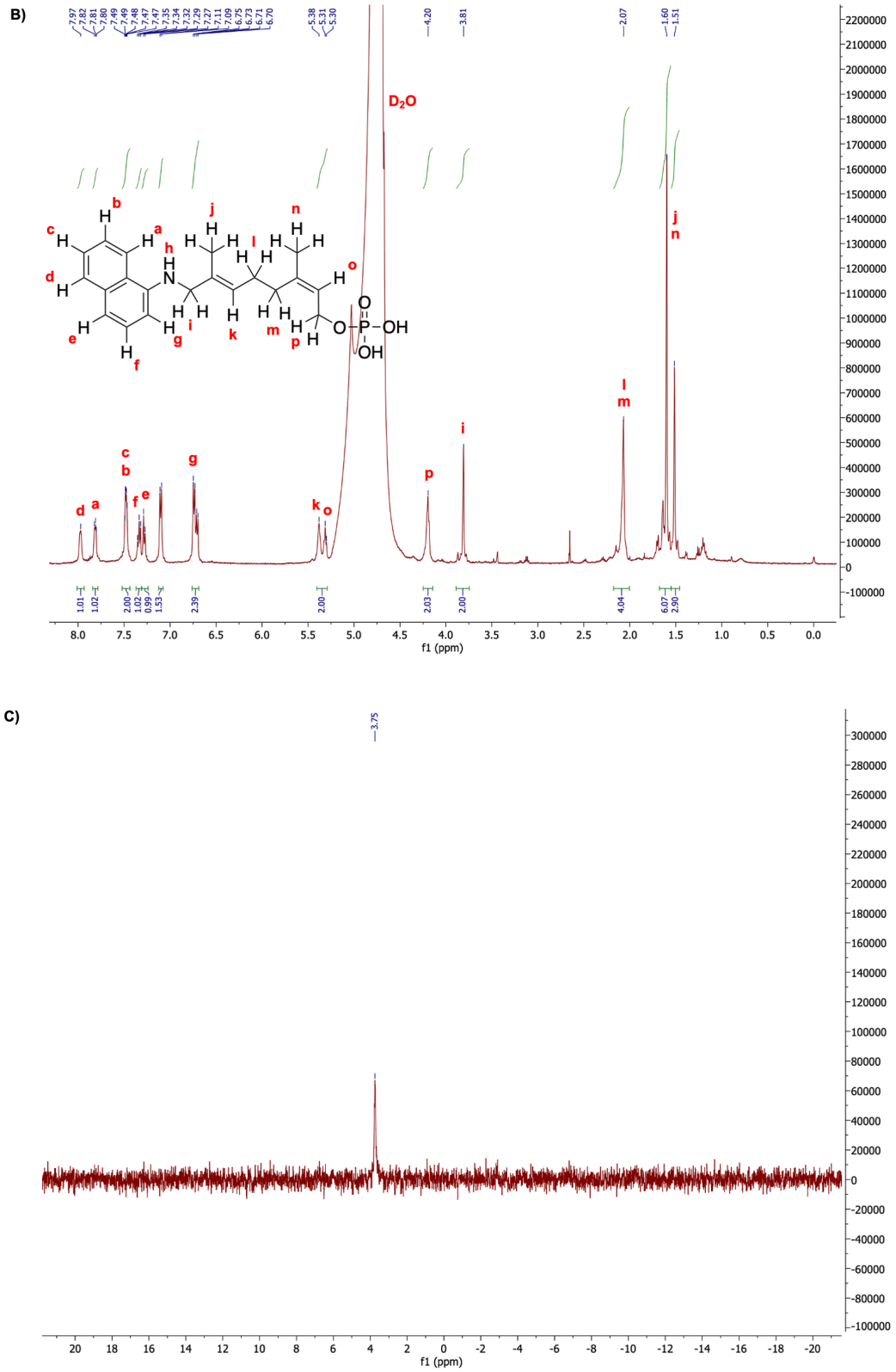

Figure 28: ^{1}H and ^{31}P NMR spectra comparing 1-NA-NP (**16**) before (**A**) and after (**B** and **C**) ion exchange

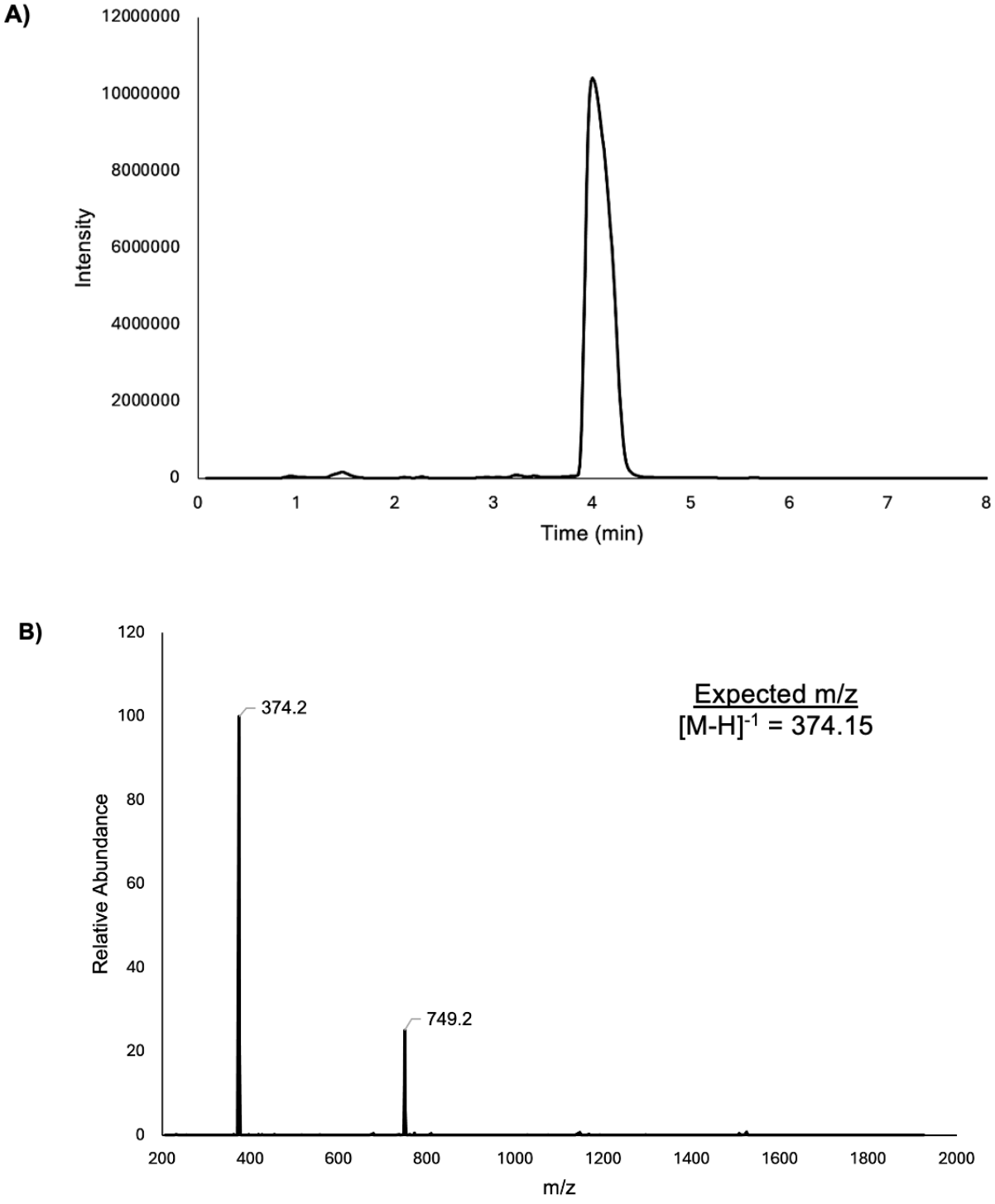

Figure 29: LC-MS chromatogram (**A**) and mass spectrum (**B**) for 1-NA-NP (**16**) after ion exchange

3.2: Chemoenzymatic Synthesis of Sugar Substrates

3.2.1: Chemoenzymatic Synthesis of UDP-diNAcBac

The monoPGT, PglC, catalyzes the transfer of phospho-diNAcBac from UDP-diNAcBac to its monophosphorylated isoprenoid substrate. UDP-diNAcBac is a rare sugar nucleotide that is reportedly formed through a series of enzymatic reactions involving PglF, PglE, and PglD in *C. jejuni* (**Figure 30**).[3, 86] The sugar is formed by converting UDP-GlcNAc to the UDP-4-keto-sugar by the dehydratase, PglF. Next, UDP-4-keto-sugar is further modified to the UDP-4-amino-sugar by the aminotransferase, PglE. And lastly, UDP-diNAcBac is formed after the *N*-acetyltransferase, PglD, reacts with the UDP-4-amino-sugar.

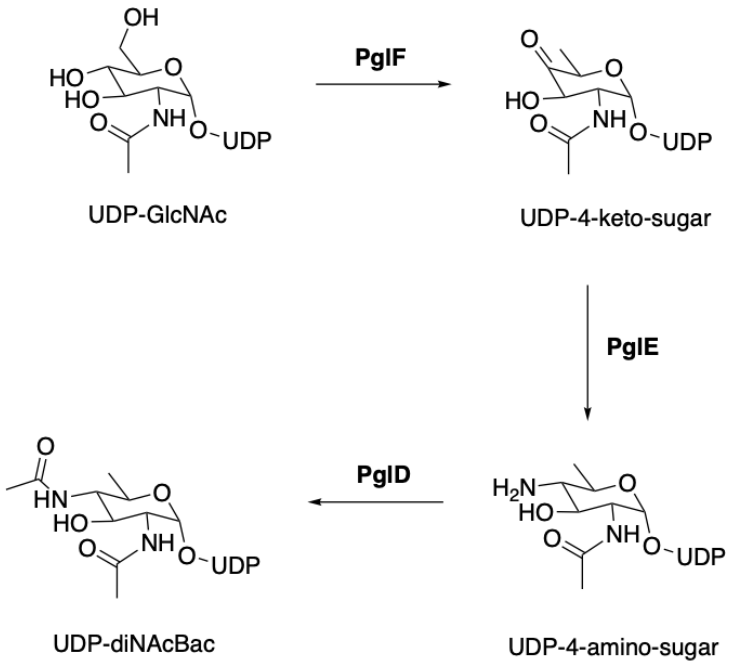

Figure 30: Chemoenzymatic synthesis of UDP-diNAcBac

The three sugar-modifying Pgl enzymes were expressed from transformed strains of *E. coli* and purified. Following expression, the proteins were analyzed by SDS-PAGE and Western

blotting (**Figure 31**), and the concentrations were calculated spectrophotometrically (**Table 3**). The chemoenzymatic reaction was initially carried out according to the previously reported specifications—adding each enzyme individually and incubating for 1 h between each addition.[86, 87] However, after multiple unsuccessful attempts, it was concluded that the Pgl enzymes were likely functioning poorly. PglF was the main culprit, which evidently needs to be isolated in the presence of NAD^+ throughout the protein expression process. It was also discovered that a two-step coupled reaction with PglF and PglE seemed to improve turnover of UDP-GlcNAc to UDP-4-amino-sugar. After the reaction conditions were modified and PglD was added, UDP-diNAcBac was formed from UDP-4-amino-sugar (**Figure 32**). UDP-diNAcBac was quantified using HPLC chromatography by integrating the product peak and comparing it to the initial UDP-GlcNAc peak with a known concentration. The reaction produced a final concentration of 0.45 mM UDP-diNAcBac.

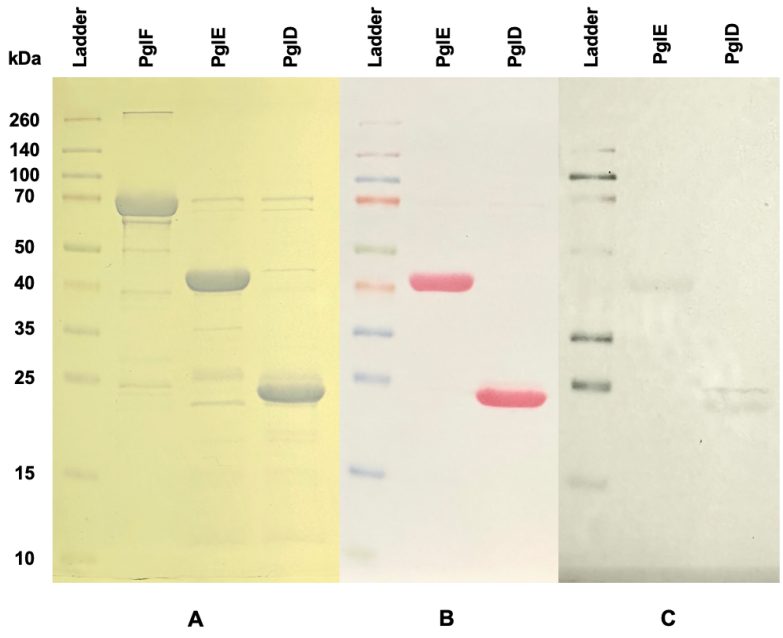

Figure 31: Protein analysis of PglF, PglE, and PglD used in the chemoenzymatic synthesis of UDP-diNAcBac. The shown techniques include SDS-PAGE (stained with Coomassie) (**A**), Ponceau staining (**B**), and Western blot (**C**).

Table 3: Molecular weight and concentration of sugar synthesis enzymes

Enzyme	Protein Molecular Weight (kDa)	Enzyme Concentration (mg/mL)
PglF	93*	2.475
PglE	44	3.989
PglD	24	5.110
WcfR	45	2.799

*GST-tagged

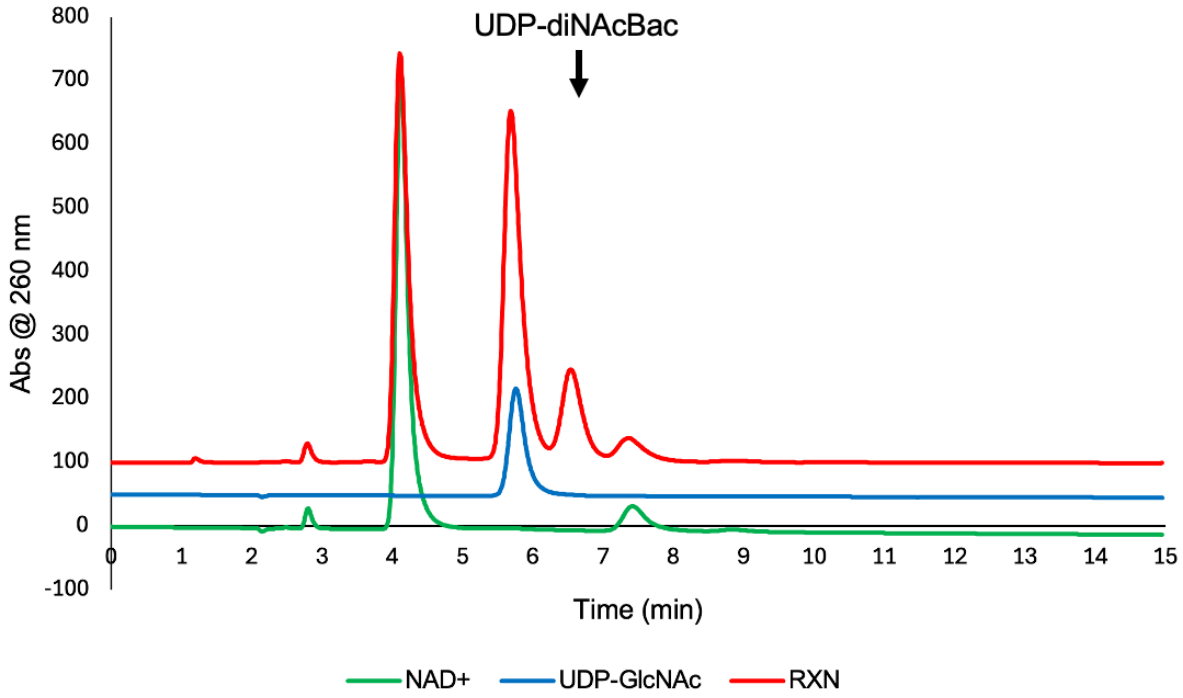

Figure 32: HPLC chromatogram of UDP-diNAcBac synthesis, showing the final reaction mixture (in red), NAD^+ (in green), and UDP-GlcNAc (in blue). Chromatograms were offset along the y-axis by 50 units for visual clarity.

3.2.2: Chemoenzymatic Synthesis of UDP-AADGal

WcfS is a monoPGT in *B. fragilis* that is predicted to catalyze the transfer of phospho-AADGal from UDP-AADGal to its monophosphorylated isoprenoid substrate. Like UDP-diNAcBac, UDP-AADGal is also a rare sugar nucleotide that can be formed

chemoenzymatically using the dehydratase, PglF, and the aminotransferase, WcfR (**Figure 33**).[44] The reaction begins with the conversion of UDP-GlcNAc to UDP-4-keto-sugar by PglF, and ends with the subsequent conversion of UDP-4-keto-sugar to UDP-AADGal by WcfR.

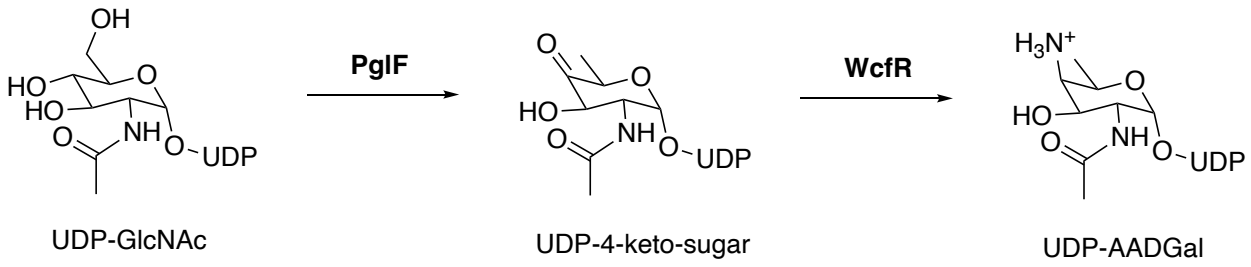

Figure 33: Chemoenzymatic synthesis of UDP-AADGal

WcfR was expressed and purified according to the usual conditions for soluble proteins along with PglF, which was isolated in the presence of NAD^+. Both proteins were analyzed by SDS-PAGE and Western blotting (**Figure 34**), and the concentrations were calculated spectrophotometrically (**Table 3**). Similarly to the UDP-diNAcBac reaction, PglF appeared to function poorly in a sequential reaction, but performed significantly better when coupled with WcfR. Conversion of UDP-GlcNAc to UDP-AADGal was achieved when the two enzymes were added to the reaction mixture simultaneously (**Figure 35**). The concentration of UDP-AADGal in the reaction mixture was quantified similarly to UDP-diNAcBac using HPLC chromatography. The integration value of the product peak was compared it to the initial UDP-GlcNAc peak with a known concentration. The reaction produced a final concentration of 0.66 mM UDP-AADGal.

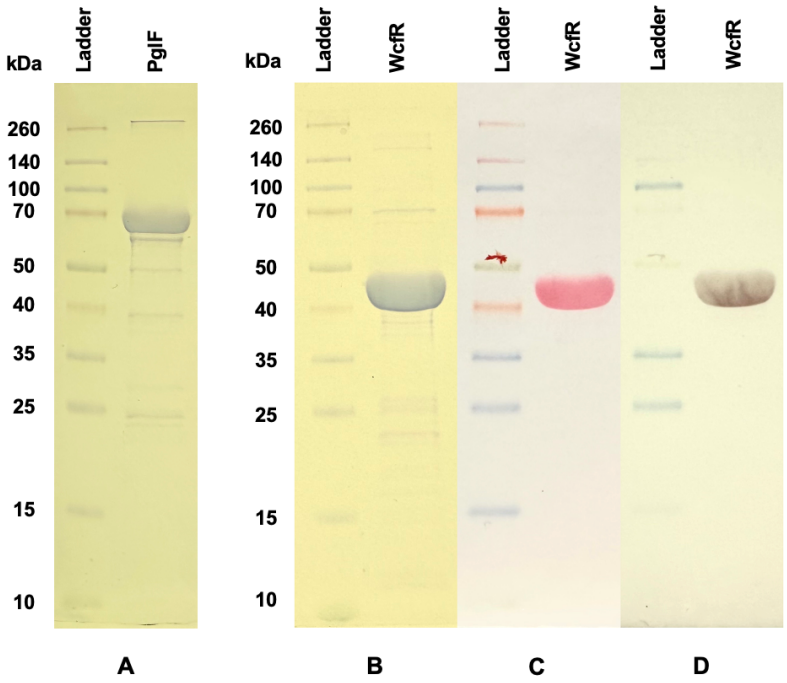

Figure 34: Protein analysis of PglF and WcfR used in the chemoenzymatic synthesis of UDP-AADGal. The shown techniques include SDS-PAGE (stained with Coomassie) (**A** and **B**), Ponceau staining (**C**), and Western blot (**D**).

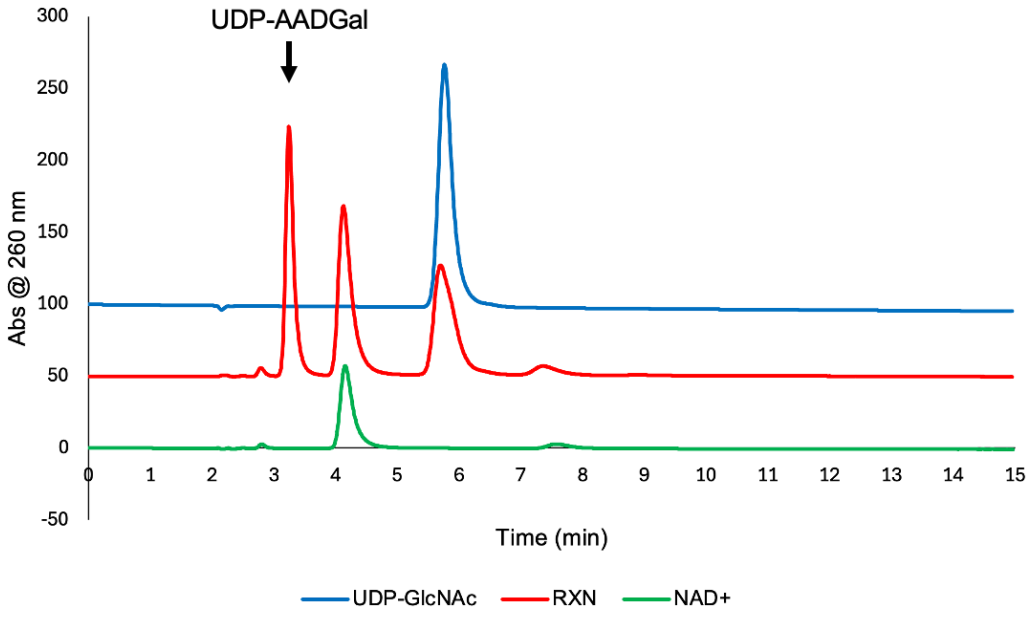

Figure 35: HPLC chromatogram of UDP-AADGal synthesis, showing the final reaction mixture (in red), NAD^+ (in green), and UDP-GlcNAc (in blue). Chromatograms were offset along the y-axis by 50 units for visual clarity.

3.3: PGT Expression and Chemoenzymatic Reactions with Bulky Analogues

3.3.1: PGT Expression

PglC and WcfS were overexpressed in a transformed strain of C41(DE3) *E. coli* expression cells. Both enzymes are integral membrane proteins and therefore are imbedded in the cellular membrane. The proteins were isolated as membrane fractions without the use of detergents. Detergents were avoided in consideration of the analytical equipment (i.e., LC-MS and C18 column), which would later be used to analyze the subsequent chemoenzymatic reactions. Since the proteins were collected as membrane fractions, an uninduced culture was used as a control to ensure that the target proteins were effectively overexpressed. Both proteins were analyzed by SDS-PAGE and Western blotting (**Figure 36** and **37**) and compared to the expected molecular weight of each protein (**Table 4**).

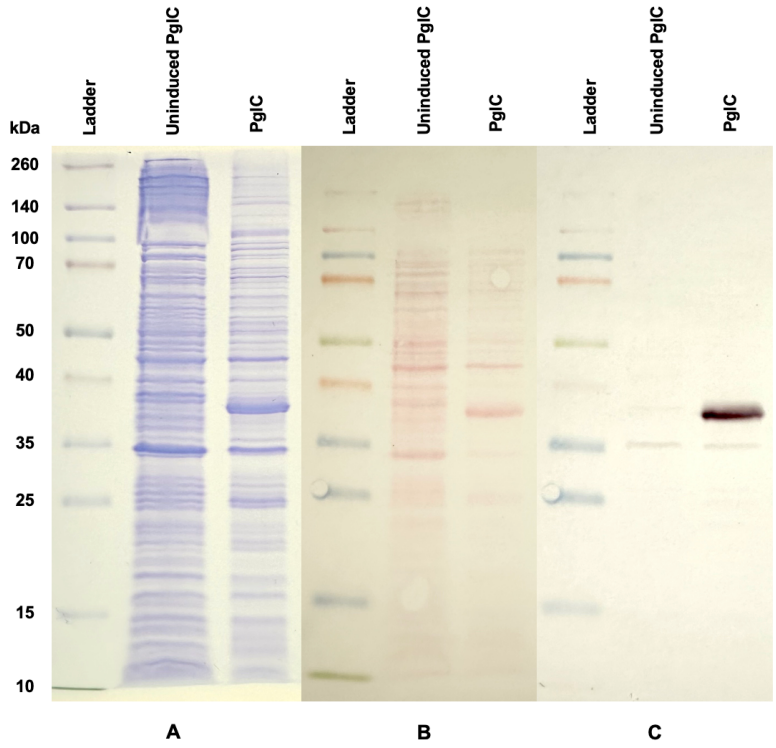

Figure 36: Protein analysis of PglC with an uninduced control. The shown techniques include SDS-PAGE (stained with Coomassie) (**A**), Ponceau staining (**B**), and Western blot (**C**).

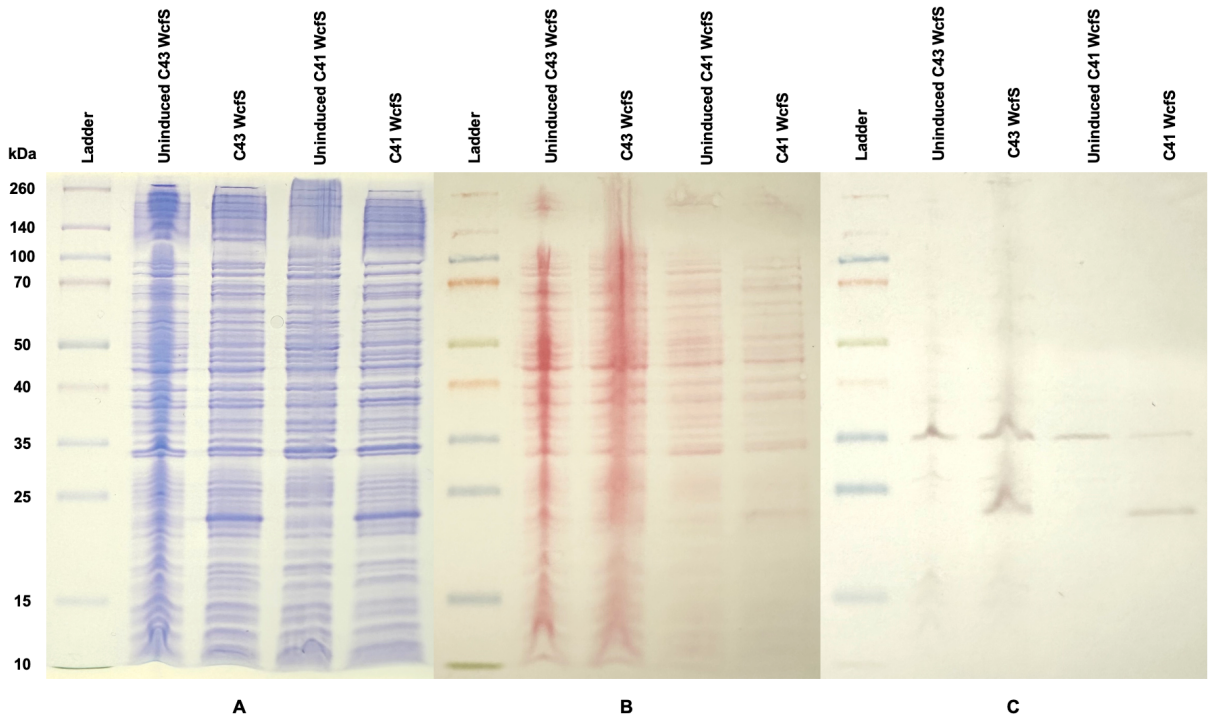

Figure 37: Protein analysis of WcfS with an uninduced control in C41 and C43 expression cells. The shown techniques include SDS-PAGE (stained with Coomassie) (**A**), Ponceau staining (**B**), and Western blot (**C**).

Table 4: Molecular weight of PGT enzymes

PGT Enzyme	Protein Molecular Weight (kDa)
PglC	38-40*
WcfS	23

*SUMO-tagged

3.3.2: Chemoenzymatic Reactions with PGTs and Bulky Analogues

The final part of this research involved combining all the individual components described above and determining what worked together in a series of chemoenzymatic reactions. In these reactions, the seven bulky isoprenoid analogues were added to separate mixtures containing the requisite sugar substrates and their corresponding monoPGT catalysts. The

reactions were carried out according to a slightly modified method that was previously published by the Troutman Group for similar chemoenzymatic reactions with polyPGTs.[36]

In the first round of reactions with PglC, 10 μM of each isoprenoid analogue was combined with 100 μM of the synthesized UDP-diNAcBac and 4 μL PglC (membrane fraction) in separate reaction mixtures. Additionally, each 40 μL mixture contained 200 mM bicine (pH 8.5), 5 mM $MgCl_2$, 100 mM KCl, and 5% (v/v) *n*-propanol. The latter was used in place of 15 mM cholate, which ordinarily serves as an emulsifier; the isoprenoids used in these reactions are water soluble and were therefore sufficiently solubilized in propanol without the need for a detergent. Cholate was also avoided in consideration of the subsequent analysis by LC-MS. After the reaction mixtures were incubated at 37 °C and shaken at 200 rpm for 2 h, 10 μL aliquots were analyzed by LC-MS in SIM mode (negative ion mode) using a gradient method with 0.1% ammonium hydroxide and *n*-propanol.

Previous research that utilized 8-anilinogeranyl diphosphate (AGPP) as an isoprenoid enzyme probe showed an isosteric relationship between aryl groups and isoprene units.[70] With respect to these findings, it was hypothesized that the aminobiphenyl probes (2-ABP-NP, 3-ABP-NP, and 4-ABP-NP) would be accepted by PGTs, whereas the naphthylamine and benzylaniline probes would not. The rationale for this hypothesis was that the fused aromatic ring system in naphthylamine (1-NA-NP) and the additional methylene separating the aromatic rings in benzylaniline (2-BA-NP, 3-BA-NP, and 4-BA-NP) would disrupt the isosteric relationship and would not mimic the native isoprenoid structure found in BP. However, this hypothesis was ultimately rejected after the first round of chemoenzymatic reactions with PglC. It was found that all seven bulky analogues were accepted by PglC and the expected $[M-H]^{-1}$ values for each

diNAcBac-linked analogue was detected in high abundance. **Figure 38** exemplifies the results of these reactions; the data for the remaining probes are provided in Appendix D (**Figures D15-21**).

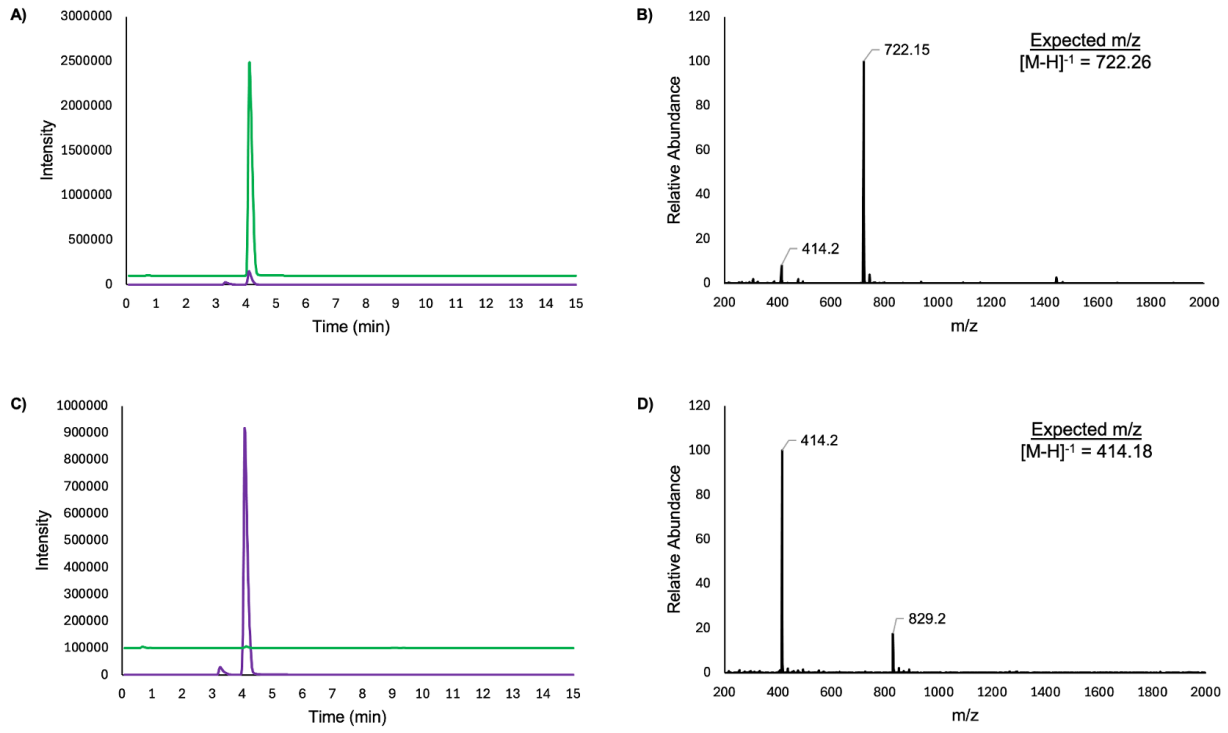

Figure 38: LC-MS chromatograms (**A** and **C**) and mass spectra (**B** and **D**) of diNAcBac-linked 4-BA-NP after reacting with PglC (**A** and **B**) compared to a control reaction (**C** and **D**) that excluded the sugar substrate. The SIM signal for diNAcBac-linked 4-BA-NP is shown in green and the signal for the 4-BA-NP (**22**) probe is shown in purple.

In the second round of chemoenzymatic reactions, WcfS and UDP-AADGal were used in place of PglC and UDP-diNAcBac. The enzyme and sugar substrate were similarly combined with the seven bulky isoprenoid analogues in separate reaction mixtures and were subjected to the same reaction conditions described above. Based on previous work with WcfS by the Troutman Group, it was hypothesized that the enzyme would not accept any of the seven bulky analogues. A published study found that the short-chain neryl phosphate probe, 2-aminobenzamide neryl phosphate (2AB-N-P), was not accepted by WcfS.[75] These results were

supported by additional unpublished preliminary studies using 2AB-N-P, 2-nitrileanilinoneryl phosphate (2CN-NP), and azide neryl phosphate (Az-NP), which were also not accepted by WcfS, despite working with PglC. However, the hypothesis regarding WcfS and the short-chain probes used in this work was ultimately rejected after finding that two of the seven bulky analogues (i.e., 3-ABP-NP and 4-BA-NP) were accepted by the enzyme and produced the expected $[M-H]^{-1}$ values for the AADGal-linked analogues (**Figures 39** and **40**).

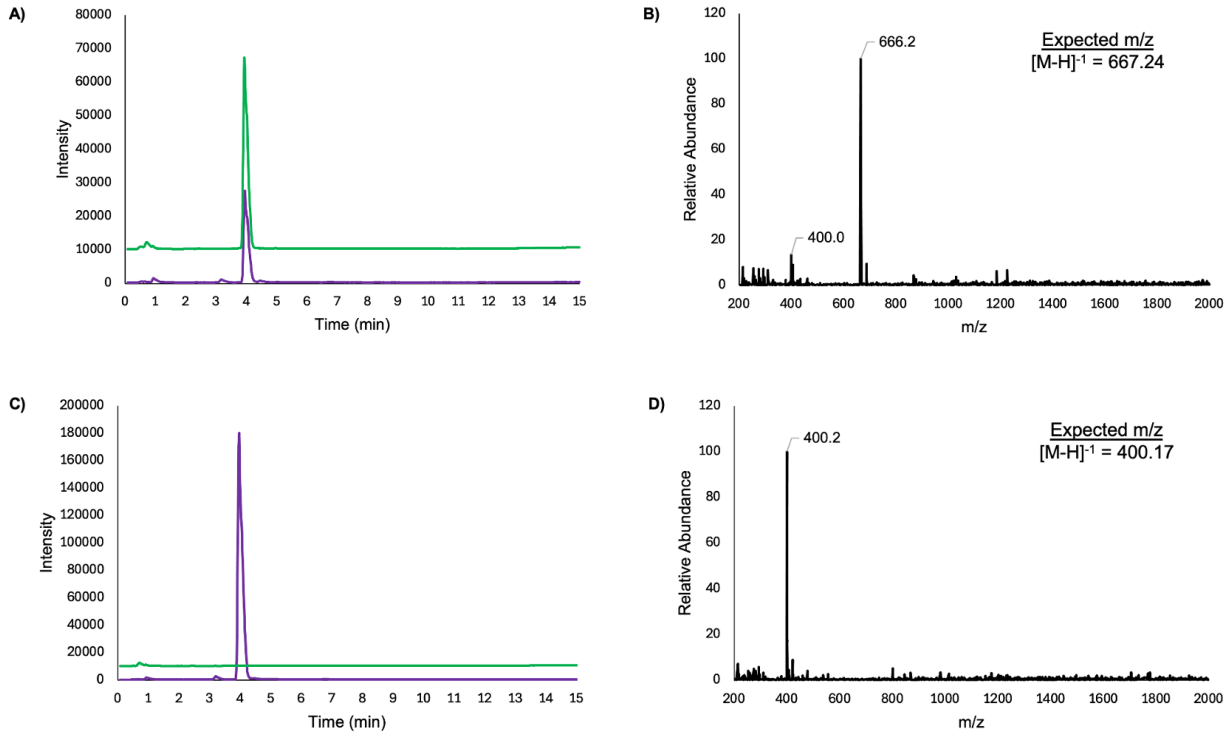

Figure 39: LC-MS chromatograms (**A** and **C**) and mass spectra (**B** and **D**) of AADGal-linked 3-ABP-NP after reacting with WcfS (**A** and **B**) compared to a control reaction (**C** and **D**) that excluded the sugar substrate. The SIM signal for AADGal-linked 3-ABP-NP is shown in green and the signal for the 3-ABP-NP (**18**) probe is shown in purple.

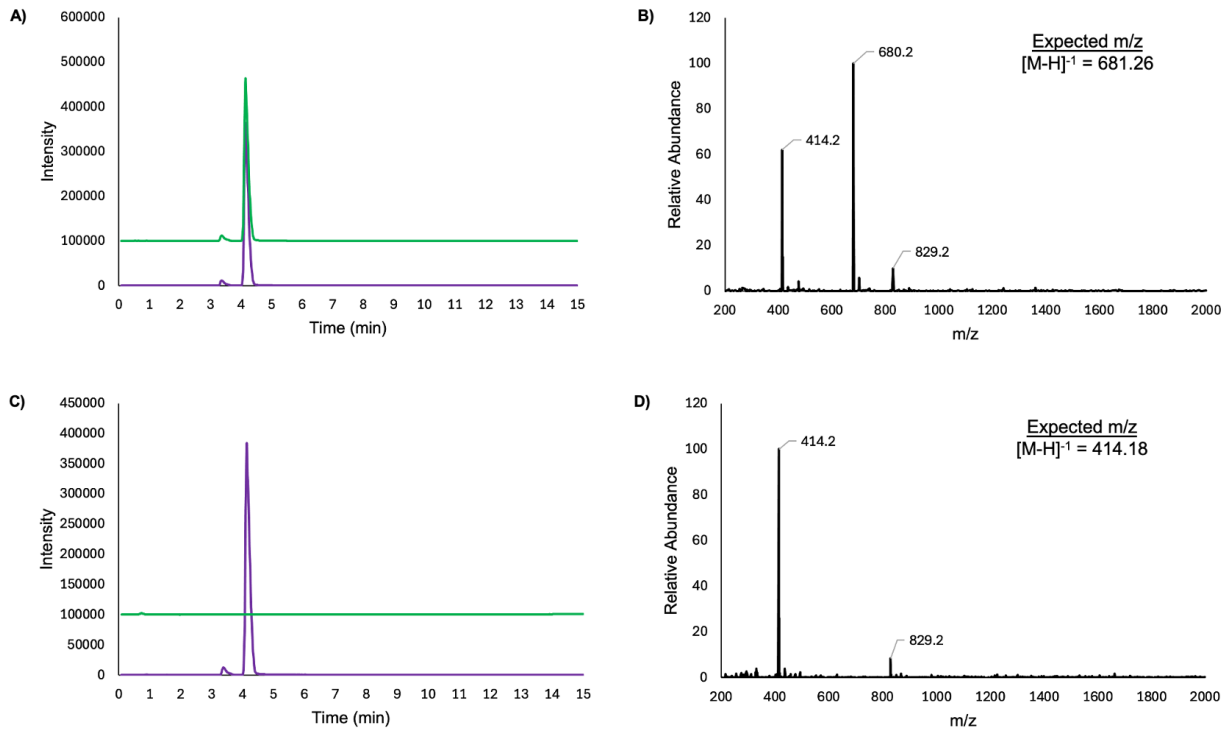

Figure 40: LC-MS chromatograms (**A** and **C**) and mass spectra (**B** and **D**) of AADGal-linked 4-BA-NP after reacting with WcfS (**A** and **B**) compared to a control reaction (**C** and **D**) that excluded the sugar substrate. The SIM signal for AADGal-linked 4-BA-NP is shown in green and the signal for the 4-BA-NP (**22**) probe is shown in purple.

After comparing the results of both rounds of chemoenzymatic reactions, it was evident that WcfS is more selective of its substrates compared to PglC. Despite setting up both reactions under the same conditions using equivalent concentrations of bulky analogues and sugar substrates, WcfS displayed poorer turnover compared to PglC. These results were not completely surprising, however, considering it has been well reported that PglC demonstrates substrate promiscuity, while WcfS is notoriously more selective of its substrates.

The LC-MS data described above provide an initial, qualitative understanding of how these two monoPGTs function with the seven bulky isoprenoid analogues. A quantitative analysis of these reactions would provide a more concise understanding of how well both enzymes function with each bulky analogue, which could be done by quantifying the turnover in each

reaction. This analysis could be carried out by measuring the integration value of the probe peak in the control reaction and comparing it to the probe peak in the chemoenzymatic reaction—for example, the purple peaks in **Figures 40C** and **40A**, respectively. Unfortunately, due to time constraints and some unexpected complications with the LC-MS, the chemoenzymatic reactions could not be repeated for analysis at present.

CHAPTER 4: CONCLUSIONS AND FUTURE WORK

4.1: Conclusions

The overall purpose of this project was to glean more information about the initiating role of PGTs in the biosynthesis of bacterial glycans and learn more about their function. One of the biggest gaps in knowledge regarding PGT function concerns the lipid substrate on which glycans are built. It is not fully understood how these enzymes select for their substrates and whether they can accept alternative lipid substrates in place of the native BP. To further elucidate the substrate specificities of PGTs, a small library of isoprenoid analogues with varying functionality was developed. The library consisted of seven different short-chain neryl phosphate analogues that were chemically synthesized with an array of bulky aromatic groups incorporated at the terminal end of the molecules. In this work, the seven bulky isoprenoid analogues were utilized to probe two different monoPGTs and determine whether either enzyme would accept the synthetic analogues.

4.1.1: Bulky Isoprenoid Analogue Chemical Synthesis

A series of short-chain isoprenoid analogues were built using neryl acetate as an abundant and affordable starting material. The oxidized neryl aldehyde served as a convenient scaffold for building PGT enzyme probes due to its short chain length and *cis* (Z) α-isoprene. One question that remained uncertain was whether short-chain isoprenoids could be used as small-molecule probes for PGTs. Despite previous studies indicating that chain length is seemingly less important than double bond geometry and α-isoprene stereochemistry, previous studies using short-chain isoprenoids offered conflicting results.[9, 75] Additionally, more evidence was needed to support the isosteric relationship between aryl groups and isoprene units that was demonstrated

with previous enzyme probes.[79, 81] To test the extent of this isosteric relationship with PGTs, a selection of bulky aromatic groups (i.e., naphthylamine, aminobiphenyl, and benzylaniline) with varying sizes and stereochemical arrangements was incorporated at the terminal end of the isoprenoid analogues.

To synthetically incorporate the chosen bulky groups, it was found that a previously reported reductive amination reaction was not suitable for these molecules.[79, 83] The decision to modify the reductive amination method and omit $TiCl_4$ proved to be more effective, as the reaction produced fewer side products, which made it easier to isolate and purify the target product in greater yields. Furthermore, the modified reductive amination method utilized for this project is a promising alternative that could be used in future work to incorporate additional aromatic groups or different functional groups.

The biggest synthetic challenge arose when attempting to form the reactive end of the PGT enzyme probes. To form the necessary monophosphate, a phosphorylation method using tetra-*n*-butylammonium dihydrogen phosphate (TNBAP) was initially attempted but was later avoided in response to numerous issues.[88] First, a bromination reaction was required prior to phosphorylation. Second, TNBAP needed to be prepared ahead of time and the synthesis required multiple difficult steps. Third, purification by ion exchange was necessary because of the massive size of TNBAP. In response to these disadvantages, an alternative method was sought out, which led to trying a phosphorylation method published by Keller et al.[84]

The Keller phosphorylation method helped eliminate some of the challenges from the initial method and offered some advantages, but it likewise had its own disadvantages. This method had the major advantage of avoiding the painstaking and time-consuming process of brominating and phosphorylating under argon gas in an overnight reaction. Instead, the Keller

reaction utilized bis-triethylammonium phosphate (TEAP), and the entire reaction could be completed in a few minutes. Additionally, TEAP is smaller than TNBAP and the resulting product may not need to be purified by ion exchange to be effective. However, the Keller reaction had the major disadvantage of producing multiple products, resulting in a lower yield compared to the initial method—especially after opting to purify by ion exchange. Overall, though, the Keller method was effective and could be used in future reactions as an alternative to the initial phosphorylation method.

4.1.2: Probing PglC and WcfS

After successfully synthesizing, purifying, and characterizing the seven bulky isoprenoid analogues, the last component of this work involved reacting the probes with various PGTs to see if they would be effective. The monoPGTs, PglC and WcfS, were chosen to fulfil this objective for multiple reasons. First, PglC is recognized in the literature as a model, prototypic monoPGT, considering its protein structure has been crystallized and published. PglC has also been reported to function as a PGT in the pathogenic species, *C. jejuni*.[9, 26] Conversely, while WcfS has been used by the Troutman Group for various purposes, more information is needed regarding its function and substrate specificity. WcfS was also chosen because the enzyme reportedly serves as a PGT in the mostly nonpathogenic and commensal species, *B. fragilis*.[29, 44]

In the first round of chemoenzymatic reactions with PglC, the results were rather surprising and surpassed the original hypothesis, considering all seven bulky analogues were accepted by the enzyme. It was hypothesized that only the aminobiphenyl probes would be accepted, since the additional phenyl group appeared to be the most similar to the aniline in AGPP. It was presumed that the fused ring system in naphthylamine and the methylene

separating the rings in benzylaniline would not be isosteric and mimic the native structure of BP. Following these results, it was later rationalized that PglC accepted all seven bulky analogues because the enzyme is known to be promiscuous and will therefore accept a variety of different substrates.[9, 89, 90] Conversely, WcfS is known to be more selective of its substrates, which was further supported by the second round of chemoenzymatic reactions showing that only two of the seven probes (i.e., 3-ABP-NP and 4-BA-NP) were accepted by the enzyme.

Based on the results of the chemoenzymatic reactions with PglC and WcfS, it is evident that short-chain probes using neryl phosphate are effective tools for probing monoPGTs, and the isosteric relationship between isoprene units and aryl groups is applicable to this class of enzymes as well. It was shown in this work that the seven bulky isoprenoid analogues are viable synthetically tractable probes that can be utilized to study the substrate specificity of various PGTs. In addition to supporting the previously reported substrate promiscuity of PglC, this small library of probes effectively led to the discovery of two short-chain isoprenoids that could potentially serve as alternative substrates for the highly selective monoPGT, WcfS.

4.2: Future Work

In continuation of this work, the chemoenzymatic reactions described herein using the seven bulky analogues with PglC and WcfS should be repeated to verify the reproducibility of the reactions. It would also be beneficial to test the bulky analogues with various polyPGTs (e.g., WecA, WecP, WbaP, and Cps2E) to determine if these enzymes show similar results to PglC or WcfS. Additionally, more could be done with small molecule probes as a technique to further elucidate the function of PGTs within the context of bacterial glycan biosynthesis. Using past and present research as a reference, more enzyme probes with diverse functionalities could be

developed to continue studying monoPGTs—including PglC and WcfS—along with the numerous other polyPGTs. In addition to studying the effects of substrate size on PGT function, it would also be interesting to see if chemical functionalities—such as polarity, for example—play a significant factor in substrate selectivity.

As a result of this research, it may one day be possible to uncover a variety of alternative substrates for PGT catalysis, which may be instrumental for differentiating the unique glycans produced by various species of bacteria. Moreover, the continued efforts to study bacterial glycan biosynthesis may one day help resolve the ongoing antibiotic resistance crisis and lead to the development of better treatment options for bacterial infections.

REFERENCES

1. Reid, A. J.; Eade, C. R.; Jones, K. J.; Jorgenson, M. A.; Troutman, J. M., Tracking Colanic Acid Repeat Unit Formation from Stepwise Biosynthesis Inactivation in Escherichia coil. *Biochemistry* **2021,** *60* (27), 2221-2230.

2. Scarbrough, B. A.; Eade, C. R.; Reid, A. J.; Williams, T. C.; Troutman, J. M., Lipopolysaccharide Is a 4-Aminoarabinose Donor to Exogenous Polyisoprenyl Phosphates through the Reverse Reaction of the Enzyme ArnT. *Acs Omega* **2021,** *6* (39), 25729-25741.

3. Glover, K. J.; Weerapana, E.; Chen, M. M.; Imperiali, B., Direct biochemical evidence for the utilization of UDP-bacillosamine by PglC, an essential glycosyl-1-phosphate transferase in the Campylobacter jejuni N-linked glycosylation pathway. *Biochemistry* **2006,** *45* (16), 5343-5350.

4. Guo, R. T.; Ko, T. P.; Chen, A. P.; Kuo, C. J.; Wang, A. H.; Liang, P. H., Crystal structures of undecaprenyl pyrophosphate synthase in complex with magnesium, isopentenyl pyrophosphate, and farnesyl thiopyrophosphate: roles of the metal ion and conserved residues in catalysis. *J Biol Chem* **2005,** *280* (21), 20762-74.

5. Eade, C. R.; Wallen, T. W.; Gates, C. E.; Oliverio, C. L.; Scarbrough, B. A.; Reid, A. J.; Jorgenson, M. A.; Young, K. D.; Troutman, J. M., Making the Enterobacterial Common Antigen Glycan and Measuring Its Substrate Sequestration. *Acs Chemical Biology* **2021,** *16* (4), 691-700.

6. Jumper, J.; Evans, R.; Pritzel, A.; Green, T.; Figurnov, M.; Ronneberger, O.; Tunyasuvunakool, K.; Bates, R.; Žídek, A.; Potapenko, A.; Bridgland, A.; Meyer, C.; Kohl, S. A. A.; Ballard, A. J.; Cowie, A.; Romera-Paredes, B.; Nikolov, S.; Jain, R.; Adler, J.; Back, T.; Petersen, S.; Reiman, D.; Clancy, E.; Zielinski, M.; Steinegger, M.; Pacholska, M.; Berghammer, T.; Bodenstein, S.; Silver, D.; Vinyals, O.; Senior, A. W.; Kavukcuoglu, K.; Kohli, P.; Hassabis, D., Highly accurate protein structure prediction with AlphaFold. *Nature* **2021,** *596* (7873), 583-589.

7. Varadi, M.; Anyango, S.; Deshpande, M.; Nair, S.; Natassia, C.; Yordanova, G.; Yuan, D.; Stroe, O.; Wood, G.; Laydon, A.; Žídek, A.; Green, T.; Tunyasuvunakool, K.; Petersen, S.; Jumper, J.; Clancy, E.; Green, R.; Vora, A.; Lutfi, M.; Figurnov, M.; Cowie, A.; Hobbs, N.; Kohli, P.; Kleywegt, G.; Birney, E.; Hassabis, D.; Velankar, S., AlphaFold Protein Structure Database: massively expanding the structural coverage of protein-sequence space with high-accuracy models. *Nucleic Acids Res* **2022,** *50* (D1), D439-d444.

8. Majumder, A.; Vuksanovic, N.; Ray, L. C.; Bernstein, H. M.; Allen, K. N.; Imperiali, B.; Straub, J. E., Synergistic computational and experimental studies of a phosphoglycosyl transferase membrane/ligand ensemble. *J Biol Chem* **2023,** *299* (10), 105194.

9. Chen, M. M.; Weerapana, E.; Ciepichal, E.; Stupak, J.; Reid, C. W.; Swiezewska, E.; Imperiali, B., Polyisoprenol specificity in the Campylobacter jejuni N-linked glycosylation pathway. *Biochemistry* **2007,** *46* (50), 14342-14348.

10. Anderson, A. J.; Seebald, L. M.; Arbour, C. A.; Imperiali, B., Probing Monotopic Phosphoglycosyl Transferases from Complex Cellular Milieu. *Acs Chemical Biology* **2022**.

11. TouzÉ, T.; Mengin-Lecreulx, D., Undecaprenyl Phosphate Synthesis. *EcoSal Plus* **2008,** *3* (1), 10.1128/ecosalplus.4.7.1.7.

12. Dodge, G. J.; Anderson, A. J.; He, Y.; Liu, W.; Viner, R.; Imperiali, B., Mapping the architecture of the initiating phosphoglycosyl transferase from S. enterica O-antigen biosynthesis in a liponanoparticle. *bioRxiv* **2023**.

13. Erlandsen, S. L.; Kristich, C. J.; Dunny, G. M.; Wells, C. L., High-resolution visualization of the microbial glycocalyx with low-voltage scanning electron microscopy: dependence on cationic dyes. *J Histochem Cytochem* **2004,** *52* (11), 1427-35.

14. Whitfield, C.; Paiment, A., Biosynthesis and assembly of Group 1 capsular polysaccharides in Escherichia coli and related extracellular polysaccharides in other bacteria. *Carbohydrate Research* **2003,** *338* (23), 2491-2502.

15. Mahanty, S.; Prigent, A.; Garraud, O., Immunogenicity of infectious pathogens and vaccine antigens. *BMC Immunol* **2015,** *16*, 31.

16. Silhavy, T. J.; Kahne, D.; Walker, S., The bacterial cell envelope. *Cold Spring Harb Perspect Biol* **2010,** *2* (5), a000414.

17. Kho, K.; Meredith, T. C., Extraction and Analysis of Bacterial Teichoic Acids. *Bio Protoc* **2018,** *8* (21), e3078.

18. Tra, V. N.; Dube, D. H., Glycans in pathogenic bacteria - potential for targeted covalent therapeutics and imaging agents. *Chemical Communications* **2014,** *50* (36), 4659-4673.

19. Hsieh, S. A.; Allen, P. M., Immunomodulatory Roles of Polysaccharide Capsules in the Intestine. *Front Immunol* **2020,** *11*, 690.

20. Cuthbertson, L.; Mainprize, I. L.; Naismith, J. H.; Whitfield, C., Pivotal Roles of the Outer Membrane Polysaccharide Export and Polysaccharide Copolymerase Protein Families in Export of Extracellular Polysaccharides in Gram-Negative Bacteria. *Microbiology and Molecular Biology Reviews* **2009,** *73* (1), 155-+.

21. Gao, Y.; Widmalm, G.; Im, W., Modeling and Simulation of Bacterial Outer Membranes with Lipopolysaccharides and Capsular Polysaccharides. *Journal of Chemical Information and Modeling* **2023,** *63* (5), 1592-1601.

22. Scott, P. M.; Erickson, K. M.; Troutman, J. M., Identification of the Functional Roles of Six Key Proteins in the Biosynthesis of Enterobacteriaceae Colanic Acid. *Biochemistry* **2019,** *58* (13), 1818-1830.

23. Raetz, C. R.; Whitfield, C., Lipopolysaccharide endotoxins. *Annu Rev Biochem* **2002,** *71*, 635-700.

24. Weintraub, A., Immunology of bacterial polysaccharide antigens. *Carbohydr Res* **2003,** *338* (23), 2539-47.

25. Campylobacter (Campylobacteriosis). Center for Disease Control and Prevention (CDC), p https://www.cdc.gov/campylobacter/index.html.

26. Rodrigues, J. A.; Blankenship, H. M.; Cha, W.; Mukherjee, S.; Sloup, R. E.; Rudrik, J. T.; Soehnlen, M.; Manning, S. D., Pangenomic analyses of antibiotic-resistant Campylobacter jejuni reveal unique lineage distributions and epidemiological associations. *Microb Genom* **2023,** *9* (8).

27. Zilbauer, M.; Dorrell, N.; Wren, B. W.; Bajaj-Elliott, M., Campylobacter jejuni-mediated disease pathogenesis: an update. *Transactions of the Royal Society of Tropical Medicine and Hygiene* **2008,** *102* (2), 123-129.

28. Sharma, A. K.; Dhasmana, N.; Dubey, N.; Kumar, N.; Gangwal, A.; Gupta, M.; Singh, Y., Bacterial Virulence Factors: Secreted for Survival. *Indian Journal of Microbiology* **2017,** *57* (1), 1-10.

29. Wexler, H. M., Bacteroides: the good, the bad, and the nitty-gritty. *Clinical Microbiology Reviews* **2007,** *20* (4), 593-+.

30. Cobo-Simón, M.; Hart, R.; Ochman, H., Escherichia Coli: What Is and Which Are? *Mol Biol Evol* **2023,** *40* (1).

31. Kaper, J. B.; Nataro, J. P.; Mobley, H. L. T., Pathogenic Escherichia coli. *Nature Reviews Microbiology* **2004,** *2* (2), 123-140.

32. Stromberg, Z. R.; Van Goor, A.; Redweik, G. A. J.; Wymore Brand, M. J.; Wannemuehler, M. J.; Mellata, M., Pathogenic and non-pathogenic Escherichia coli colonization and host inflammatory response in a defined microbiota mouse model. *Dis Model Mech* **2018,** *11* (11).

33. Ventola, C. L., The antibiotic resistance crisis: part 1: causes and threats. *P t* **2015,** *40* (4), 277-83.

34. Melander, R. J.; Zurawski, D. V.; Melander, C., Narrow-Spectrum Antibacterial Agents. *Medchemcomm* **2018,** *9* (1), 12-21.

35. Dickey, S. W.; Cheung, G. Y. C.; Otto, M., Different drugs for bad bugs: antivirulence strategies in the age of antibiotic resistance. *Nature Reviews Drug Discovery* **2017,** *16* (7), 457-471.

36. Reid, A. J.; Scarbrough, B. A.; Williams, T. C.; Gates, C. E.; Eade, C. R.; Troutman, J. M., General Utilization of Fluorescent Polyisoprenoids with Sugar Selective Phosphoglycosyltransferases. *Biochemistry* **2020,** *59* (4), 615-626.

37. Oinam, L.; Minoshima, F.; Tateno, H., Glycan profiling of the gut microbiota by Glycan-seq. *ISME Communications* **2022,** *2* (1), 1.

38. Whitfield, C., Biosynthesis and assembly of capsular polysaccharides in Escherichia coli. *Annual Review of Biochemistry* **2006,** *75*, 39-68.

39. Troutman, J. M.; Erickson, K. M.; Scott, P. M.; Hazel, J. M.; Martinez, C. D.; Dodbele, S., Tuning the Production of Variable Length, Fluorescent Polyisoprenoids Using Surfactant-Controlled Enzymatic Synthesis. *Biochemistry* **2015,** *54* (18), 2817-2827.

40. Tatar, L. D.; Marolda, C. L.; Polischuk, A. N.; van Leeuwen, D.; Valvano, M. A., An Escherichia coli undecaprenyl-pyrophosphate phosphatase implicated in undecaprenyl phosphate recycling. *Microbiology (Reading)* **2007,** *153* (Pt 8), 2518-2529.

41. Dodbele, S.; Martinez, C. D.; Troutman, J. M., Species Differences in Alternative Substrate Utilization by the Antibacterial Target Undecaprenyl Pyrophosphate Synthase. *Biochemistry* **2014,** *53* (30), 5042-5050.

42. Lukose, V.; Walvoort, M. T. C.; Imperiali, B., Bacterial phosphoglycosyl transferases: initiators of glycan biosynthesis at the membrane interface. *Glycobiology* **2017,** *27* (9), 820-833.

43. O'Toole, K. H.; Imperiali, B.; Allen, K. N., Glycoconjugate pathway connections revealed by sequence similarity network analysis of the monotopic phosphoglycosyl transferases. *Proceedings of the National Academy of Sciences of the United States of America* **2021,** *118* (4).

44. Mostafavi, A. Z.; Troutman, J. M., Biosynthetic Assembly of the Bacteroides fragilis Capsular Polysaccharide A Precursor Bactoprenyl Diphosphate-Linked Acetamido-4-amino-6-deoxygalactopyranose. *Biochemistry* **2013,** *52* (11), 1939-1949.

45. Amer, A. O.; Valvano, M. A., Conserved amino acid residues found in a predicted cytosolic domain of the lipopolysaccharide biosynthetic protein WecA are implicated in the recognition of UDP-N-acetylglucosamine. *Microbiology (Reading)* **2001,** *147* (Pt 11), 3015-25.

46. Valvano, M. A., Export of O-specific lipopolysaccharide. *Front Biosci* **2003,** *8*, s452-71.

47. Cartee, R. T.; Forsee, W. T.; Bender, M. H.; Ambrose, K. D.; Yother, J., CpsE from type 2 Streptococcus pneumoniae catalyzes the reversible addition of glucose-1-phosphate to a polyprenyl phosphate acceptor, initiating type 2 capsule repeat unit formation. *J Bacteriol* **2005,** *187* (21), 7425-33.

48. Das, D.; Kuzmic, P.; Imperiali, B., Analysis of a dual domain phosphoglycosyl transferase reveals a ping-pong mechanism with a covalent enzyme intermediate. *Proceedings of the National Academy of Sciences of the United States of America* **2017,** *114* (27), 7019-7024.

49. Anderson, A. J.; Dodge, G. J.; Allen, K. N.; Imperiali, B., Co-conserved sequence motifs are predictive of substrate specificity in a family of monotopic phosphoglycosyl transferases. *Protein Science* **2023,** *32* (6).

50. Entova, S.; Guan, Z. Q.; Imperiali, B., Investigation of the conserved reentrant membrane helix in the monotopic phosphoglycosyl transferase superfamily supports key molecular interactions with polyprenol phosphate substrates. *Archives of Biochemistry and Biophysics* **2019,** *675*.

51. Carpenter, E. P.; Beis, K.; Cameron, A. D.; Iwata, S., Overcoming the challenges of membrane protein crystallography. *Curr Opin Struct Biol* **2008,** *18* (5), 581-6.

52. International Consortium Completes Human Genome Project. https://www.genome.gov/11006929/2003-release-international-consortium-completes-hgp.

53. Lopez Aguilar, A.; Briard, J. G.; Yang, L.; Ovryn, B.; Macauley, M. S.; Wu, P., Tools for Studying Glycans: Recent Advances in Chemoenzymatic Glycan Labeling. *ACS Chem Biol* **2017,** *12* (3), 611-621.

54. Wu, X.; Wang, R.; Kwon, N.; Ma, H.; Yoon, J., Activatable fluorescent probes for in situ imaging of enzymes. *Chem Soc Rev* **2022,** *51* (2), 450-463.

55. Li, Y. X.; Xie, D. T.; Yang, Y. X.; Chen, Z.; Guo, W. Y.; Yang, W. C., Development of Small-Molecule Fluorescent Probes Targeting Enzymes. *Molecules* **2022,** *27* (14).

56. Arrowsmith, C. H.; Audia, J. E.; Austin, C.; Baell, J.; Bennett, J.; Blagg, J.; Bountra, C.; Brennan, P. E.; Brown, P. J.; Bunnage, M. E.; Buser-Doepner, C.; Campbell, R. M.; Carter, A. J.; Cohen, P.; Copeland, R. A.; Cravatt, B.; Dahlin, J. L.; Dhanak, D.; Edwards, A. M.; Frederiksen, M.; Frye, S. V.; Gray, N.; Grimshaw, C. E.; Hepworth, D.; Howe, T.; Huber, K. V.; Jin, J.; Knapp, S.; Kotz, J. D.; Kruger, R. G.; Lowe, D.; Mader, M. M.; Marsden, B.; Mueller-Fahrnow, A.; Müller, S.; O'Hagan, R. C.; Overington, J. P.; Owen, D. R.; Rosenberg, S. H.; Roth, B.; Ross, R.; Schapira, M.; Schreiber, S. L.; Shoichet, B.; Sundström, M.; Superti-Furga, G.; Taunton, J.; Toledo-Sherman, L.; Walpole, C.; Walters, M. A.; Willson, T. M.; Workman, P.; Young, R. N.; Zuercher, W. J., The promise and peril of chemical probes. *Nat Chem Biol* **2015,** *11* (8), 536-41.

57. Fang, H.; Peng, B.; Ong, S. Y.; Wu, Q.; Li, L.; Yao, S. Q., Recent advances in activity-based probes (ABPs) and affinity-based probes (AfBPs) for profiling of enzymes. *Chem Sci* **2021,** *12* (24), 8288-8310.

58. Jugniot, N.; Voisin, P.; Bentaher, A.; Mellet, P., Neutrophil Elastase Activity Imaging: Recent Approaches in the Design and Applications of Activity-Based Probes and Substrate-Based Probes. *Contrast Media Mol Imaging* **2019,** *2019*, 7417192.

59. Marshall, A. P.; Shirley, J. D.; Carlson, E. E., Enzyme-targeted fluorescent small-molecule probes for bacterial imaging. *Curr Opin Chem Biol* **2020,** *57*, 155-165.

60. Nicolau, I.; Hădade, N. D.; Matache, M.; Funeriu, D. P., Synthetic Approaches of Epoxysuccinate Chemical Probes. *Chembiochem* **2023,** *24* (16), e202300157.

61. Liu, Y.; Patricelli, M. P.; Cravatt, B. F., Activity-based protein profiling: the serine hydrolases. *Proc Natl Acad Sci U S A* **1999,** *96* (26), 14694-9.

62. Vandermoten, S.; Haubruge, E.; Cusson, M., New insights into short-chain prenyltransferases: structural features, evolutionary history and potential for selective inhibition. *Cell Mol Life Sci* **2009,** *66* (23), 3685-95.

63. Zhang, F. L.; Casey, P. J., Protein prenylation: molecular mechanisms and functional consequences. *Annu Rev Biochem* **1996,** *65*, 241-69.

64. Withers, S. T.; Keasling, J. D., Biosynthesis and engineering of isoprenoid small molecules. *Applied Microbiology and Biotechnology* **2007,** *73* (5), 980-990.

65. Ogura, K.; Koyama, T., Enzymatic aspects of isoprenoid chain elongation. *Chemical Reviews* **1998,** *98* (4), 1263-1276.

66. Palsuledesai, C. C.; Distefano, M. D., Protein prenylation: enzymes, therapeutics, and biotechnology applications. *ACS Chem Biol* **2015,** *10* (1), 51-62.

67. Ramazi, S.; Zahiri, J., Posttranslational modifications in proteins: resources, tools and prediction methods. *Database (Oxford)* **2021,** *2021*.

68. Wang, Y. C.; Distefano, M. D., Synthetic isoprenoid analogues for the study of prenylated proteins: Fluorescent imaging and proteomic applications. *Bioorganic Chemistry* **2016,** *64*, 59-65.

69. Turek, T. C.; Gaon, I.; Distefano, M. D.; Strickland, C. L., Synthesis of farnesyl diphosphate analogues containing ether-linked photoactive benzophenones and their application in studies of protein prenyltransferases. *Journal of Organic Chemistry* **2001,** *66* (10), 3253-3264.

70. Troutman, J. M.; Subramanian, T.; Andres, D. A.; Spielmann, H. P., Selective modification of CaaX peptides with ortho-substituted anilinogeranyl lipids by protein farnesyl

transferase: competitive substrates and potent inhibitors from a library of farnesyl diphosphate analogues. *Biochemistry* **2007,** *46* (40), 11310-21.

71. Teng, K. H.; Chen, A. P.; Kuo, C. J.; Li, Y. C.; Liu, H. G.; Chen, C. T.; Liang, P. H., Fluorescent substrate analog for monitoring chain elongation by undecaprenyl pyrophosphate synthase in real time. *Anal Biochem* **2011,** *417* (1), 136-41.

72. Lujan, D. K.; Stanziale, J. A.; Mostafavi, A. Z.; Sharma, S.; Troutman, J. M., Chemoenzymatic synthesis of an isoprenoid phosphate tool for the analysis of complex bacterial oligosaccharide biosynthesis. *Carbohydr Res* **2012,** *359*, 44-53.

73. Troutman, J. M.; Imperiali, B., Campylobacter jejuni PglH is a single active site processive polymerase that utilizes product inhibition to limit sequential glycosyl transfer reactions. *Biochemistry* **2009,** *48* (12), 2807-16.

74. Hartley, M. D.; Imperiali, B., At the membrane frontier: a prospectus on the remarkable evolutionary conservation of polyprenols and polyprenyl-phosphates. *Arch Biochem Biophys* **2012,** *517* (2), 83-97.

75. Mostafavi, A. Z.; Lujan, D. K.; Erickson, K. M.; Martinez, C. D.; Troutman, J. M., Fluorescent probes for investigation of isoprenoid configuration and size discrimination by bactoprenol-utilizing enzymes. *Bioorganic & Medicinal Chemistry* **2013,** *21* (17), 5428-5435.

76. Glover, K. J.; Weerapana, E.; Imperiali, B., In vitro assembly of the undecaprenylpyrophosphate-linked heptasaccharide for prokaryotic N-linked glycosylation. *Proc Natl Acad Sci U S A* **2005,** *102* (40), 14255-9.

77. Sharma, S.; Erickson, K. M.; Troutman, J. M., Complete Tetrasaccharide Repeat Unit Biosynthesis of the Immunomodulatory Bacteroides fragilis Capsular Polysaccharide A. *ACS Chem Biol* **2017,** *12* (1), 92-101.

78. Subramanian, T.; Wang, Z.; Troutman, J. M.; Andres, D. A.; Spielmann, H. P., Directed library of anilinogeranyl analogues of farnesyl diphosphate via mixed solid- and solution-phase synthesis. *Org Lett* **2005,** *7* (11), 2109-12.

79. Chehade, K. A. H.; Andres, D. A.; Morimoto, H.; Spielmann, H. P., Design and synthesis of a transferable farnesyl pyrophosphate analogue to Ras by protein farnesyltransferase. *Journal of Organic Chemistry* **2000,** *65* (10), 3027-3033.

80. Liu, F.; Vijayakrishnan, B.; Faridmoayer, A.; Taylor, T. A.; Parsons, T. B.; Bernardes, G. J.; Kowarik, M.; Davis, B. G., Rationally designed short polyisoprenol-linked PglB substrates for engineered polypeptide and protein N-glycosylation. *J Am Chem Soc* **2014,** *136* (2), 566-9.

81. Chehade, K. A. H.; Kiegiel, K.; Isaacs, R. J.; Pickett, J. S.; Bowers, K. E.; Fierke, C. A.; Andres, D. A.; Spielmann, H. P., Photoaffinity analogues of farnesyl pyrophosphate transferable by protein farnesyl transferase. *Journal of the American Chemical Society* **2002,** *124* (28), 8206-8219.

82. Umbreit, M. A.; Sharpless, K. B., ALLYLIC OXIDATION OF OLEFINS BY CATALYTIC AND STOICHIOMETRIC SELENIUM DIOXIDE WITH TERT-BUTYL HYDROPEROXIDE. *Journal of the American Chemical Society* **1977,** *99* (16), 5526-5528.

83. Abdel-Magid, A. F.; Carson, K. G.; Harris, B. D.; Maryanoff, C. A.; Shah, R. D., Reductive Amination of Aldehydes and Ketones with Sodium Triacetoxyborohydride. Studies on Direct and Indirect Reductive Amination Procedures(1). *J Org Chem* **1996,** *61* (11), 3849-3862.

84. Keller, R. K.; Thompson, R., Rapid synthesis of isoprenoid diphosphates and their isolation in one step using either thin layer or flash chromatography. *J Chromatogr* **1993,** *645* (1), 161-7.

85. Lund, S.; Courtney, T.; Williams, G. J., Probing the Substrate Promiscuity of Isopentenyl Phosphate Kinase as a Platform for Hemiterpene Analogue Production. *Chembiochem* **2019,** *20* (17), 2217-2221.

86. Olivier, N. B.; Chen, M. M.; Behr, J. R.; Imperiali, B., In vitro biosynthesis of UDP-N,N'-diacetylbacillosamine by enzymes of the Campylobacter jejuni general protein glycosylation system. *Biochemistry* **2006,** *45* (45), 13659-69.

87. Reid, A. J.; Erickson, K. M.; Hazel, J. M.; Lukose, V.; Troutman, J. M., Chemoenzymatic Preparation of a Campylobacter jejuni Lipid-Linked Heptasaccharide on an Azide-Linked Polyisoprenoid. *ACS Omega* **2023,** *8* (17), 15790-15798.

88. Dixit, V. M.; Laskovics, F. M.; Noall, W. I.; Poulter, C. D., Tris(tetrabutylammonium) hydrogen pyrophosphate. A new reagent for the preparation of allylic pyrophosphate esters. *The Journal of Organic Chemistry* **1981,** *46* (9), 1967-1969.

89. Arbour, C. A.; Vuksanovic, N.; Bernstein, H. M.; Allen, K. N.; Imperiali, B., Characterization of PglJ, a Glycosyltransferase in the Campylobacter concisus N-Linked Protein Glycosylation Pathway that Expands Glycan Diversity. *Biochemistry* **2024,** *63* (1), 141-151.

90. Lukose, V.; Whitworth, G.; Guan, Z.; Imperiali, B., Chemoenzymatic Assembly of Bacterial Glycoconjugates for Site-Specific Orthogonal Labeling. *J Am Chem Soc* **2015,** *137* (39), 12446-9.

APPENDIX A: SUPPLEMENTAL FIGURES

Figure A1: A photo demonstrating the fluorescence assay used to distinguish fractions containing fluorescent compounds following ion exchange chromatography. Each 10 mL sample was collected in glass culture tubes and placed under a 254 nm UV lamp. The samples that fluoresced—such as the blue-colored, 1-naphthylamine solution (shown on the right)—were collected, while those that did not appear visibly different from the control tube—containing deionized water (shown on the left)—were discarded.

APPENDIX B: THIN-LAYER CHROMATOGRAPHY DATA

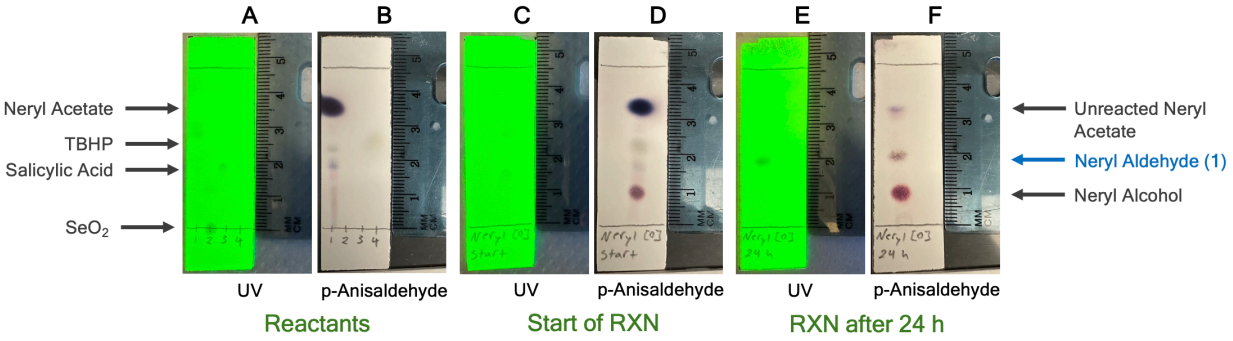

Figure B1: TLC analysis of neryl acetate oxidation, forming neryl aldehyde (**1**). Silica gel plates were visualized under 254 nm UV light (**A**, **C**, **E**), treated with p-anisaldehyde spray, and heated (**B**, **D**, **F**).

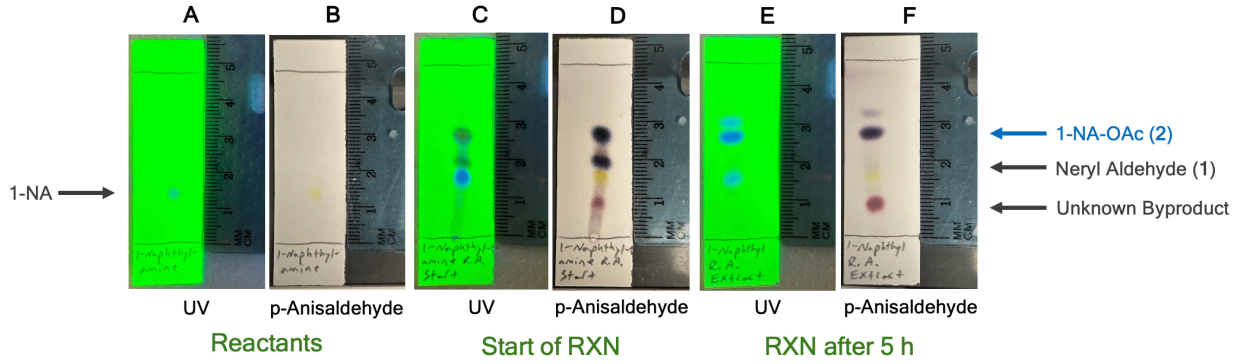

Figure B2: TLC analysis of 1-naphthylamine reductive amination, forming 1-naphthylamine neryl acetate (**2**). Silica gel plates were visualized under 254 nm UV light (**A**, **C**, **E**), treated with p-anisaldehyde spray, and heated (**B**, **D**, **F**).

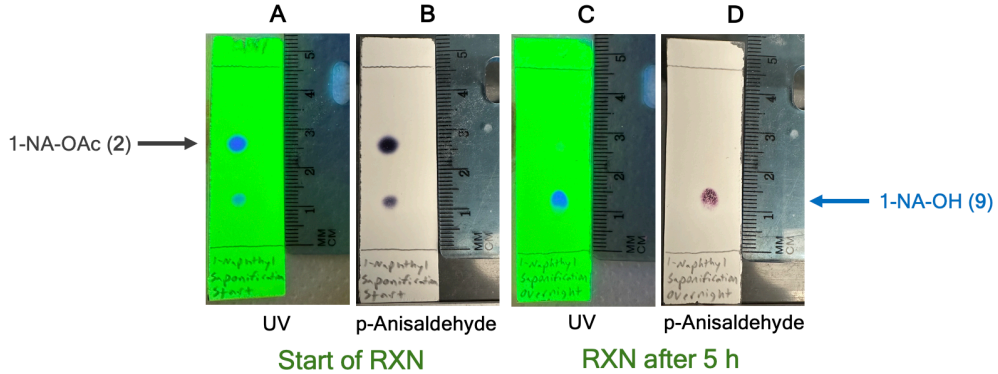

Figure B3: TLC analysis of 1-naphthylamine neryl acetate saponification, forming 1-naphthylamine neryl alcohol (**9**). Silica gel plates were visualized under 254 nm UV light (**A** and **C**), treated with p-anisaldehyde spray, and heated (**B** and **D**).

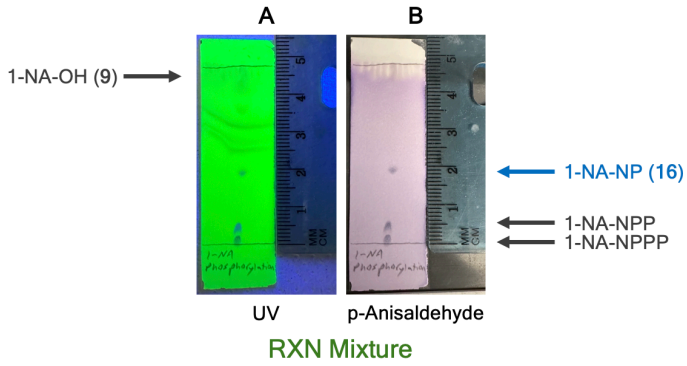

Figure B4: TLC analysis of 1-naphthylamine neryl alcohol phosphorylation, forming 1-naphthylamine neryl monophosphate (**16**). Silica gel plates were visualized under 254 nm UV light (**A**), treated with p-anisaldehyde spray, and heated (**B**).

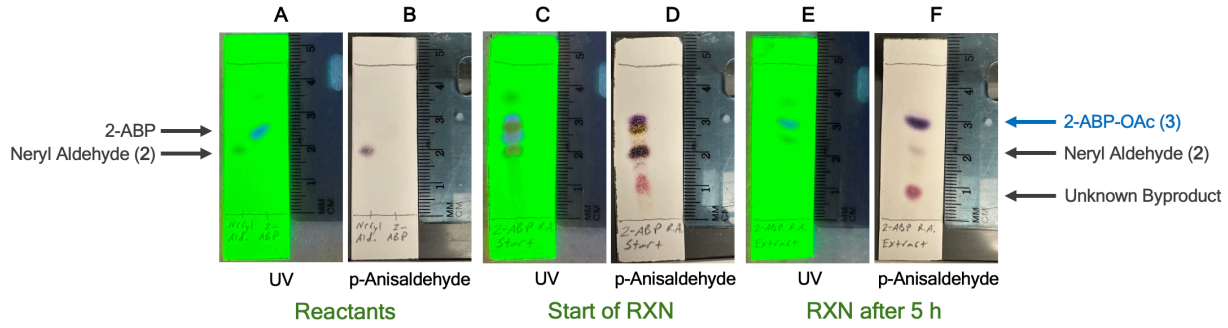

Figure B5: TLC analysis of 2-aminobiphenyl reductive amination, forming 2-aminobiphenyl neryl acetate (**3**). Silica gel plates were visualized under 254 nm UV light (**A**, **C**, **E**), treated with p-anisaldehyde spray, and heated (**B**, **D**, **F**).

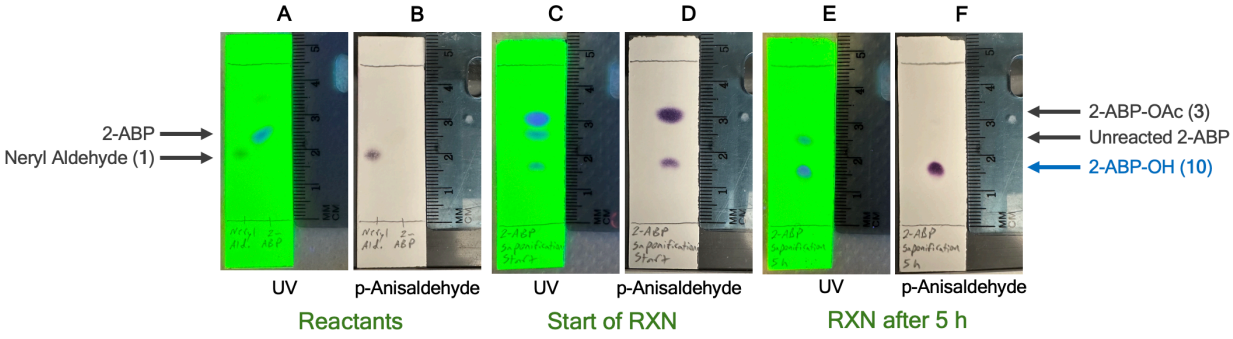

Figure B6: TLC analysis of 2-aminobiphenyl neryl acetate saponification, forming 2-aminobiphenyl neryl alcohol (**10**). Silica gel plates were visualized under 254 nm UV light (**A**, **C**, **E**), treated with p-anisaldehyde spray, and heated (**B**, **D**, **F**).

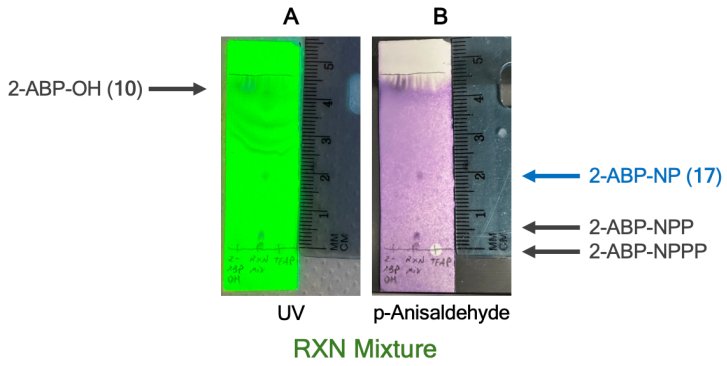

Figure B7: TLC analysis of 2-aminobiphenyl neryl alcohol phosphorylation, forming 2-aminobiphenyl neryl monophosphate (**17**). Silica gel plates were visualized under 254 nm UV light (**A**), treated with p-anisaldehyde spray, and heated (**B**).

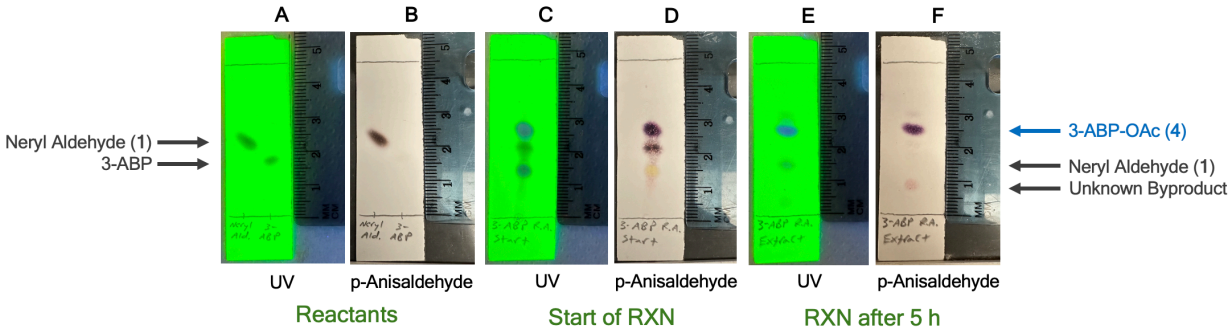

Figure B8: TLC analysis of 3-aminobiphenyl reductive amination, forming 3-aminobiphenyl neryl acetate (**4**). Silica gel plates were visualized under 254 nm UV light (**A**, **C**, **E**), treated with p-anisaldehyde spray, and heated (**B**, **D**, **F**).

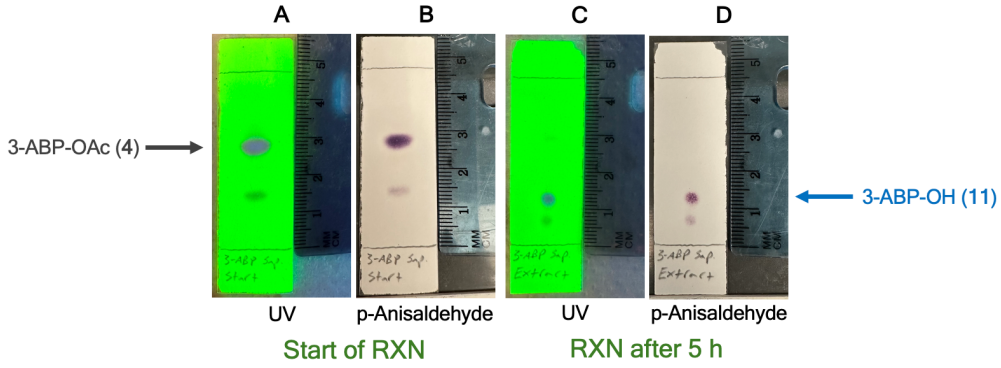

Figure B9: TLC analysis of 3-aminobiphenyl neryl acetate saponification, forming 3-aminobiphenyl neryl alcohol (**11**). Silica gel plates were visualized under 254 nm UV light (**A** and **C**), treated with p-anisaldehyde spray, and heated (**B** and **D**).

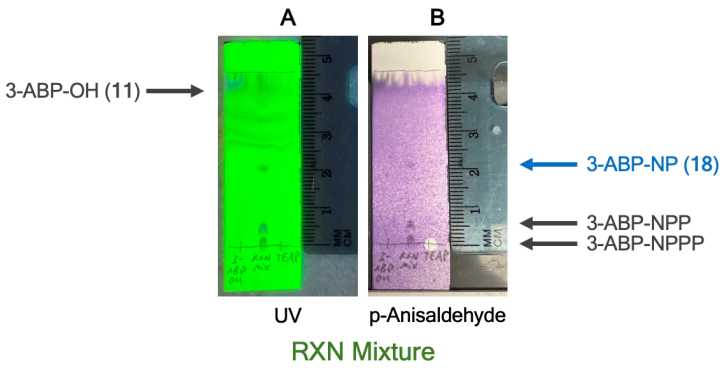

Figure B10: TLC analysis of 3-aminobiphenyl neryl alcohol phosphorylation, forming 3-aminobiphenyl neryl monophosphate (**18**). Silica gel plates were visualized under 254 nm UV light (**A**), treated with p-anisaldehyde spray, and heated (**B**).

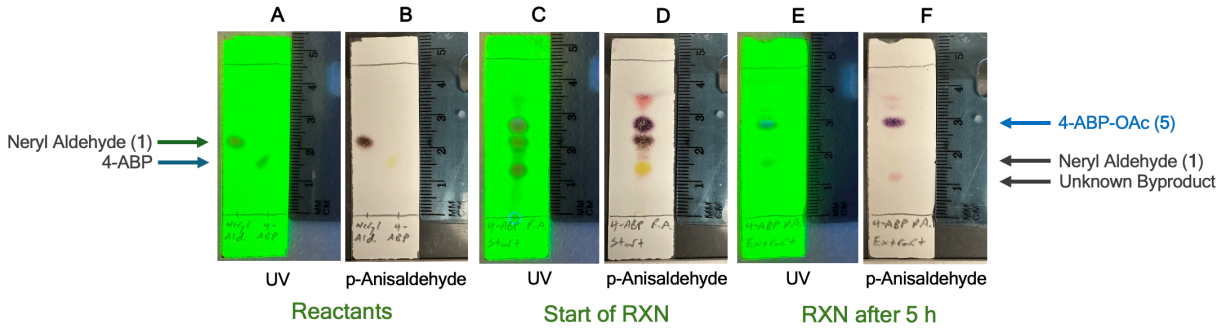

Figure B11: TLC analysis of 4-aminobiphenyl reductive amination, forming 4-aminobiphenyl neryl acetate (**5**). Silica gel plates were visualized under 254 nm UV light (**A**, **C**, **E**), treated with p-anisaldehyde spray, and heated (**B**, **D**, **F**).

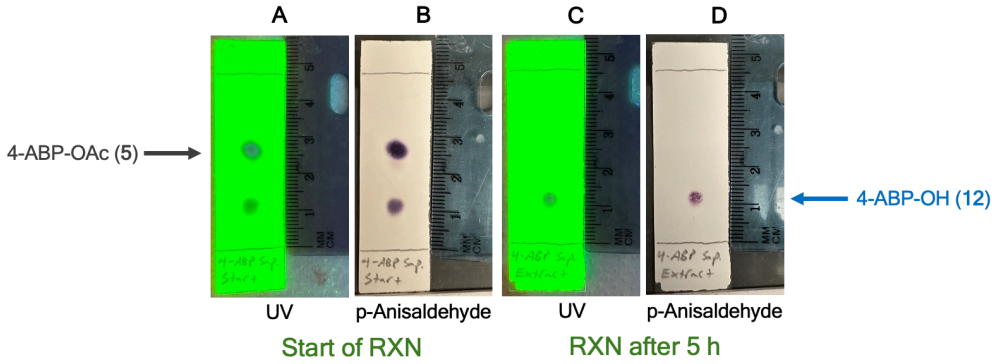

Figure B12: TLC analysis of 4-aminobiphenyl neryl acetate saponification, forming 4-aminobiphenyl neryl alcohol (**12**). Silica gel plates were visualized under 254 nm UV light (**A** and **C**), treated with p-anisaldehyde spray, and heated (**B** and **D**).

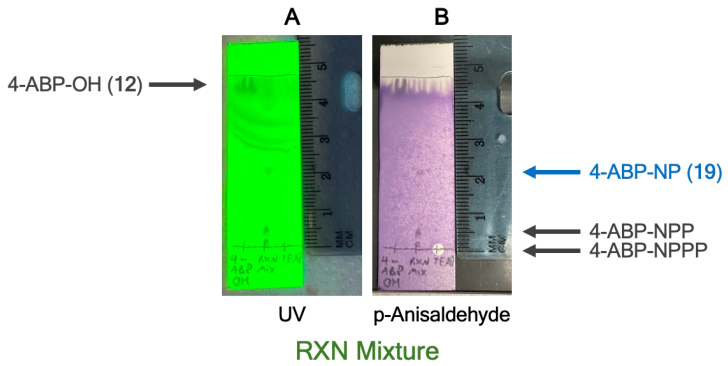

Figure B13: TLC analysis of 4-aminobiphenyl neryl alcohol phosphorylation, forming 4-aminobiphenyl neryl monophosphate (**19**). Silica gel plates were visualized under 254 nm UV light (**A**), treated with p-anisaldehyde spray, and heated (**B**).

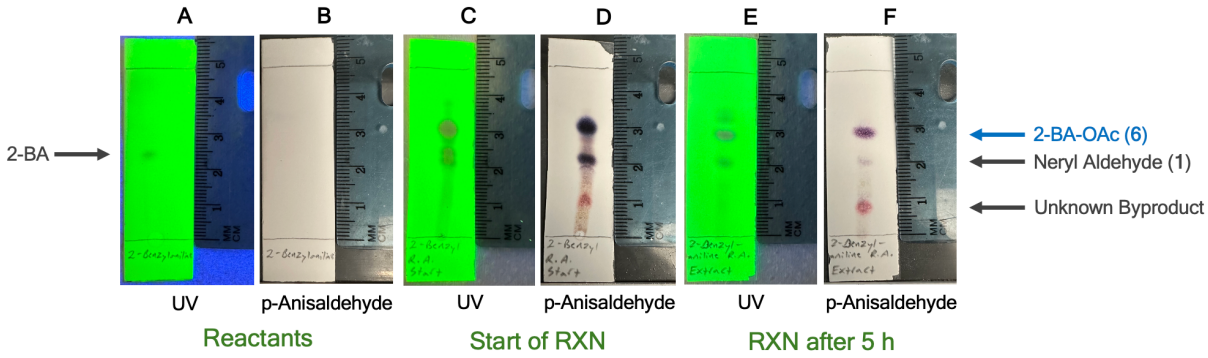

Figure B14: TLC analysis of 2-benzylaniline reductive amination, forming 2-benzylaniline neryl acetate (**6**). Silica gel plates were visualized under 254 nm UV light (**A**, **C**, **E**), treated with p-anisaldehyde spray, and heated (**B**, **D**, **F**).

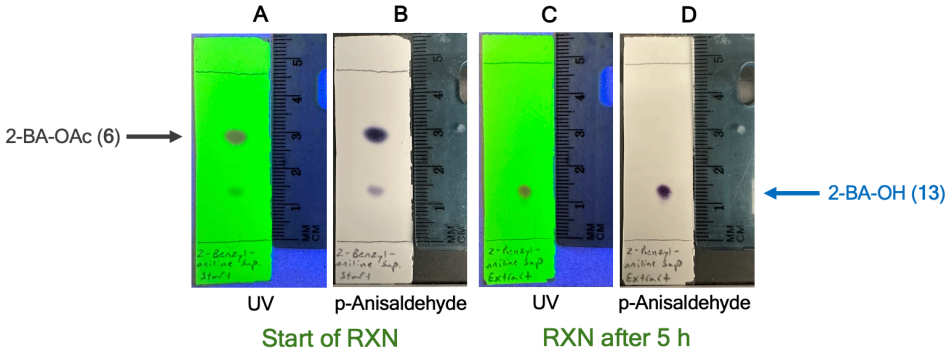

Figure B15: TLC analysis of 2-benzylaniline neryl acetate saponification, forming 2-benzylaniline neryl alcohol (**13**). Silica gel plates were visualized under 254 nm UV light (**A** and **C**), treated with p-anisaldehyde spray, and heated (**B** and **D**).

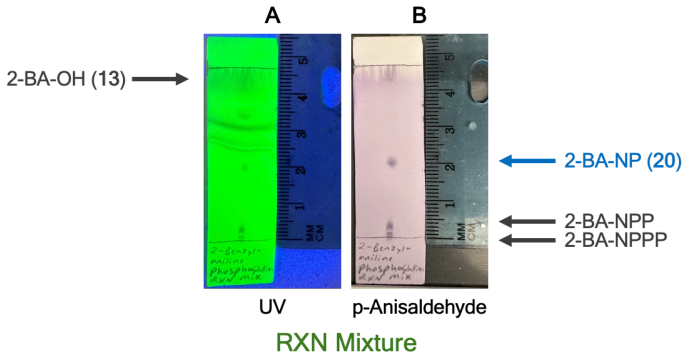

Figure B16: TLC analysis of 2-benzylaniline neryl alcohol phosphorylation, forming 2-benzylaniline neryl monophosphate (**20**). Silica gel plates were visualized under 254 nm UV light (**A**), treated with p-anisaldehyde spray, and heated (**B**).

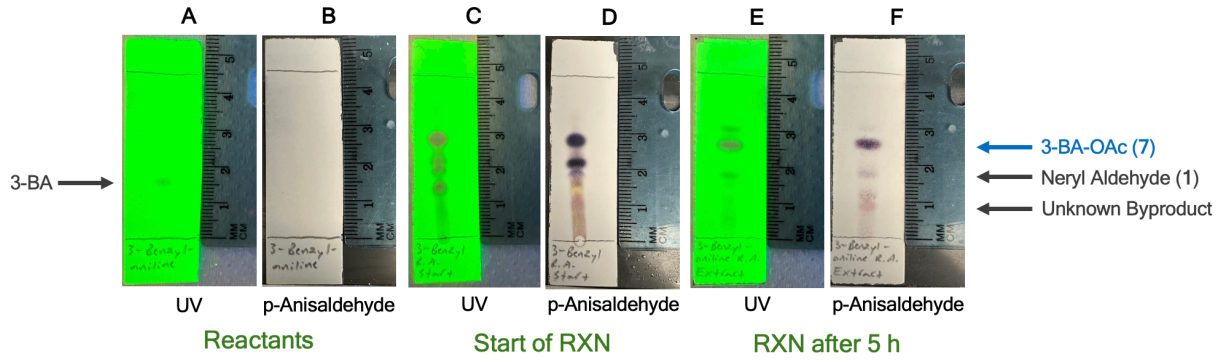

Figure B17: TLC analysis of 3-benzylaniline reductive amination, forming 3-benzylaniline neryl acetate (**7**). Silica gel plates were visualized under 254 nm UV light (**A**, **C**, **E**), treated with p-anisaldehyde spray, and heated (**B**, **D**, **F**).

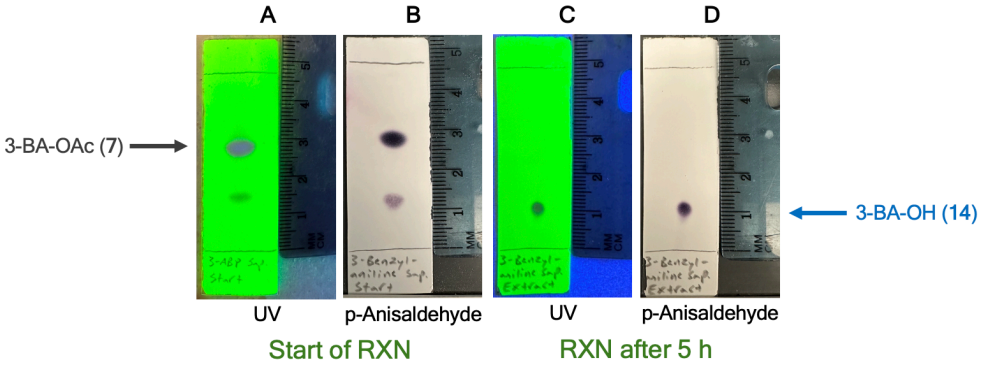

Figure B18: TLC analysis of 3-benzylaniline neryl acetate saponification, forming 3-benzylaniline neryl alcohol (**14**). Silica gel plates were visualized under 254 nm UV light (**A** and **C**), treated with p-anisaldehyde spray, and heated (**B** and **D**).

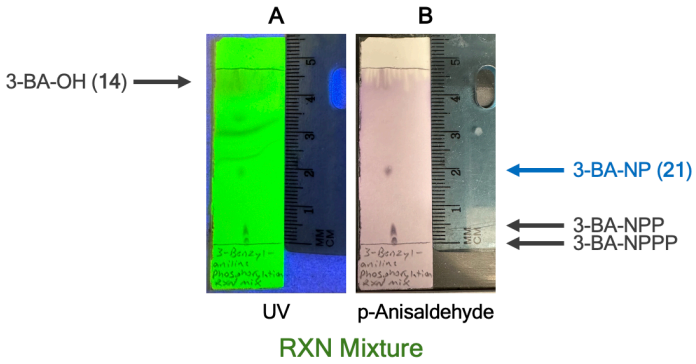

Figure B19: TLC analysis of 3-benzylaniline neryl alcohol phosphorylation, forming 3-benzylaniline neryl monophosphate (**21**). Silica gel plates were visualized under 254 nm UV light (**A**), treated with p-anisaldehyde spray, and heated (**B**).

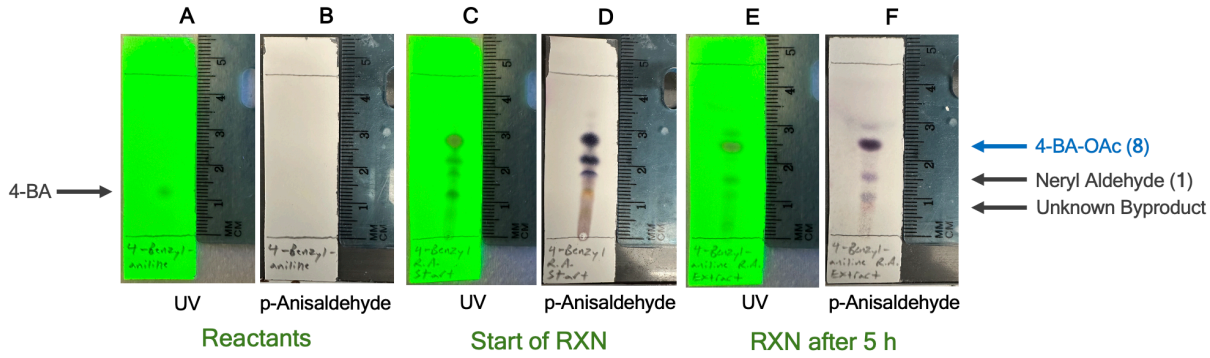

Figure B20: TLC analysis of 4-benzylaniline reductive amination, forming 4-benzylaniline neryl acetate (**8**). Silica gel plates were visualized under 254 nm UV light (**A**, **C**, **E**), treated with p-anisaldehyde spray, and heated (**B**, **D**, **F**).

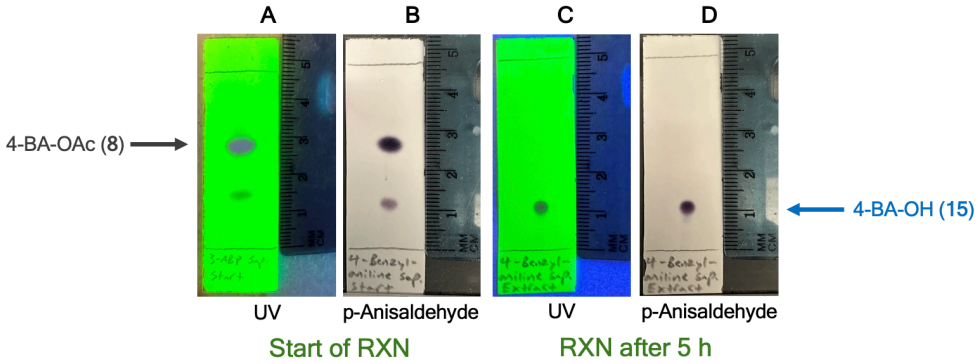

Figure B21: TLC analysis of 4-benzylaniline neryl acetate saponification, forming 4-benzylaniline neryl alcohol (**15**). Silica gel plates were visualized under 254 nm UV light (**A** and **C**), treated with p-anisaldehyde spray, and heated (**B** and **D**).

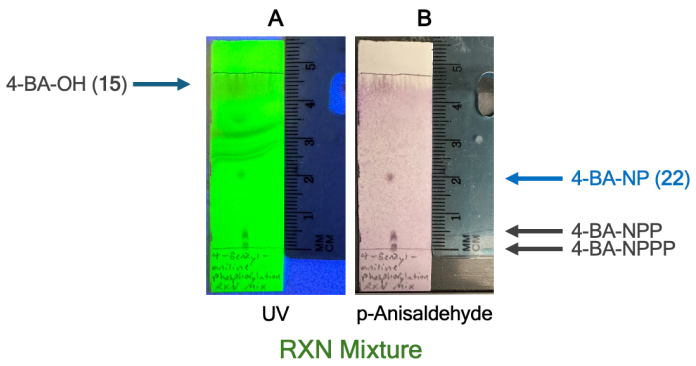

Figure B22: TLC analysis of 4-benzylaniline neryl alcohol phosphorylation, forming 4-benzylaniline neryl monophosphate (**22**). Silica gel plates were visualized under 254 nm UV light (**A**), treated with p-anisaldehyde spray, and heated (**B**).

APPENDIX C: NMR SPECTRA

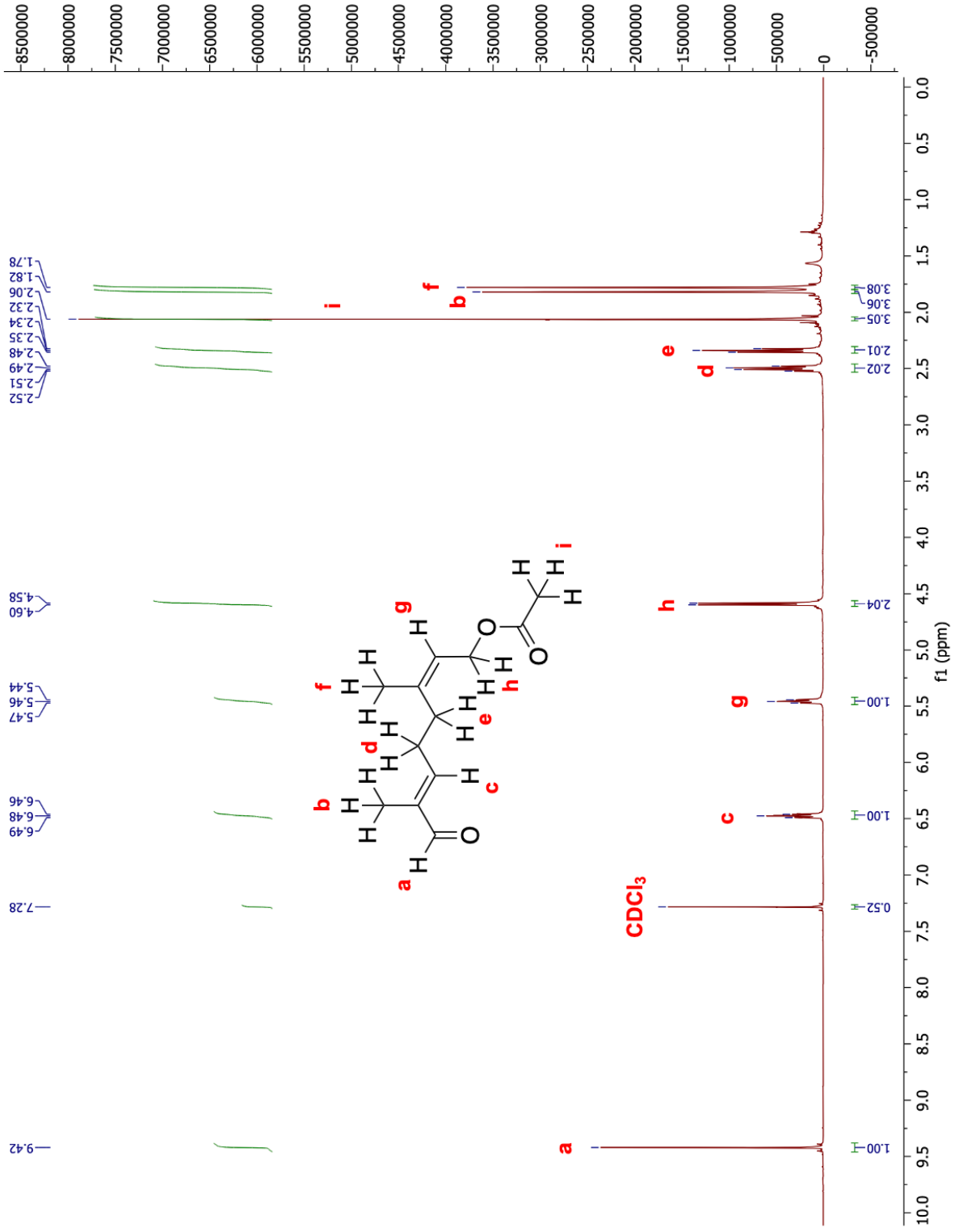

Figure C1: ^{1}H NMR spectrum of neryl aldehyde (**1**) with structure overlay and assigned peaks

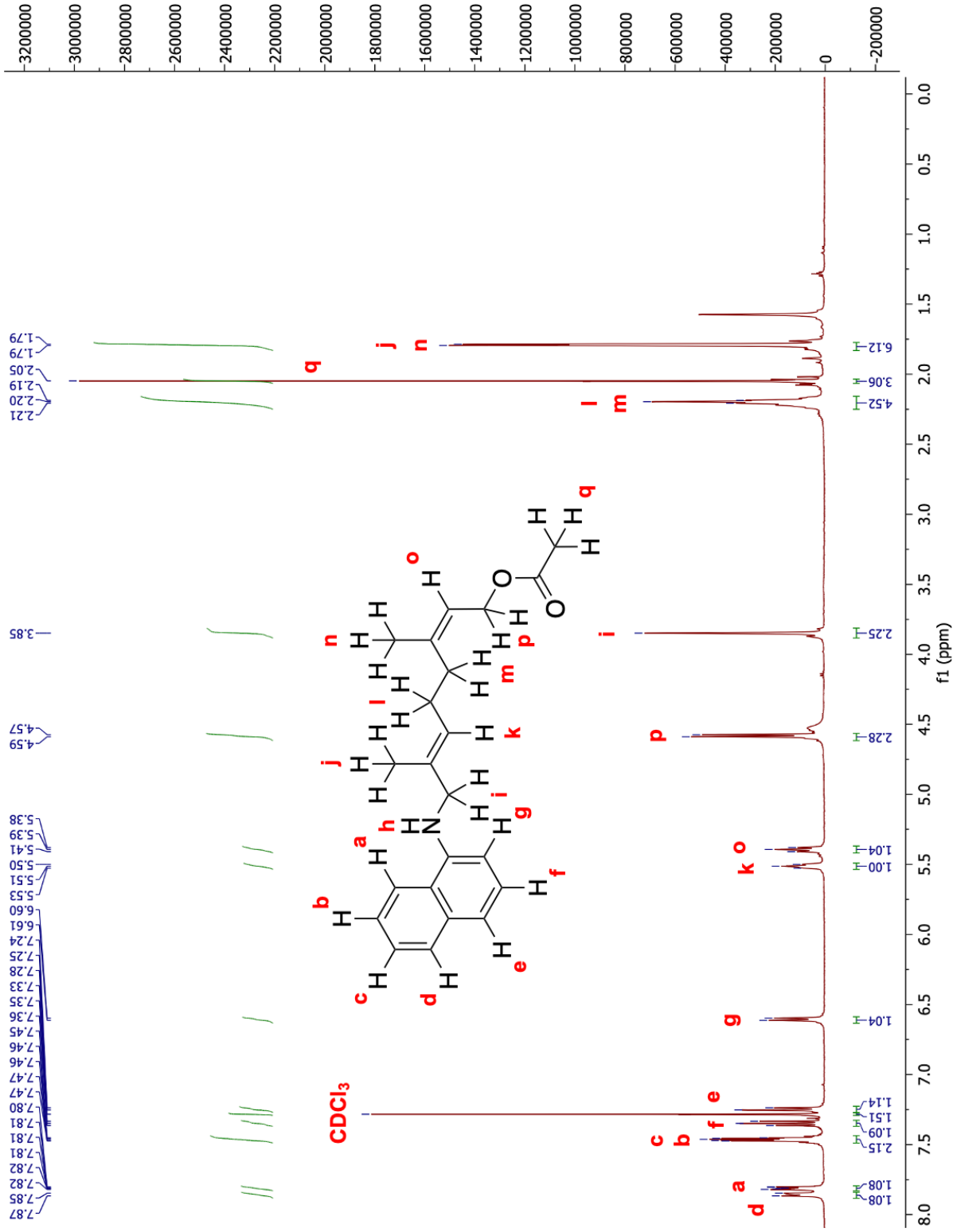

Figure C2: ^{1}H NMR spectrum of 1-naphthylamine acetate (**2**) with structure overlay and assigned peaks

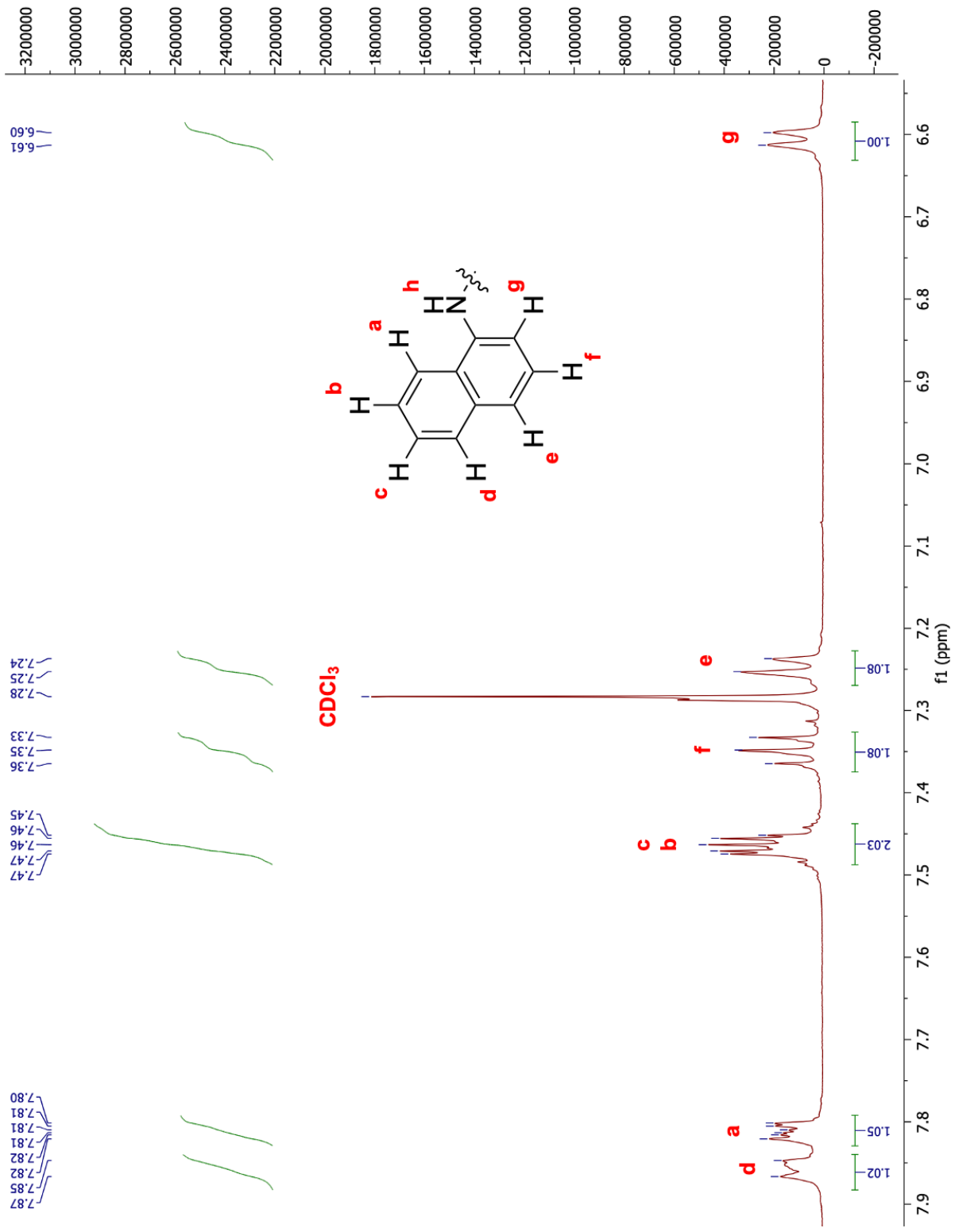

Figure C3: ^{1}H NMR spectrum of 1-naphthylamine neryl acetate (**2**) zoomed in at the aromatic region with structure overlay and assigned peaks

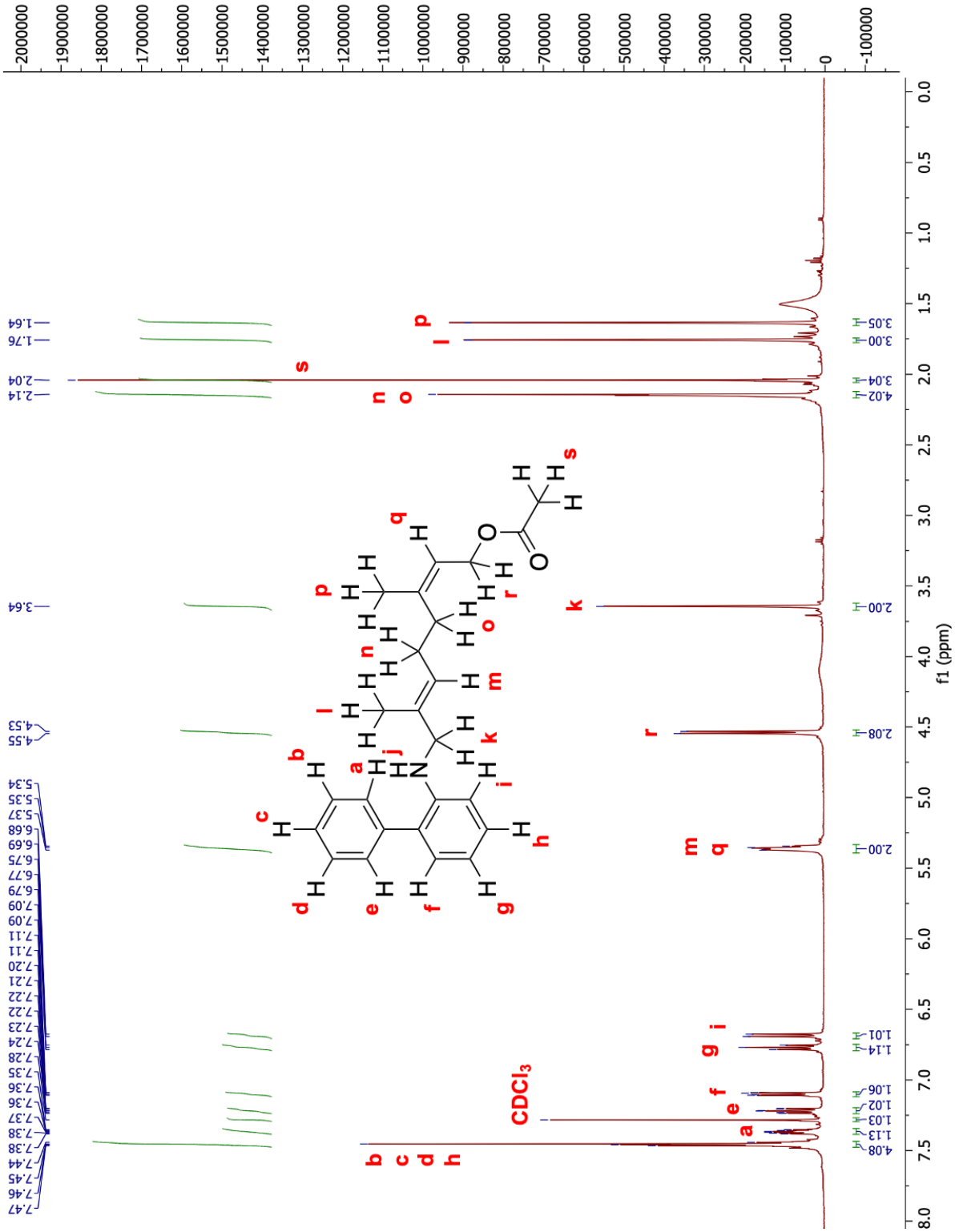

Figure C4: ^{1}H NMR spectrum of 2-aminobiphenyl neryl acetate (**3**) with structure overlay and assigned peaks

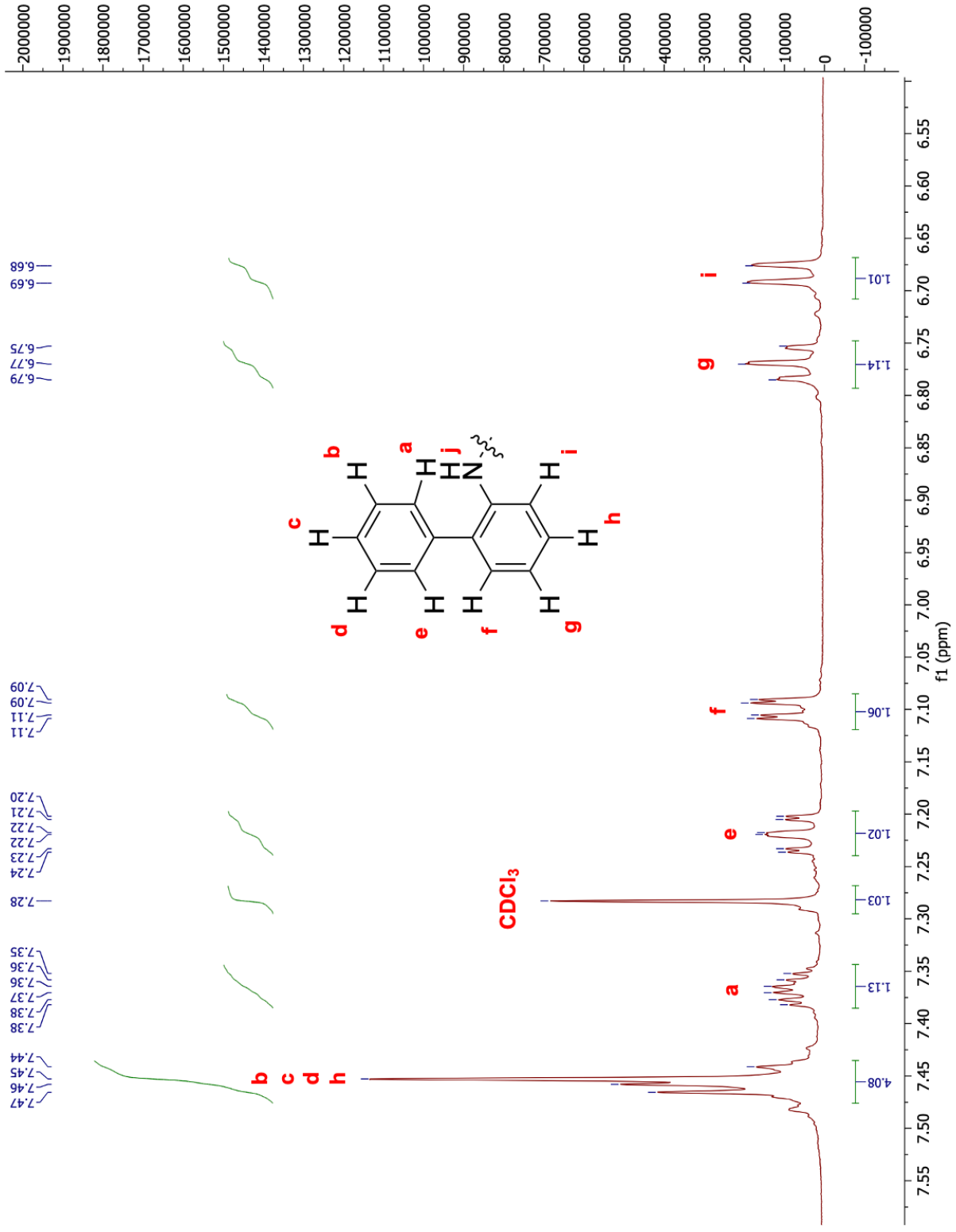

Figure C5: ^{1}H NMR spectrum of 2-aminobiphenyl neryl acetate (**3**) zoomed in at the aromatic region with structure overlay and assigned peaks

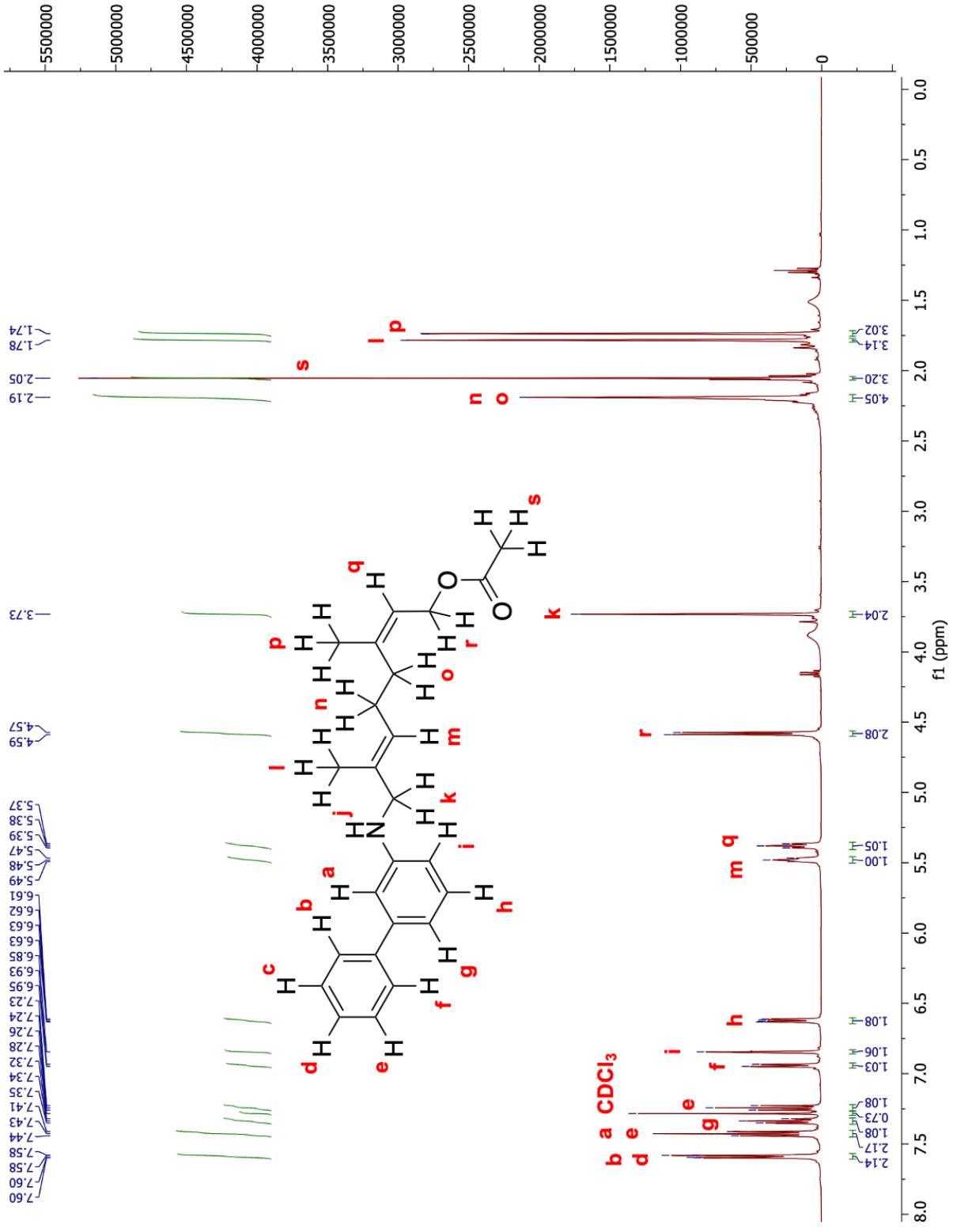

Figure C6: ^{1}H NMR spectrum of 3-aminobiphenyl neryl acetate (**4**) with structure overlay and assigned peaks

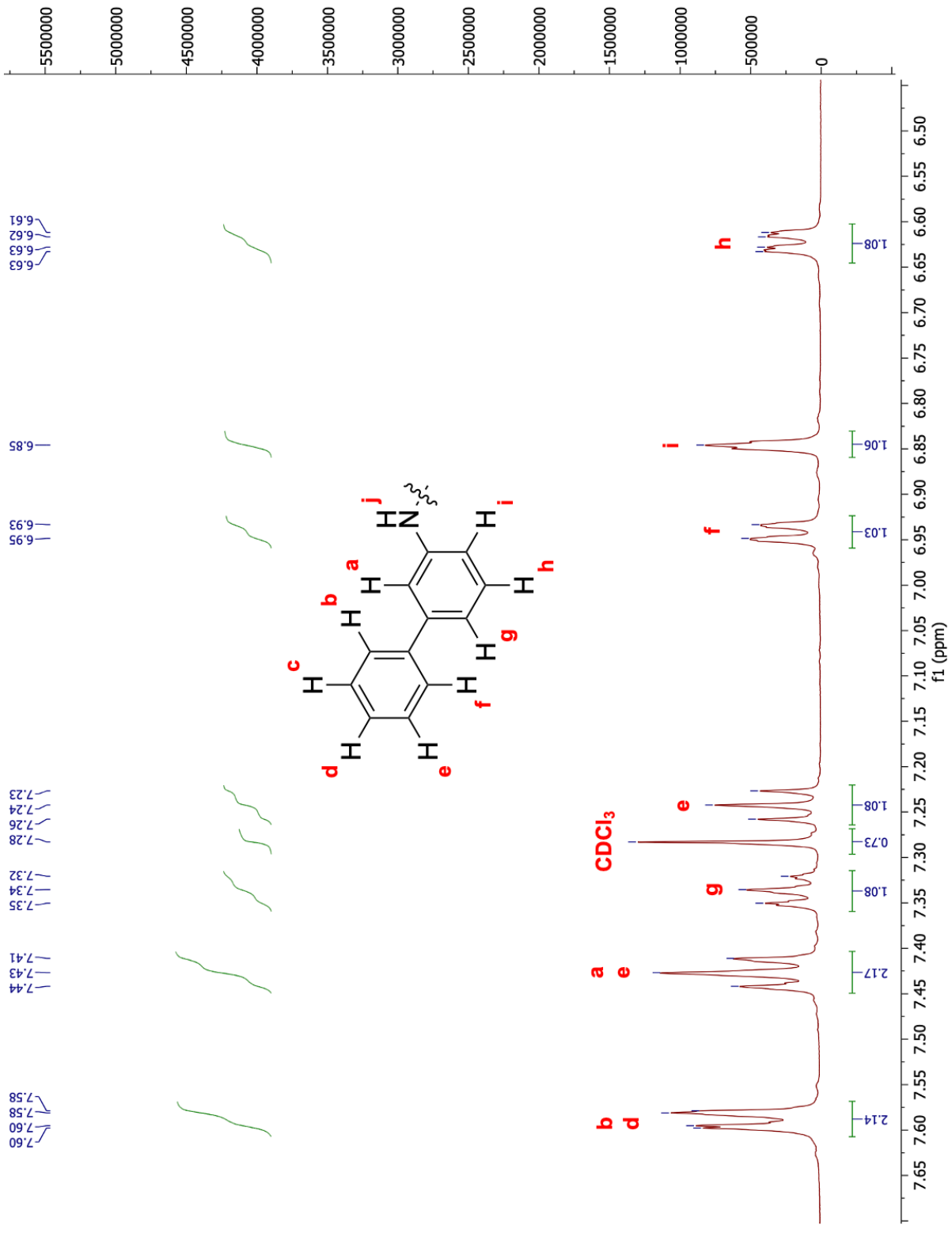

Figure C7: ^{1}H NMR spectrum of 3-aminobiphenyl neryl acetate (**4**) zoomed in at the aromatic region with structure overlay and assigned peaks

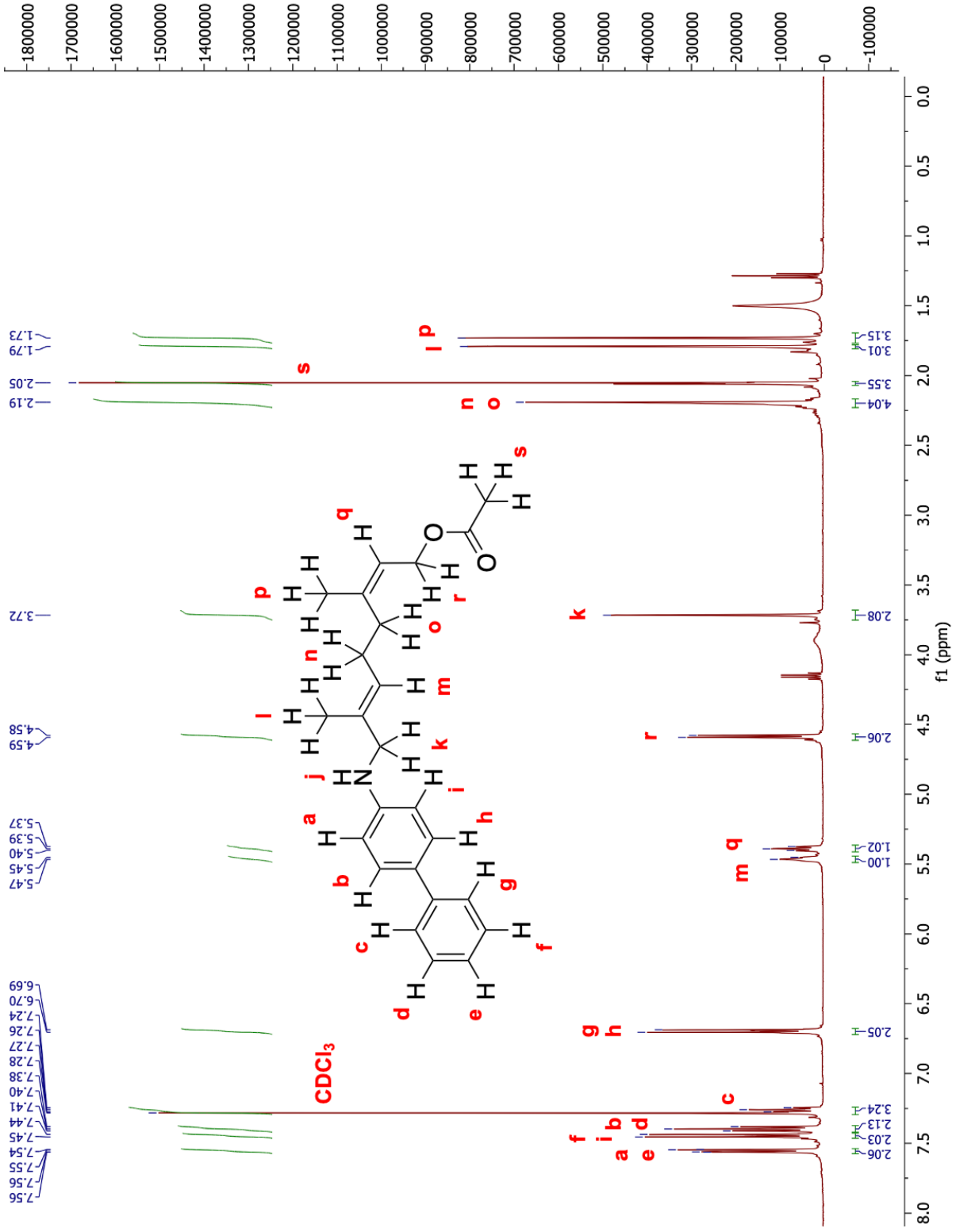

Figure C8: ^{1}H NMR spectrum of 4-aminobiphenyl neryl acetate (**5**) with structure overlay and assigned peaks

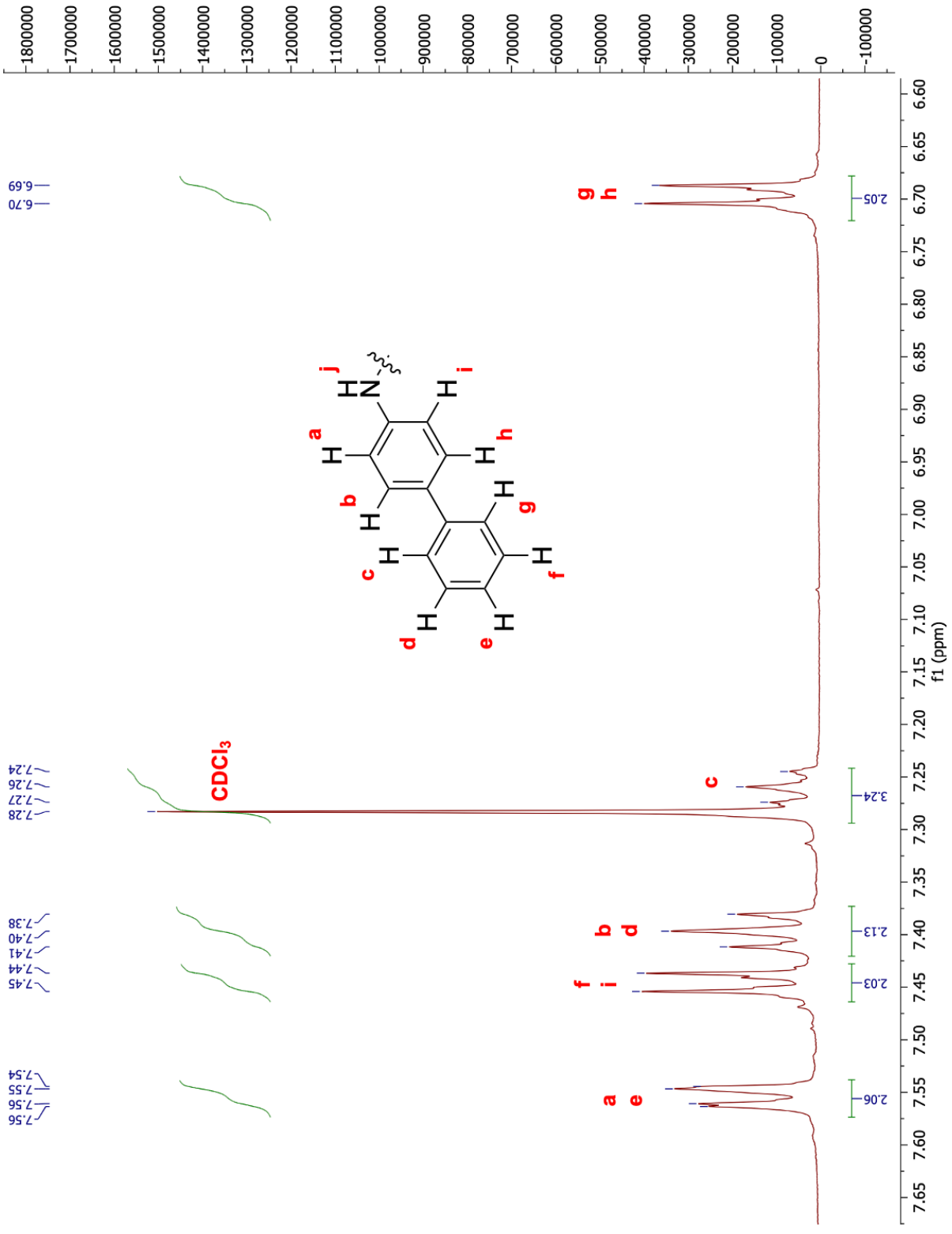

Figure C9: ^{1}H NMR spectrum of 4-aminobiphenyl neryl acetate (**5**) zoomed in at the aromatic region with structure overlay and assigned peaks

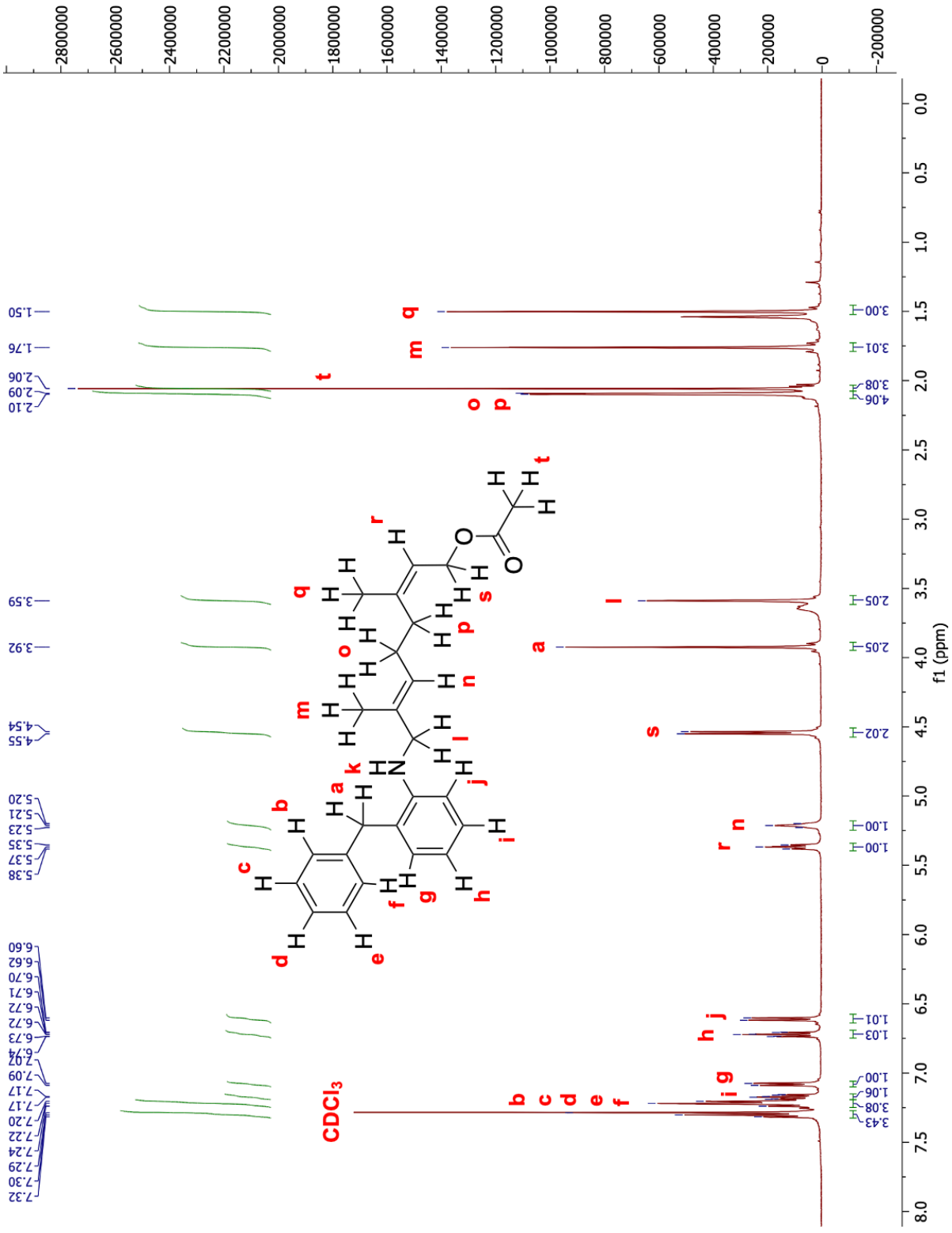

Figure C10: ^{1}H NMR spectrum of 2-benzylaniline neryl acetate (**6**) with structure overlay and assigned peaks

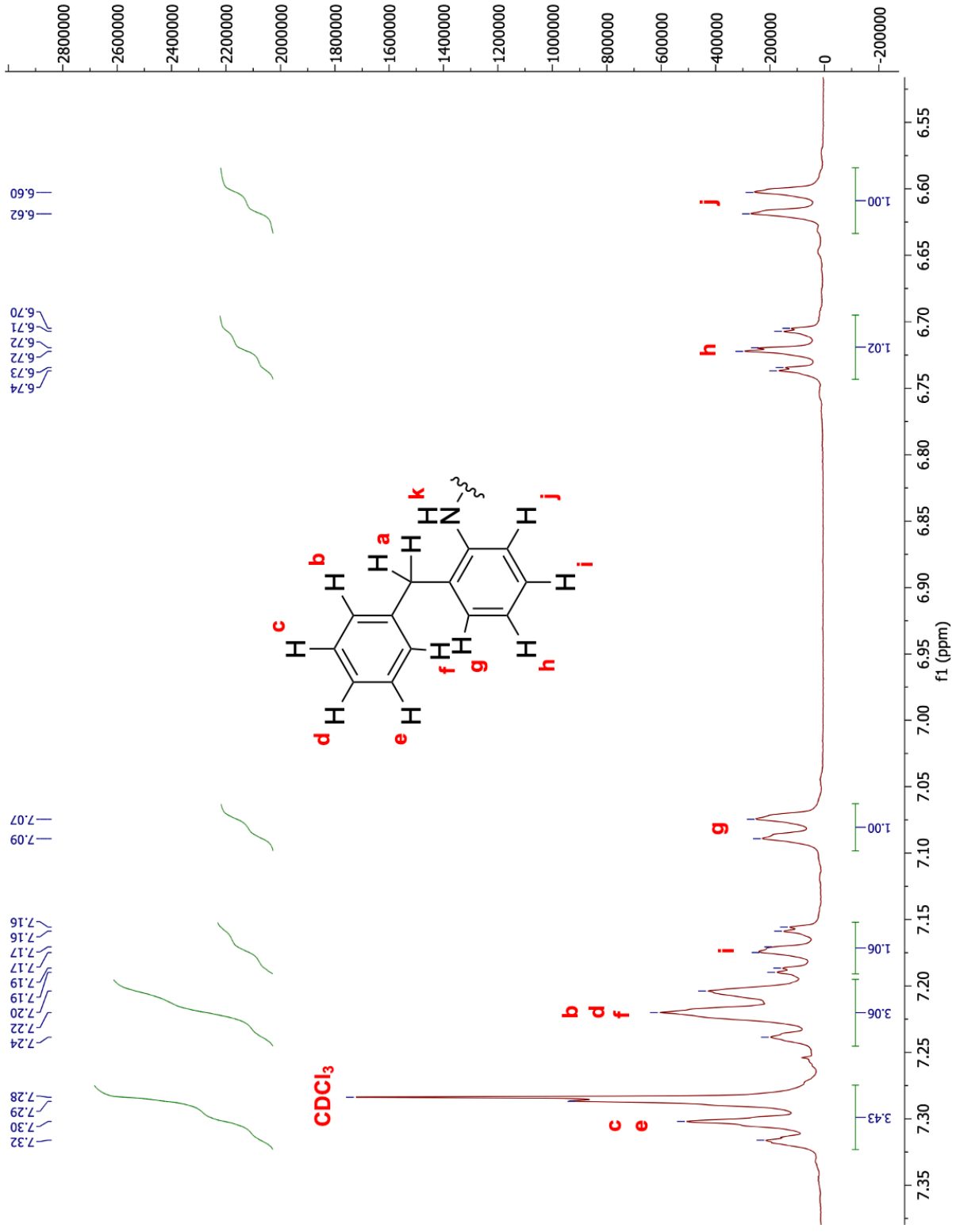

Figure C11: ^{1}H NMR spectrum of 2-benzylaniline neryl acetate (**6**) zoomed in at the aromatic region with structure overlay and assigned peaks

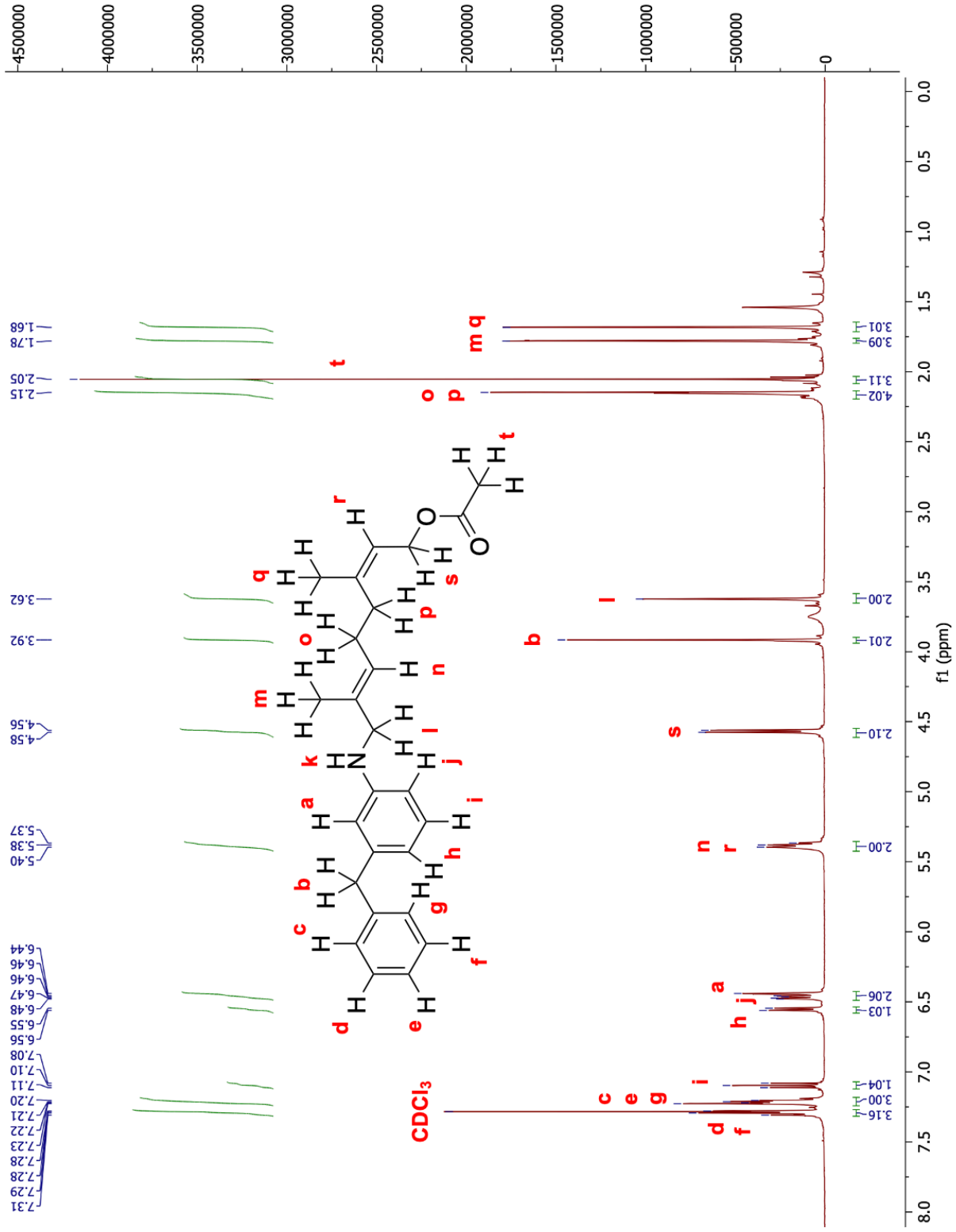

Figure C12: ^{1}H NMR spectrum of 3-benzylaniline neryl acetate (**7**) with structure overlay and assigned peaks

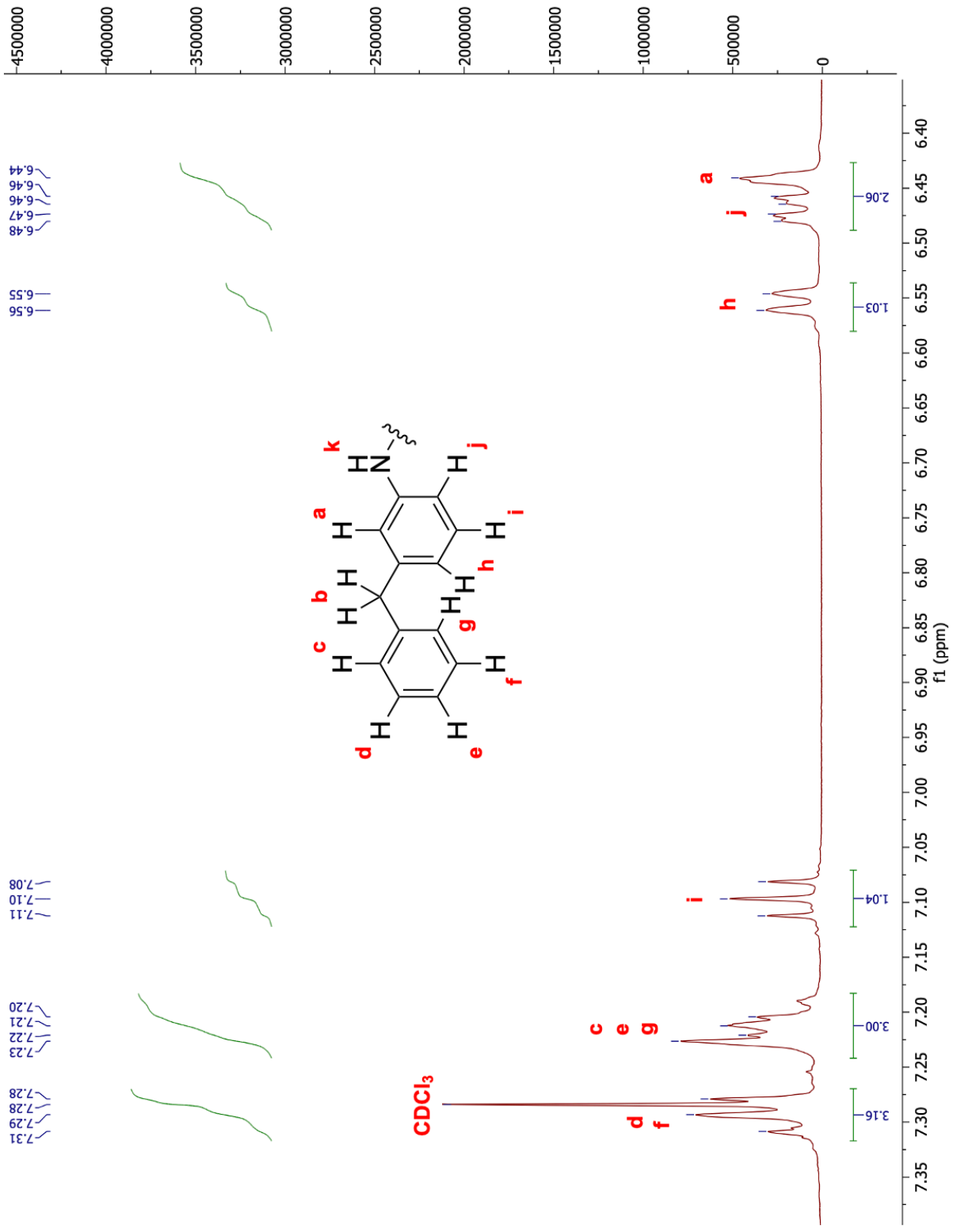

Figure C13: ^{1}H NMR spectrum of 3-benzylaniline neryl acetate (**7**) zoomed in at the aromatic region with structure overlay and assigned peaks

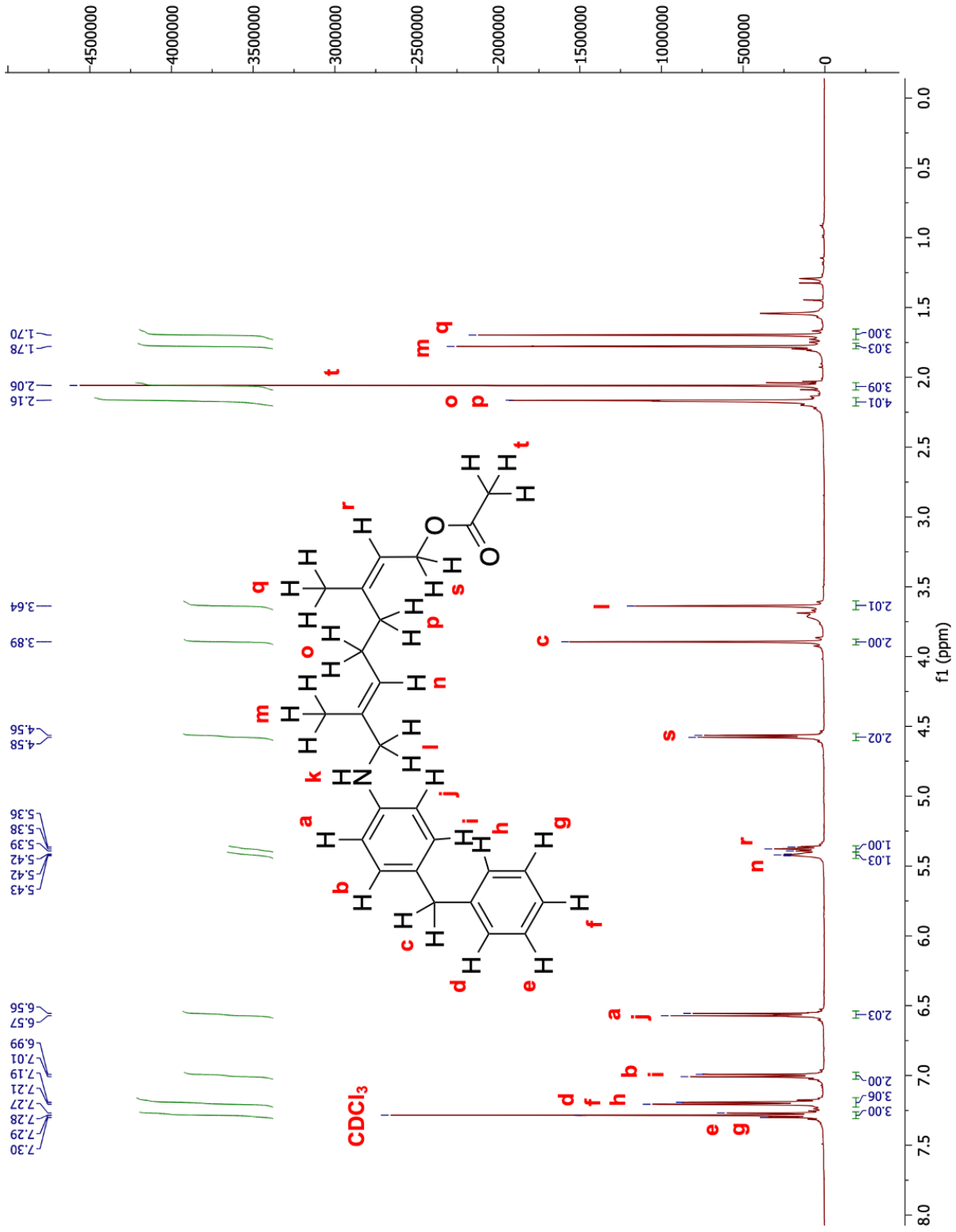

Figure C14: ^{1}H NMR spectrum of 4-benzylaniline neryl acetate (**8**) with structure overlay and assigned peaks

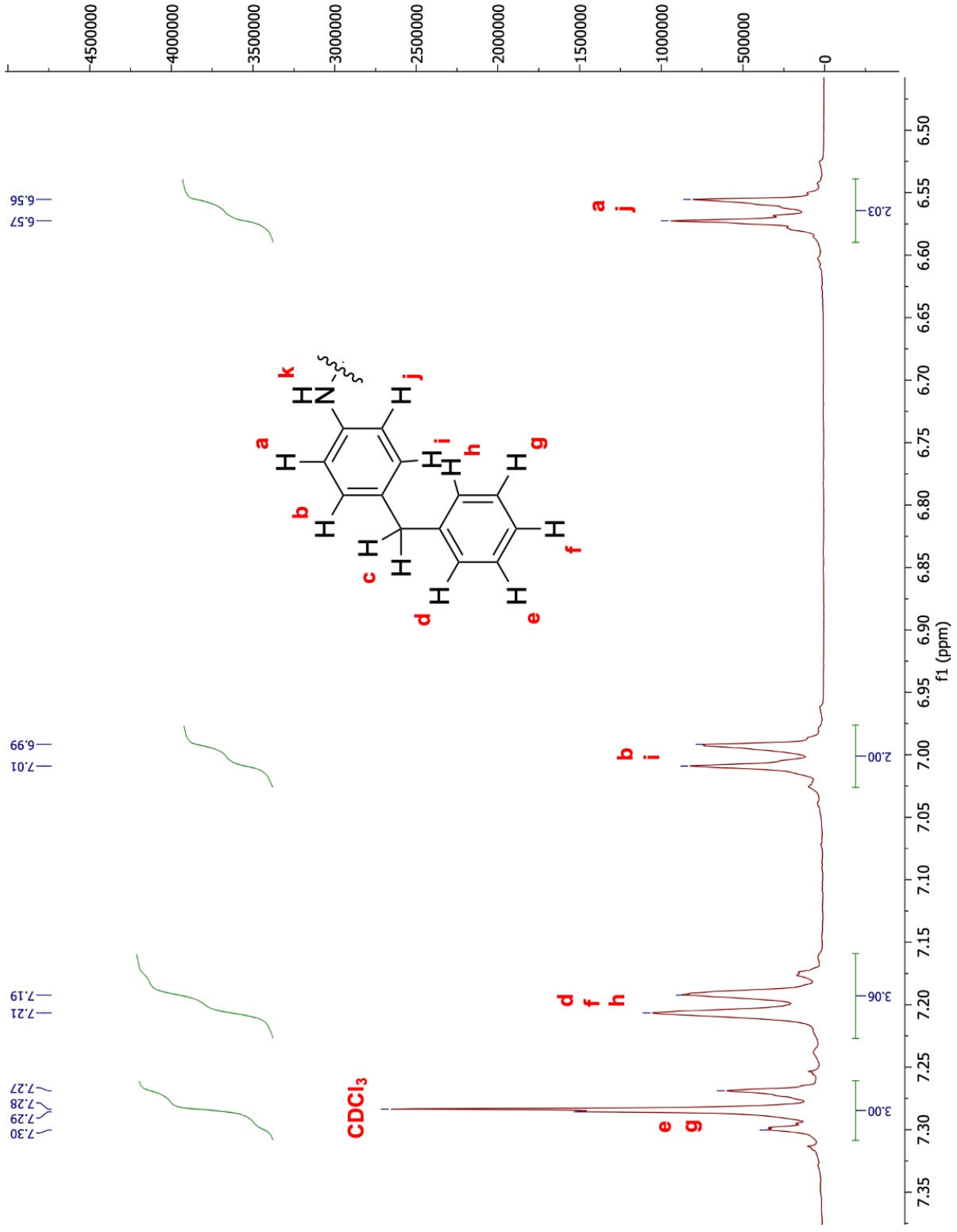

Figure C15: [1]H NMR spectrum of 4-benzylaniline neryl acetate (**8**) zoomed in at the aromatic region with structure overlay and assigned peaks

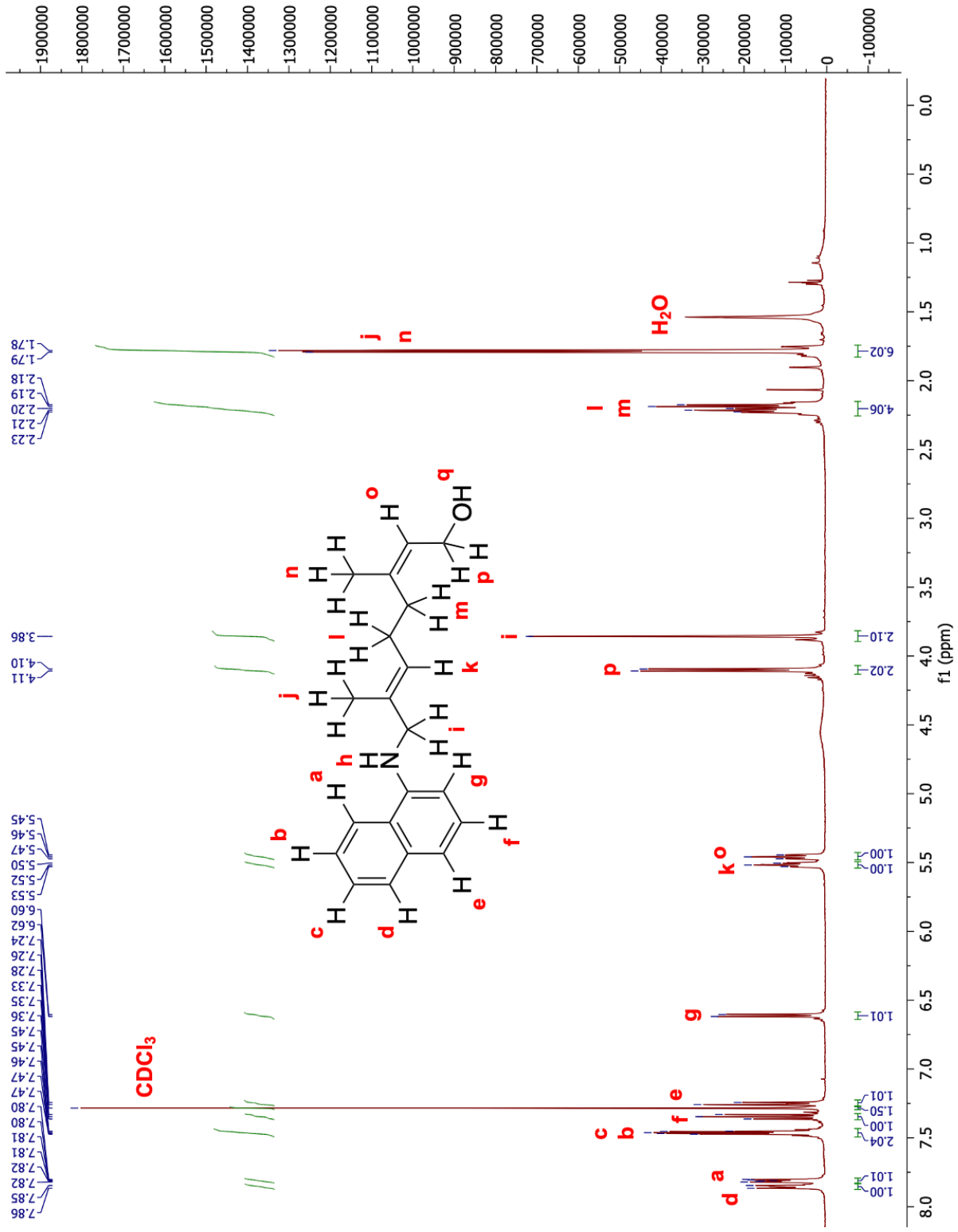

Figure C16: ^{1}H NMR spectrum of 1-naphthylamine neryl alcohol (**9**) with structure overlay and assigned peaks

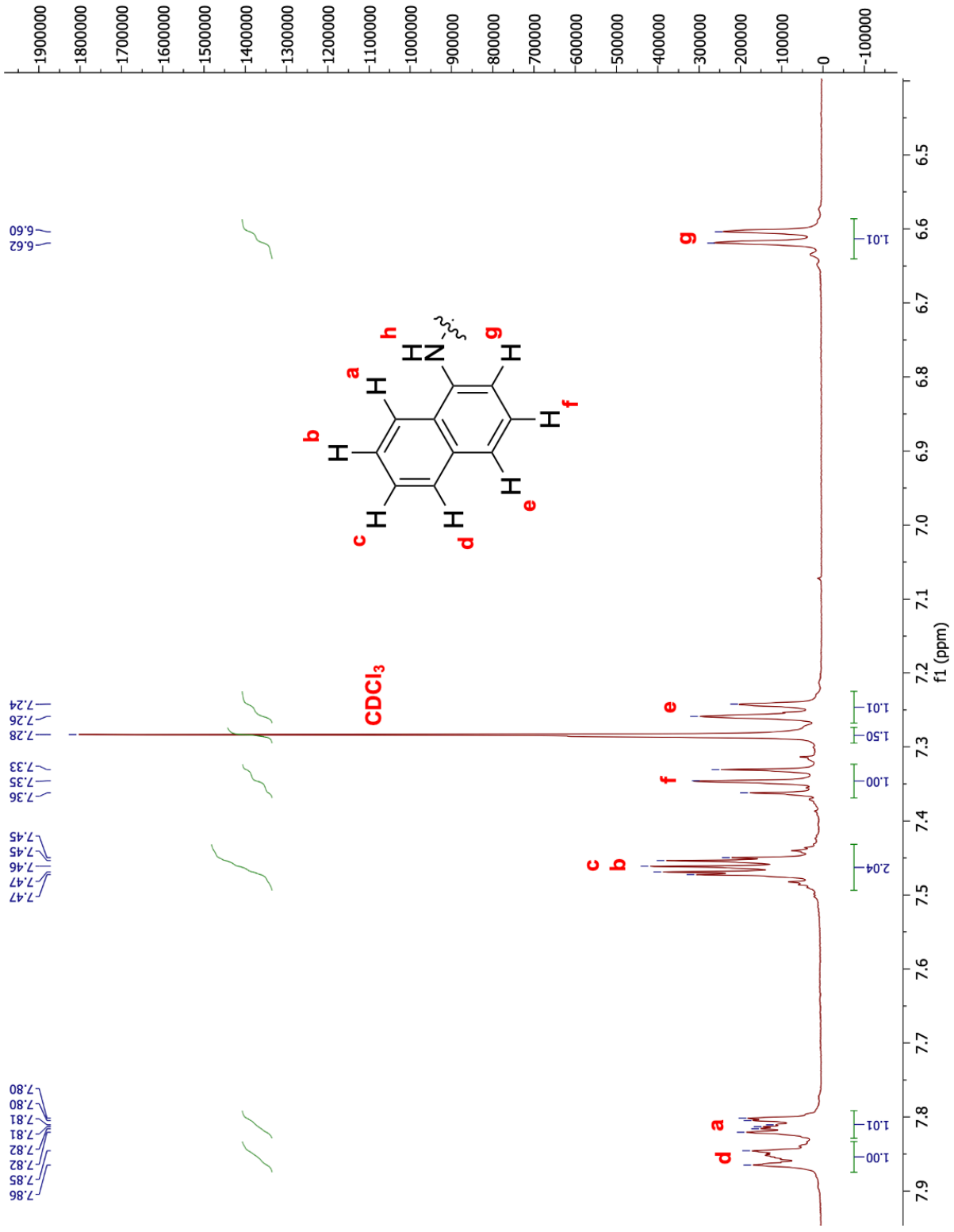

Figure C17: ^{1}H NMR spectrum of 1-naphthylamine neryl alcohol (**9**) zoomed in at the aromatic region with structure overlay and assigned peaks

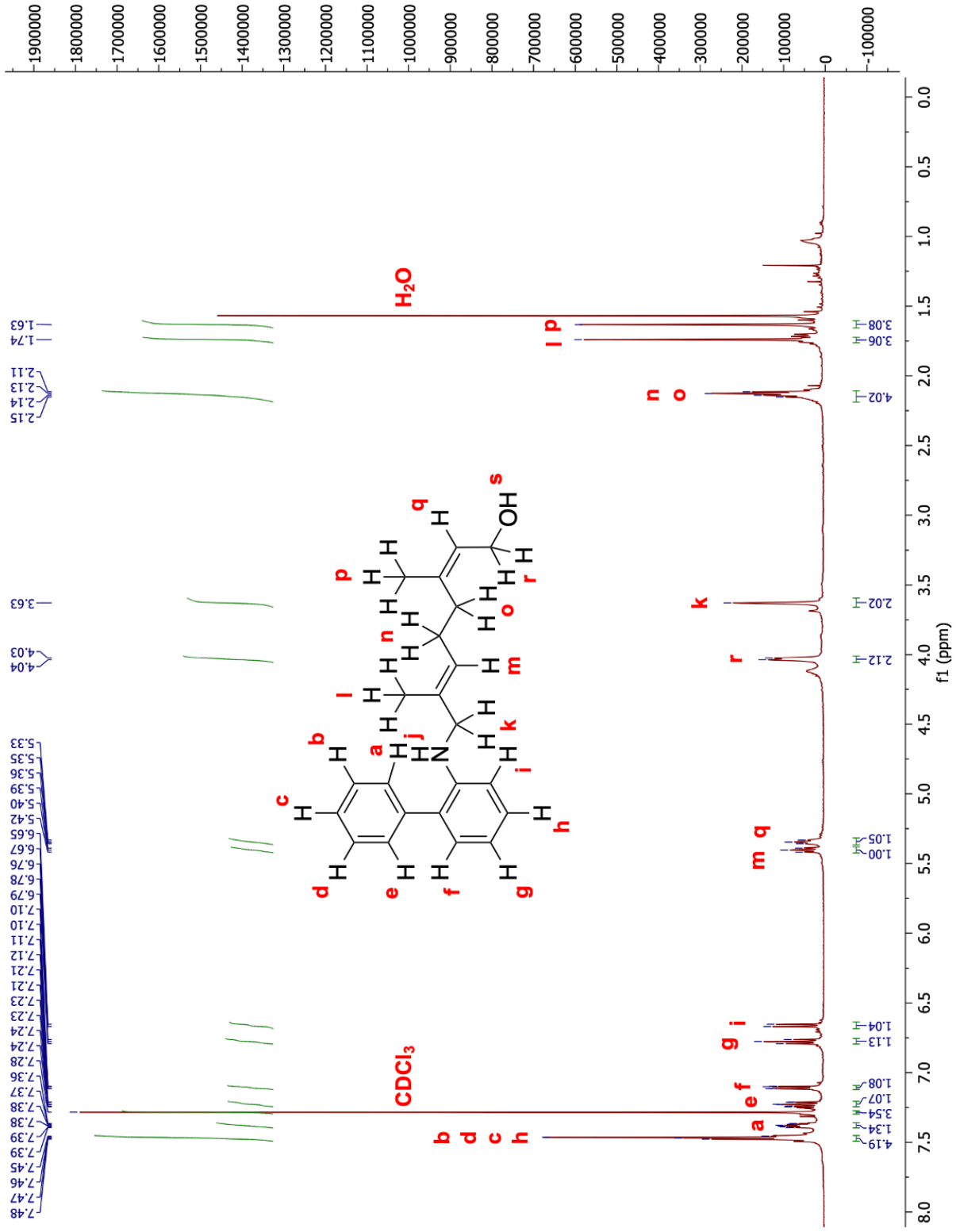

Figure C18: ^{1}H NMR spectrum of 2-aminobiphenyl neryl alcohol (**10**) with structure overlay and assigned peaks

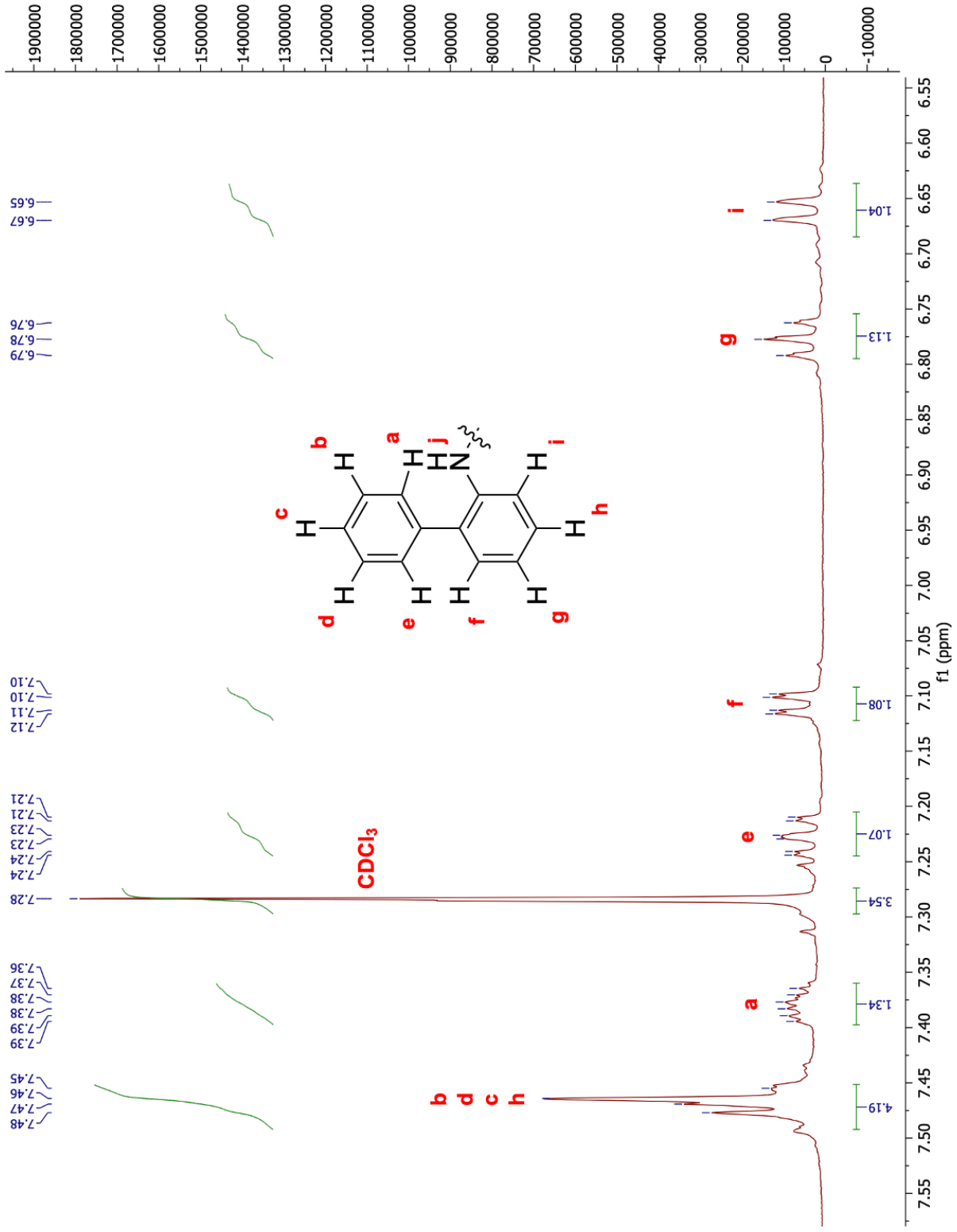

Figure C19: ^{1}H NMR spectrum of 2-aminobiphenyl neryl alcohol (**10**) zoomed in at the aromatic region with structure overlay and assigned peaks

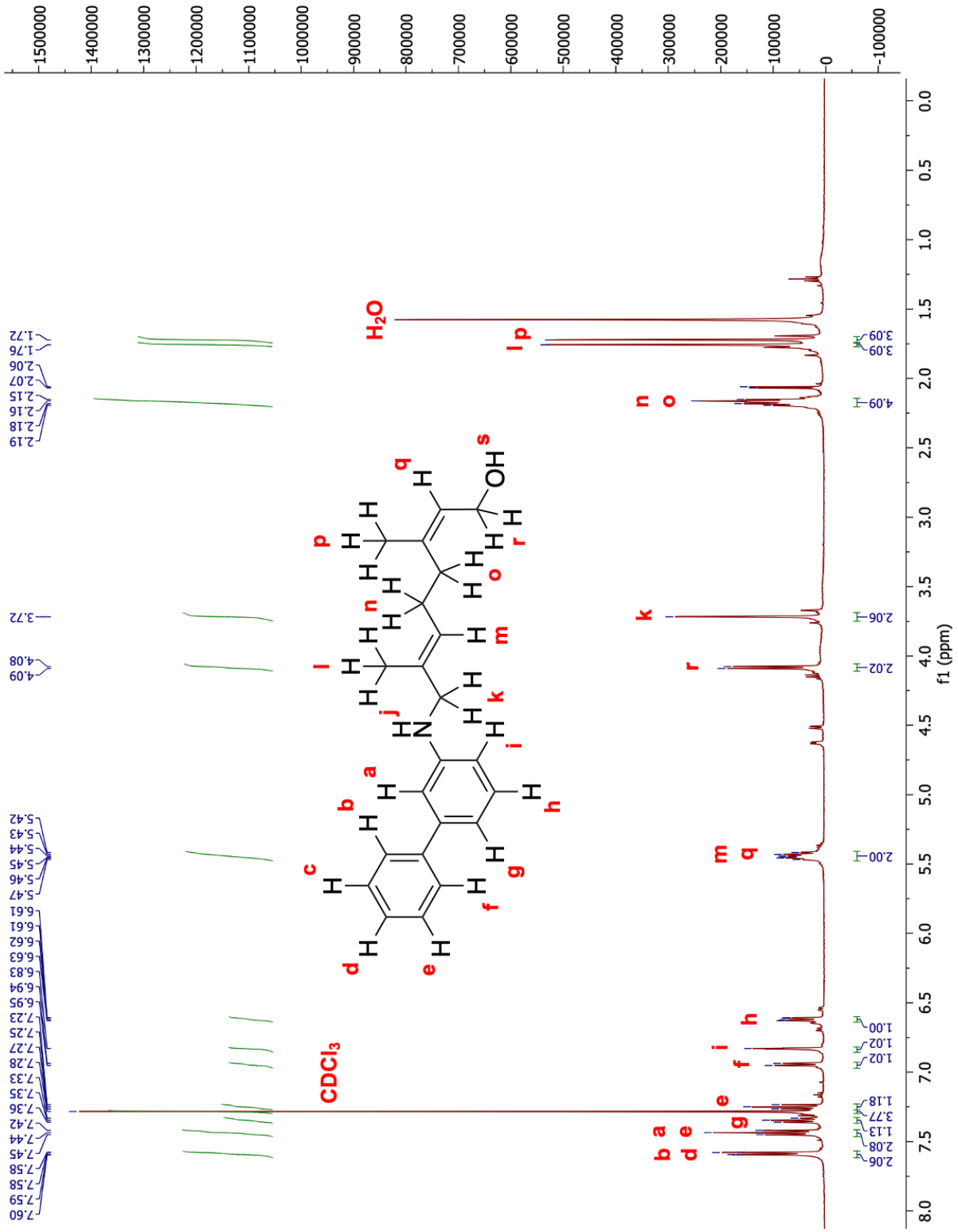

Figure C20: ^{1}H NMR spectrum of 3-aminobiphenyl neryl alcohol (**11**) with structure overlay and assigned peaks

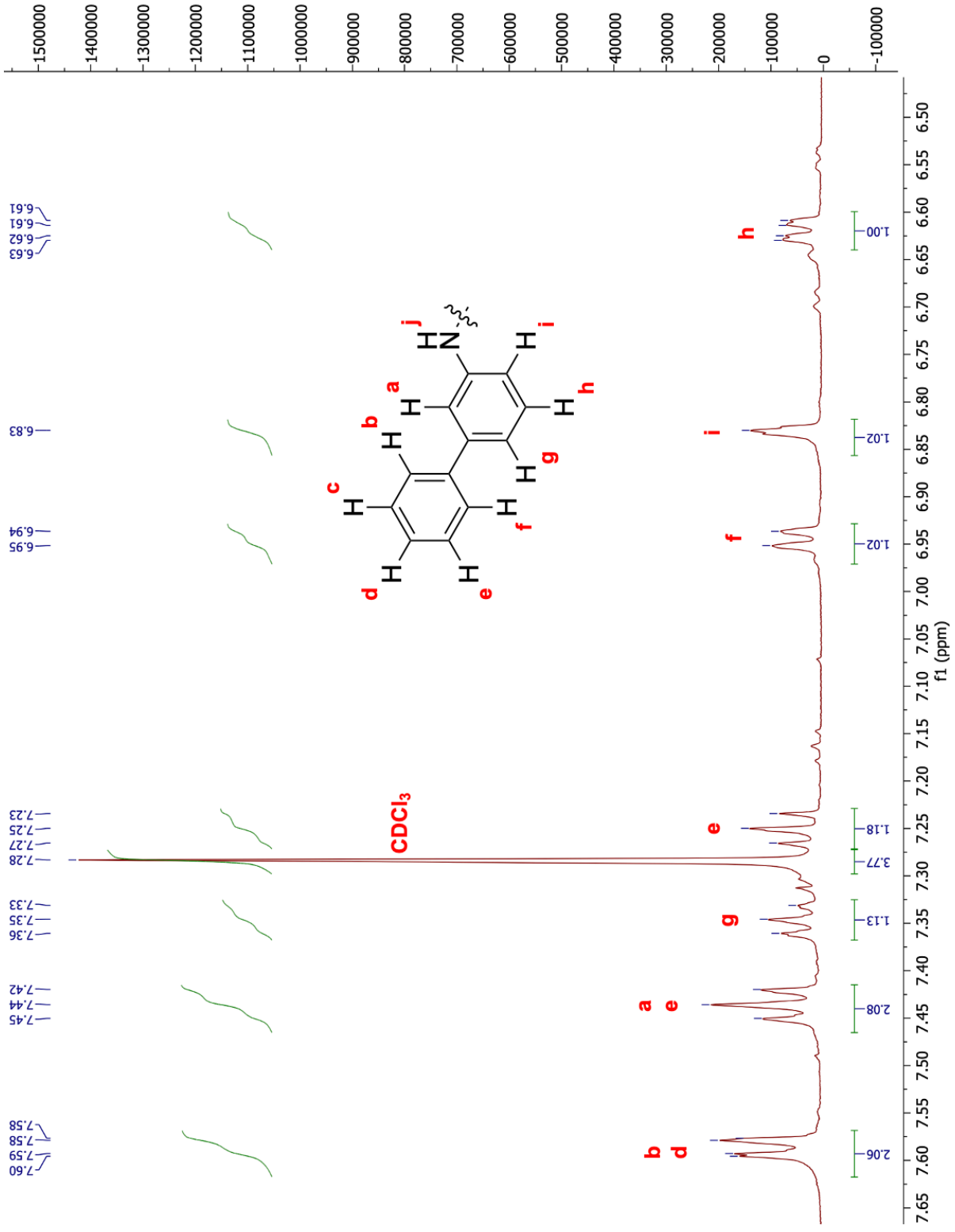

Figure C21: ^{1}H NMR spectrum of 3-aminobiphenyl neryl alcohol (**11**) zoomed in at the aromatic region with structure overlay and assigned peaks

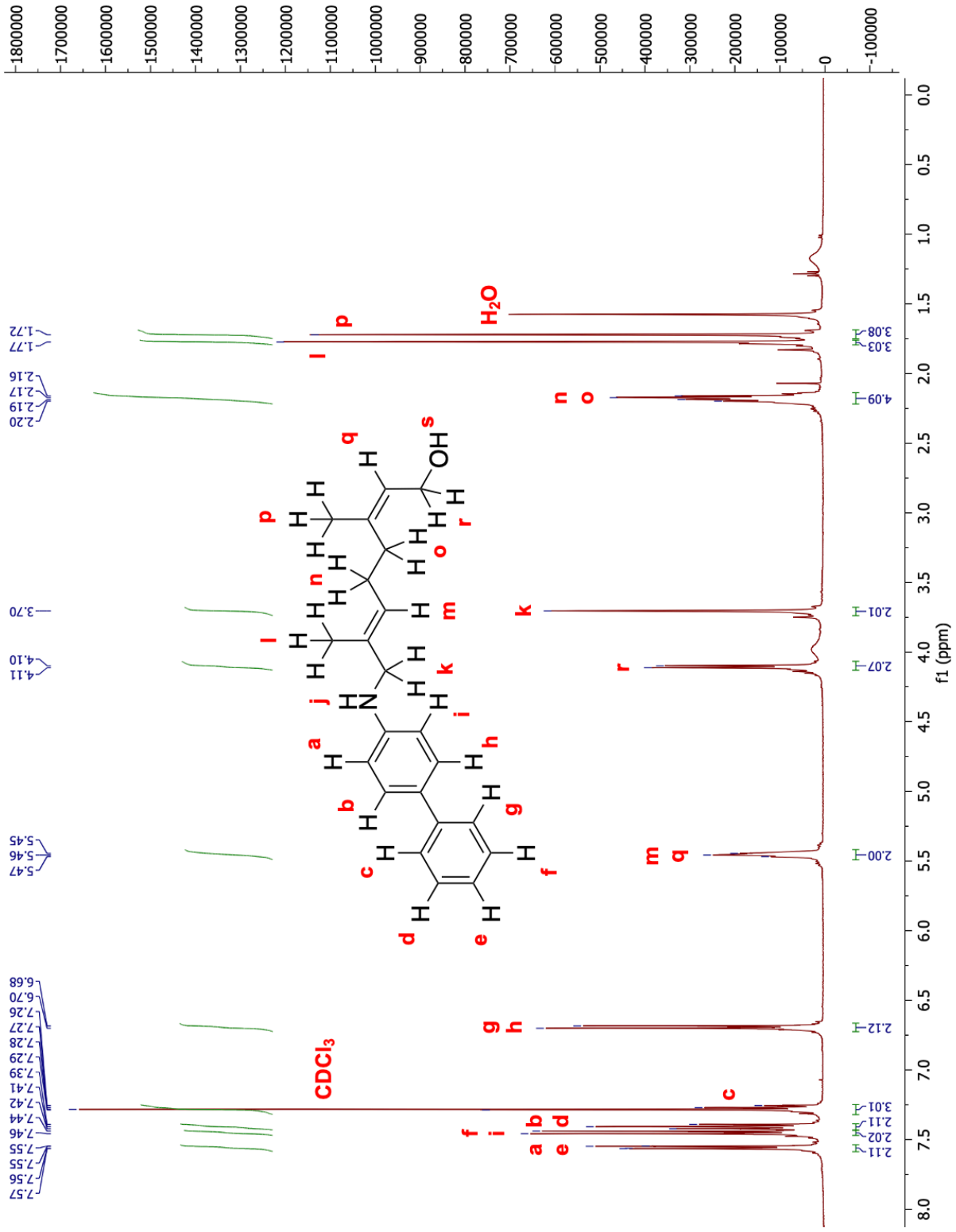

Figure C22: ^{1}H NMR spectrum of 4-aminobiphenyl neryl alcohol (**12**) with structure overlay and assigned peaks

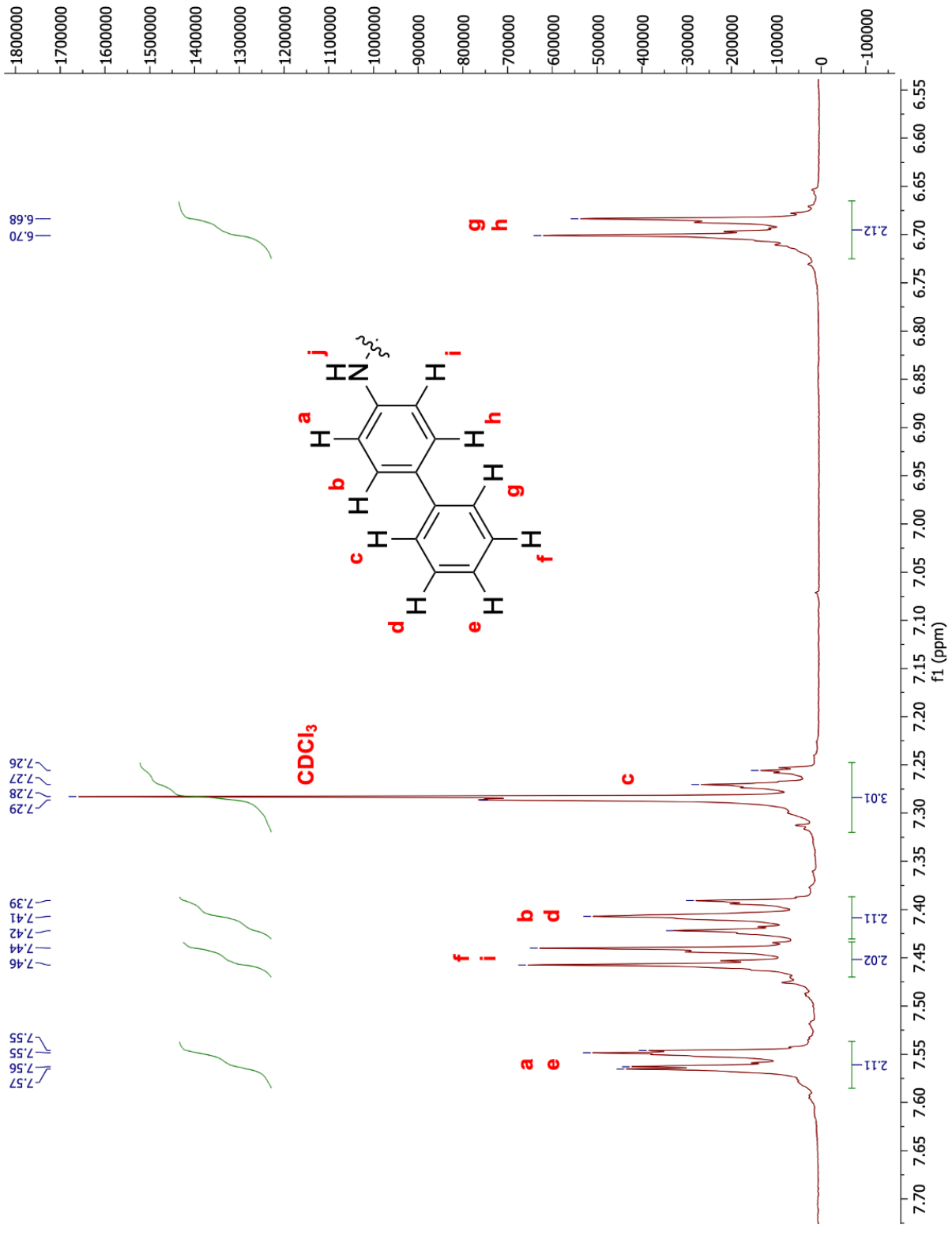

Figure C23: ^{1}H NMR spectrum of 4-aminobiphenyl neryl alcohol (**12**) zoomed in at the aromatic region with structure overlay and assigned peaks

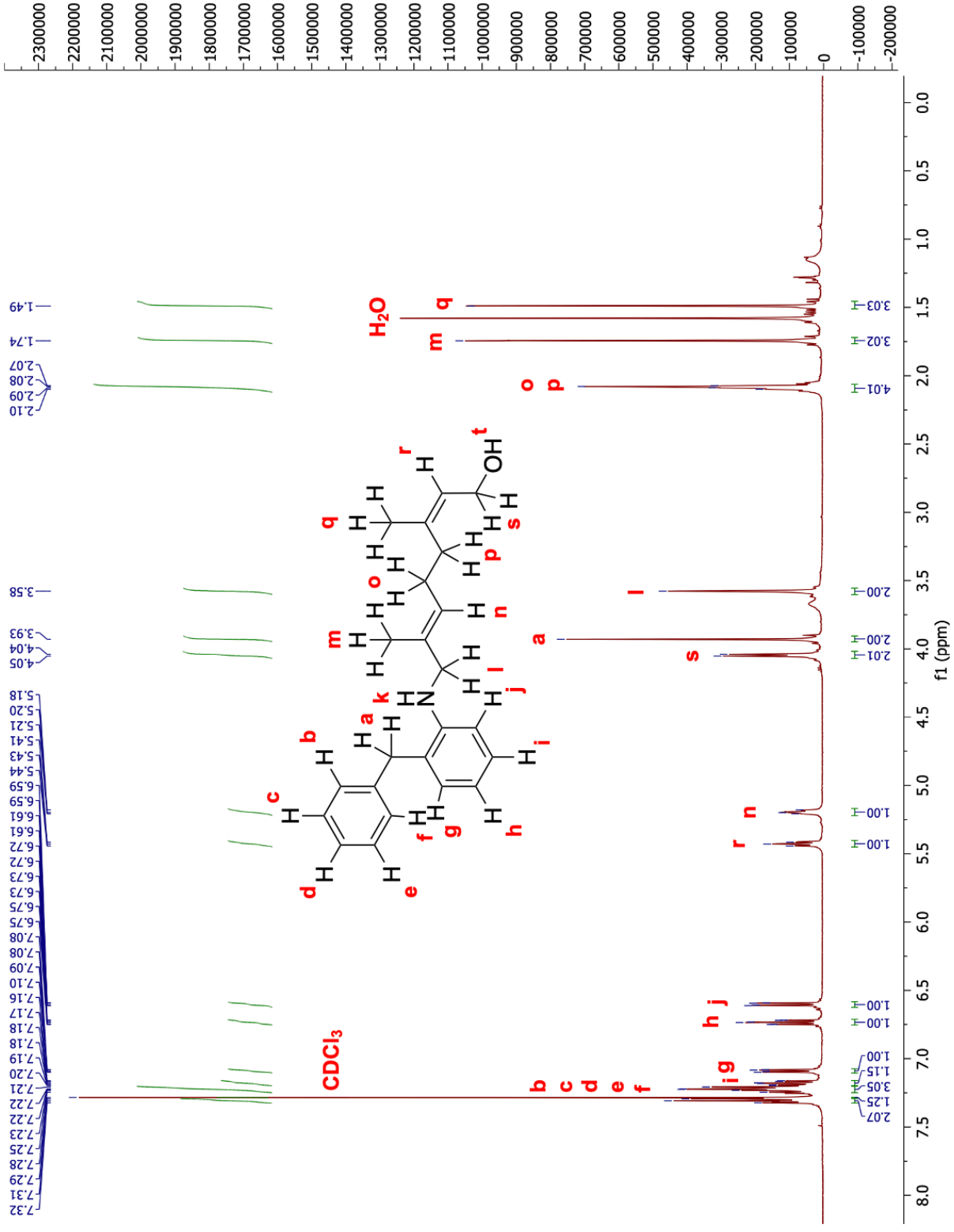

Figure C24: ^{1}H NMR spectrum of 2-benzylaniline neryl alcohol (**13**) with structure overlay and assigned peaks

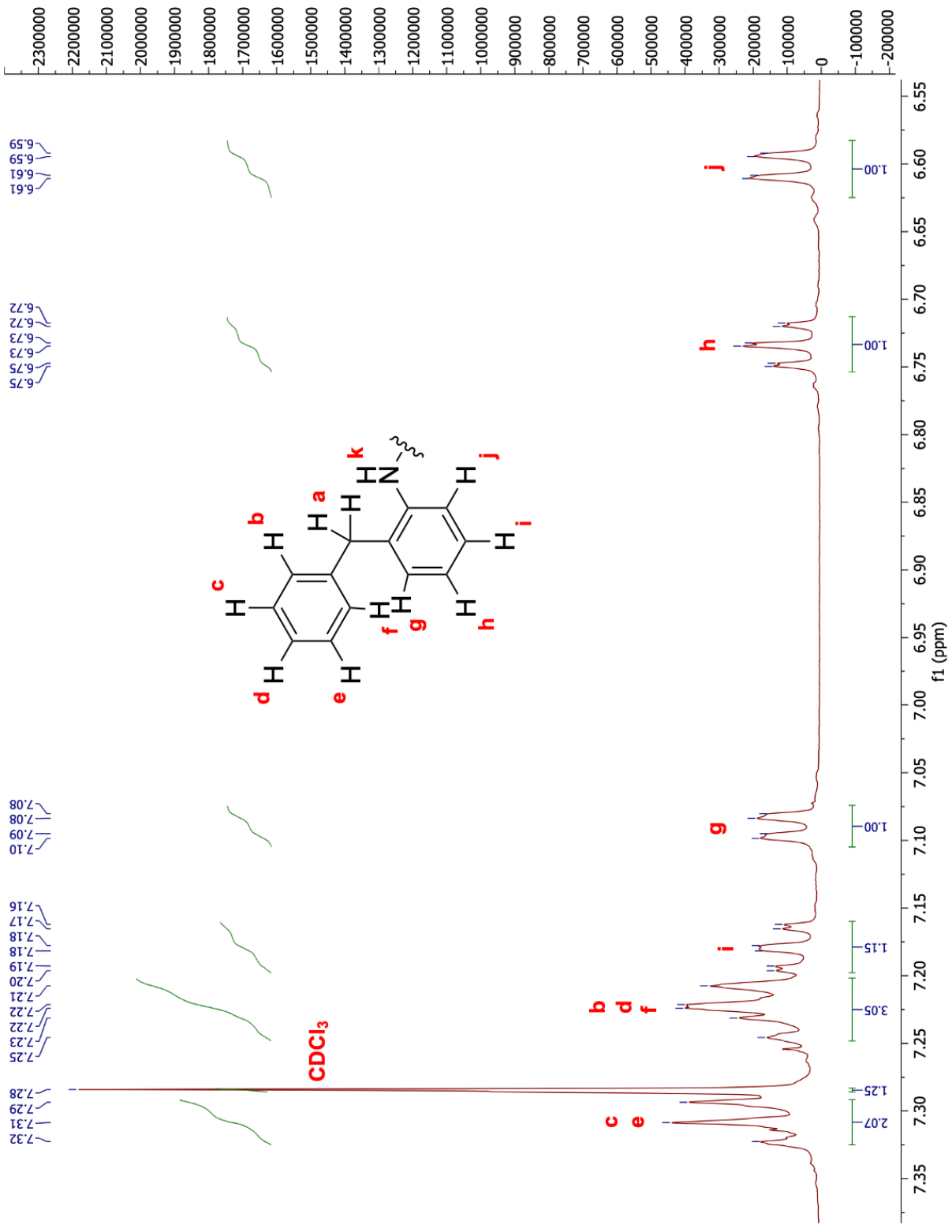

Figure C25: ^{1}H NMR spectrum of 2-benzylaniline neryl alcohol (**13**) zoomed in at the aromatic region with structure overlay and assigned peaks

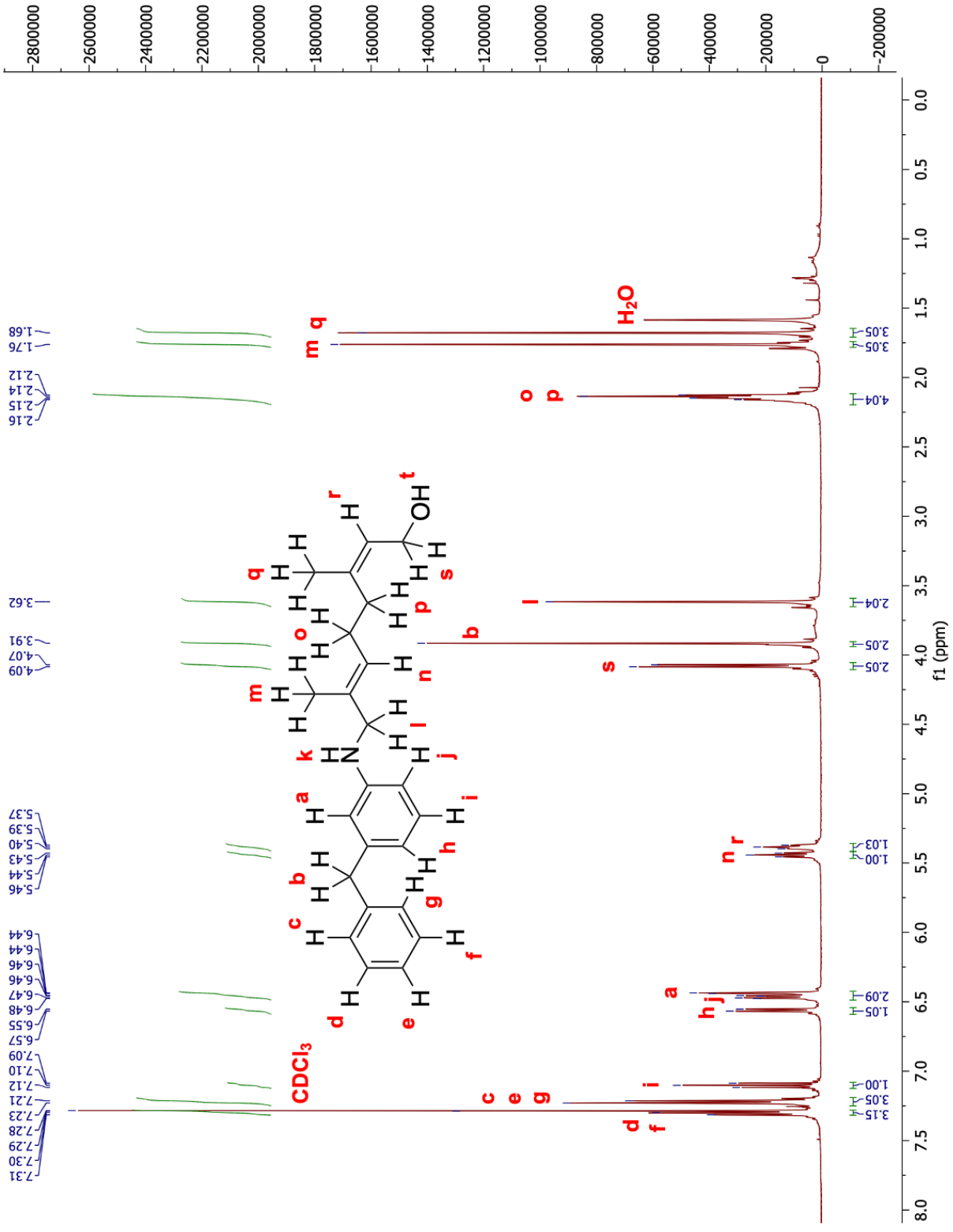

Figure C26: ^{1}H NMR spectrum of 3-benzylaniline neryl alcohol (**14**) with structure overlay and assigned peaks

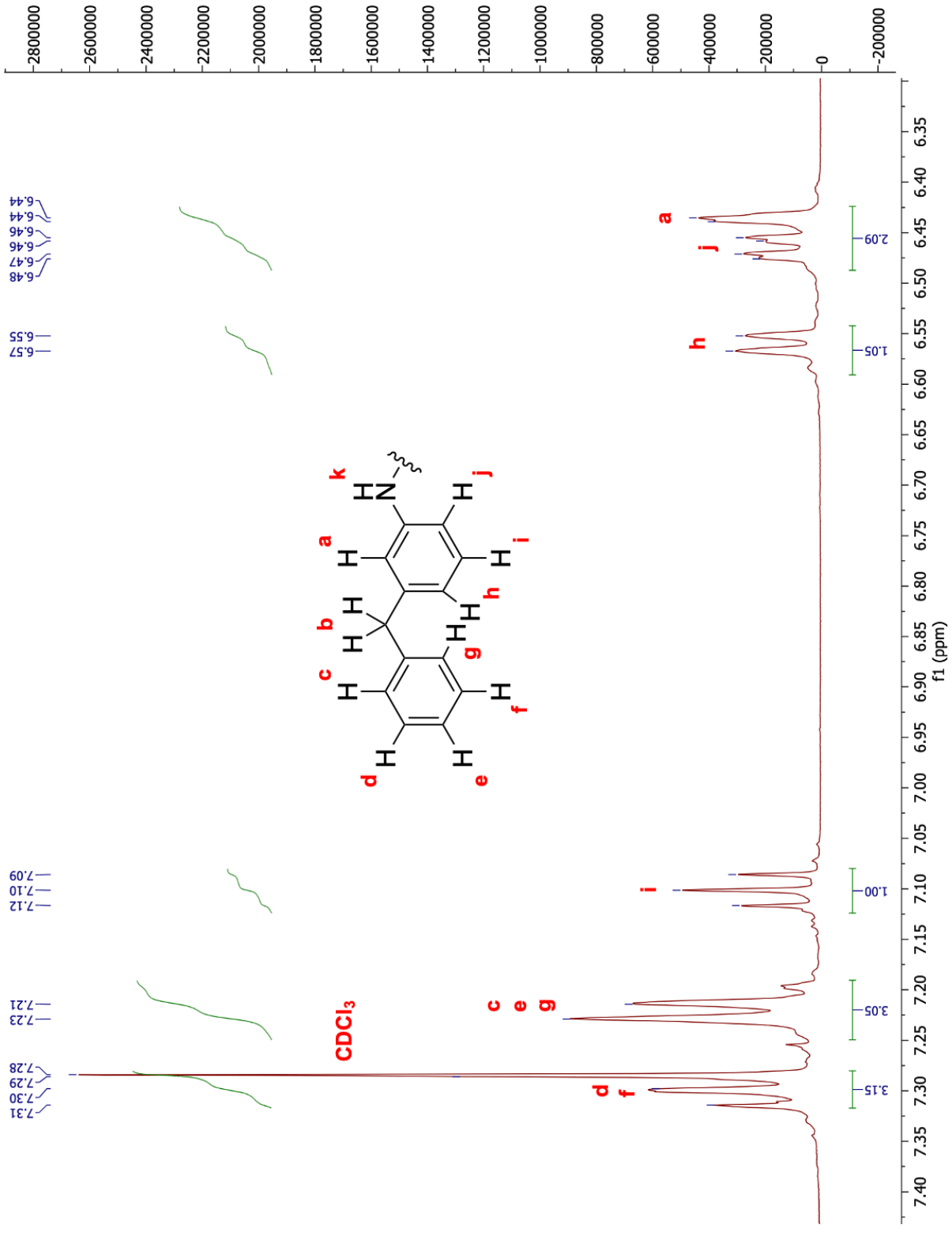

Figure C27: ^{1}H NMR spectrum of 3-benzylaniline neryl alcohol (**14**) zoomed in at the aromatic region with structure overlay and assigned peaks

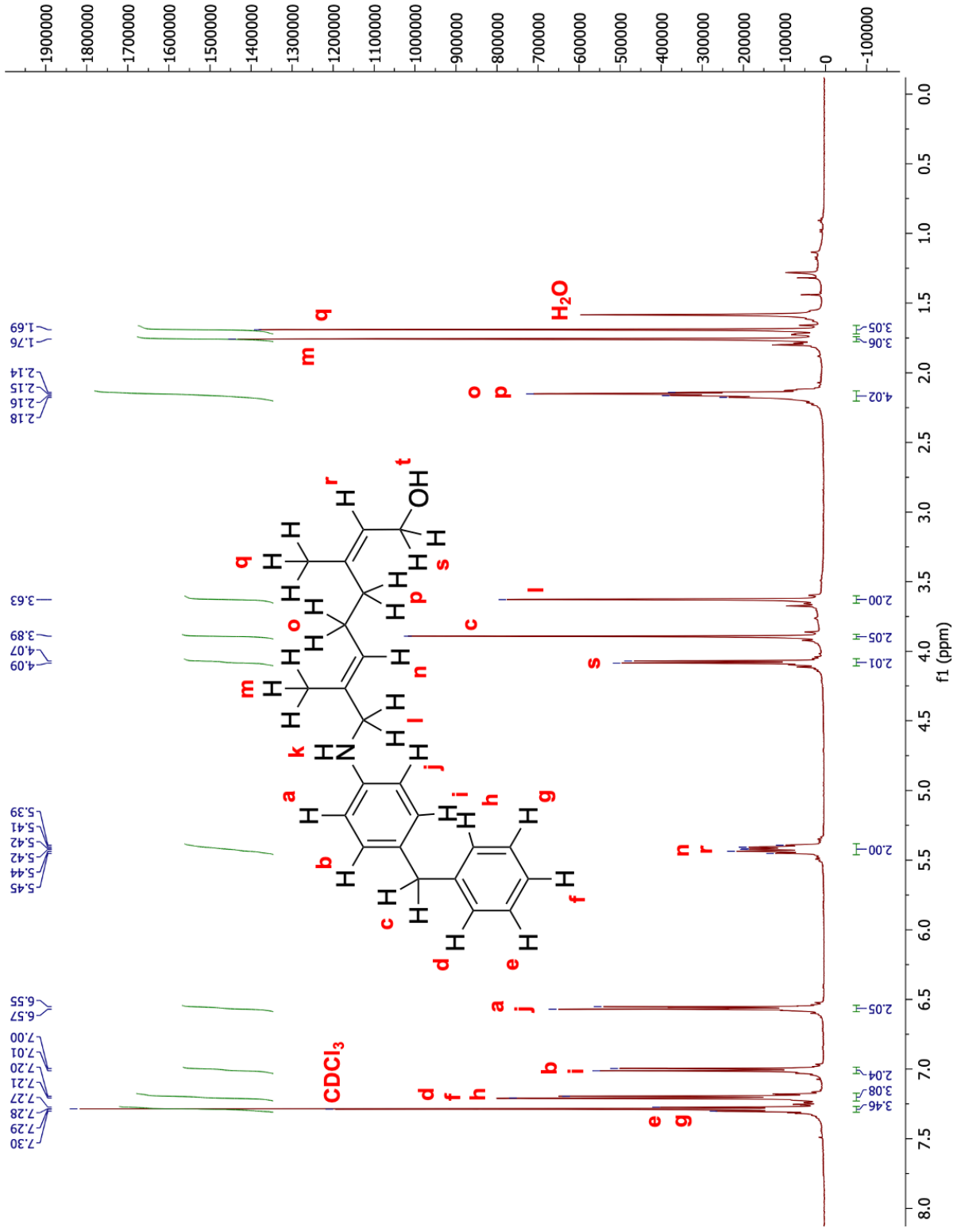

Figure C28: ^{1}H NMR spectrum of 4-benzylaniline neryl alcohol (**15**) with structure overlay and assigned peaks

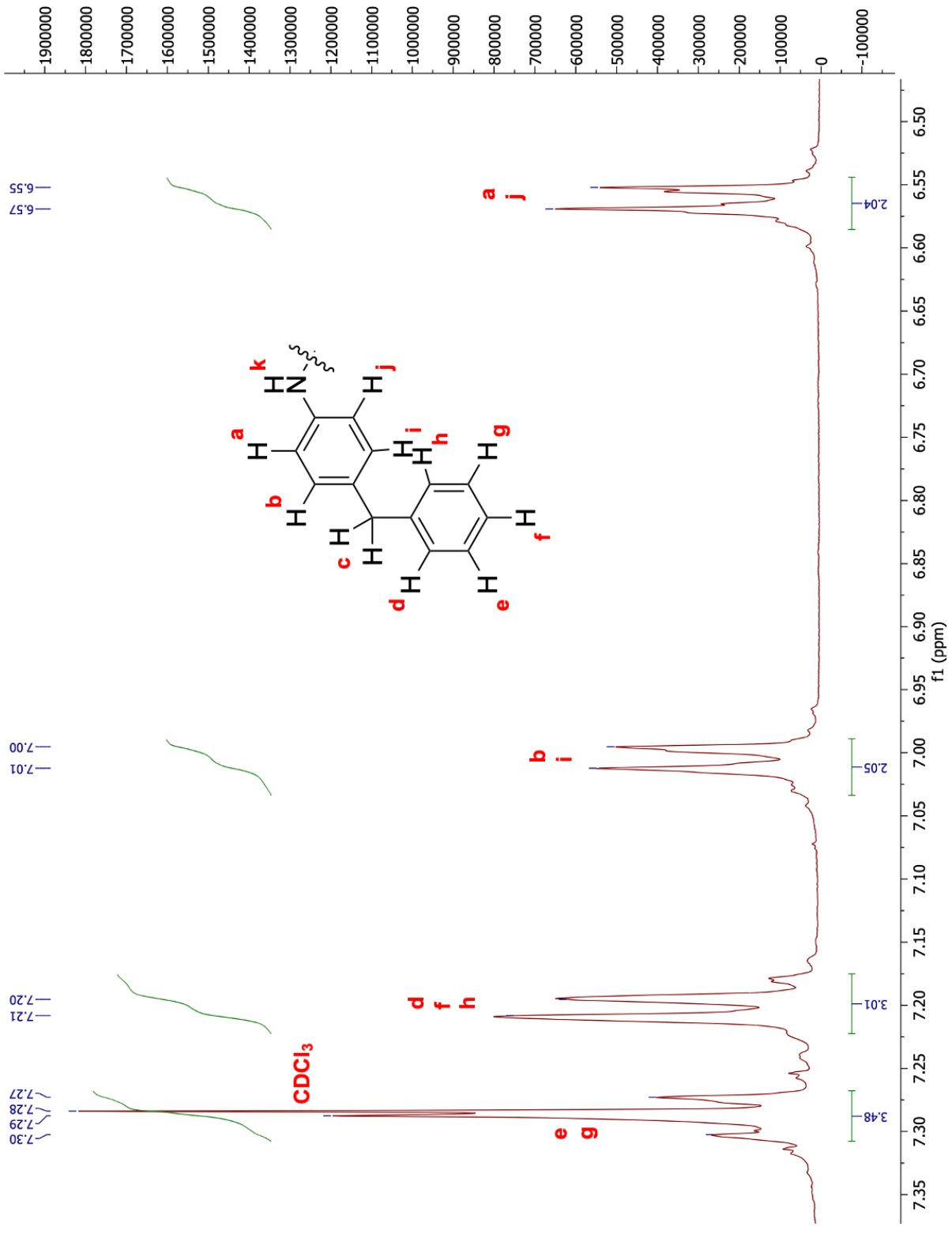

Figure C29: ^{1}H NMR spectrum of 4-benzylaniline neryl alcohol (**15**) zoomed in at the aromatic region with structure overlay and assigned peaks

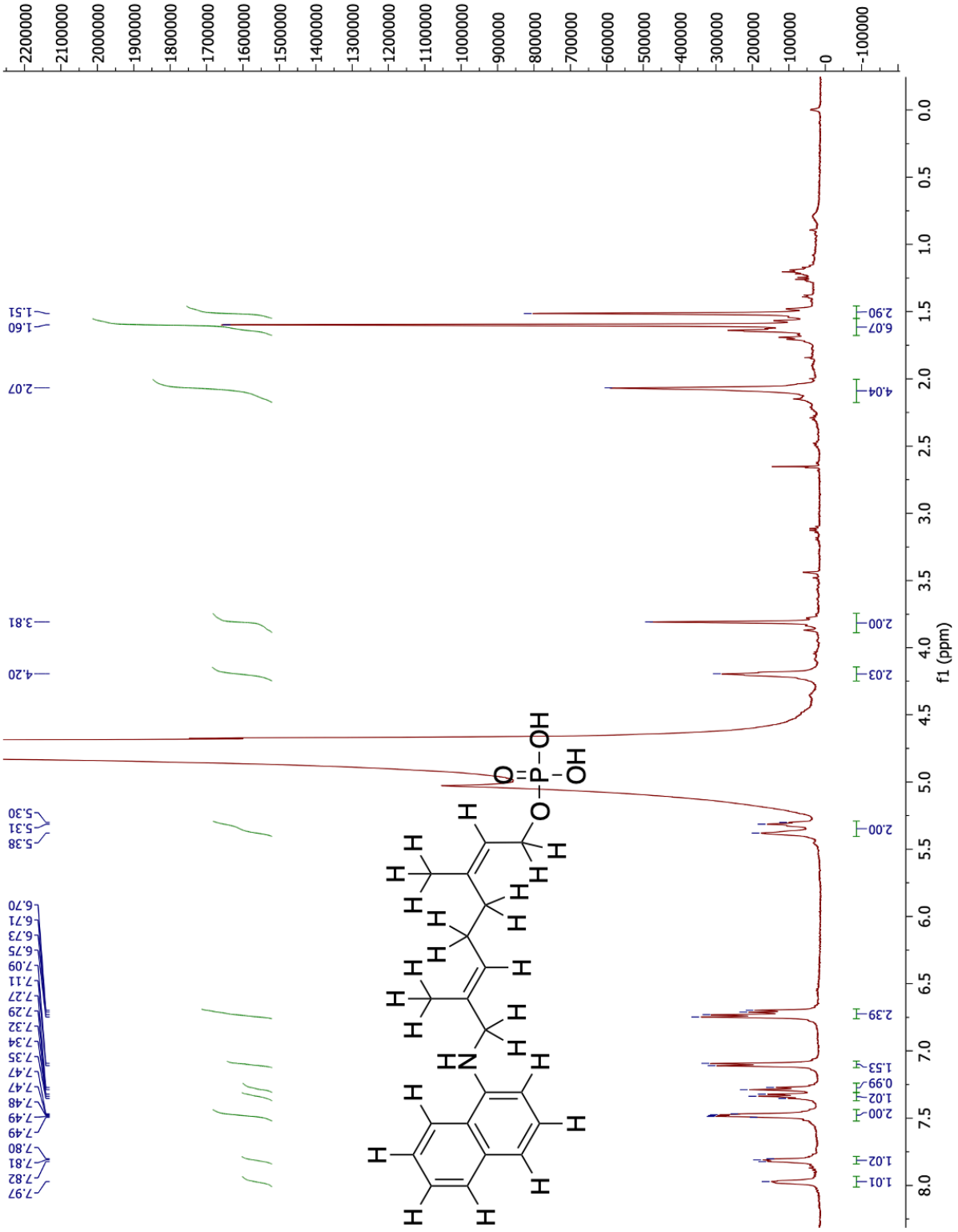

Figure C30: ^{1}H NMR spectrum of 1-naphthylamine neryl monophosphate (**16**) with structure overlay

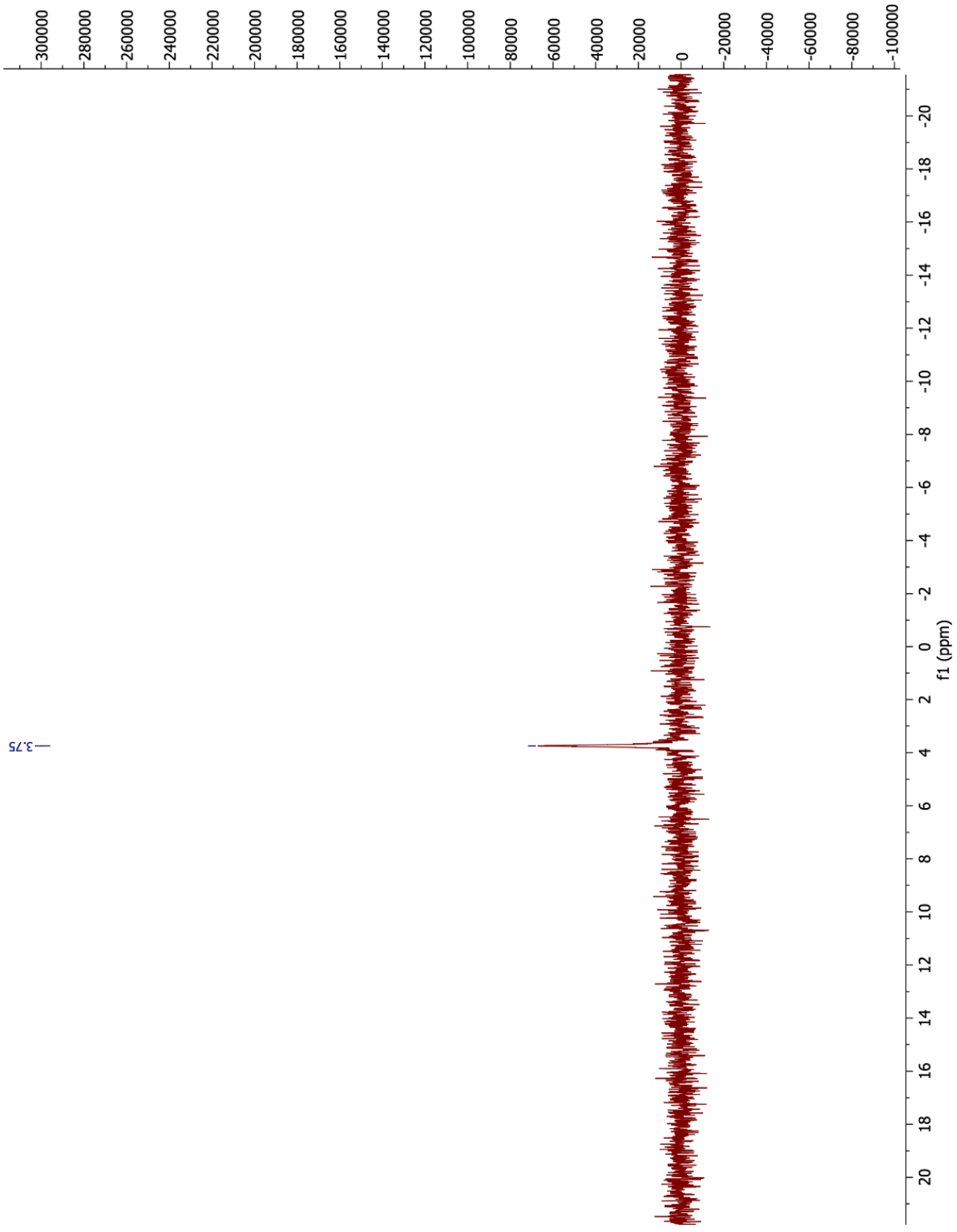

Figure C31: ^{31}P NMR spectrum of 1-naphthylamine neryl monophosphate (**16**)

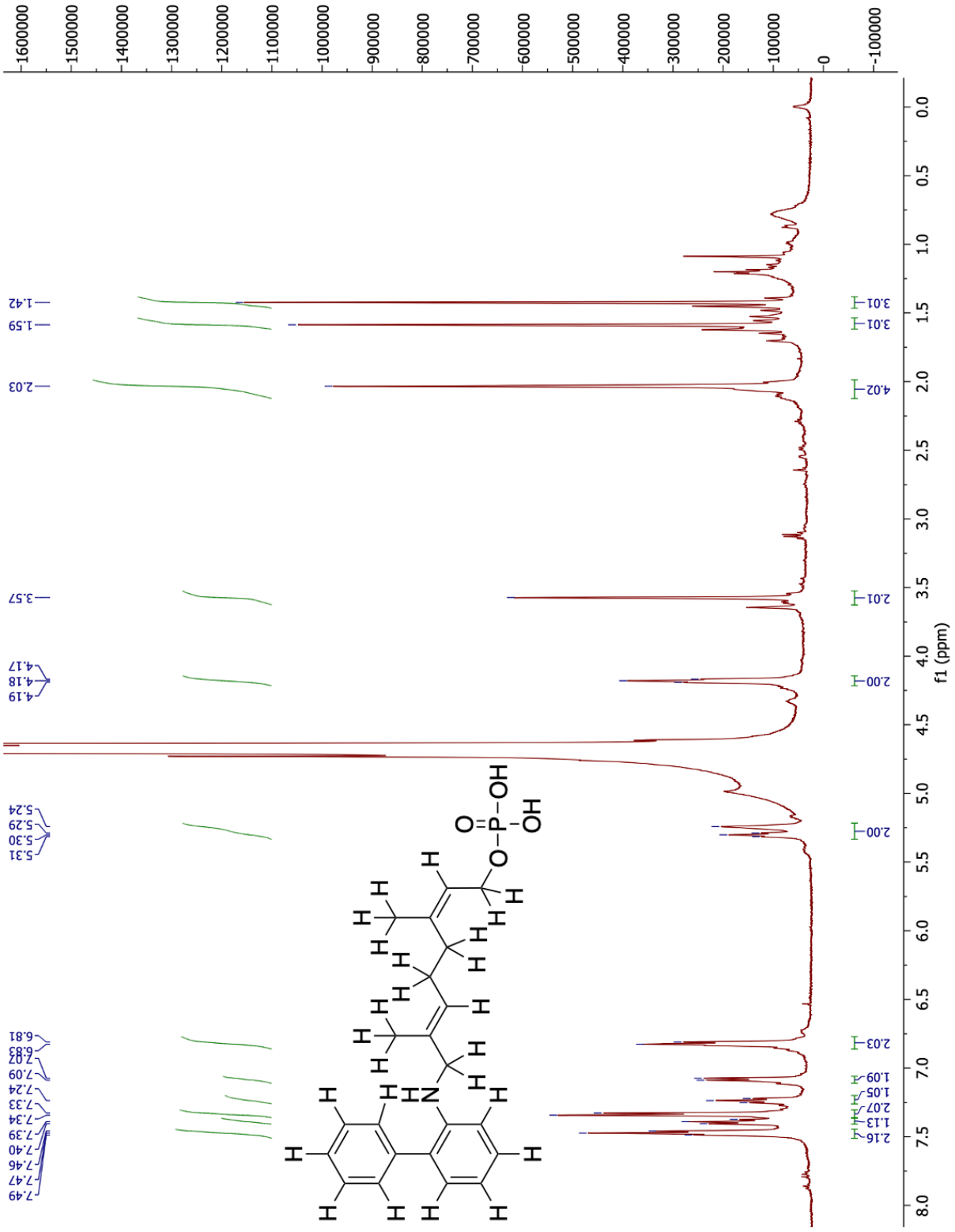

Figure C32: ^{1}H NMR spectrum of 2-aminobiphenyl neryl monophosphate (**17**) with structure overlay

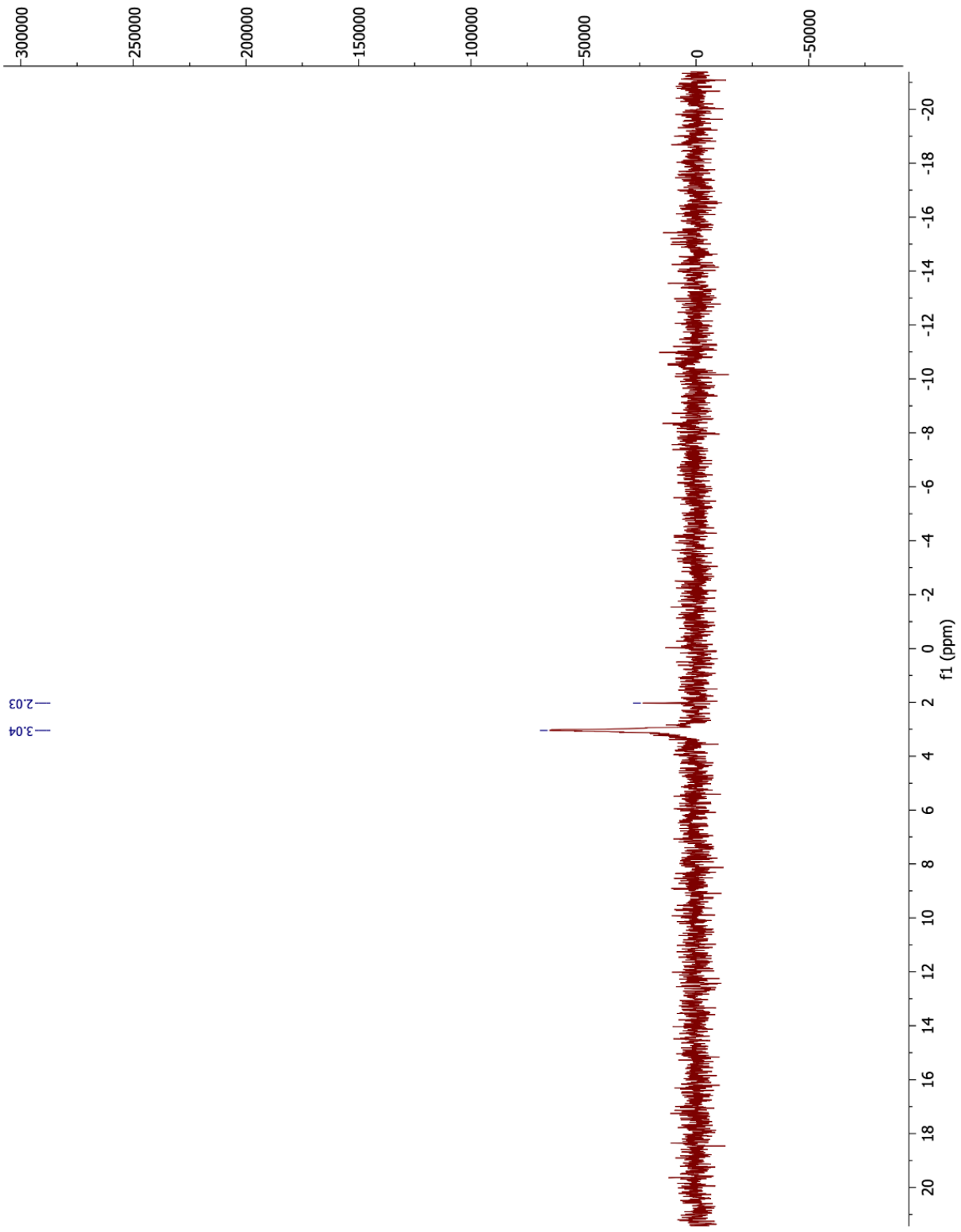

Figure C33: ^{31}P NMR spectrum of 2-aminobiphenyl neryl monophosphate (**17**)

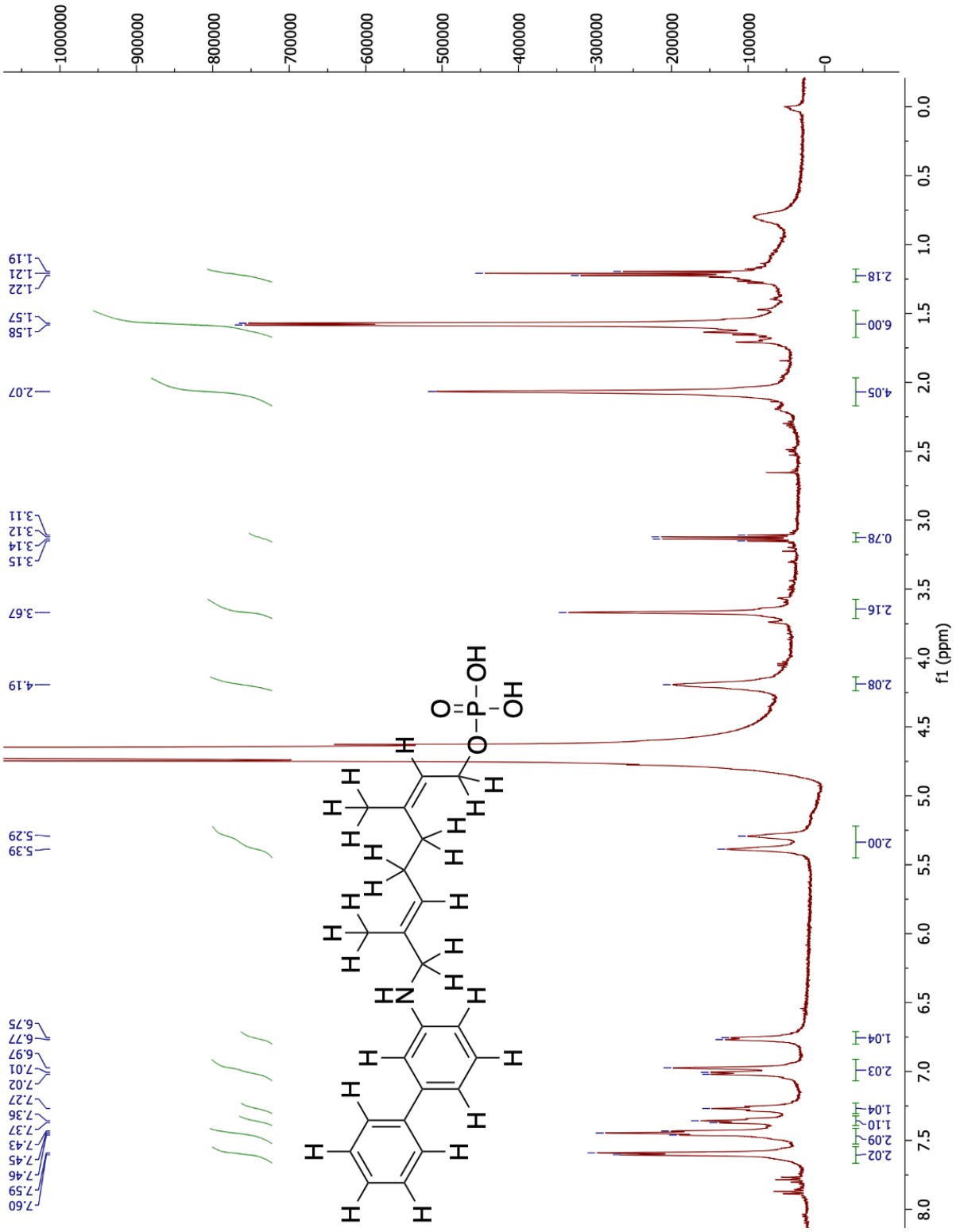

Figure C34: ^{1}H NMR spectrum of 3-aminobiphenyl neryl monophosphate (**18**) with structure overlay

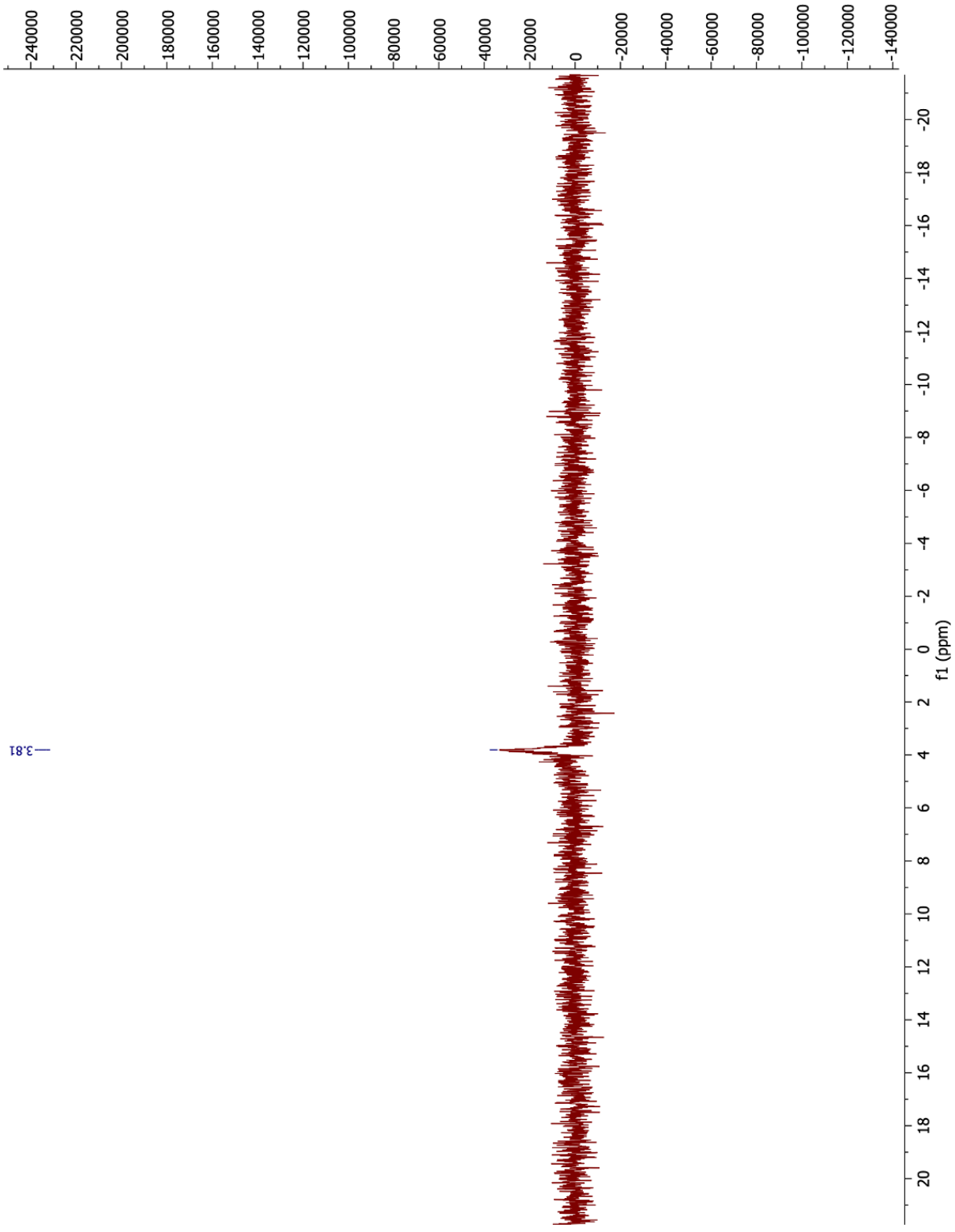

Figure C35: ^{31}P NMR spectrum of 3-aminobiphenyl neryl monophosphate (**18**)

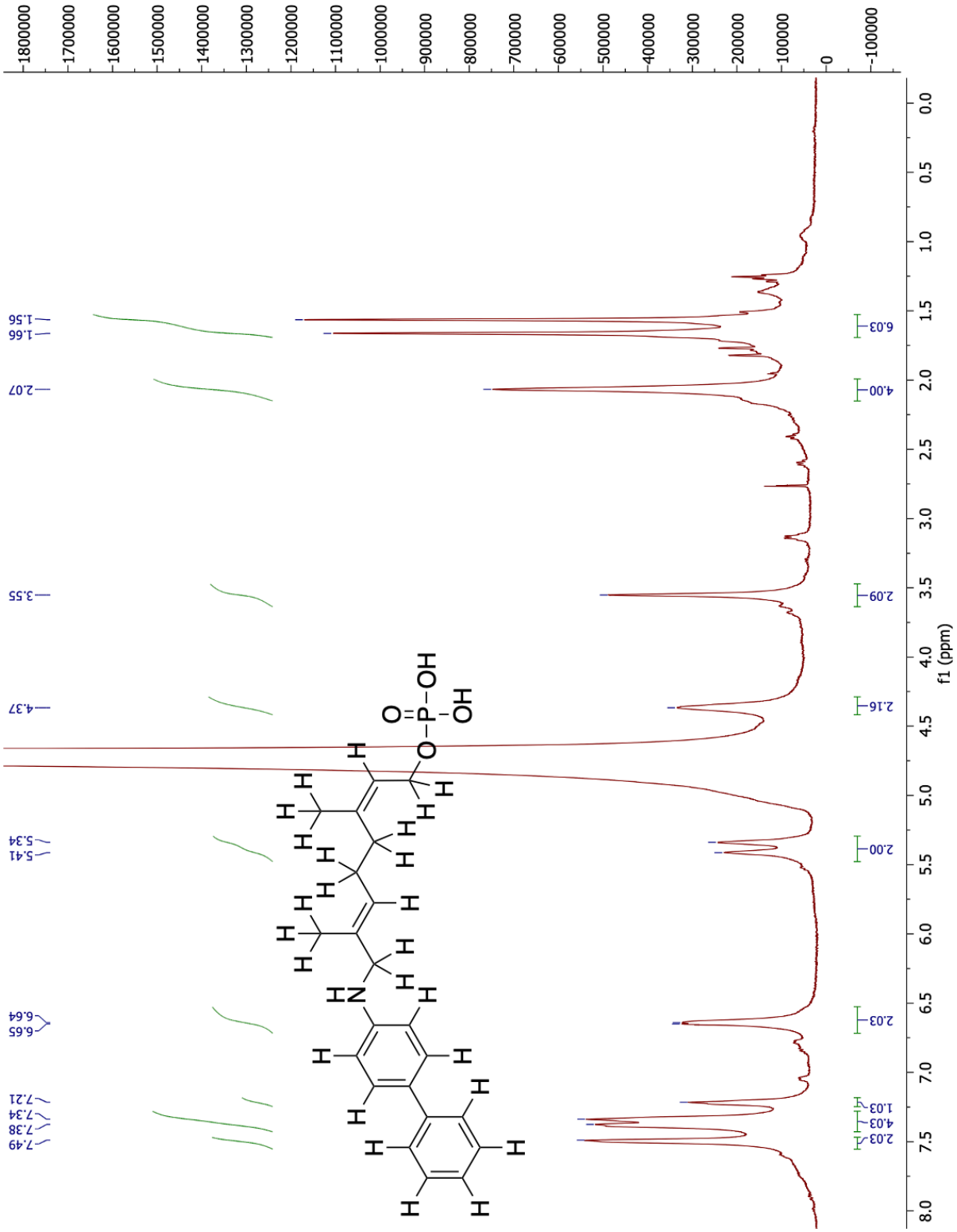

Figure C36: ^{1}H NMR spectrum of 4-aminobiphenyl neryl monophosphate (**19**) with structure overlay

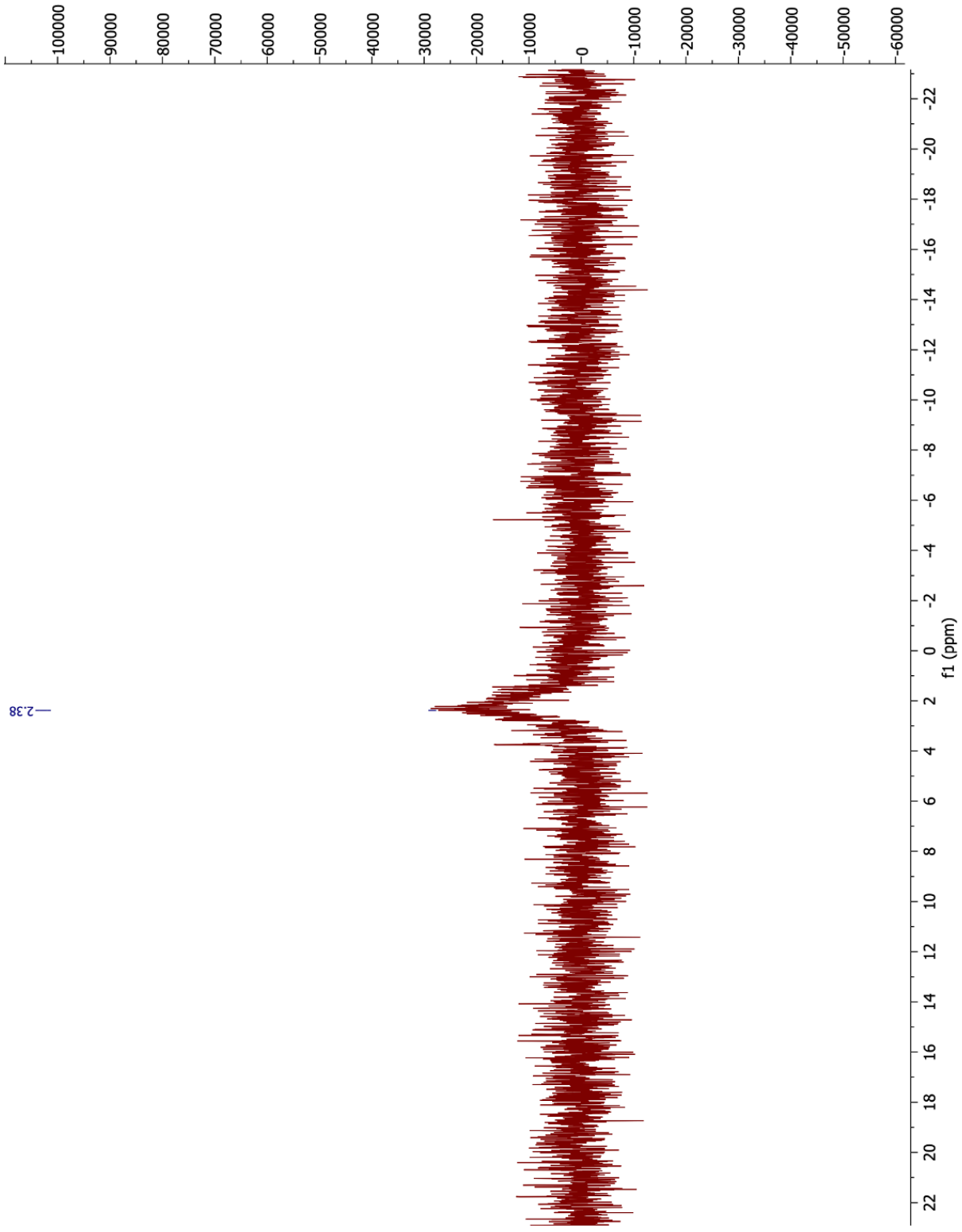

Figure C37: ^{31}P NMR spectrum of 4-aminobiphenyl neryl monophosphate (**19**)

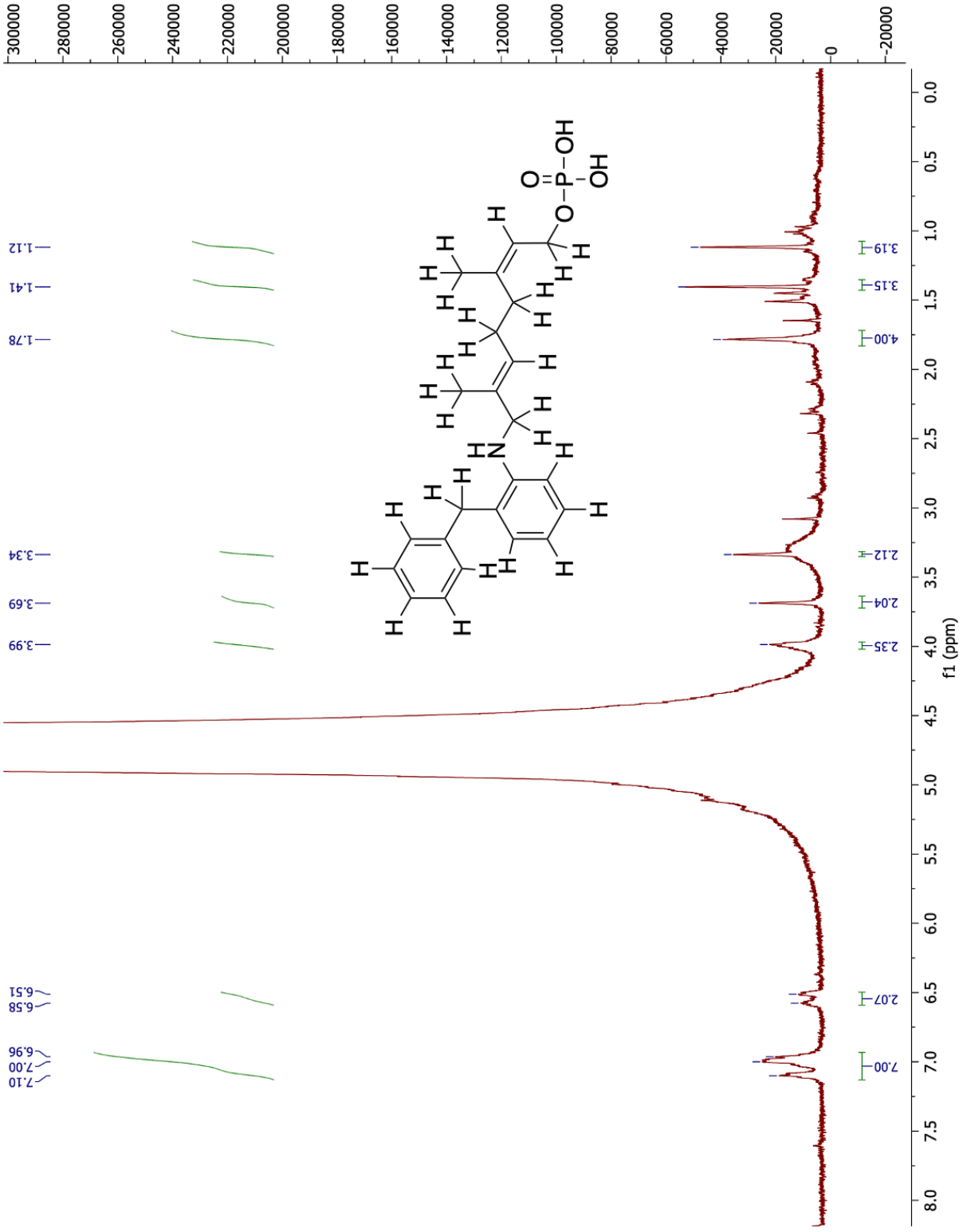

Figure C38: ^{1}H NMR spectrum of 2-benzylaniline neryl monophosphate (**20**) with structure overlay

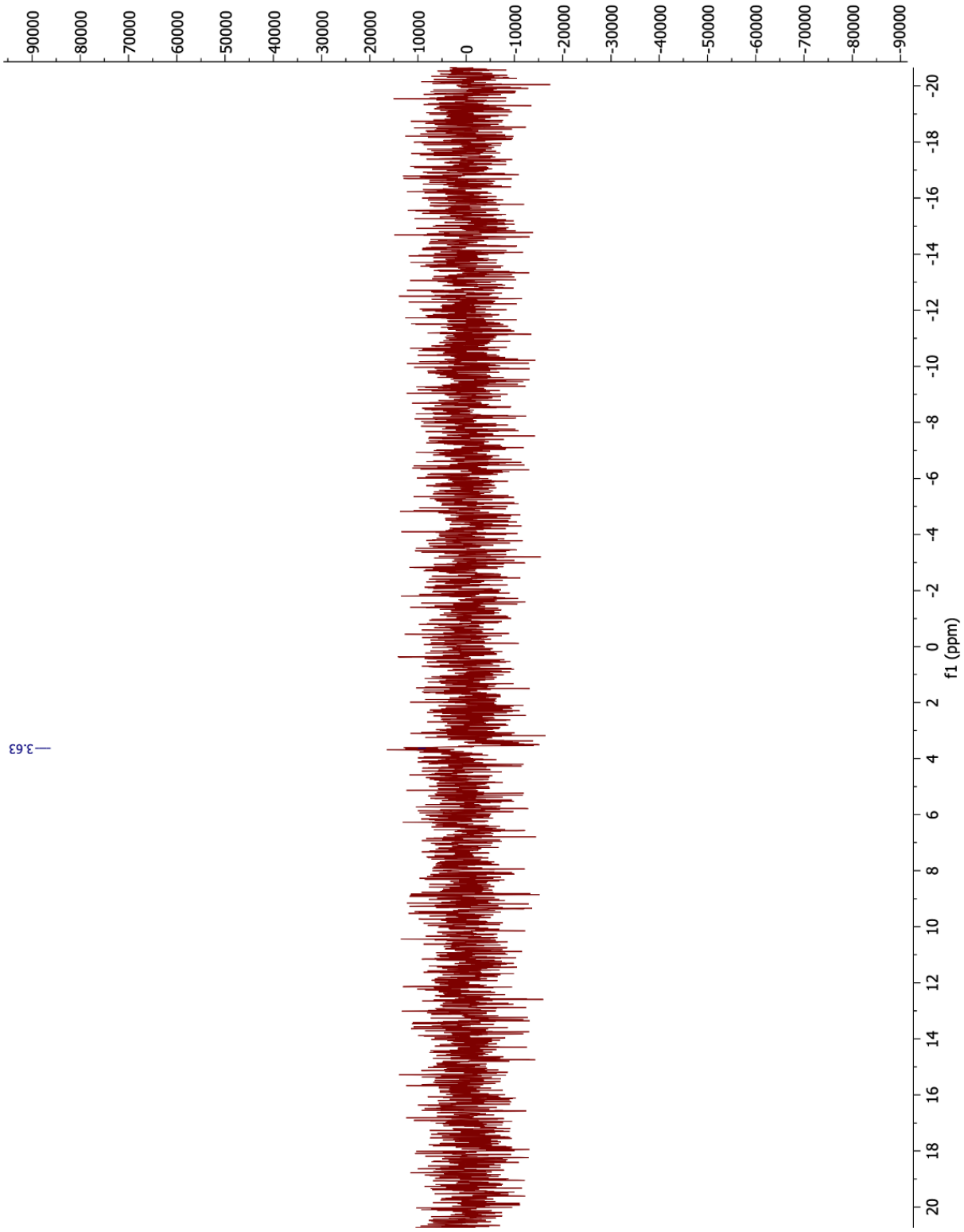

Figure C39: ^{31}P NMR spectrum of 2-benzylaniline neryl monophosphate (**20**)

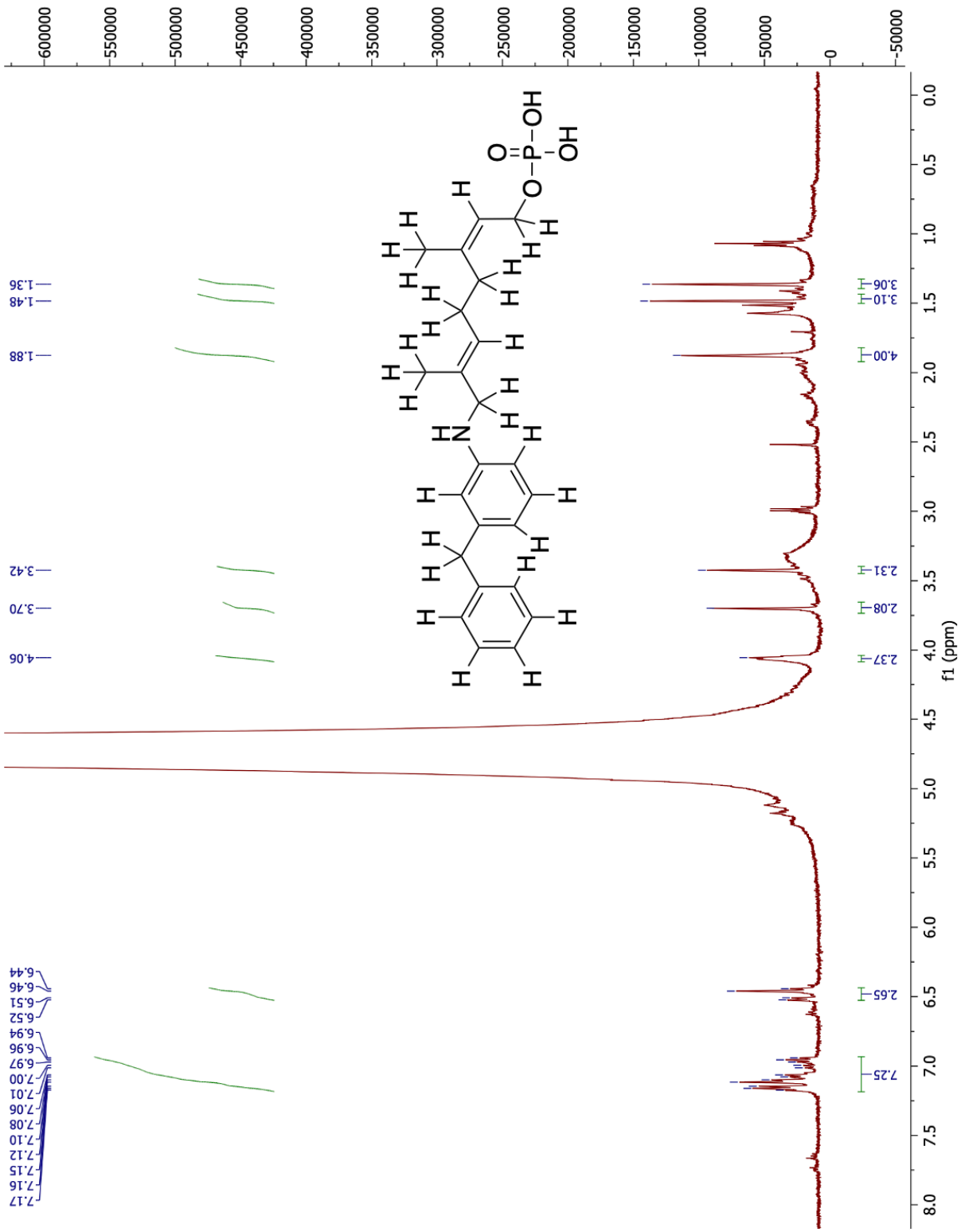

Figure C40: ^{1}H NMR spectrum of 3-benzylaniline neryl monophosphate (**21**) with structure overlay

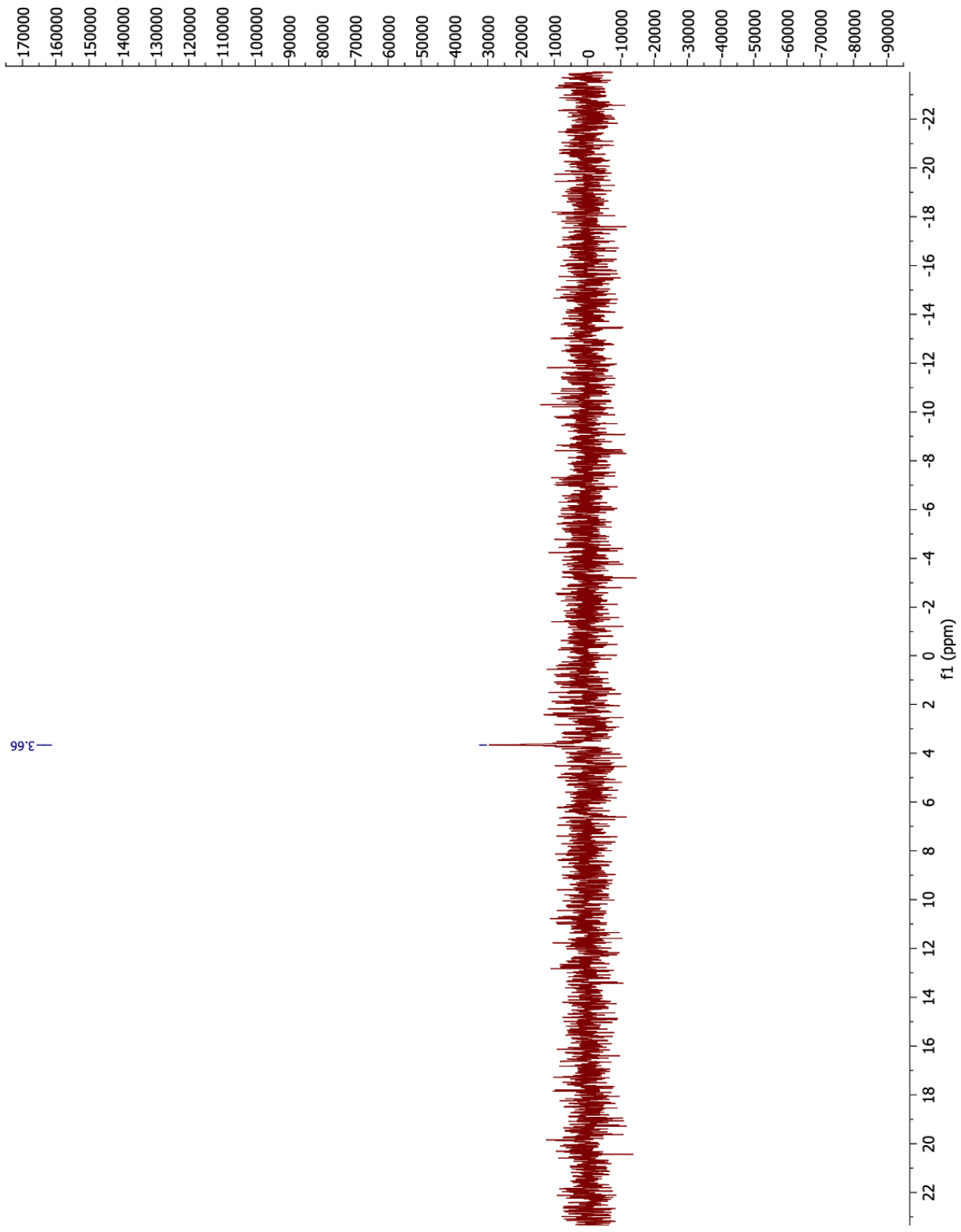

Figure C41: ^{31}P NMR spectrum of 3-benzylaniline neryl monophosphate (**21**)

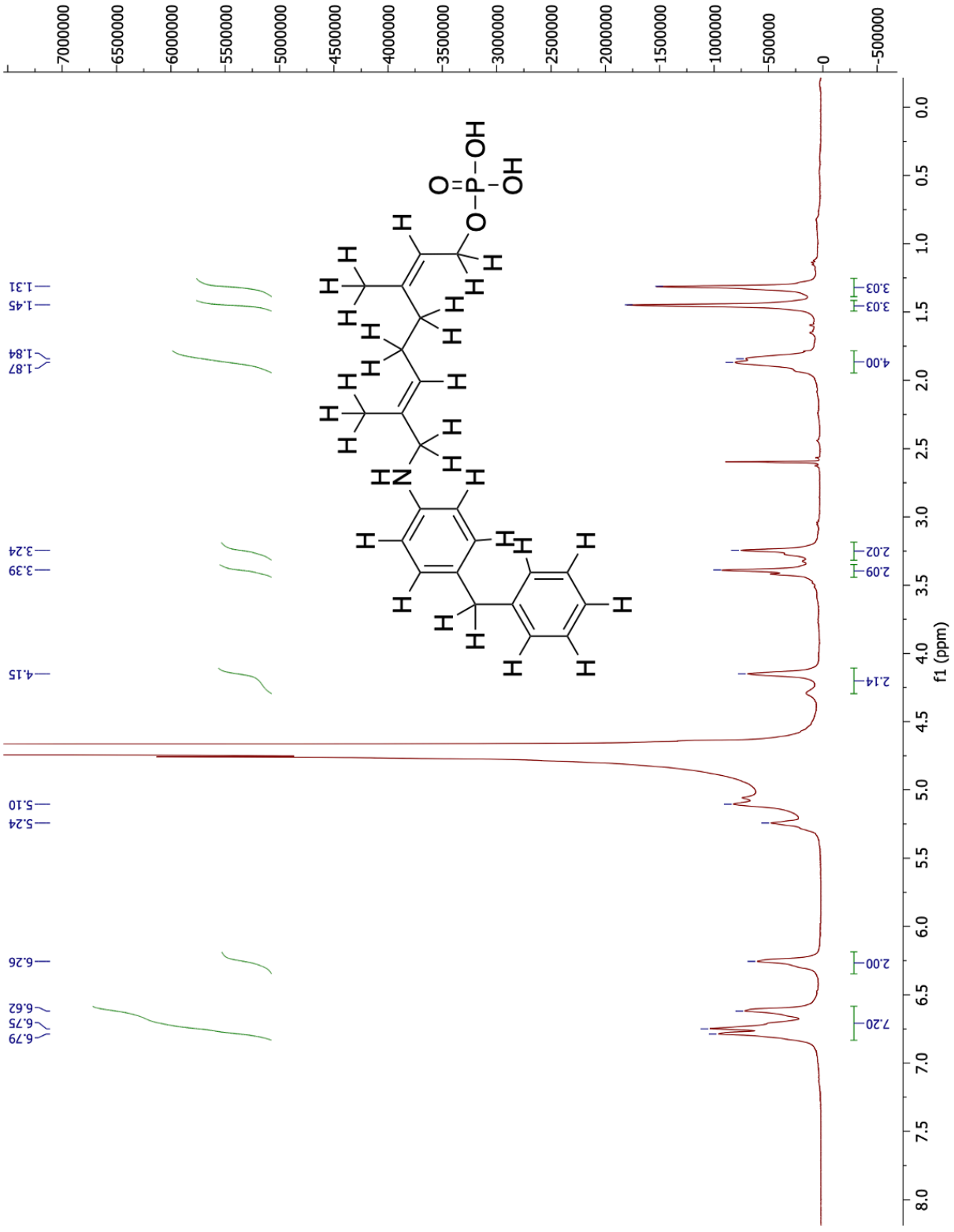

Figure C42: ^{1}H NMR spectrum of 4-benzylaniline neryl monophosphate (**22**) with structure overlay

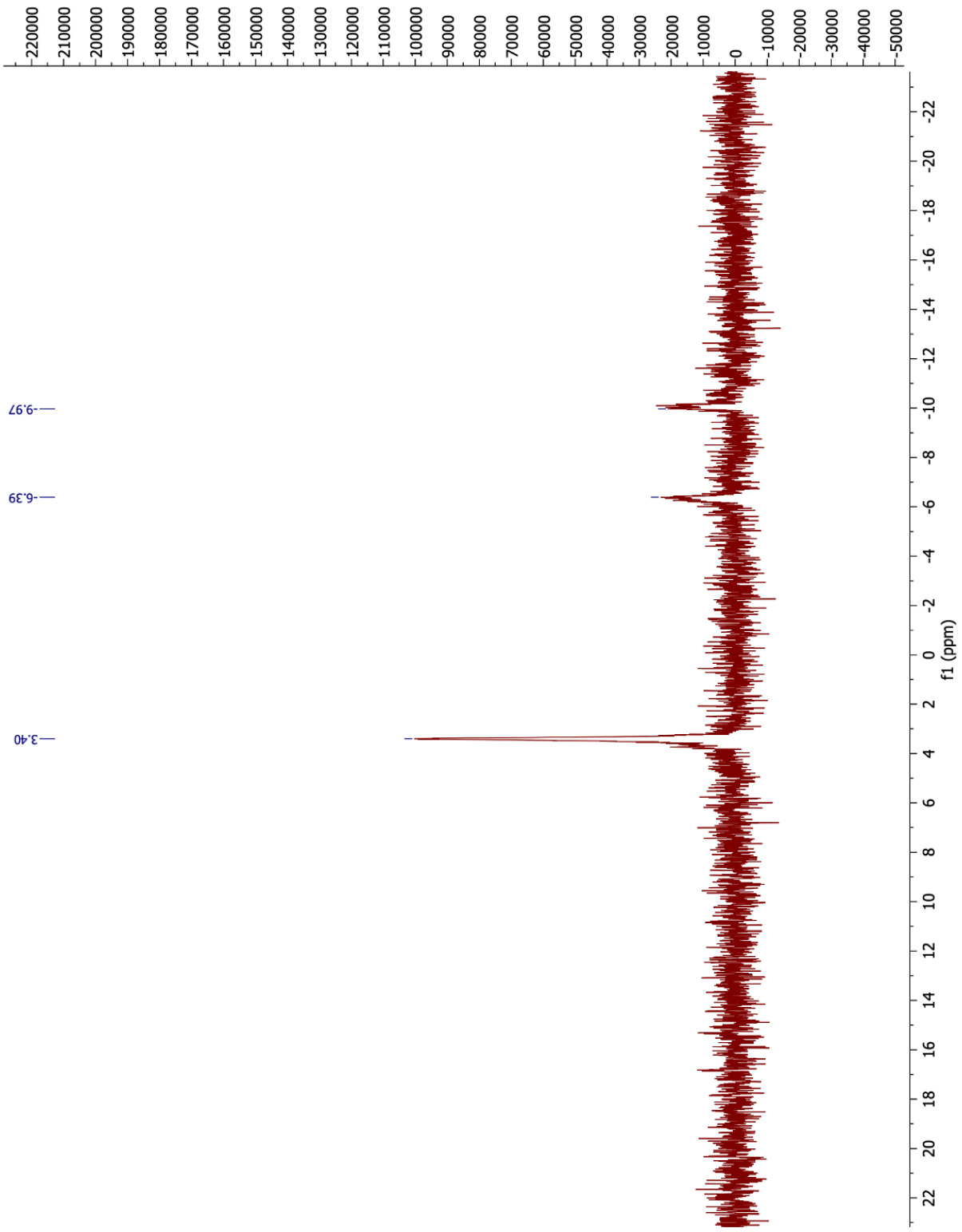

Figure C43: ^{31}P NMR spectrum of 4-benzylaniline neryl monophosphate (**22**)

APPENDIX D: CHROMATOGRAMS AND MASS SPECTRA

HPLC Chromatograms

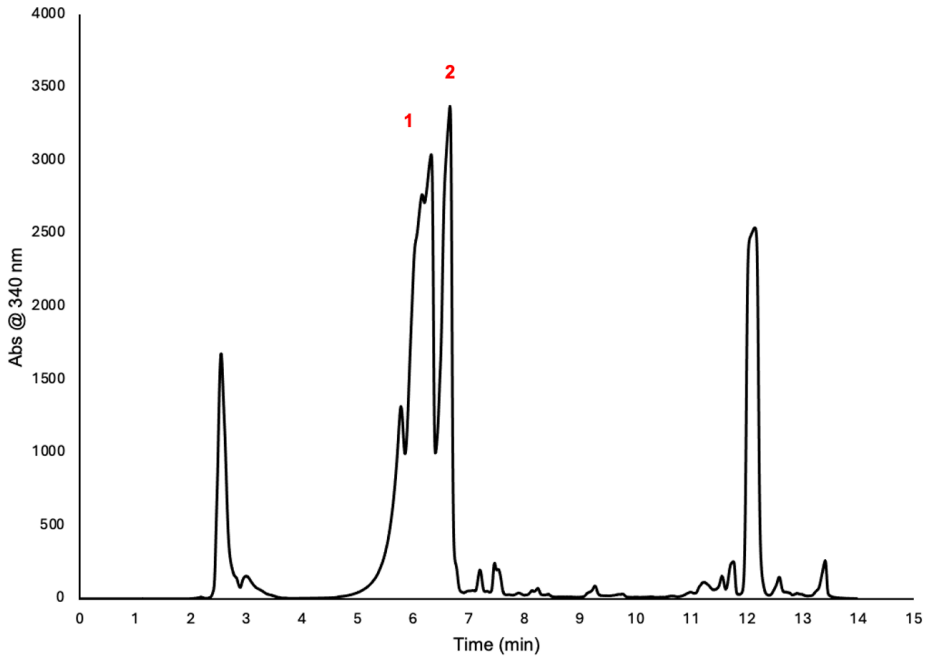

Figure D1: HPLC isolation of 1-naphthylamine neryl monophosphate (**16**) (peak 2) from the di- and triphosphates (peak 1)

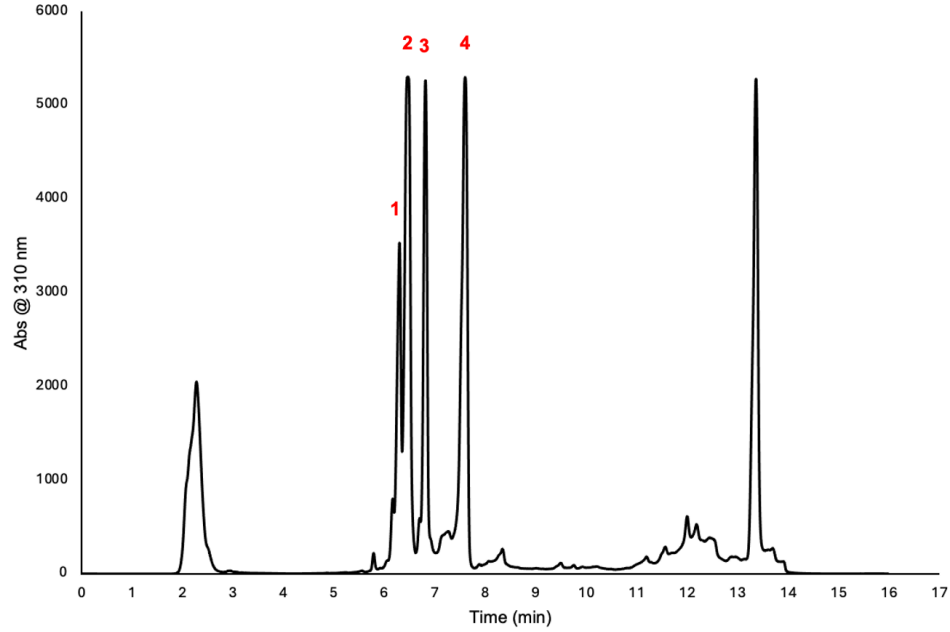

Figure D2: HPLC isolation of 2-aminobiphenyl neryl monophosphate (**17**) (peak 3) from the phosphorylation reaction mixture of diphosphate (peak 2), triphosphate (peak 1), and alcohol (peak 4)

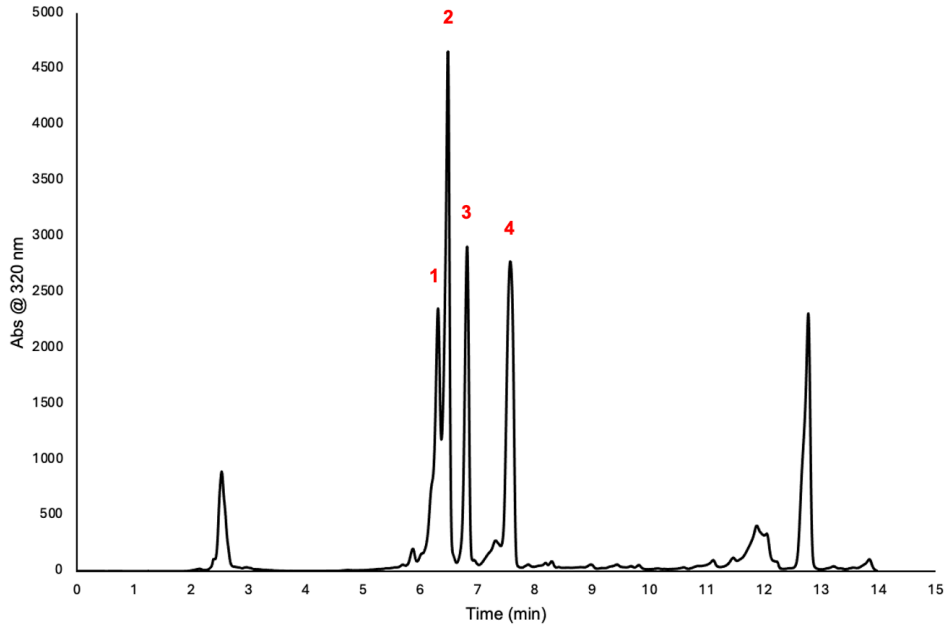

Figure D3: HPLC isolation of 3-aminobiphenyl neryl monophosphate (**18**) (peak 3) from the phosphorylation reaction mixture of diphosphate (peak 2), triphosphate (peak 1), and alcohol (peak 4)

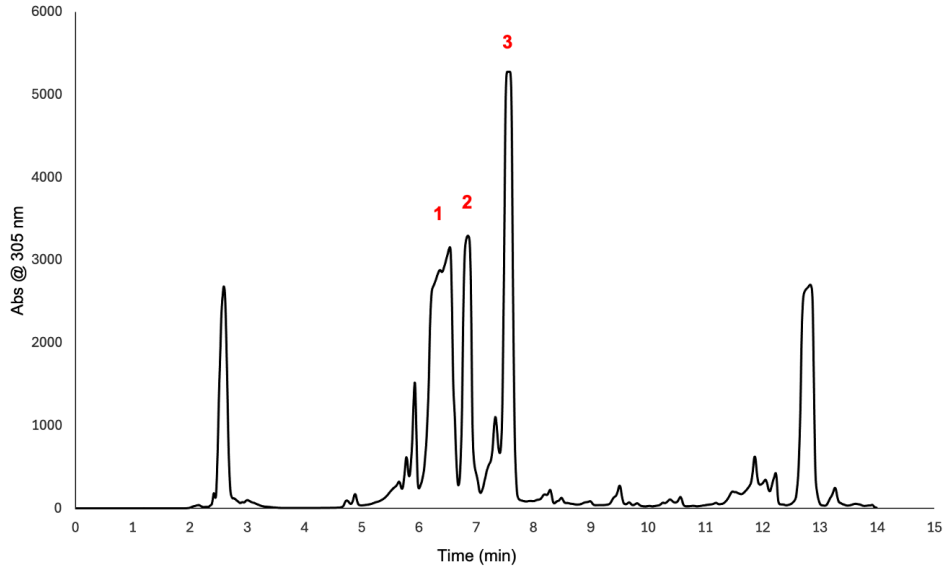

Figure D4: HPLC isolation of 4-aminobiphenyl neryl monophosphate (**19**) (peak 2) from the phosphorylation reaction mixture of di- and triphosphates (peak 1) and alcohol (peak 3)

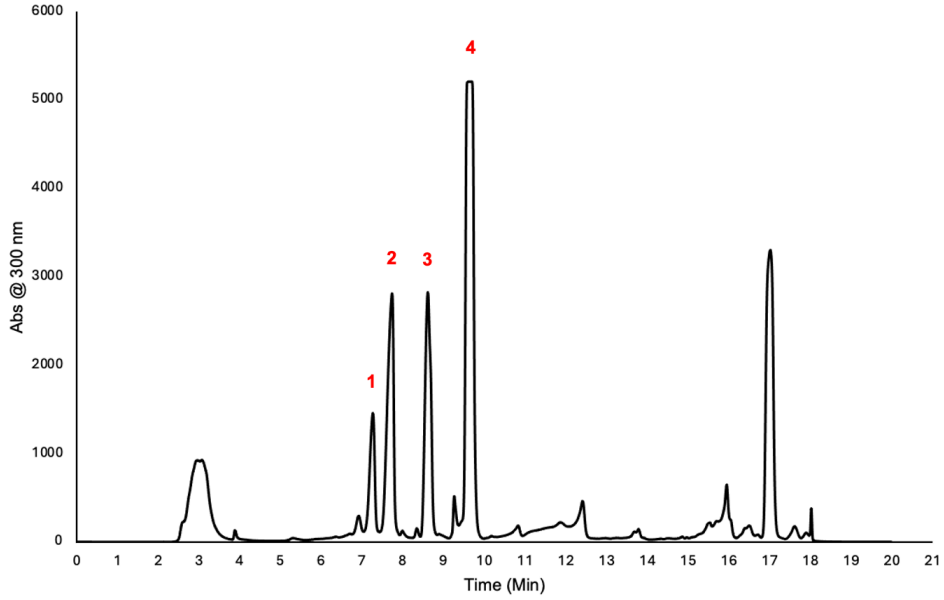

Figure D5: HPLC isolation of 2-benzylaniline neryl monophosphate (**20**) (peak 3) from the phosphorylation reaction mixture of diphosphate (peak 2), triphosphate (peak 1), and alcohol (peak 4)

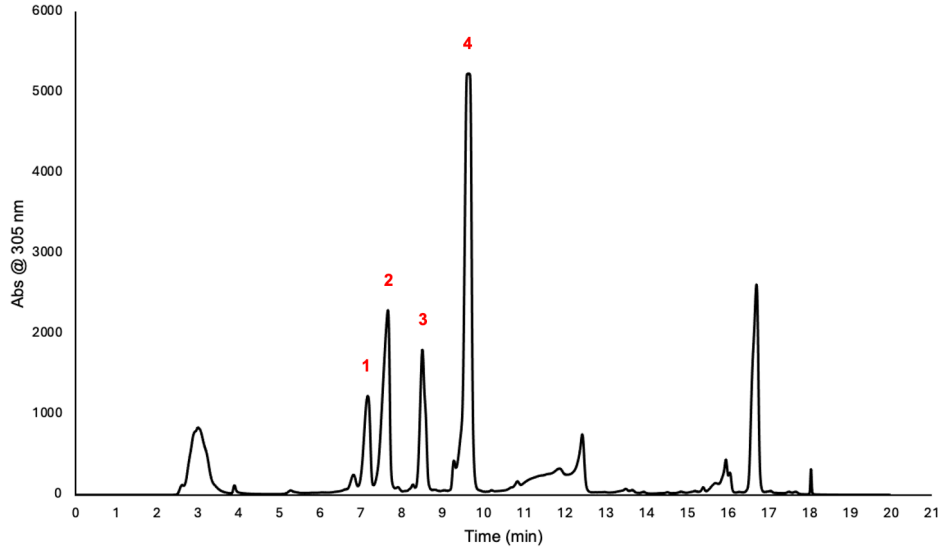

Figure D6: HPLC isolation of 3-benzylaniline neryl monophosphate (**21**) (peak 3) from the phosphorylation reaction mixture of diphosphate (peak 2), triphosphate (peak 1), and alcohol (peak 4)

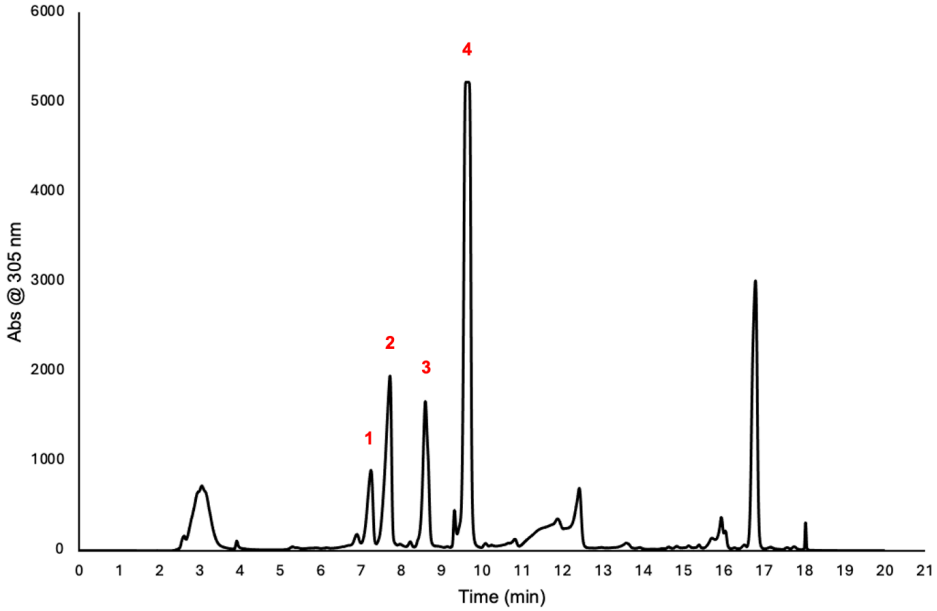

Figure D7: HPLC isolation of 4-benzylaniline neryl monophosphate (**22**) (peak 3) from the phosphorylation reaction mixture of diphosphate (peak 2), triphosphate (peak 1), and alcohol (peak 4)

LC-MS Chromatograms and Mass Spectra

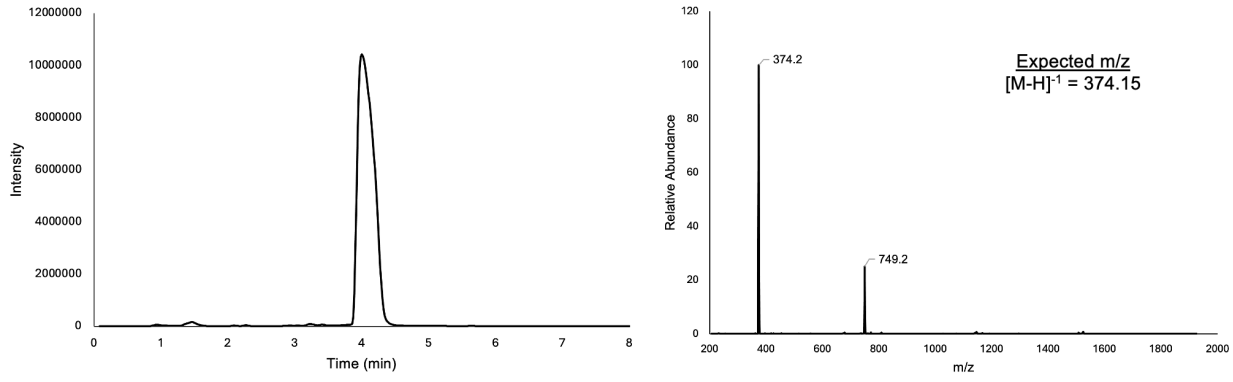

Figure D8: LC-MS analysis of 1-naphthylamine neryl monophosphate (**16**)

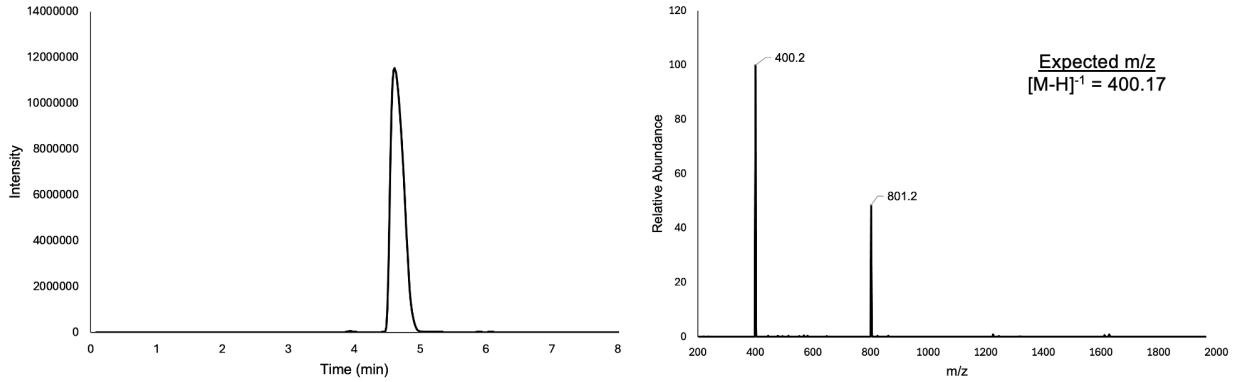

Figure D9: LC-MS analysis of 2-aminobiphenyl neryl monophosphate (**17**)

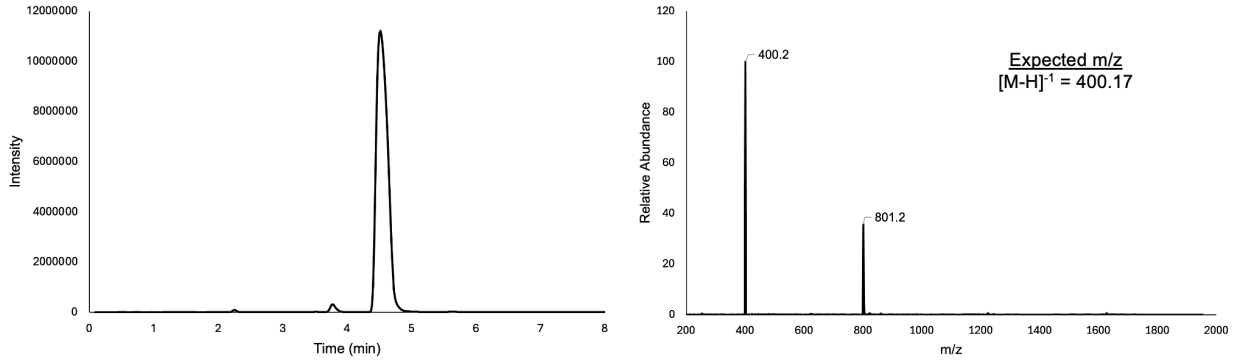

Figure D10: LC-MS analysis of 3-aminobiphenyl neryl monophosphate (**18**)

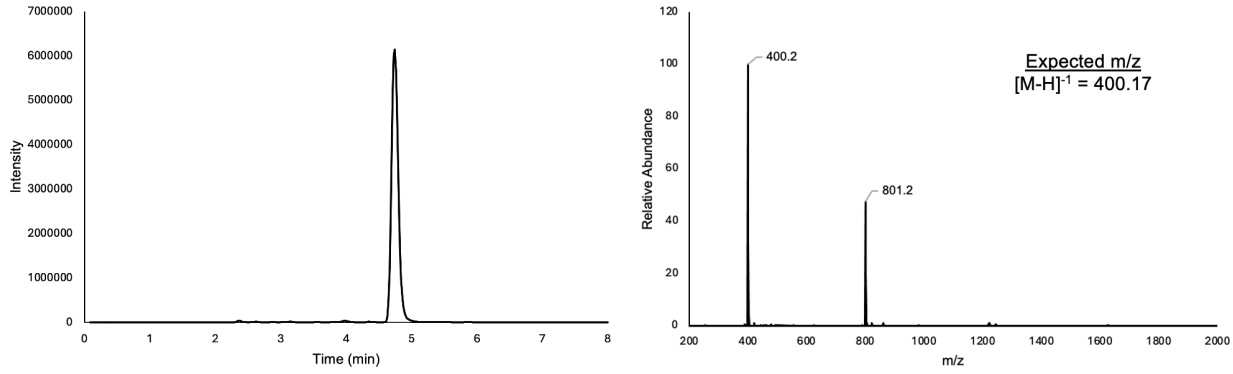

Figure D11: LC-MS analysis of 4-aminobiphenyl neryl monophosphate (**19**)

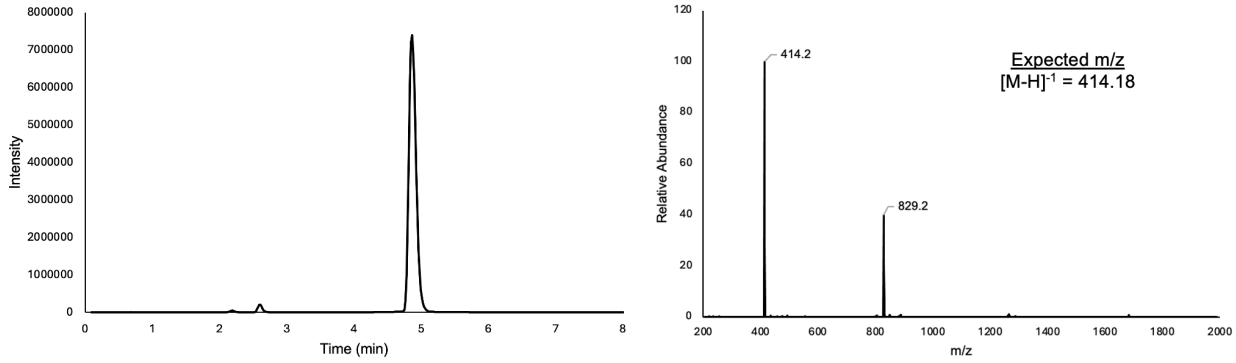

Figure D12: LC-MS analysis of 2-benzylaniline neryl monophosphate (**20**)

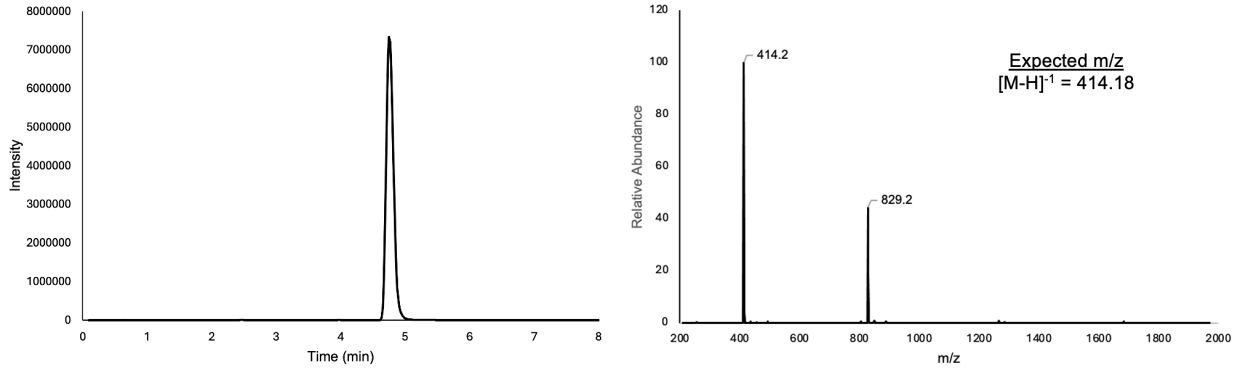

Figure D13: LC-MS analysis of 3-benzylaniline neryl monophosphate (**21**)

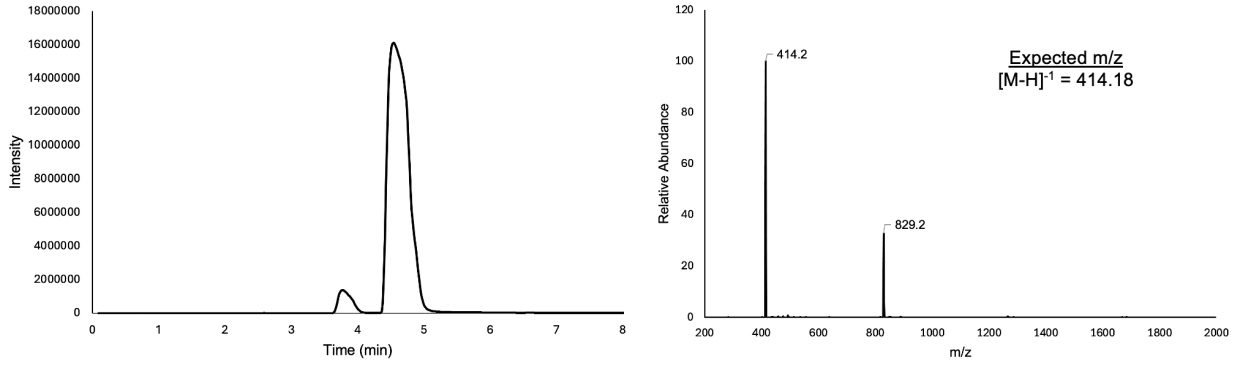

Figure D14: LC-MS analysis of 4-benzylaniline neryl monophosphate (**22**)

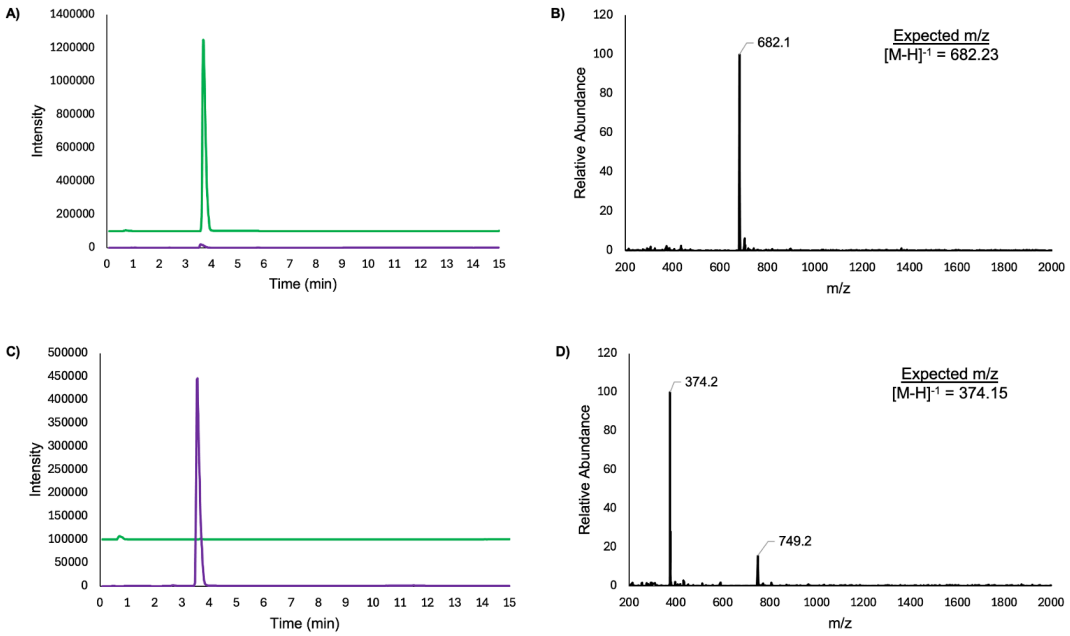

Figure D15: LC-MS chromatograms (**A** and **C**) and mass spectra (**B** and **D**) of diNAcBac-linked 1-NA-NP after reacting with PglC (**A** and **B**) compared to a control reaction (**C** and **D**) that excluded the sugar substrate. The SIM signal for diNAcBac-linked 1-NA-NP is shown in green and the signal for the 1-NA-NP (**16**) probe is shown in purple.

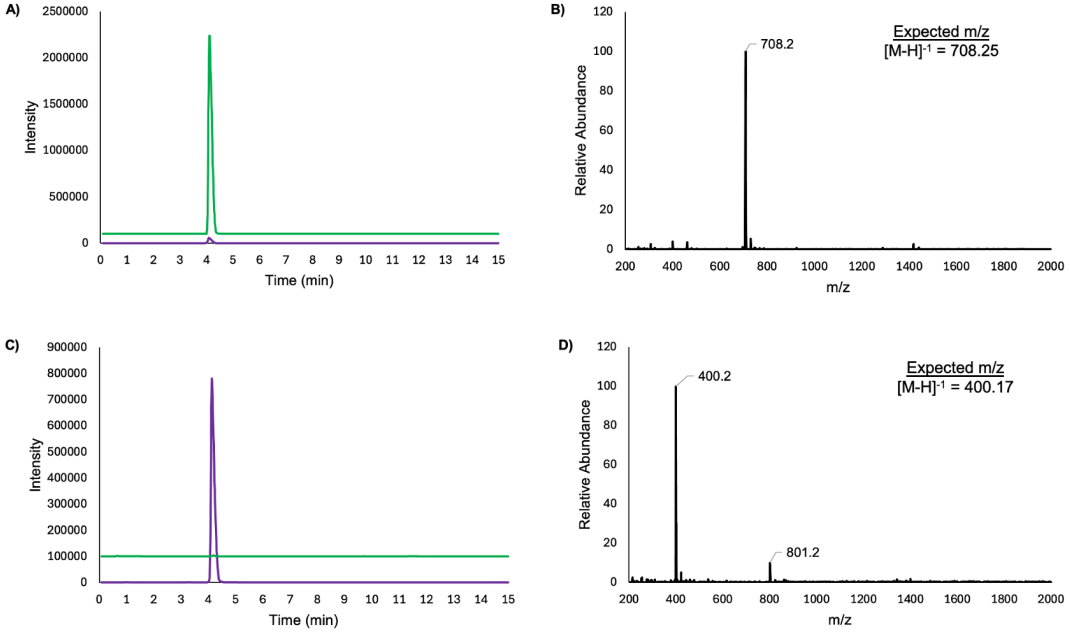

Figure D16: LC-MS chromatograms (**A** and **C**) and mass spectra (**B** and **D**) of diNAcBac-linked 2-ABP-NP after reacting with PglC (**A** and **B**) compared to a control reaction (**C** and **D**) that excluded the sugar substrate. The SIM signal for diNAcBac-linked 2-ABP-NP is shown in green and the signal for the 2-ABP-NP (**17**) probe is shown in purple.

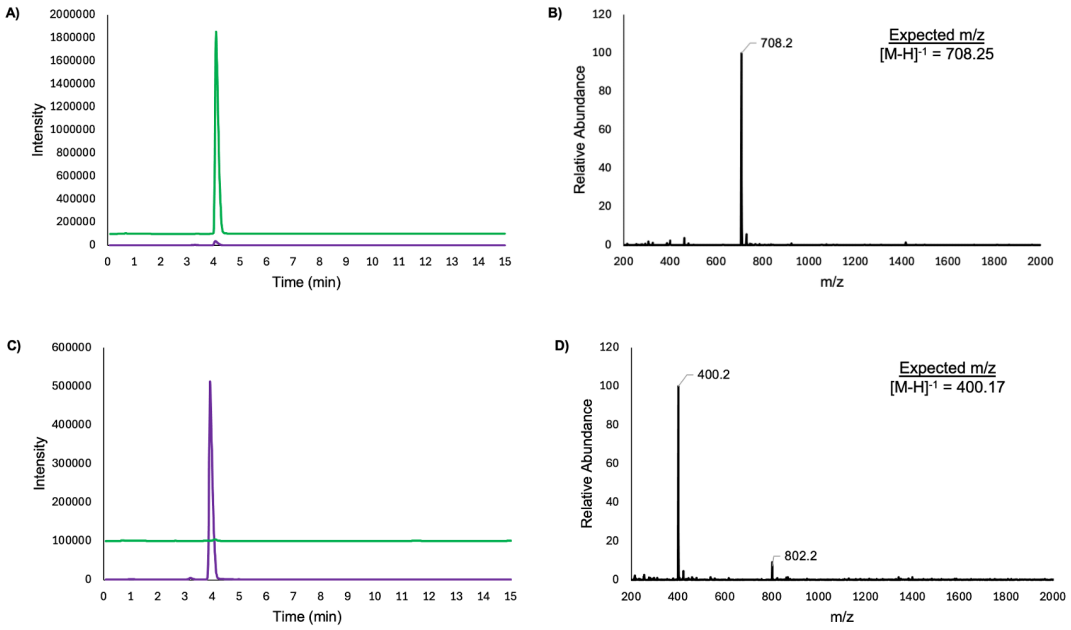

Figure D17: LC-MS chromatograms (**A** and **C**) and mass spectra (**B** and **D**) of diNAcBac-linked 3-ABP-NP after reacting with PglC (**A** and **B**) compared to a control reaction (**C** and **D**) that excluded the sugar substrate. The SIM signal for diNAcBac-linked 3-ABP-NP is shown in green and the signal for the 3-ABP-NP (**18**) probe is shown in purple.

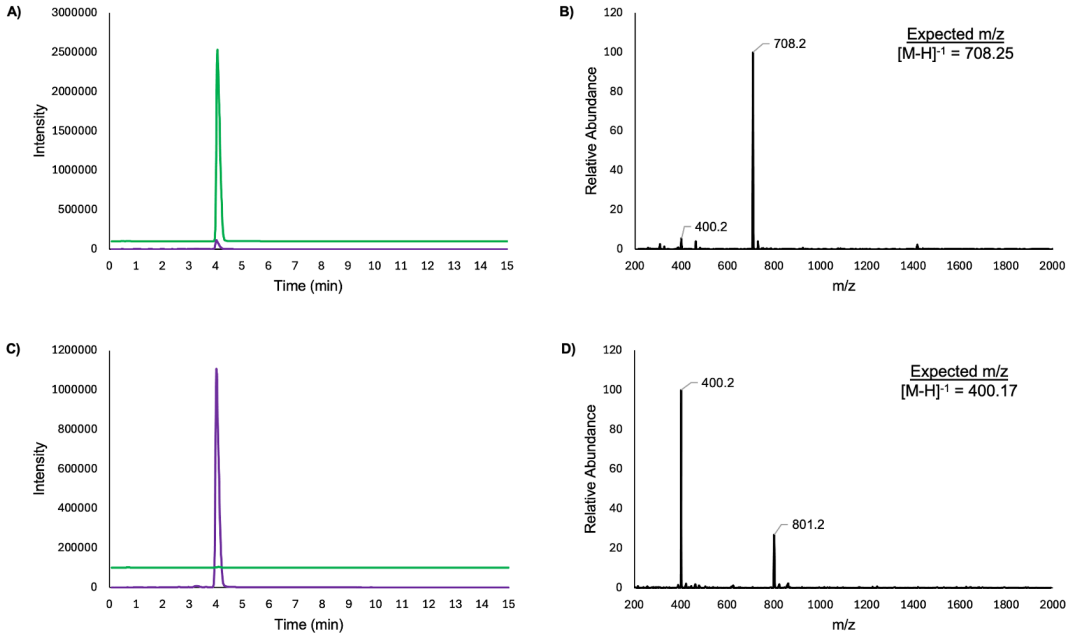

Figure D18: LC-MS chromatograms (**A** and **C**) and mass spectra (**B** and **D**) of diNAcBac-linked 4-ABP-NP after reacting with PglC (**A** and **B**) compared to a control reaction (**C** and **D**) that excluded the sugar substrate. The SIM signal for diNAcBac-linked 4-ABP-NP is shown in green and the signal for the 4-ABP-NP (**19**) probe is shown in purple.

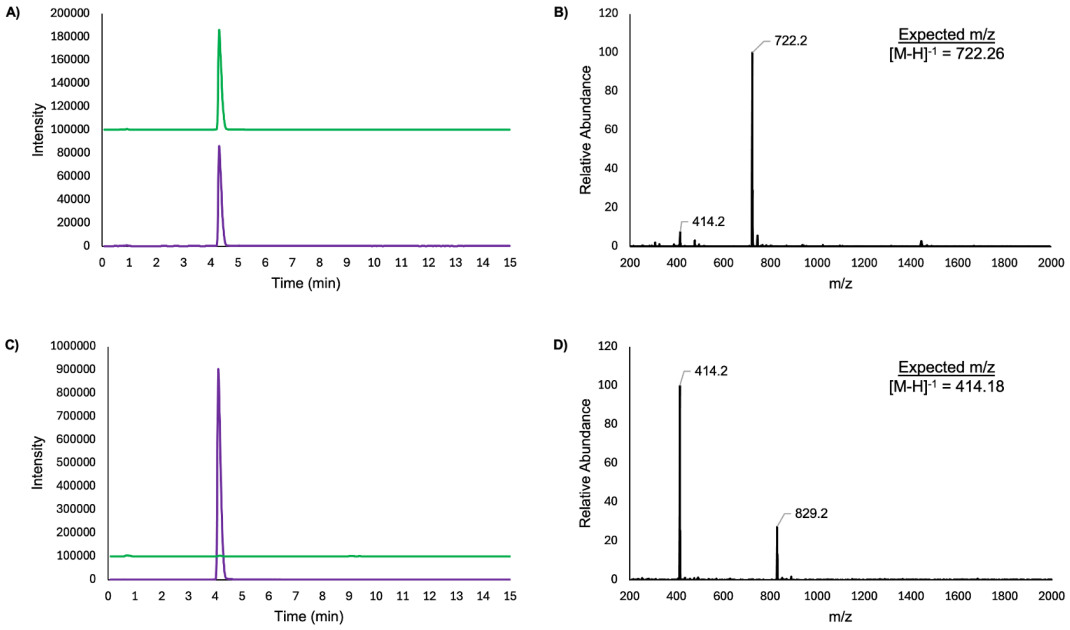

Figure D19: LC-MS chromatograms (**A** and **C**) and mass spectra (**B** and **D**) of diNAcBac-linked 2-BA-NP after reacting with PglC (**A** and **B**) compared to a control reaction (**C** and **D**) that excluded the sugar substrate. The SIM signal for diNAcBac-linked 2-BA-NP is shown in green and the signal for the 2-BA-NP (**20**) probe is shown in purple.

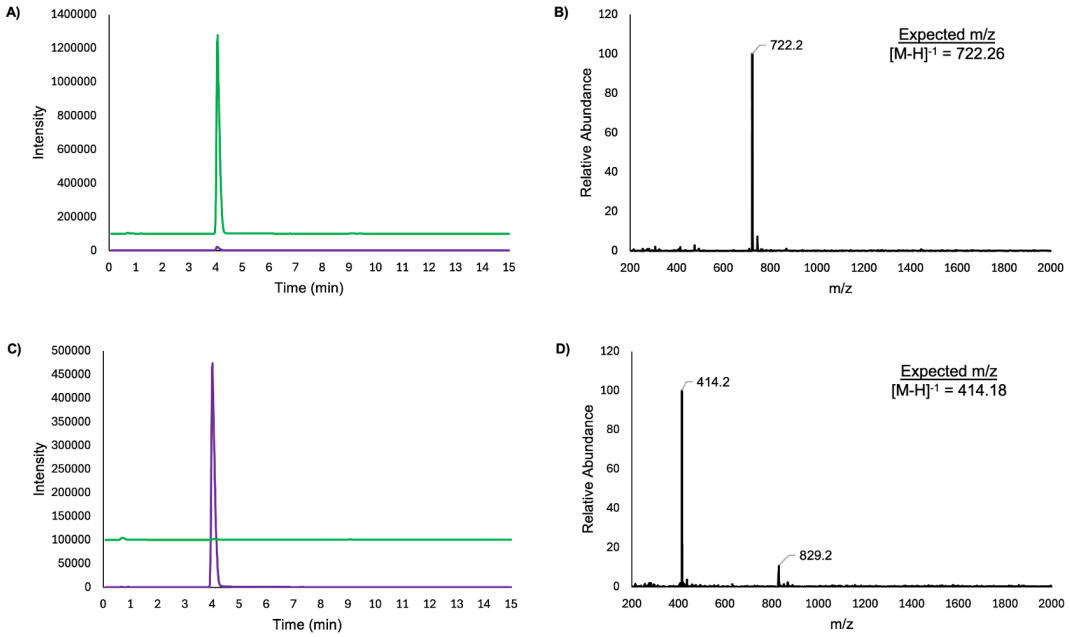

Figure D20: LC-MS chromatograms (**A** and **C**) and mass spectra (**B** and **D**) of diNAcBac-linked 3-BA-NP after reacting with PglC (**A** and **B**) compared to a control reaction (**C** and **D**) that excluded the sugar substrate. The SIM signal for diNAcBac-linked 3-BA-NP is shown in green and the signal for the 3-BA-NP (**21**) probe is shown in purple.

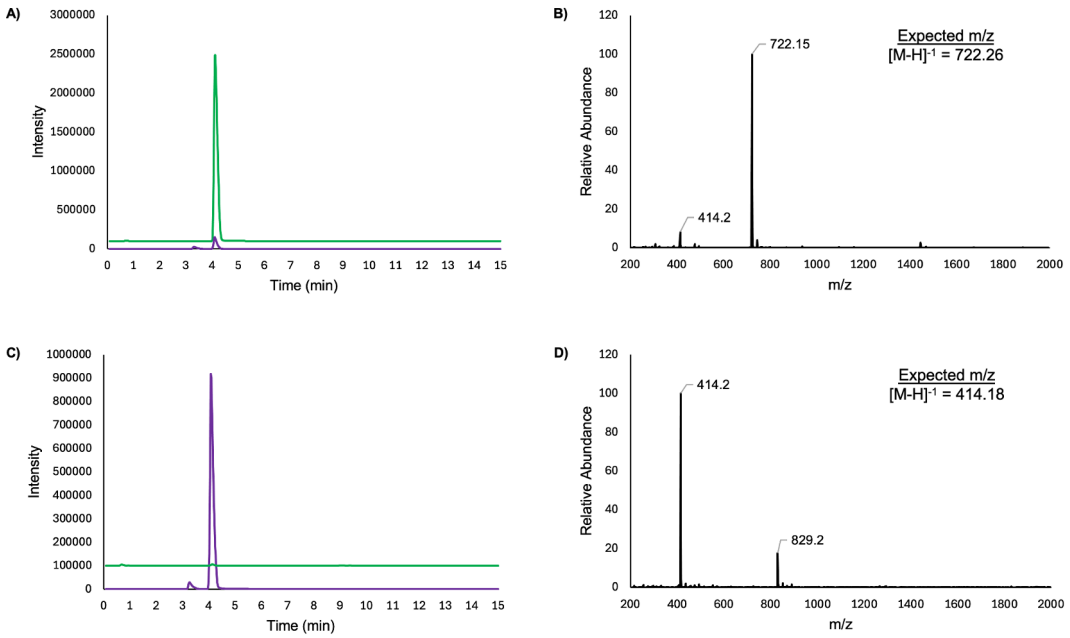

Figure D21: LC-MS chromatograms (**A** and **C**) and mass spectra (**B** and **D**) of diNAcBac-linked 4-BA-NP after reacting with PglC (**A** and **B**) compared to a control reaction (**C** and **D**) that excluded the sugar substrate. The SIM signal for diNAcBac-linked 4-BA-NP is shown in green and the signal for the 4-BA-NP (**22**) probe is shown in purple.

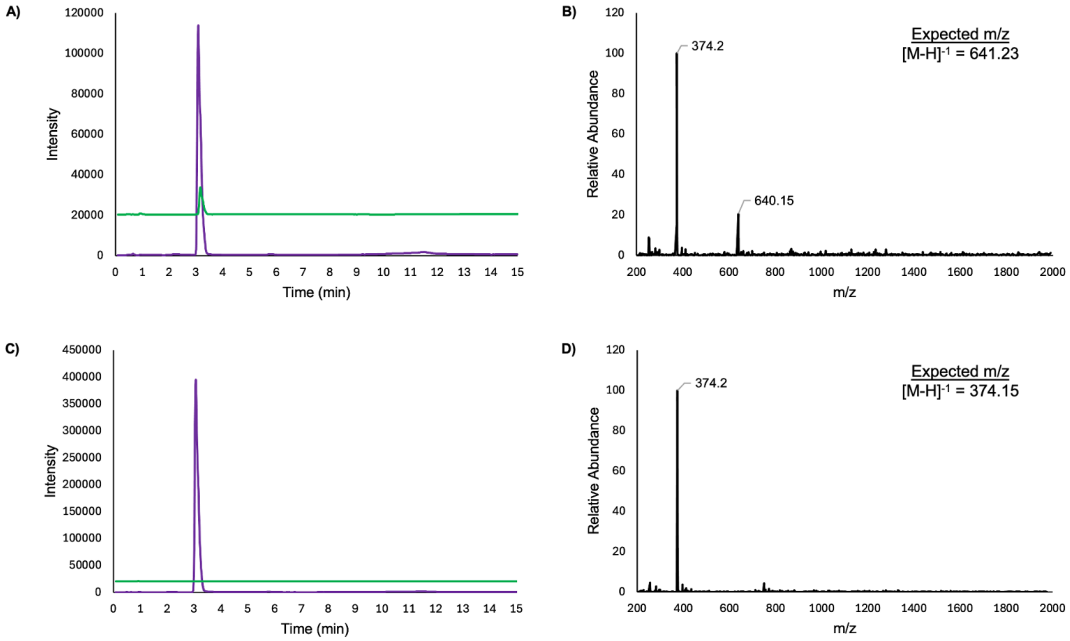

Figure D22: LC-MS chromatograms (**A** and **C**) and mass spectra (**B** and **D**) of AADGal-linked 1-NA-NP after reacting with WcfS (**A** and **B**) compared to a control reaction (**C** and **D**) that excluded the sugar substrate. The SIM signal for AADGal-linked 1-NA-NP is shown in green and the signal for the 1-NA-NP (**16**) probe is shown in purple.

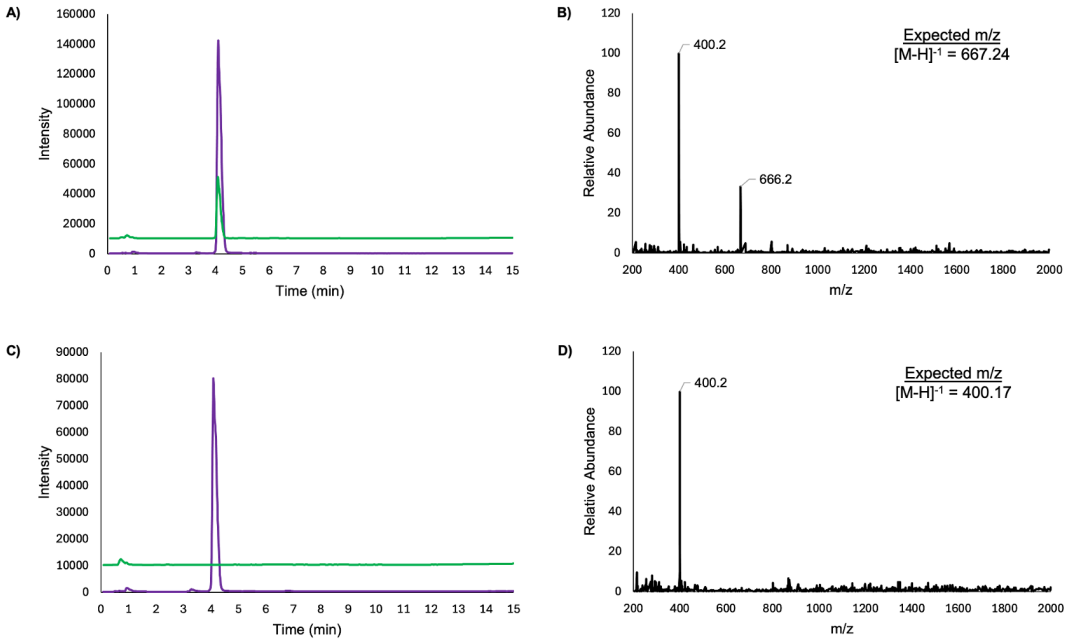

Figure D23: LC-MS chromatograms (**A** and **C**) and mass spectra (**B** and **D**) of AADGal-linked 2-ABP-NP after reacting with WcfS (**A** and **B**) compared to a control reaction (**C** and **D**) that excluded the sugar substrate. The SIM signal for AADGal-linked 2-ABP-NP is shown in green and the signal for the 2-ABP-NP (**17**) probe is shown in purple.

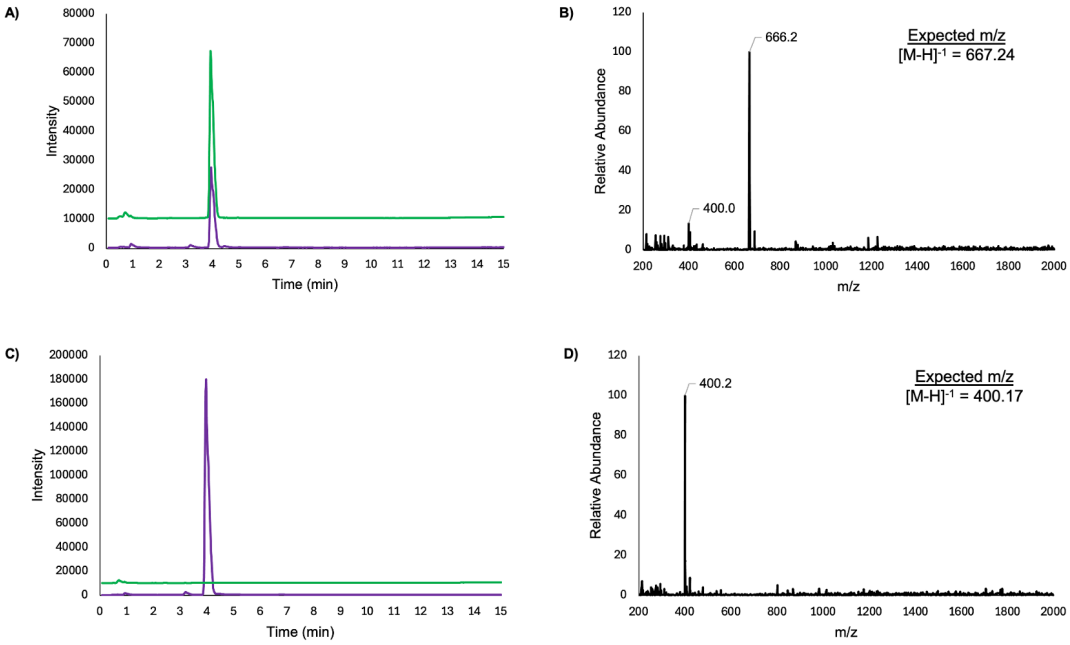

Figure D24: LC-MS chromatograms (**A** and **C**) and mass spectra (**B** and **D**) of AADGal-linked 3-ABP-NP after reacting with WcfS (**A** and **B**) compared to a control reaction (**C** and **D**) that excluded the sugar substrate. The SIM signal for AADGal-linked 3-ABP-NP is shown in green and the signal for the 3-ABP-NP (**18**) probe is shown in purple.

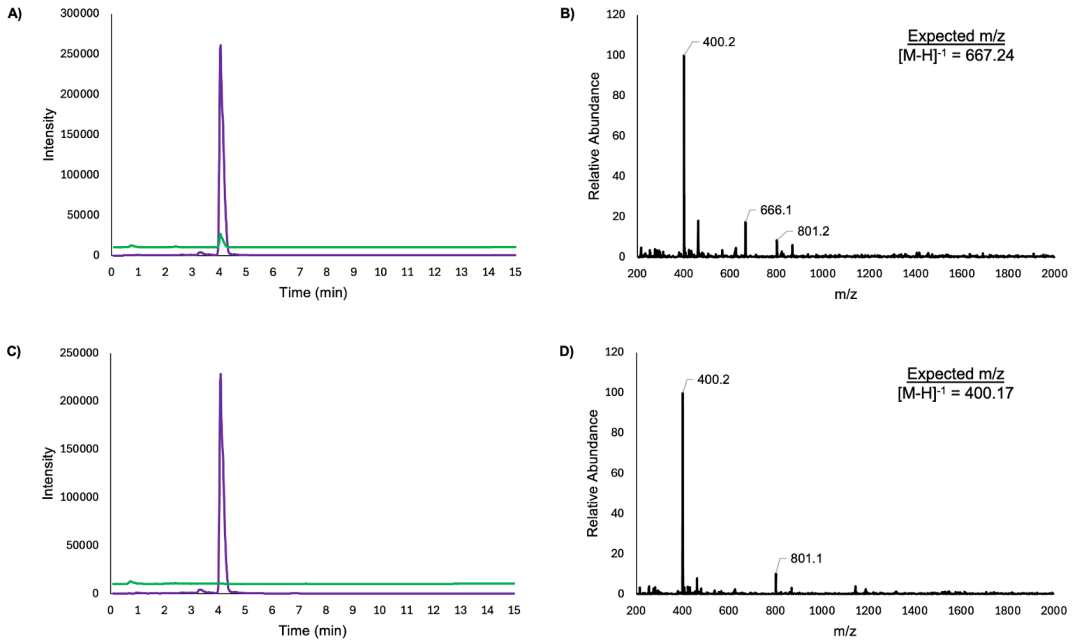

Figure D25: LC-MS chromatograms (**A** and **C**) and mass spectra (**B** and **D**) of AADGal-linked 4-ABP-NP after reacting with WcfS (**A** and **B**) compared to a control reaction (**C** and **D**) that excluded the sugar substrate. The SIM signal for AADGal-linked 4-ABP-NP is shown in green and the signal for the 4-ABP-NP (**19**) probe is shown in purple.

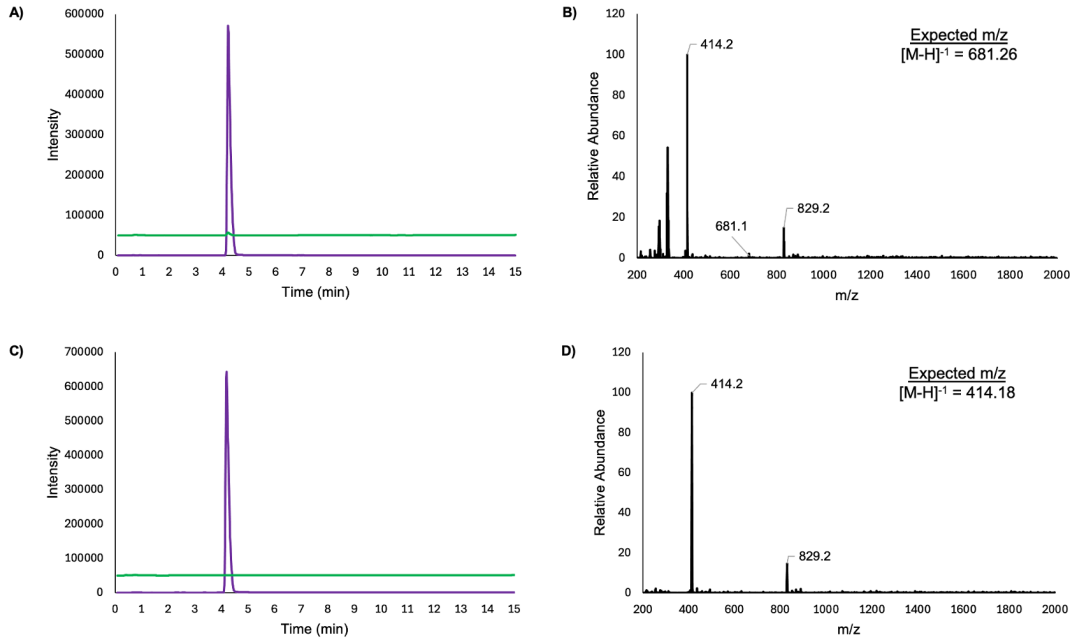

Figure D26: LC-MS chromatograms (**A** and **C**) and mass spectra (**B** and **D**) of AADGal-linked 2-BA-NP after reacting with WcfS (**A** and **B**) compared to a control reaction (**C** and **D**) that excluded the sugar substrate. The SIM signal for AADGal-linked 2-BA-NP is shown in green and the signal for the 2-BA-NP (**20**) probe is shown in purple.

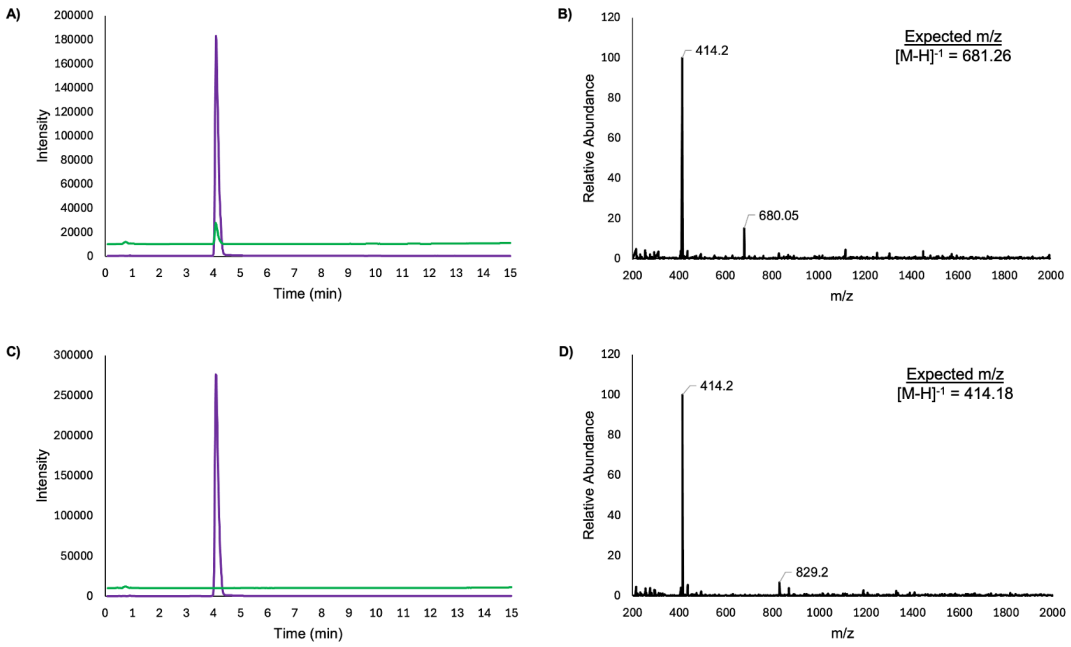

Figure D27: LC-MS chromatograms (**A** and **C**) and mass spectra (**B** and **D**) of AADGal-linked 3-BA-NP after reacting with WcfS (**A** and **B**) compared to a control reaction (**C** and **D**) that excluded the sugar substrate. The SIM signal for AADGal-linked 3-BA-NP is shown in green and the signal for the 3-BA-NP (**21**) probe is shown in purple.

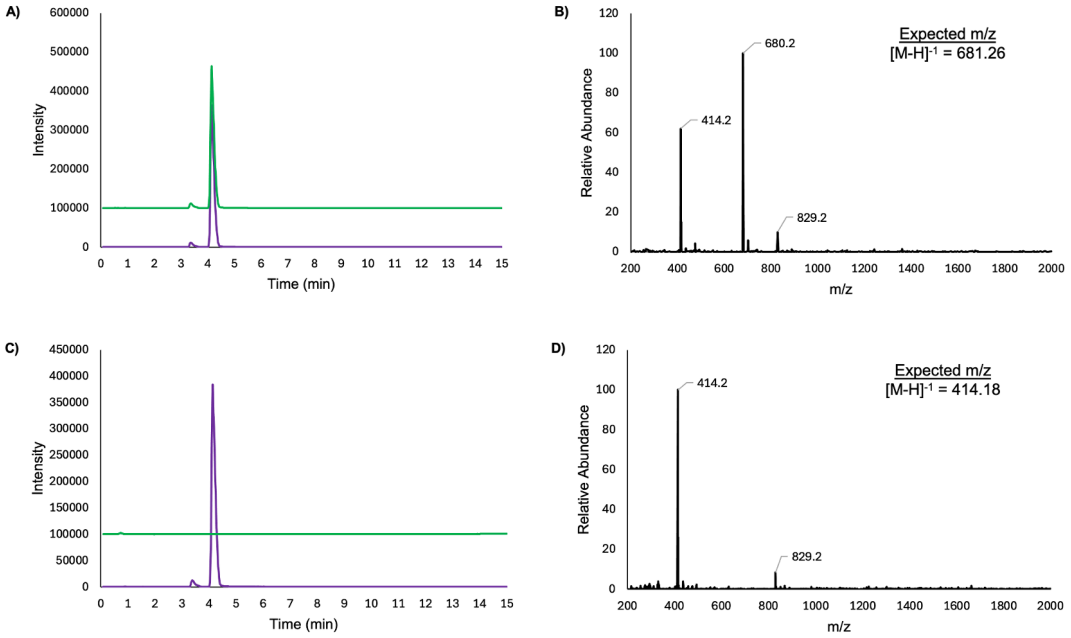

Figure D28: LC-MS chromatograms (**A** and **C**) and mass spectra (**B** and **D**) of AADGal-linked 4-BA-NP after reacting with WcfS (**A** and **B**) compared to a control reaction (**C** and **D**) that excluded the sugar substrate. The SIM signal for AADGal-linked 4-BA-NP is shown in green and the signal for the 4-BA-NP (**22**) probe is shown in purple.

APPENDIX E: SPECTROPHOTOMETRIC ANALYSIS DATA

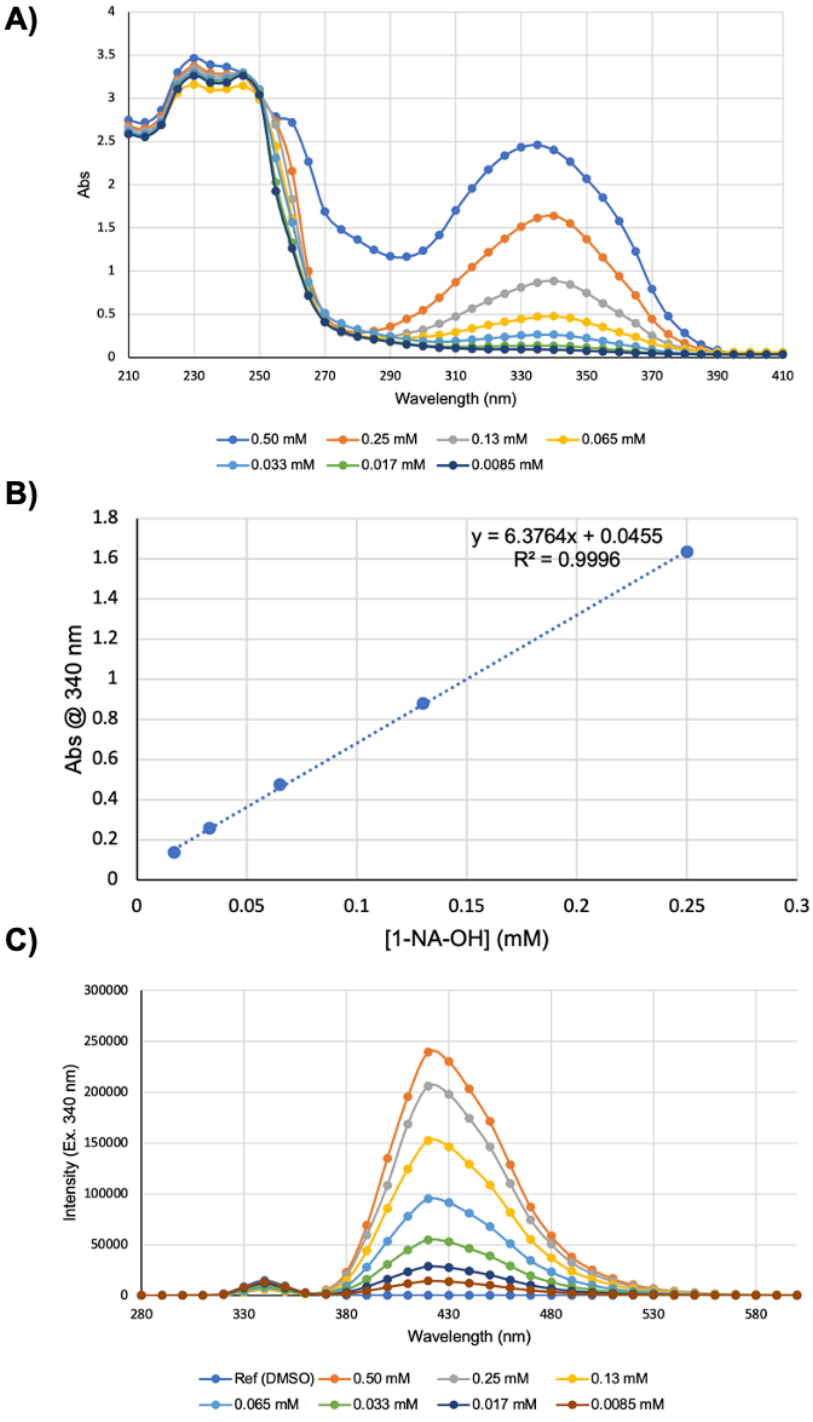

Figure E1: Spectrophotometric analysis of 1-naphthylamine neryl alcohol (1-NA-OH) (**9**), including an absorbance spectrum (**A**), standard curve (**B**), and fluorescence spectrum (**C**)

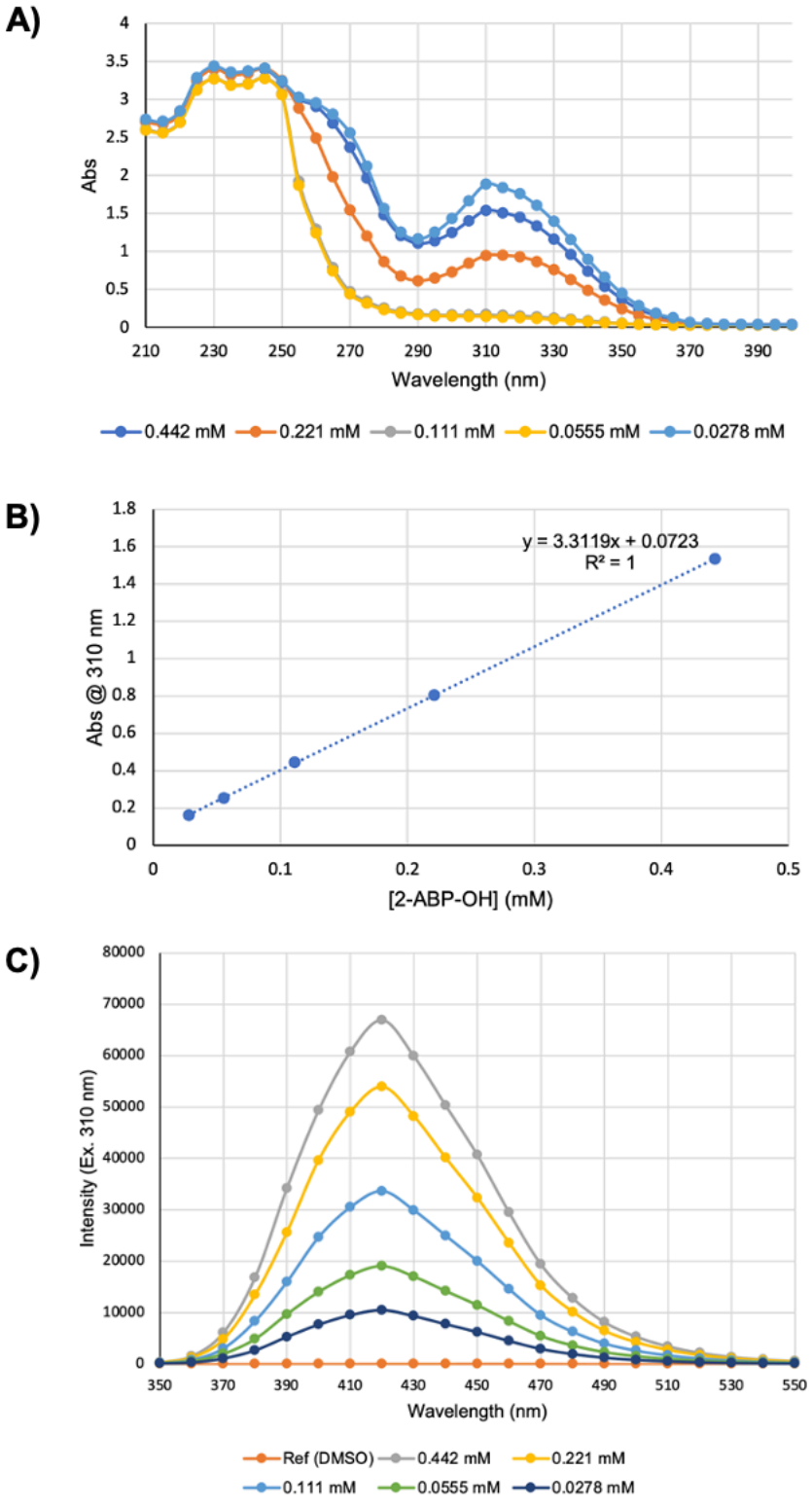

Figure E2: Spectrophotometric analysis of 2-aminobiphenyl neryl alcohol (2-ABP-OH) (**10**), including an absorbance spectrum (**A**), standard curve (**B**), and fluorescence spectrum (**C**)

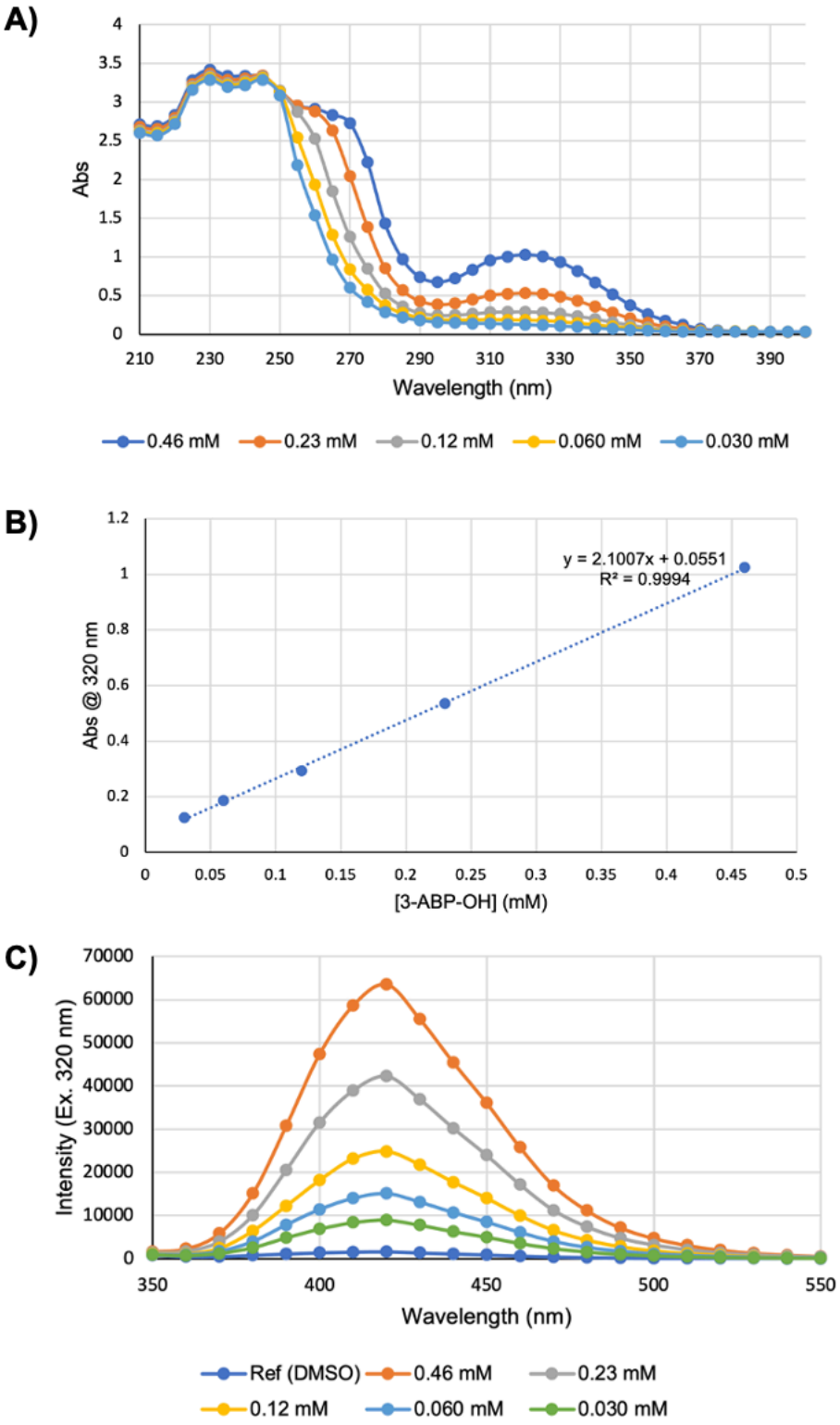

Figure E3: Spectrophotometric analysis of 3-aminobiphenyl neryl alcohol (3-ABP-OH) (**11**), including an absorbance spectrum (**A**), standard curve (**B**), and fluorescence spectrum (**C**)

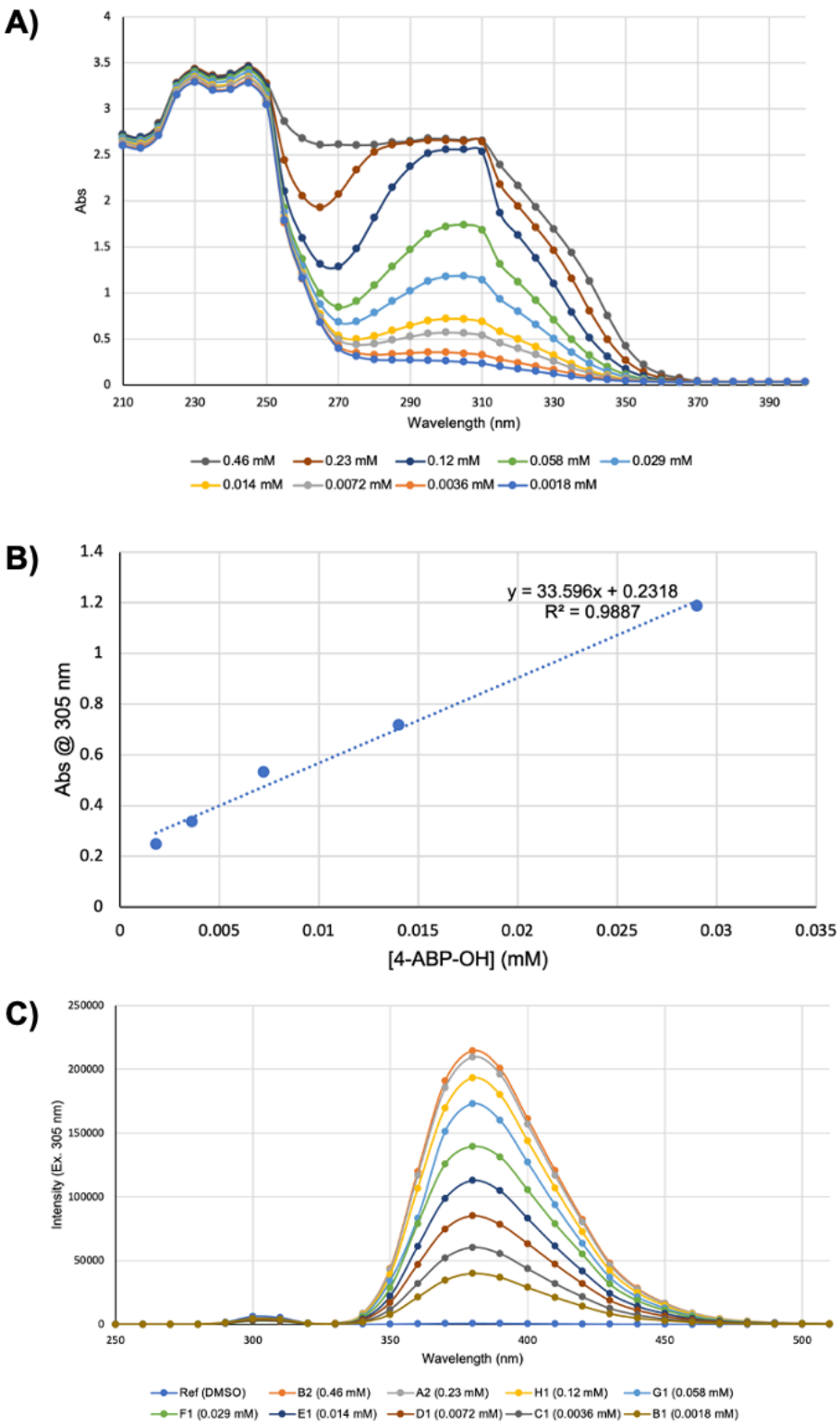

Figure E4: Spectrophotometric analysis of 4-aminobiphenyl neryl alcohol (4-ABP-OH) (**12**), including an absorbance spectrum (**A**), standard curve (**B**), and fluorescence spectrum (**C**)

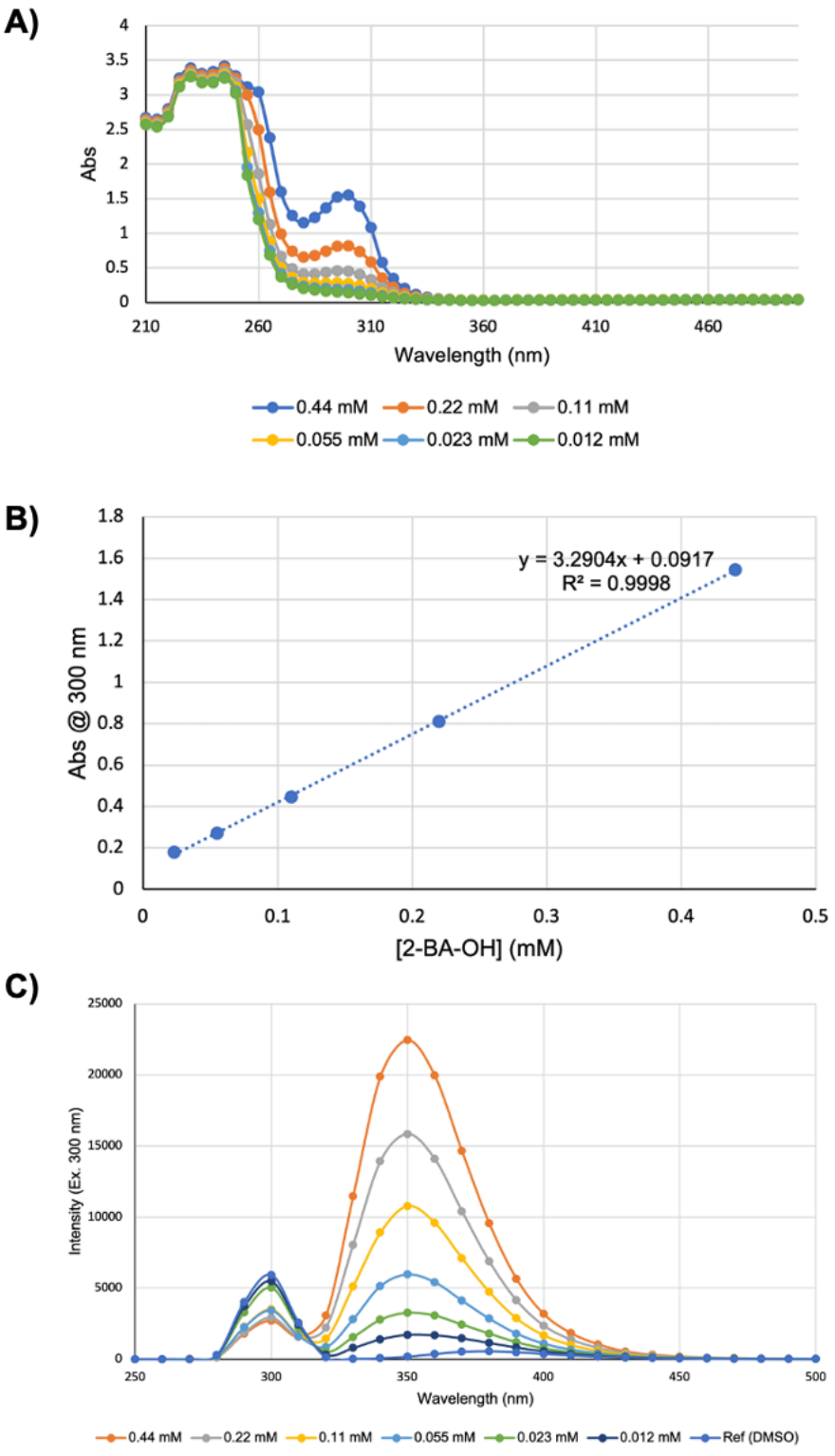

Figure E5: Spectrophotometric analysis of 2-benzylaniline neryl alcohol (2-BA-OH) (**13**), including an absorbance spectrum (**A**), standard curve (**B**), and fluorescence spectrum (**C**)

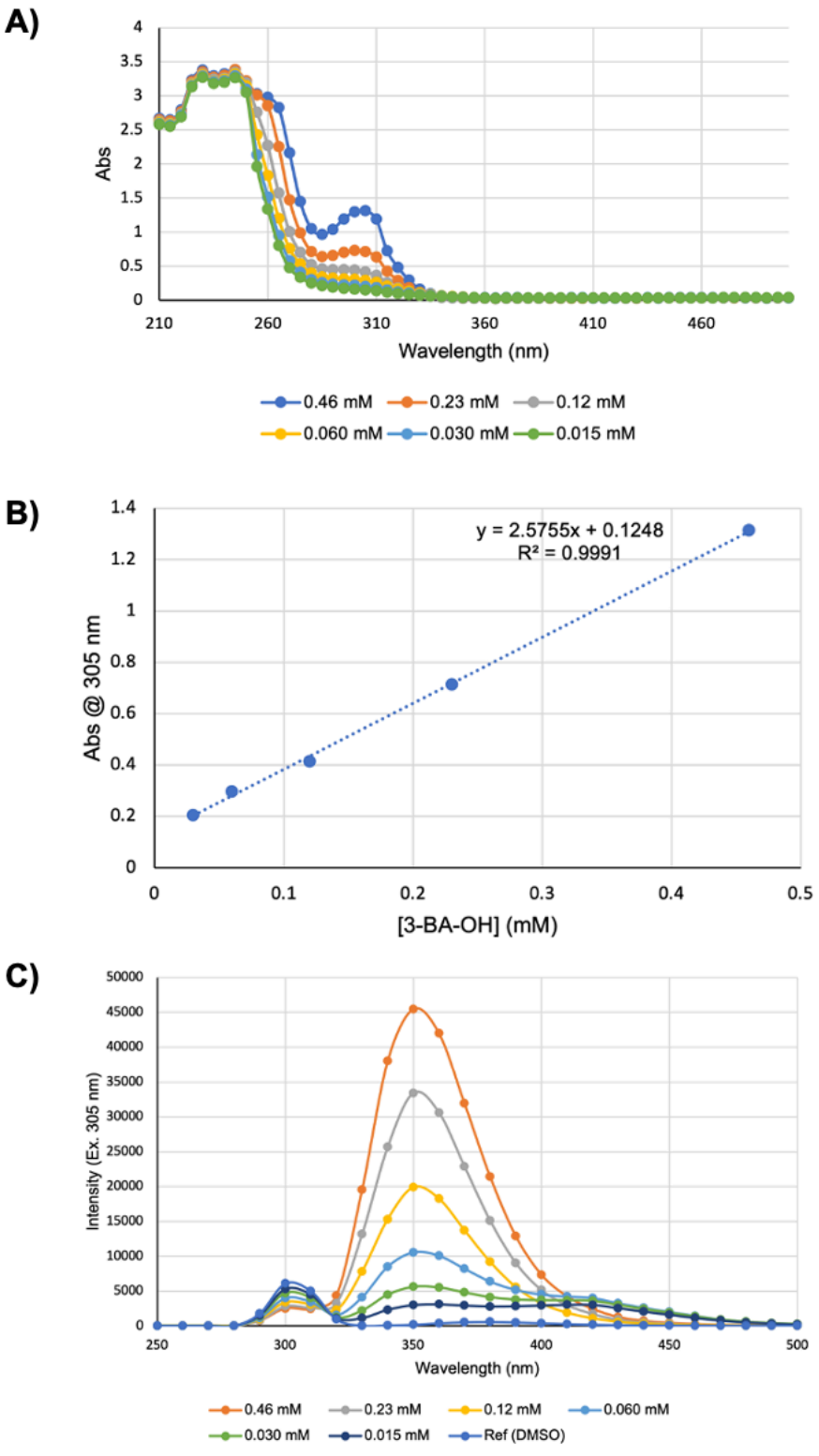

Figure E6: Spectrophotometric analysis of 3-benzylaniline neryl alcohol (3-BA-OH) (**14**), including an absorbance spectrum (**A**), standard curve (**B**), and fluorescence spectrum (**C**)

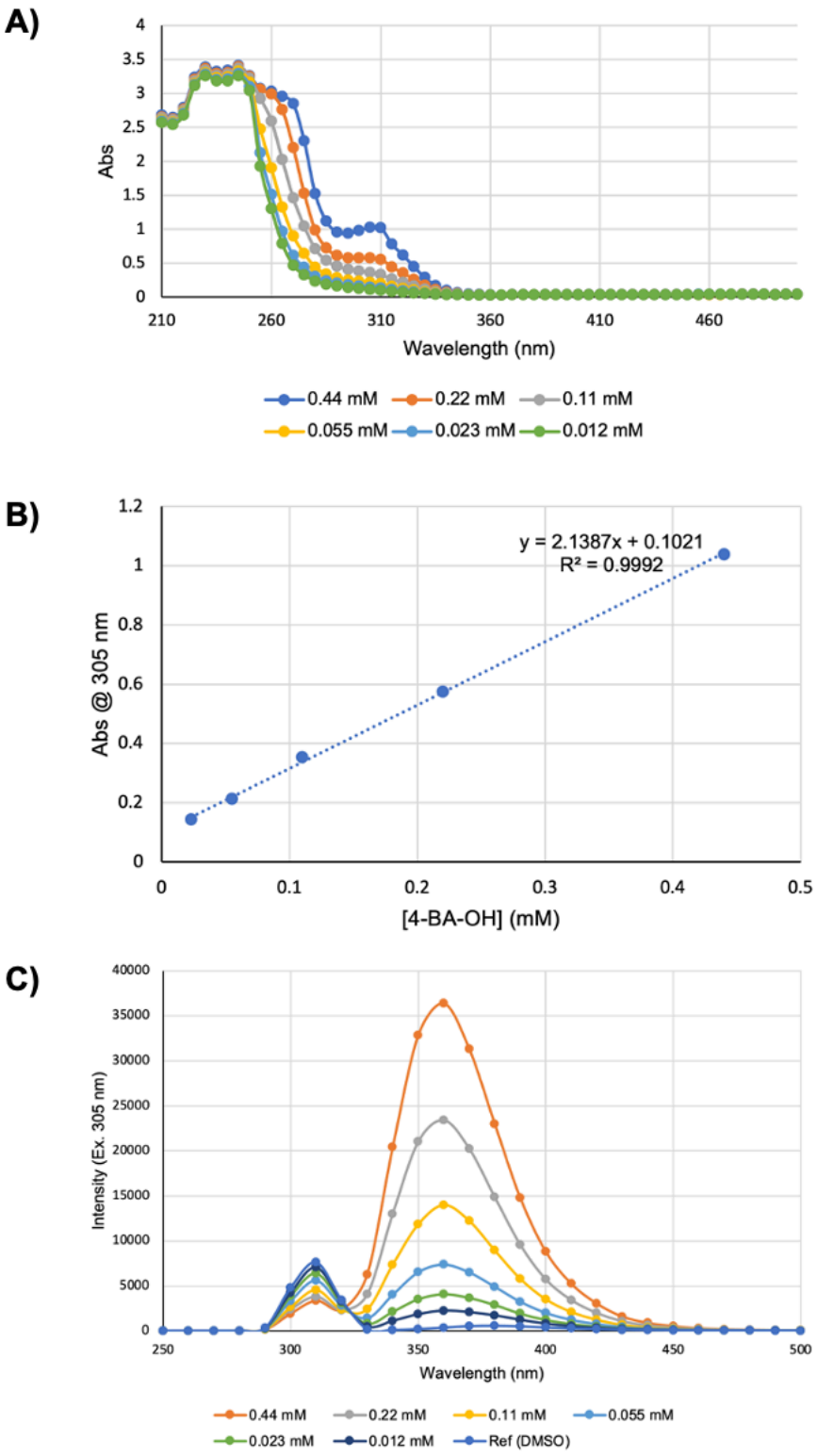

Figure E7: Spectrophotometric analysis of 4-benzylaniline neryl alcohol (4-BA-OH) (**15**), including an absorbance spectrum (**A**), standard curve (**B**), and fluorescence spectrum (**C**)